Early brain development in infants born with congenital heart disease

Kelly, Christopher John

Awarding institution:
King's College London

Early brain development in infants born with congenital heart disease

Christopher J. Kelly

A thesis submitted in partial fulfilment of the requirement for the degree of

Doctor of Philosophy, King's College London

April 2018

Abstract

Improving neurodevelopmental outcomes has become one of the biggest remaining challenges for infants born with congenital heart disease (CHD). Despite a dramatic reduction in CHD mortality over the past few decades, there have been comparatively modest improvements in neurodevelopmental outcomes. The burden of the problem is significant, affecting a wide range of developmental domains that impact upon future educational achievement, employability and quality of life for millions of children born with CHD. While it was initially assumed that adverse outcomes were due to brain injury sustained around the time of cardiac surgery, it is now clear that there is a complex interplay between the circulation and brain, involving both fetal and postnatal development. Promising early work has suggested the role of reduced cerebral oxygenation as a key factor in altered early brain development in CHD, although the precise mechanisms through which this is mediated remain unclear.

This thesis aims to test the hypotheses that congenital heart disease is associated with impaired early brain development, and that reduced cerebral oxygen delivery in CHD is associated with impaired cortical development in newborn infants prior to surgery. This is achieved through the study of a new prospective cohort of newborn infants born with major CHD prior to surgery, and the use of both qualitative and quantitative magnetic resonance image analysis of brain tissue macrostructure and microstructure, in order to compare early brain development with age-matched healthy infants.

Evidence is provided that complexity of cortical folding and cortical grey matter volumes are both reduced in newborns with CHD when compared to healthy age-matched controls, and that the degree of impairment is associated with reduced cerebral oxygen delivery. At the microstructural level, fractional anisotropy (FA) is demonstrated to be elevated and cortical orientation dispersion index (ODI) reduced in a number of cortical regions compared to healthy controls, supporting the interpretation that dendritic arborisation in cortical grey matter may be the primary component that is negatively affected. Both findings are convergent with recent animal studies and provide support to the development of future interventional strategies to optimise cerebral oxygenation during early brain development.

Declaration of originality

The work presented in this thesis was conducted by the author at the Centre for the Developing Brain, King's College London between March 2015 and March 2018. All sources are appropriately referenced.

This work has not been submitted for the purpose of obtaining any other degree at this University or any other institution.

Christopher Kelly

Copyright declaration

Acknowledgements

The work presented in this thesis would not have been possible without the generous help and support from a large number of people. I would like to thank Prof Serena Counsell, my primary supervisor, for her indefatigable enthusiasm, guidance, and encouragement. Thank you to Prof Mary Rutherford, my second supervisor, for her support, inspiration, and thoughtful guidance when working with families in the study. Thank you to my third supervisor Prof John Simpson for his expertise and advice. Finally, thank you to my fourth supervisor Prof David Edwards for his mentorship, analytical mind, and for always encouraging me to pursue interesting ideas.

There are many friends and colleagues to thank from the Centre for the Developing Brain and St Thomas' Hospital: Jana Hutter, Anthony Price, Rui Teixeira, Lucilio Cordero-Grande, and Prof Jo Hajnal for their help developing acquisition protocols; Dafnis Batalle, Antonis Makropoulos, Daan Christiaens, Max Pietsch, Diliana Pecheva, Jonathan O'Muircheartaigh, Donald Tournier, and Gareth Ball for help with imaging analysis; the clinical fellows including Tomoki Arichi, Maddy Barnett, Sophie Arulkumaran, Johannes Steinweg, Katy Vecchiato, Harriet Cullen, Nora Tusor, David Cox and Michelle Krishnan for their friendship and support; Andrew Chew for his enthusiastic stewardship of the CHD follow up programme; our research radiologists Sophie Arulkumaran, Olivia Carney, and Kelly Pegoretti; our research nurses Julia Wurie, Maryann Sharma, Jose Bueno Conde, Beatriz Santamaria, Millie O'Keeffe and Jakki Brandon; our research radiographers Joanna Allsop, Emer Hughes, Matt Fox, Ana Dos Santos Gomes, and Elaine Green; Saheli Dodhia, Devinder Mehet, Amin Alamshah, Laura McCabe, and Veena Supramaniam for assistance with ethics, governance, and logistics; all the doctors and nurses on the St Thomas' Neonatal Unit, particularly Hammad Khan and Geraint Lee, who advocated the project and supported me with scanning; the doctors and nurses from the cardiology service at the Evelina Children's Hospital, and particularly Kuberan Pushparajah for all his advice and support; Soba Akinwunmi and Andrew Cantell for their IT assistance; and Michelle Hetherington for making sure everything always ran smoothly.

Thank you to the British Heart Foundation for funding my Clinical Research Training Fellowship, to the Medical Research Council for providing additional funding, and to the National Institute for Health Research for funding my academic clinical fellowship for pilot work prior to starting this PhD.

Finally, thank you to my parents, family, and friends for all their encouragement over the years. And of course, most importantly, thank you to Charlotte for somehow putting up with me, without whose love and support this would not have been possible.

Table of Contents

List of Figures

List of Tables

List of Abbreviations

ASD	Atrial septal defect
ASO	Arterial switch operation
AVSD	Atrio-ventricular septal defect
BAV	Bicuspid aortic valve
CoA	Coarctation of the aorta
CBF	Cerebral blood flow
DGM	Deep grey matter
DILV	Double inlet right ventricle
DORV	Double outlet right ventricle
DTI	Diffusion tensor imaging
FA	Fractional anisotropy
GA	Gestational age
GI	Gyrificatiom index
GM	Grey matter
HARDI	High angular resolution diffusion imaging
HLHS	Hypoplastic left heart syndrome
HRV	Hypoplastic right ventricle
IUGR	Intrauterine growth restriction
MAPCAs	Major aortopulmonary collateral arteries
MD	Mean diffusivity
MRI	Magnetic resonance imaging
NODDI	Neurite orientation dispersion and density imaging
NDI	Neurite density index
NEC	Necrotising enterocolitis
ODI	Orientation dispersion index
PA	Pulmonary atresia
PC-MR	Phase contrast magnetic resonance imaging
PDA	Patent ductus arteriosus
PMA	Post-menstrual age
PS	Pulmonary stenosis
PVL	Periventricular leucomalacia
SD	Standard deviation
TA	Truncus arteriosus
TBSS	Tract-based spatial statistics
TGA	Transposition of the great arteries
TOF	Tetralogy of Fallot
TS	Tricuspid stenosis
VSD	Ventricular septal defect
WM	White matter

Publications

The following publications were written during the course of the PhD fellowship:

Kelly CJ, Makropoulos A, Cordero-Grande L, et al. Impaired development of the cerebral cortex in infants with congenital heart disease is correlated to reduced cerebral oxygen delivery. *Sci Rep*, Springer US; 2017; **7**: 15088
Available from: http://www.nature.com/articles/s41598-017-14939-z

Kelly CJ, Arulkumaran S, Tristão Pereira C, Cordero-Grande L, Hughes EJ, Teixeira RPAG, Steinweg JK, Victor S, Pushparajah K, Hajnal JV, Simpson J, Edwards AD, Rutherford MA, Counsell SJ. Neuroimaging findings in newborns with congenital heart disease prior to surgery: an observational study. Submitted.

Kelly CJ, Christiaens D, Batalle D, Makropoulos A, Cordero-Grande L, Steinweg JK, O'Muircheartaigh J, Khan H, Lee G, Victor S, Alexander DC, Zhang H, Simpson J, Hajnal JV, Edwards AD, Rutherford MA, Counsell SJ. Abnormal microstructural development of the cortex in congenital heart disease is related to impaired cerebral oxygen delivery. Submitted.

Claessens NHP, **Kelly CJ**, Counsell SJ, Benders MJNL. Neuroimaging, cardiovascular physiology, and functional outcomes in infants with congenital heart disease. *Dev Med Child Neurol* 2017; 59: 894–902 http://doi.wiley.com/10.1111/dmcn.13461

Kelly CJ, Hughes EJ, Rutherford MA, Counsell SJ. Advances in neonatal magnetic resonance imaging of the brain: From research to practice. Archives of Disease in Childhood 2018. http://dx.doi.org/10.1136/archdischild-2018-314778

Makropoulos A, Robinson EC, Schuh A, Wright R, Fitzgibbon S, Bozek J, Counsell SJ, Steinweg J, Vecchiato K, Passerat-Palmbach J, Lenz G, Mortari F, Tenev T, Duff EP, Bastiani M, Cordero-Grande L, Hughes E, Tusor N, Tournier J-D, Hutter J, Price A, Teixeria RPA, Murgasova M, Victor S, **Kelly CJ**, Rutherford MA, Smith SM, Edwards AD, Hajnal JV, Jenkinson M, Rueckert D. The Developing Human Connectome Project: A Minimal Processing Pipeline for Neonatal Cortical Surface Reconstruction. NeuroImage 2018. Neuroimage 173, 88-112.
http://dx.doi.org/10.1016/j.neuroimage.2018.01.054

Batalle D, O'Muircheartaigh J, Makropoulos A, **Kelly CJ**, Dimitrova R, Hughes EJ, Hajnal JV, Zhang H, Alexander DC, Edwards AD, Counsell SJ. Different patterns of cortical maturation before and after 38 weeks gestational age demonstrated by diffusion MRI in vivo. NeuroImage 2018. Submitted.

Conference Abstracts

Hughes E, Winchman T, Mager L, Wurie J, Sharma M, Fox M, Allsop J, Padormo F, Arichi T, Tusor N, **Kelly CJ**, Barnett M, Kapetanakis A, Krishnan M, Price A, Teixeira RPAG, Bequiri A, Hutter J, Rutherford M, Counsell S, Edwards AD, Hajnal J. A dedicated neonatal magnetic resonance brain imaging system. ESMRMB 2015, Edinburgh, 1-3 October 2015.

Kelly CJ et al. “Cortical Grey Matter Volume is reduced in neonates with complex congenital heart disease”, Pediatric Academic Societies 2016, Baltimore, MA, US, 30 April – 3 May 2016.

Kelly CJ, Pietsch M, Counsell SJ, Tournier JD, “Transfer learning and convolutional neural net fusion for motion artefact detection”, ISMRM, Honolulu, Hawaii, US, 22-27 April 2017.

Hughes EJ, Carney O, Pegoretti K, Arulkumaran S, Cordero-Grande L, **Kelly CJ**, Barnett M, Krishnan M, Steinweg J, Allsop J, Dos Santos Gomes A, Wurie J, Bueno-Conde J, Fox M, Strang A, Sharma M, Victor S, Counsell SJ, Edwards AD, Hajnal JV, Rutherford MA, The type and prevalence of incidental findings on magnetic resonance imaging of the low risk term born neonatal brain, ISMRM, Honolulu, Hawaii, US, 22-27 April 2017.

Kelly CJ, Makropoulos A, Cordero-Grande L, et al. Impaired development of the cerebral cortex in infants with congenital heart disease is correlated to reduced cerebral oxygen delivery, BHF Fellows Meeting, Cambridge UK, 25-26 September 2017. Runner up – Best abstract.

Kelly CJ, Makropoulos A, Cordero-Grande L, et al. Impaired development of the cerebral cortex in infants with congenital heart disease is correlated to reduced cerebral oxygen delivery, BPNA 44th BPNA Annual Scientific Meeting, London, UK, 3 January 2018.

Steinweg JK, Vecchiato K, **Kelly CJ**, Chew A, Falconer S, Arulkumaran S, Tusor N, Brandon J, O'Keeffe C, Wurie J, Hughes EJ, Allsop J, Dos Santos Gomes A, Green E, Harper N, Rawn Z, Victor S, Counsell SJ, Rutherford MA, Edwards AD. The Developing Human Connectome Project: Update, Pediatric Academic Societies (PAS) 2018 Meeting, Toronto, Canada, 5-8 May 2018.

Bravar G, Vecchiato K, Steinweg J, **Kelly CJ**, Hughes E, Victor S, Singh R, Edwards AD, Arichi T, Correlation between Functional Resting State Networks and Cerebral Function Monitoring in Hypoxic Ischemic Encephalopathy, Pediatric Academic Societies (PAS) 2018 Meeting, Toronto, Canada, 5-8 May 2018.

Kelly CJ, Christiaens D, Batalle D, Makropoulos A, Cordero-Grande L, Steinweg JK, O'Muircheartaigh J, Khan H, Lee G, Victor S, Alexander DC, Zhang H, Simpson J, Hajnal JV, Edwards AD, Rutherford MA, Counsell SJ. Abnormal microstructural development of the cortex in congenital heart disease is related to impaired cerebral oxygen delivery. Neonatal Society Spring Meeting 2018, Royal Society of Medicine, London, 22 March 2018. Winner – Best trainee presentation.

Invited Talks

Kelly CJ, "Brain lesion prevalence and cortical folding in CHD", Neurology in Fetuses and Neonates with Congenital Heart Disease Symposium, European Association Brain and Congenital Heart Disease (European-ABC), Utrecht, Netherlands, 8 February 2018.

Chapter 1

Introduction

1.1 BACKGROUND AND MOTIVATION

Improving neurodevelopmental outcome has become one of the greatest remaining challenges for infants born with congenital heart disease (CHD). Despite dramatic improvements in mortality over the past few decades (Khairy et al., 2010), improvements in motor and cognitive neurodevelopmental outcomes have been comparatively modest (Gaynor et al., 2015).

The burden of the problem is significant – CHD is the most common congenital abnormality affecting newborns (Bernier et al., 2010). Approximately one third will require surgery in their first year of life (Wernovsky and Licht, 2016) and roughly half of this group will currently experience some form of neurodevelopmental problem in childhood (Marino et al., 2012). Young children with CHD may exhibit deficits in multiple domains, including gross and fine motor, speech and language, memory, and visuospatial skills. Follow-up studies suggest that deficits persist into adolescence and adulthood (Bellinger et al., 2015b, 2015a, 2011; Schaefer et al., 2013; Tyagi et al., 2017), with survivors of CHD found to experience deficits in specific domains including hyperactivity and inattention (Hansen et al., 2012) and executive function (Calderon and Bellinger, 2015), which can have widespread repercussions for later neurocognitive, behavioural and psychosocial development. This poses a serious threat to educational achievement, employability and later quality of life (and in many countries insurability) for millions of children born with CHD.

As clinicians and researchers working with children born with CHD, our shared goal is threefold: 1) to understand the necessary environment in utero for normal brain development, and to develop appropriate interventions to ensure that this is possible in pregnancies complicated by CHD, 2) to undertake cardiac surgery while protecting the brain from acquired injury, and 3) for these children to thrive during childhood and live a fulfilled adult life with no significant difference in neurodevelopmental outcomes compared to their healthy peers.

The first step towards achieving these goals in a systematic way is to understand the underlying biological processes that are responsible for altered brain development in CHD. This knowledge will enable focused identification of candidate therapeutic options. We also need to define a set of measures, using magnetic resonance imaging (MRI) or other biological markers, that can reliably quantify early brain dysmaturation in CHD *in vivo*, allowing us to distinguish abnormal brain development. This provides the ability to perform intervention studies using these validated measures as primary outcomes to demonstrate efficacy in the neonatal period. Determining efficacy as early as possible is crucial, as it enables faster iteration of the clinical trials process, and will ultimately improve outcomes for children with CHD sooner.

Despite a growing body of experimental work, our understanding of the biological mechanisms that underpin how CHD affects brain development remains limited. Nevertheless, there is converging evidence of the role of reduced cerebral oxygenation in abnormal neuronal development and migration that may be responsible in CHD (Dean et al., 2013; Morton et al., 2017; Ortega et al., 2017; Sun et al., 2015; Yuen et al., 2014). In the same way, although imaging studies in CHD have identified a number of measures of brain dysmaturation, including alterations of macrostructural brain growth and morphology, microstructural tissue differences, metabolic alterations, and structural and functional connectivity differences, our ability to define a quantifiable short-term primary outcome for an interventional trial is surprisingly inadequate.

A systematic approach will take time to translate into tangible outcomes. In the meantime, there is an immediate opportunity to exploit the considerable differences in clinical practice between cardiac centres, using historical data that have been collected over many years. Injury rates vary considerably between cohorts (Mebius et al., 2017). The natural assumption is that such variation must be, at least in part, due to modifiable local differences in clinical management.

In this thesis, I prospectively recruit, assess and describe a new contemporary cohort of infants born with CHD, and use a range of analysis techniques to assess differences compared to healthy controls. Through this work, I aim to both contribute to our understanding of brain dysmaturation in this important population and identify MR imaging measures that could be used to quantify brain dysmaturation in the context of future interventional trials.

1.2 HYPOTHESIS AND AIMS

This thesis aims to test the following hypotheses:

- Infants born with major congenital heart disease have impaired early brain development compared to healthy controls and are more susceptible to perinatal brain injury.
- Reduced cerebral oxygen delivery in congenital heart disease is associated with impaired development of the cerebral cortex.

This is conducted with the following aims:

1. To describe the prevalence and types of acquired brain injury in newborn infants with congenital heart disease and identify clinical variables that are associated with injury.
2. To use quantitative macrostructural measures to investigate developmental differences of the cerebral cortex between infants with CHD and healthy controls using structural MRI, and to determine if abnormalities are associated with reduced cerebral oxygen delivery.
3. To use diffusion MRI to quantify microstructural changes in the cerebral cortex of infants born with CHD, and to investigate if cerebral oxygen delivery is associated with microstructural development.

1.3 THESIS OUTLINE

Chapter 2 introduces the fundamentals of MRI, diffusion-weighted imaging, phase contrast imaging, the challenges that are involved in scanning a vulnerable newborn population, and introduces methods of MR image analysis that are discussed in this thesis.

In Chapter 3, I introduce the burden of neurodevelopmental problems in children with CHD and discuss evidence of abnormal early brain development in CHD. I consider different hypotheses for brain dysmaturation, including reduced cerebral oxygen delivery, and explore recent studies that have attempted to test these. I finish by considering the effect of cerebral oxygen delivery on neurodevelopmental outcomes.

In Chapter 4, I determine the prevalence of lesions in a prospective cohort of infants born with CHD and characterise these lesions using a mixture of qualitative and quantitative methods. I then explore clinical risk factors that are associated with injury.

Macrostructural differences between a group of infants with CHD and a matched group of healthy controls are assessed in Chapter 5. I show that brain volumes and measures of cortical folding are both reduced in newborn infants compared to healthy age-matched controls, and that these measures are related to reduced cerebral oxygen delivery.

In Chapter 6, I use diffusion MRI to investigate the cortical microstructural development of the brain in infants with CHD compared to healthy controls, and relate these changes to cerebral oxygen delivery. I finish by exploring the link between macrostructural appearance (using gyrification index as a quantitative measure) and microstructural measures of tissue development.

Chapter 7 provides a summary of the work presented in this thesis, its limitations, and examines potential avenues for future study.

Chapter 2

Background

2.1 INTRODUCTION

Three main methodological approaches are employed in this thesis. The first involves qualitative analysis of brain lesions of pre-surgical MR brain imaging of infants with CHD. The second uses quantitative methods to compare macroscopic differences in brain size and cortical folding between infants with CHD and healthy controls. The third uses diffusion MRI to assess the cortical microstructure of infants with CHD compared to healthy controls.

In this chapter, I provide an outline of the general principles of MRI, including diffusion-weighted imaging and phase contrast angiography. I then explain the segmentation and cortical surface reconstruction methods that are used for the macrostructural analysis. This is followed by an outline of the methods used for assessing cortical microstructure, including image registration and the statistical methods that are employed to analyse group diffusion data. Specific methodological details for each study are provided in each experimental chapter.

2.2 BIOPHYSICAL PRINCIPLES OF MRI

Magnetic resonance imaging provides a unique opportunity to gain a better understanding of the structure and function of living biological tissue. Given that MRI does not involve ionising radiation and provides imaging with high spatial resolution and good tissue contrast, it has become a widely used tool. This section reviews the essential parameters of MRI acquisition, provides a conceptual overview of diffusion imaging and microstructural imaging, followed by the principles governing the analysis of structural, diffusion, and phase contrast data.

2.2.1 Magnetic fields

MRI is based upon the principle of nuclear magnetic resonance (NMR) discovered by Purcell and Bloch in the 1940s (Bloch, 1946; Purcell et al., 1946). All atomic nuclei possess the quantum property of spin. Different MRI techniques measure the effect of

altering the spin of specific atomic nuclei, such as hydrogen nuclei, which have an odd number of protons and/or neutrons, making them NMR active atomic isotopes.

In the human body, there is an abundant source of protons in the form of hydrogen atoms (^{1}H) present in the body's water. Indeed, the mass of the human brain consists of approximately three-quarters water. Protons have a spin, and therefore the associated electrical charge of the protons also moves, inducing a small local magnetic field. As a result, the proton has its own magnetic field, and can be considered as a small bar magnet.

In the absence of an external magnetic field, the protons are randomly orientated with no net magnetisation. However, in the presence of an external magnetic field, B0, the protons align themselves longitudinally with the field, either parallel (in line with the field) or anti-parallel (flipped in the opposite direction), as shown in Figure 1.

If the spins of the protons are not completely aligned with the direction of the external magnetic field B0, the protons start to revolve or "precess" around the field's longitudinal direction (Figure 1). The frequency with which the protons precess is called the resonance or "Larmor" frequency and is proportional to the strength of the magnetic field B0, measured in Tesla.

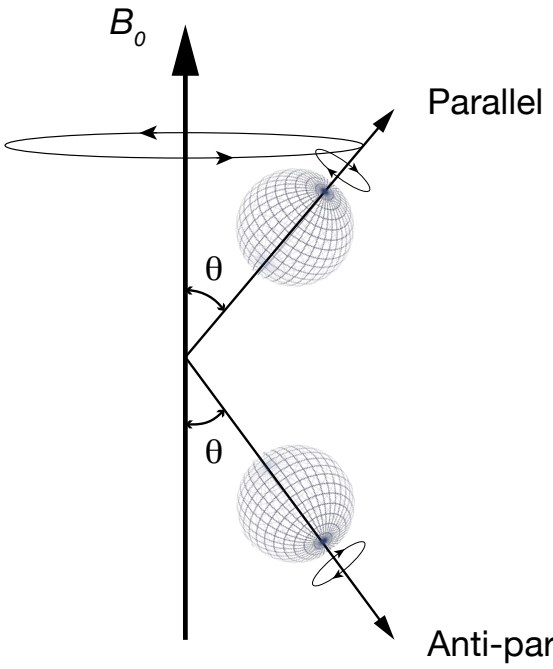

Figure 1 Alignment of protons in a magnetic field - spin precession and alignment
Protons in a strong magnetic field demonstrating alignment that is either parallel or anti-parallel to the external magnetic field B0. In this environment, protons develop a secondary spinning motion around the direction of the magnetic field, called precession.

A spin can have different energy levels depending on the orientation of its magnetic moment in relation to the external magnetic field. For a simple spin system such as that of the proton, when the magnetic moment is aligned with the field it is in a lower energy state (the parallel position), while when it opposes the field (the anti-parallel position) it is elevated to a higher-energy state. The difference is however very small, and even normal thermal energy at room temperature is enough to flip spins. The signals generated in MRI are based upon this imbalance between energy states, and the small differences involved help explain why MR techniques are commonly limited by signal strength.

Parallel and antiparallel protons cancel each other out, but there are slightly more parallel protons at the lower energy level, leading to a net magnetic moment along the direction of the applied magnetic field. However, magnetisation that is longitudinal to the external magnetic field cannot be measured directly. To allow direct measurement, a magnetisation that is transverse to the external magnetic field is necessary.

2.2.2 Generating an MR signal

Spins can be excited from a low energy state to high energy state by applying an oscillating radiofrequency (RF) pulse (Figure 2). This pulse consists of an oscillating electromagnetic field, B1, perpendicular to the static field B0. The most efficient transfer of energy occurs when the B1 pulse is delivered at the same frequency as the spin's Larmor frequency (128 MHz for a proton in a 3 Tesla magnetic field, which is the field strength used in this thesis).

The RF pulse has two main effects. Firstly, it lifts some protons to a higher energy level (flipping to anti-parallel), reducing the net magnetisation vector in the longitudinal direction. Secondly, it induces the protons to precess in phase, tipping the net magnetisation vector towards the transverse x-y plane (Figure 2, green arrow).

When sufficient energy is provided to cause a 90° shift in net magnetisation, the flip angle is said to be 90°. A receiver coil orientated perpendicular to B0 measures the transverse magnetisation vector through current induction.

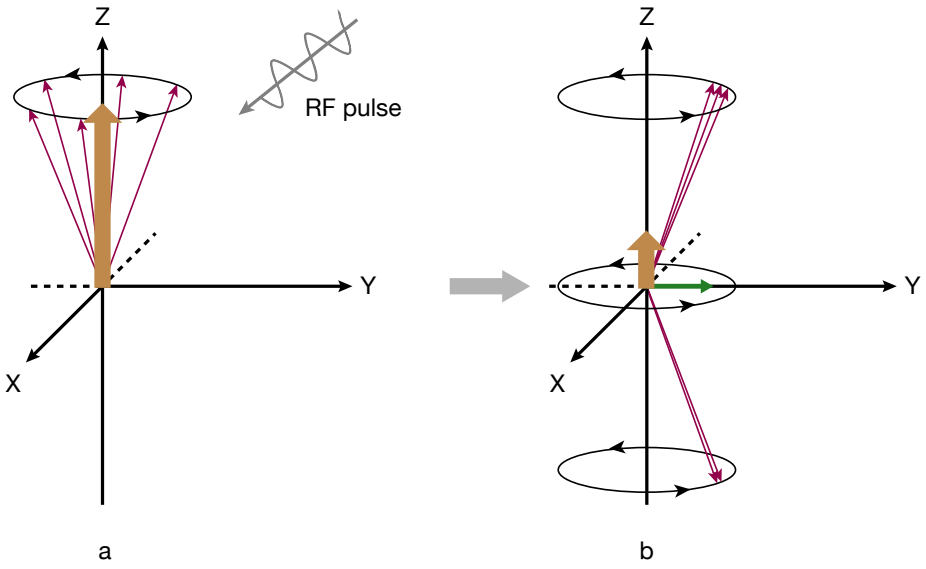

Figure 2 Generating an MR signal

A radiofrequency (RF) pulse has two effects on the protons: 1. It lifts some protons to a higher level of energy (arrows pointing down in b), resulting in reduced longitudinal magnetisation along the z-axis; 2. It causes the protons to precess in step, or in 'phase', establishing a new transverse magnetisation in the x-y plane, which moves around with the precessing protons.

After the RF pulse is switched off, protons return to their lower state of energy, resulting in longitudinal magnetisation growing back to its original value. The energy gained from the RF pulse is lost in one of two ways. Firstly, the energy is lost to surrounding tissue (the 'lattice'), in a process called longitudinal relaxation or spin-lattice-relaxation. The time taken for the longitudinal magnetisation to recover back to its original value is determined by a constant called by the longitudinal relaxation time, or T1. T1 can vary depending on the atomic structure of the material: for example, fat has a faster T1 than water because the carbon bonds in fat resonate close to the Larmor frequency, facilitating faster transfer of energy to the surrounding tissue.

Secondly, protons lose energy to other nuclei, referred to as transversal relaxation, or spin-spin-relaxation. Transverse magnetisation decays against time at a rate determined by a constant called the transversal relaxation time, or T2. T2-relaxation occurs when protons get out of phase, a process that is caused by both inhomogeneities of the external magnetic field, and inhomogeneities of local magnetic fields within the tissues. If a substance is impure – e.g. containing larger molecules, there are bigger variations in local magnetic fields, causing greater differences in precession frequencies, and so protons become out of phase faster, causing a shorter T2. This is the case for fat, which demonstrates a short T2. In contrast, the smaller

and homogenous molecules in water results in smaller net differences in internal magnetic fields from location to location, allowing the protons to stay in step for a longer time, and hence resulting in a longer measured T2.

These differences in T1 and T2 between different tissue compositions provide the contrast mechanism necessary to image the soft tissues of the brain.

2.2.3 Image formation

Placing a biological tissue such as the brain into a static B0 magnetic field will not allow a three-dimensional MR image to be generated, as all protons will be subjected to roughly the same magnetic field, and hence will emit identical frequencies, irrespective of the spatial location that it has been received from.

To encode spatial information, a second magnetic field is required to allow slice-selective excitation. Slice selection is achieved by varying the magnetic field gradients to cause variation in the precessional frequency in a linear fashion along a single axis of the coil (Lauterbur, 1973). The resultant MR signal is a mixture of precessional frequencies that are related to the position along the gradient axis x, a process that is termed ‘frequency encoding’. An additional gradient applied along the y axis can be used to alter the phase of the precessing spins, termed ‘phase encoding’. A combination of these allows the position of a signal to be encoded in a two-dimensional plane, according to both the phase and frequency of the received signal. In order to build a three-dimensional image, an RF pulse is used to selectively excite spins at specific positions along the z-axis, where its oscillatory frequency matches the resonant frequency of the spins, and where differences in resonant frequencies are induced as a function of the varying gradient strength that has been applied.

The characteristics of the gradients that are applied to the tissue determine the resolution of the acquired images. By increasing the gradients in a step-wise manner, it becomes possible to separate the sample into small cuboids, referred to as ‘voxels’. The size of the steps therefore determines the voxel size. Each voxel is subjected to the same frequency and phase encoding conditions, and so the biological components of the tissue within each voxel behave in the same way. It is therefore possible to adjust the scan resolution by varying the step size of the gradients. Lower resolution has the advantage of a better signal-to-noise ratio (SNR), but also the disadvantage of grouping a larger number of protons with potentially very different

properties together, which could result in a misleading mixed signal. The choice of resolution for a particular application is ultimately a compromise between these two different factors.

2.2.4 Scanning parameters

Image contrast in MRI depends on both modifiable and non-modifiable parameters. Extrinsic parameters can be adjusted as part of the scan sequence, and include time to echo (TE), repetition time (TR) and flip angle. Intrinsic contrast parameters are related to the composition of the tissue being studied, and are therefore fixed – for example, T1 recovery and T2 decay.

Repetition time (TR): The TR describes the amount of time between sequential 90° RF pulses, and determines the longitudinal relaxation, or T1 relaxation that occurs between pulses.

Time to echo (TE): The TE determines the amount of T2 decay that occurs before the signal is received. By choosing different TEs, the signals can be T2-weighted to varying degrees. With very short TEs, T2 effects have not yet had time to appear. With longer TEs, the signal intensity difference between tissues will depend on their transversal relaxation times.

For example, a short TR and TE will emphasise the T1 characteristics of tissue, producing a “T1-weighted” image. In contrast, a long TR and TE will emphasise T2 characteristics of tissue, producing a “T2-weighted” image.

Flip angle: To increase speed, it is possible to use pulses that cause flip angles smaller than 90°. In this case, longitudinal magnetisation is not totally abolished as would be the case with the full 90°, and there is still a substantial amount of longitudinal magnetisation left, which can be tilted by the next pulse. This gives a reasonable signal even if the next pulse is produced after a very short TR.

2.2.5 Diffusion MRI

2.2.5.1 The concept of diffusion

Diffusion MRI offers a unique insight into tissue microstructure. It is the most promising method to investigate tissue microstructure *in vivo* and provides quantitative measures of brain injury and development. It works by sensitising MRI measurements to the displacement pattern of water molecules undergoing diffusion.

Each molecule in a fluid is in constant motion due to its thermal energy, and changes direction when it encounters a collision with another molecule. In a homogenous fluid, the path that a molecule takes describes a random walk – a chain of statistically-independent steps – in a process that is now known as Brownian motion, named after Robert Brown, a botanist who first described the random motion of grains of pollen grains suspended in water under a microscope (Brown, 1828). This observed phenomenon was later formalised independently by both Albert Einstein and Marian Smoluchowski (Einstein, 1905; von Smoluchowski, 1906), demonstrating that the mean displacement of freely-diffusing particles is dependent on both the time taken to diffuse, and the diffusion coefficient (or diffusivity) of the medium in which they are in (Equation [2.1]).

$$\lambda = \sqrt{6D\tau} \qquad [2.1]$$

where λ is the root mean square displacement of a molecule in three dimensions over time interval τ, and D is the diffusion coefficient of the medium. In the case of water at body temperature, D is approximately 2.5 μm^2/ms. This is particularly fortuitous, as with a different value of D, diffusion MRI would not be possible. With measureable diffusion times between 10-200 ms on modern MRI scanners, this diffusion coefficient provides a length scale in the order of 10-50 μm, which is far below imaging resolution, and enables us to probe the microstructure of living biological tissue microstructure on the micrometre scale.

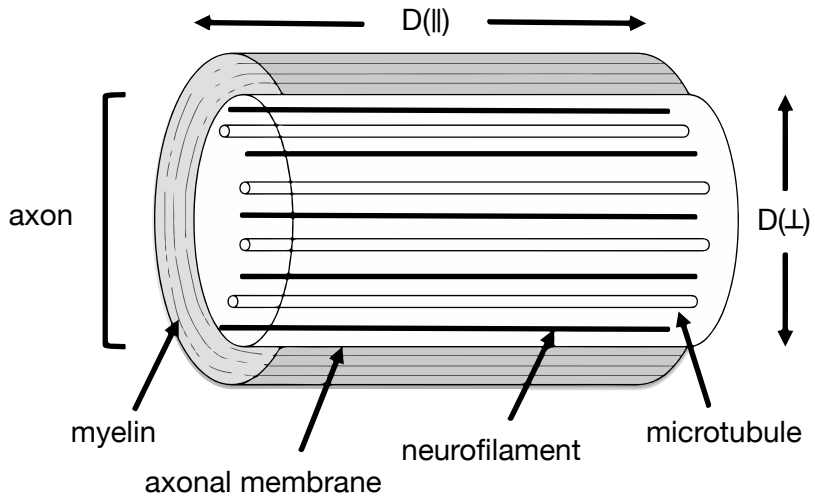

Figure 3 Schematic of the longitudinal view of a myelinated axon

Myelin, microtubules and neurofilaments are all longitudinally-orientated structures that hinder diffusion of water perpendicular to the length of the axon. This would cause the perpendicular diffusion coefficient D(⊥) to be smaller than the parallel diffusion coefficient D(∥). Adapted from Beaulieu 2002, with permission from John Wiley and Sons.

Within a homogenous medium such as water, displacement due to diffusion can be described as 'isotropic'. However, the brain is a heterogeneous organ, with various types of cellular compartments creating barriers to diffusion, and so reducing their mean displacement over time (Beaulieu, 2002). In addition, the organisation of long neuronal axons into tracts within the cerebral white matter preferentially favours diffusion along, rather than across, the length of the axons (Figure 3).

Differential anisotropy within the brain was first demonstrated in the cat brain (Moseley et al., 1990), and has gone on to form the basis for clinical diffusion MRI.

2.2.5.2 Diffusion-weighted imaging (DWI)

A pulsed field gradient spin-echo sequence is commonly used to measure the magnitude of diffusion within the brain (Stejskal and Tanner, 1965), which measures diffusion of water molecules along the direction of diffusion gradient G. The sequence induces diffusion weighting through two pulsed gradients applied on either side of a 180° RF pulse (Figure 4). Static spins will demonstrate the same MR signal following these gradients, as the two pulses will cancel each other out. However, spins that have moved will result in signal loss, allowing the macroscopic diffusion of water in each voxel to be measured. By applying different directions to the diffusion gradients, the direction of water diffusion can be estimated in three-dimensions.

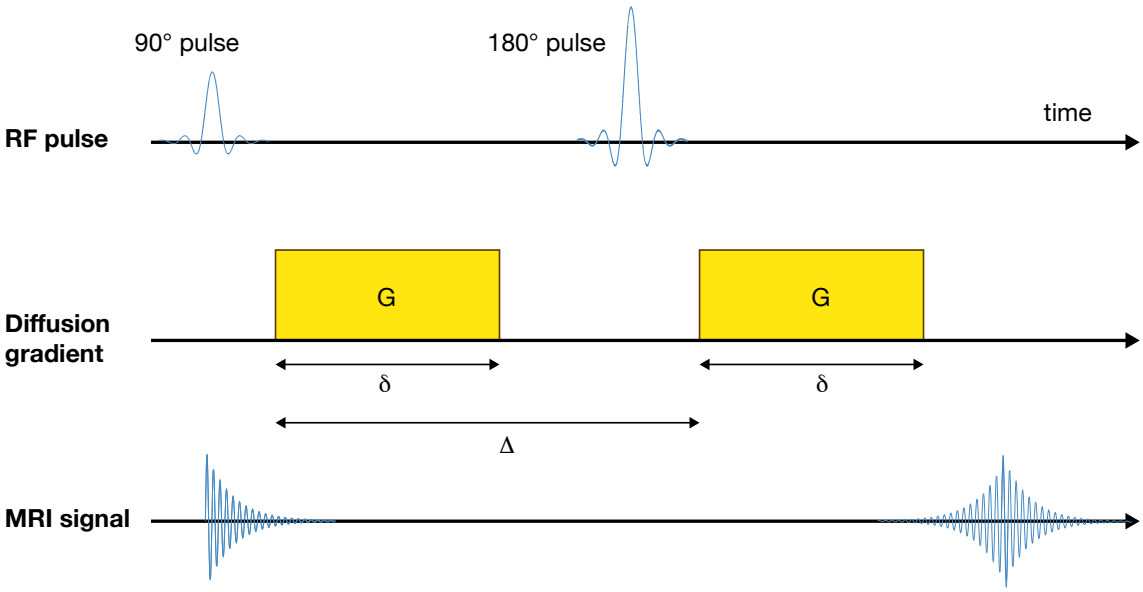

Figure 4 Pulse diagram of the Stejskal-Tanner acquisition sequence for diffusion-weighted imaging
Initially all spins are aligned in a strong magnetic field B0. A 90° RF pulse maps the spins on to the transverse plane. A magnetic field gradient in direction G then causes dephasing of the proton spins. A 180° RF pulse flips the proton spins to the opposite side of the transverse plane. A second diffusion gradient then causes rephrasing of the proton spins. Finally a signal read out at maximal rephrasing occurs – if diffusion has occurred, the proton spins are not completely refocused, resulting in signal loss. δ = Duration of diffusion encoding gradient; Δ = diffusion time interval.

Differences in diffusion signal can be seen across the various structures of the brain. In the cerebrospinal fluid (CSF) of the ventricles, diffusion is unhindered, and hence can be described as isotropic. In contrast, in the white matter, diffusion occurs preferentially along the white matter tracts, resulting in anisotropic diffusion. Signal differences observed between these two areas are not due to differences in the diffusivity of water in each compartment (which is approximately 2.3 x 10 mm^2/s). Instead the *apparent* difference in diffusivity is due to constraints imposed on that water by various cellular barriers in the parenchyma, restricting diffusion, and therefore reducing signal attenuation. The apparent diffusion coefficient (ADC) is commonly used in diffusion MRI to describe the extent of water diffusivity, accounting for impedance due to cellular barriers.

ADC is maximally sensitive to water diffusion occurring in the direction of the applied gradient and is unable to quantify diffusion in a perpendicular axis. This problem is overcome by applying three diffusion gradients (i.e. left-right, anterior-posterior and inferior-superior), and taking an average of the resultant ADC values. Alternatively, through application of several different diffusion-weighted gradient directions, it is possible to calculate rotationally-invariant estimates of tissue diffusivity.

2.2.5.3 Diffusion tensor imaging (DTI)

Diffusion tensor imaging is a sensitive probe of cellular structure that works by measuring the diffusion of water molecules using a Gaussian model. The diffusion tensor D is a symmetric, positive-definitive matrix, meaning that it has 3 orthogonal (mutually perpendicular) eigenvectors, and three positive eigenvalues. This can be used to characterise the anisotropy, magnitude and orientation of the diffusion tensor (Basser et al., 1994). The tensor is represented by a 3 x 3 matrix that describes the diffusion profile in a given voxel, as shown in Equation 2.2:

$$D = \begin{bmatrix} D_{xx} & D_{xy} & D_{xz} \\ D_{xy} & D_{yy} & D_{yz} \\ D_{xz} & D_{yz} & D_{zz} \end{bmatrix} \quad [2.2]$$

where the diagonal elements D_{xx}, D_{yy}, and D_{zz} represent the diffusivity along the three orthogonal axes of the tensor, and the off-diagonal elements describe the correlation between these displacements. Together, the eigenvectors and eigenvalues of the diffusion tensor define an ellipsoid that represents an isosurface of the Gaussian diffusion probability.

The elements of the tensor D are estimated from ADC measurements in a large number of gradient directions. This can be performed if at least 6 diffusion-weighted images are acquired in non-collinear gradient directions, in addition to at least one further image acquired at a different b-value, usually b=0 s/mm^2. As the number of gradients increases, the estimate becomes more robust to noise, and it has been shown that at least 30 unique gradient directions are required to achieve a robust estimation of the tensor (Jones, 2004; Papadakis et al., 2000). For comparison, a diffusion acquisition with 300 directions is used in the microstructural study in Chapter 6.

2.2.5.4 DTI parameters

A number of DTI scalar measures have been introduced from the eigenvalue decomposition that can be used as surrogate measures of underlying tissue microstructure. These measures depend only on the eigenvalues (and not eigenvectors), and hence are rotationally invariant. Commonly used quantitative measures include mean diffusivity (MD), fractional anisotropy (FA), axial diffusivity

(AD), and radial diffusivity (RD), demonstrated in Figure 5. MD is the average ADC across all directions. AD is calculated from the eigenvalue of the principle eigenvector, while RD is the mean ADC in the radial direction (i.e. the plane that is perpendicular to the principle direction). FA is computed from the three principle eigenvalues, and is a measure of the degree of anisotropy of water diffusion. For perfectly isotropic diffusion, FA equals 0, while in the case of a pencil-shaped tensor, FA approaches 1.

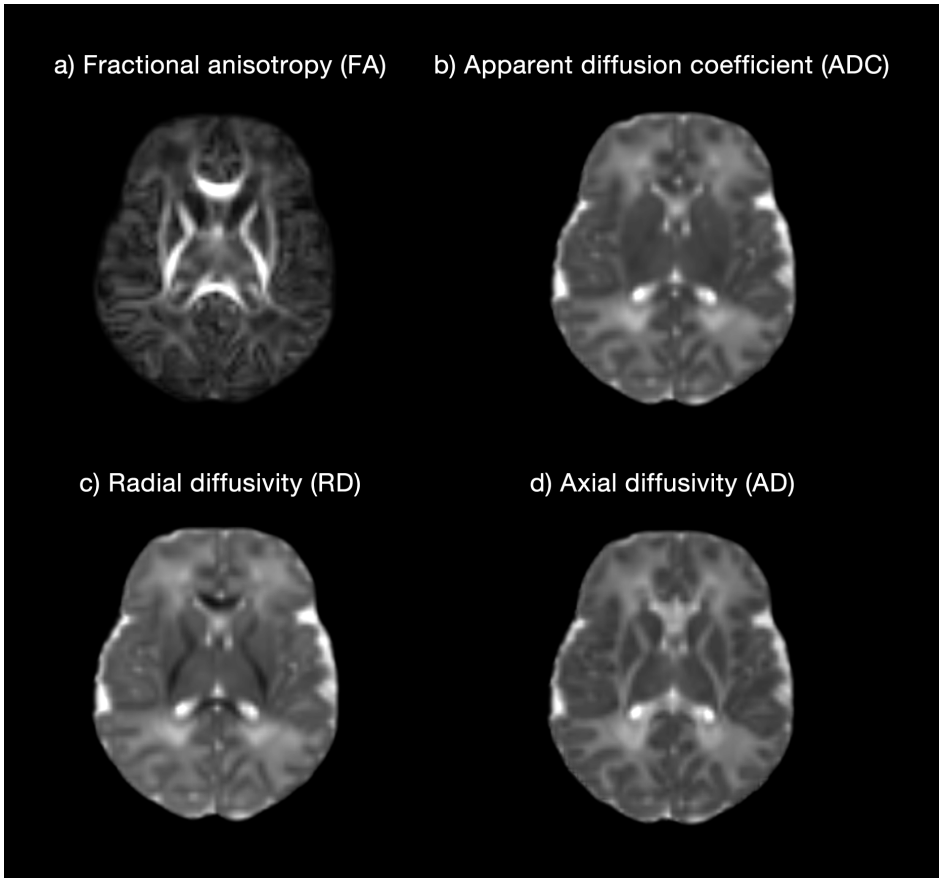

Figure 5 Illustration of common metrics used in diffusion tensor imaging (DTI)
Common diffusion tensor metrics calculated from diffusion-weighted images of a healthy control infant from Chapter 6, born at 38+4 and scanned at 38+5.

2.2.5.5 High angular resolution diffusion imaging

There are a number of limitations of standard DTI. Anisotropy indices based upon DTI are not only a function of microscopic tissue features, but are confounded by orientation dispersion and fibre crossings, both of which are ubiquitous in the brain (Schmahmann and Pandya, 2006). Therefore, it is not possible to confidently attribute changes in signal to intrinsic alterations in tissue microstructure, where they might instead have been caused by variations in the neural circuitry that have altered the neurite orientation distribution. DTI also ignores the presence of multiple tissue

compartments that might include neurones, neuroglia, and extracellular space – each compartmentalises water and may have different signal properties.

A newer set of methods have therefore been developed that are based upon the high angular resolution diffusion imaging (HARDI) acquisition protocol (Tuch et al., 2002). In essence, this consists of measuring the diffusion-weighted signal using a much larger number of uniformly distributed gradient directions than is required for DTI, so as to capture the higher angular frequency features of the diffusion-weighted signal that are not adequately modelled by a single diffusion tensor. In such methods, the *q*-space is sampled on a single shell, with gradients of a fixed *b*-value in equally-distributed directions. High *b* values are used to maximise angular contrast, and acquisition sequences utilise as many directions as time allows. This is commonly around 60, but may be as many as 300, such as for the diffusion acquisition sequence used in this thesis. HARDI acquisitions enable the use of more advanced models than the diffusion tensor, which can better-delineate crossing fibres. It also becomes possible to quantify neurite morphology using more complex microstructural models, discussed in the next section, which require shells at a number of different *b*-values.

2.2.6 Microstructural imaging

It was recognised early in the development of diffusion MRI that it could potentially be used as a probe into neural tissue microstructure (Thomsen et al., 1987). These early findings gave rise to a variety of methods that have attempted to directly relate DWI to tissue microstructure, although such modelling techniques remain controversial and are a hotly-debated topic of research.

Regional variation in ADC was described in human brains as early as 1987, with contrast noted between grey and white matter, and alterations in patients with infarction (Thomsen et al., 1987). Tissue differences were subsequently confirmed in the cat brain, with anisotropic diffusion described in white matter and isotropic diffusion in grey matter (Moseley et al., 1990). Similar findings were reported in the human brain, including anisotropic diffusion in the spinal cord and major fibre tracts in the brain (Hajnal et al., 1991). DTI is now a popular method used clinically for the assessment of pathological changes in brain microstructure. However, as discussed previously, DTI-based anisotropy indices are not only related to microscopic tissue features but are confounded by crossing fibres and orientation dispersion of fibres –

features that are ubiquitous in the brain. It is therefore difficult to understand the origin of an observed signal abnormality with DTI alone.

Compartment models attempt to provide specific measurements including axon diameter and neurite dispersion by decomposing the DWI signal into two or three compartments. Typically, compartments include restricted intra-axonal diffusion, extracellular diffusion, and water trapped in glial cells or membranes. Examples include the two-compartment ball and stick model (Behrens et al., 2003), the composite hindered and restricted model of diffusion (CHARMED) (Assaf and Basser, 2005), and later AxCaliber (Assaf et al., 2008). Criticisms have revolved around model assumptions that are difficult to justify, conclusions that are hard to validate, or practical complexity that makes them unsuitable for clinical practice (e.g. AxCaliber required many diffusion measurements perpendicular to the nerves, which required prior knowledge of the fibre orientation).

2.2.6.1 Modelling fibre dispersion

Early diffusion models assumed that there were one or more fibre populations with parallel axons in each voxel, and so could not accurately represent the widespread regions of fanning or bending fibre bundles in the brain.

A model by Jespersen et al. attempted to capture the distribution of axons and dendrites both in white matter and grey matter (Jespersen et al., 2007). They used a two-compartment model with an isotropic tensor (ball) to represent diffusion in the extracellular space, and cylindrically-symmetric anisotropic tensors to describe intra-axonal diffusion. Model predictions appeared to agree well with ex-vivo experimental data from a monkey brain.

Zhang et al developed a model to estimate axon diameter in the presence of dispersion using a parametric Watson distribution – a cylindrically symmetric directional distribution, characterised by a single concentration parameter (Zhang et al., 2011). This technique could be performed in-vivo using just four *b*-values and multiple gradient directions (4 HARDI shells), due to a reduced number of model parameters.

Zhang's model was simplified in subsequent work to create neurite orientation dispersion and density imaging (NODDI), which was targeted at routine clinical imaging and required only two different *b*-values (Zhang et al., 2012). The model

attempts to recover the neurite orientation dispersion index (ODI) and neurite density index (NDI) by modelling the contribution of signal from three compartments: 1) intra-neurite, represented by sticks following a Watson distribution; 2) extra-neurite, modelled by a cylindrically symmetric tensor; 3) CSF, which has free isotropic diffusion.

While NODDI makes improvements on previous methods, some limitations remain. Due to the use of a single Watson distribution, it cannot model crossing fibres – a feature commonly found in the white matter. By default, it also assumes a fixed intrinsic diffusivity throughout the brain of 1.7 x 10^{-3} mm^2 s^{-1} and across different protocols, which is perhaps unlikely, resulting in an overestimation of free water content in the white matter compared to that known from neuroanatomy studies (Nieuwenhuys et al., 2008). The use of NODDI has been demonstrated in healthy newborn imaging (Kunz et al., 2014), in encephalopathic infants (Kansagra et al., 2016), and longitudinally from infancy through to early childhood (Jelescu et al., 2015). Two neonatal papers report the NODDI parameters used, with both fixing axial diffusivity in the intra-axonal and extra-axonal space to a value of 2 x 10^{-3} mm^2 s^{-1} (Jelescu et al., 2015; Kunz et al., 2014), likely reflecting the higher water content of the neonatal brain compared to an adult (Dobbing and Sands, 1973). Quantitative estimates obtained from microstructural MR imaging studies remain heavily model-dependent, exhibiting biases and limitations that are related to the model assumptions. The ultimate model that achieves an optimum compromise between precision and constraints is yet to be developed.

2.2.7 Phase contrast MR

Phase contrast angiography is a technique that is capable of encoding moving spins' velocity in their phase and can be used to visualise moving fluid such as blood. Spins moving along a magnetic field gradient develop a phase shift that is proportional to their velocity. Bipolar gradients (two gradients in opposite directions but with equal magnitude) are applied to encode the velocity of the moving spins. Spins that are stationary will experience two equal and opposite changes in phase, resulting in no net change. Moving spins will experience two different gradients of different magnitude due to their different spatial position between each pulse, resulting in a net phase shift that is proportional to their velocity. Therefore, by measuring changes in phase, the velocity of the spins can be computed.

Bipolar gradients were originally applied along only one anatomic axis at a time, in order to provide flow sensitivity in that particular direction. However, by using flow-encoding gradients along two or more axes simultaneously, it is possible to measure flow sensitivity along any arbitrary direction. This is the basis for phase contrast flow measurements that are most commonly used in cardiovascular imaging.

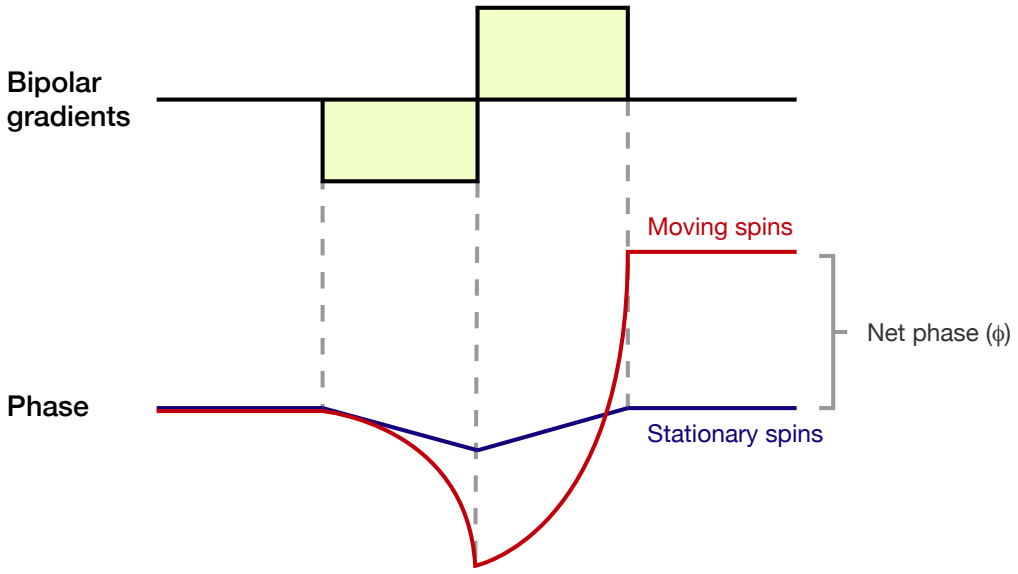

Figure 6 The effect of bipolar phase-encoding gradients in phase contrast angiography (PCA)
The net phase gain is zero for stationary spins (blue) but positive for spins that are moving in the direction of the gradients (red).

The sequence's sensitivity to slow or fast flows is determined by the amplitude, duration and spacing of the bipolar gradients. These are controlled by a parameter called velocity encoding (v_{enc}), which is critical to the performance of the study, and hence needs to be carefully chosen beforehand.

As velocity is encoded in the spin's phase, the measured velocity exhibits some particular characteristics. Phase measurements that vary by n*2π, where n is an integer, will be mapped back (or 'aliased') to the -π to π interval. Velocity measurements are therefore constrained to -v_{enc} to v_{enc}, where v_{enc} corresponds to a phase difference of π. Blood velocities that are higher than the v_{enc} parameter will be misrepresented in the final image, due to being incorrectly assigned back to the -v_{enc} to v_{enc} interval, resulting in 'velocity aliasing'. This can be avoided by picking a value for v_{enc} that encompasses the expected range of velocities in the image.

Data acquired using a phase contrast technique can be processed to obtain phase difference and magnitude images (Figure 7). In phase difference images, the signal obtained is proportional to the velocity of the spins moving along the direction of the gradient. Spins moving in one direction are given a bright signal (white), while spins moving in the opposite direction are assigned a dark (black) signal. Flow can then be inferred from a product of the average flow velocity and the cross-sectional area of the vessel.

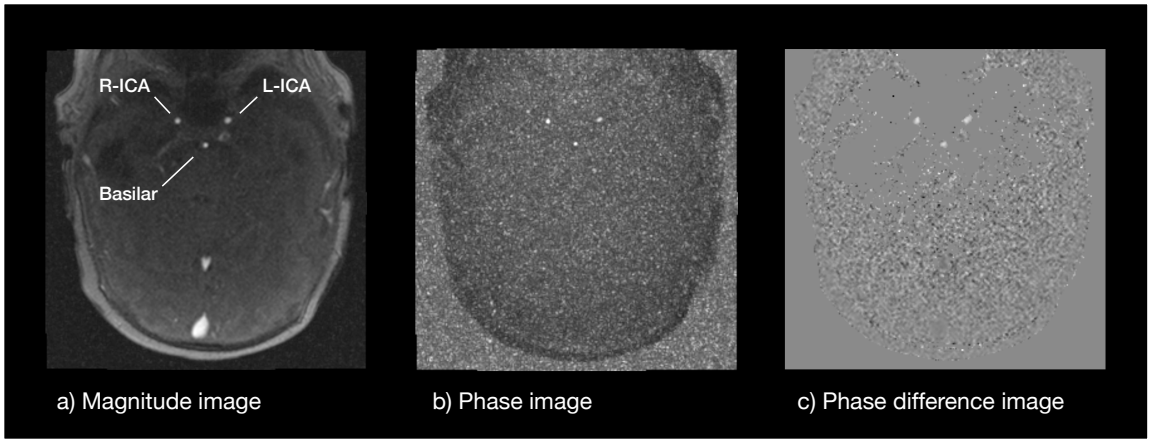

Figure 7 Transverse phase contrast angiography of the neonatal cerebral vessels
a) Magnitude image from PCA acquired in a term infant in a plane perpendicular to both internal carotid and basilar arteries, at the level of the sphenoid bone. R-ICA = right internal carotid; L-ICA = left internal carotid. b) Phase image, where bright voxels indicate flow towards the head (positive velocity). c) Phase difference image where bright voxels indicate flow towards the head.

Measurement accuracy is retained even if the measurement plane is not perfectly perpendicular to the velocity of blood flow, but instead deviated by a small angle β. An angulated plane results in alterations to both the velocity measurement and also the cross-sectional area. Blood velocity v will be underestimated, as $v * \cos \beta$ will be measured instead (Figure 8). Conversely, the cross-sectional area will be overestimated by a factor of $1/\cos \beta$, due to the oblique slice through the tubular vessel (Figure 8). These two effects cancel out each other to the first order. However, as the slice has a non-zero thickness, the angulated slice will suffer from more severe partial volume effects, resulting in decreased accuracy of flow measurements, as is outlined in the following section.

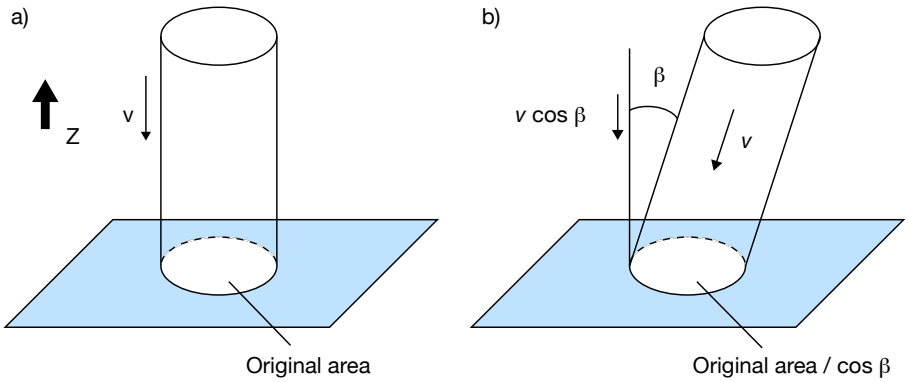

Figure 8 The effect of measuring flow through a vessel at an oblique angle (β) to the direction of flow (*v*) using phase contrast angiography

Illustration of the effect of introducing an angle β between the direction of flow (*v*) and the flow measurement direction (Z). While blood velocity will be underestimated, cross sectional area will be overestimated. Both effects cancel each other out. Figure adapted from (Bernstein et al., 2004).

2.2.7.1 Random error in flow estimation using PCA

The random error in PCA can be computed from the error in the phase images that are used to calculate flow velocity and is inversely related to the signal-to-noise ratio (SNR) of the magnitude image. Regions with very low signal intensity in the magnitude images, such as air and bone, will therefore result in very high uncertainty for phase measurement. The marked imprecision of phase measurements in these areas can be seen by the speckled pattern in Figure 7b.

The variance of the error in velocity measurement is proportional to the velocity encoding (v_{enc}) parameter mentioned earlier, and so a lower v_{enc} will help to minimise this variance. For this reason, v_{enc} should be set carefully to the lowest possible level that will not lead to velocity aliasing as discussed previously.

2.2.7.2 Systematic error in flow estimation using PCA

There are a number of different types of systematic error in PCA flow measurements, which are described in detail elsewhere (Bakker et al., 1999; Wolf et al., 1993). As a brief summary, the primary sources of systematic error include:

a. **Intravoxel phase dispersion** – the signal magnitude can be significantly reduced by intravoxel dephasing, caused in particular by turbulent flow. This is often caused by stenotic or otherwise diseased arteries, which is not a factor that is commonly a problem in newborn imaging. This source of error can be minimised by using a low echo time.

b. **Partial volume effects** – flow measures in a vessel are inferred by a product of measured velocity and cross-sectional area. In the middle of a vessel, it is possible to be confident that the contents of the voxel in question is exclusively blood. However, at the peripheries of the vessel, a number of voxels may contain both blood and static vessel wall tissue. The degree to which this causes error depends on both the in-plane resolution and the diameter of the vessel. While there are other techniques including approximating the fraction of blood in the voxel, the most effective way to reduce the impact of partial volume effects is to increase the in-plane resolution. Previous studies have suggested that the minimum number of voxels required to make this error negligible is most commonly 16 voxels/vessel area (Bakker et al., 1999, 1995), although another study found good agreement between PCA and Doppler ultrasound measurements in a canine femoral artery with only 3 voxels/vessel area (Hofman et al., 1995). In the experiments in this thesis, each cerebral vessel of interest contained approximately 20 – 30 voxels/vessel area.
c. **Vessel angulation** – as discussed previously, if the velocity-encoding direction is at an angle to the direction of flow, the number of voxels affected by partial volume effects increases. The most effective way to reduce this error is to increase resolution both the in-plane resolution and slice thickness. Gradient moment nulling can also be used to minimise the effect of flow perpendicular to the velocity-encoding direction. The PCA sequence used in this thesis employed both approaches to reduce the effects of vessel angulation, along with careful (and exhaustive) adjustments to the placement of the acquisition plane to achieve the best results.
d. **Phase introduced by eddy currents** – eddy currents are known to introduce artefacts in phase imaging, although in modern scanners, this error should be negligible.

2.2.7.3 Cardiac synchronisation

In order to calculate average flow measurements across the cardiac cycle, the MR acquisition requires synchronisation with the cardiac cycle. Imaging is performed alongside an electrocardiogram (ECG), and the R-R interval is used as an easy way to measure the interval between QRS complexes.

The most efficient way of performing synchronisation for PCA is retrospective gating, whereby data is continuously acquired along with an ECG recording of the subject's cardiac cycle. MRI data is labelled with the duration since the most recent R wave, which marks the beginning of systole. The cardiac cycle is then divided into segments, or 'phases', and multiple measurements of repeated cardiac cycles can be accumulated in order to acquire data with acceptable levels of signal across time.

2.3 NEONATAL MRI CONSIDERATIONS

MRI is a relatively new and evolving technology – the first human scans were performed in the late 1970s (Brant Zawadzki et al., 1983), and the first neonatal brain scans followed shortly after in the early 1980s (Johnson et al., 1983). Since then, the typical magnetic field strength used in clinical scanners has increased from approximately 0.15 Tesla to 1.5 - 3 Tesla, making higher resolution imaging possible, which is particularly important for the small anatomical structures in the neonatal brain. Performing MRI scans in neonates can be technically challenging for a number of reasons:

a) **Size** – the average brain volume of a term newborn is in the range of 200-600 millilitres, in contrast to an average adult brain volume of greater than 1 litre (Allen et al., 2002; Makropoulos et al., 2016; Orasanu et al., 2014). To clearly delineate the smaller neonatal structures, the use of higher spatial resolution is required;
b) **Movement** – motion corruption can lead to unusable images. Babies are unable to follow instructions to lie still, and the combination of a noisy machine and unfamiliar environment can make it difficult to remain asleep;
c) **Physiology** – higher resting heart rates and respiratory rates in neonates require careful adaptation of cardiac and flow-based imaging;
d) **Biological differences** – the immature brain has a higher water content with immature myelination of the white matter compared to adults, resulting in the inversion of MRI contrast when compared to adult brain scans (Prastawa et al., 2005). These differences require careful optimisation of MR sequences for the neonatal brain, and also explain the use of T2-weighted rather than T1-weighted imaging to be most commonly used for image processing in neonatal subjects.

Scans acquired as part of this thesis used novel image acquisition and reconstruction techniques, and imaging hardware that had been designed specifically for neonatal imaging, as part of the Developing Human Connectome Project (Hughes et al., 2017b).

The resulting Neonatal Brain Imaging System (NBIS) brought together a number of innovations to improve the scanning procedure for neonates (Figure 9). A dedicated 32-channel receive array coil and positioning device allows placement of the infant's

head deep into the coil, to maximise the signal-to-noise ratio (Hughes et al., 2017b; Keil et al., 2011), enabling faster imaging at higher resolution. Disturbance to the infant is minimised by using a custom-designed MRI-compatible trolley to transport the settled infant and shell to the scanner for swift transfer onto the scanning bed.

Sequences were optimised for neonatal scanning. To avoid startling the infant, a slow ramp-up in scanner noise was employed. Synthetic coil noise was used to fill in the usual gaps in gradient noise, in order to create continuous gradient sound while scanning. To work within time restraints (scan times greater than 60 minutes become difficult in natural sleep), multiband acquisitions were used for structural and diffusion imaging in order to acquire the greatest amount of data in the shortest possible time.

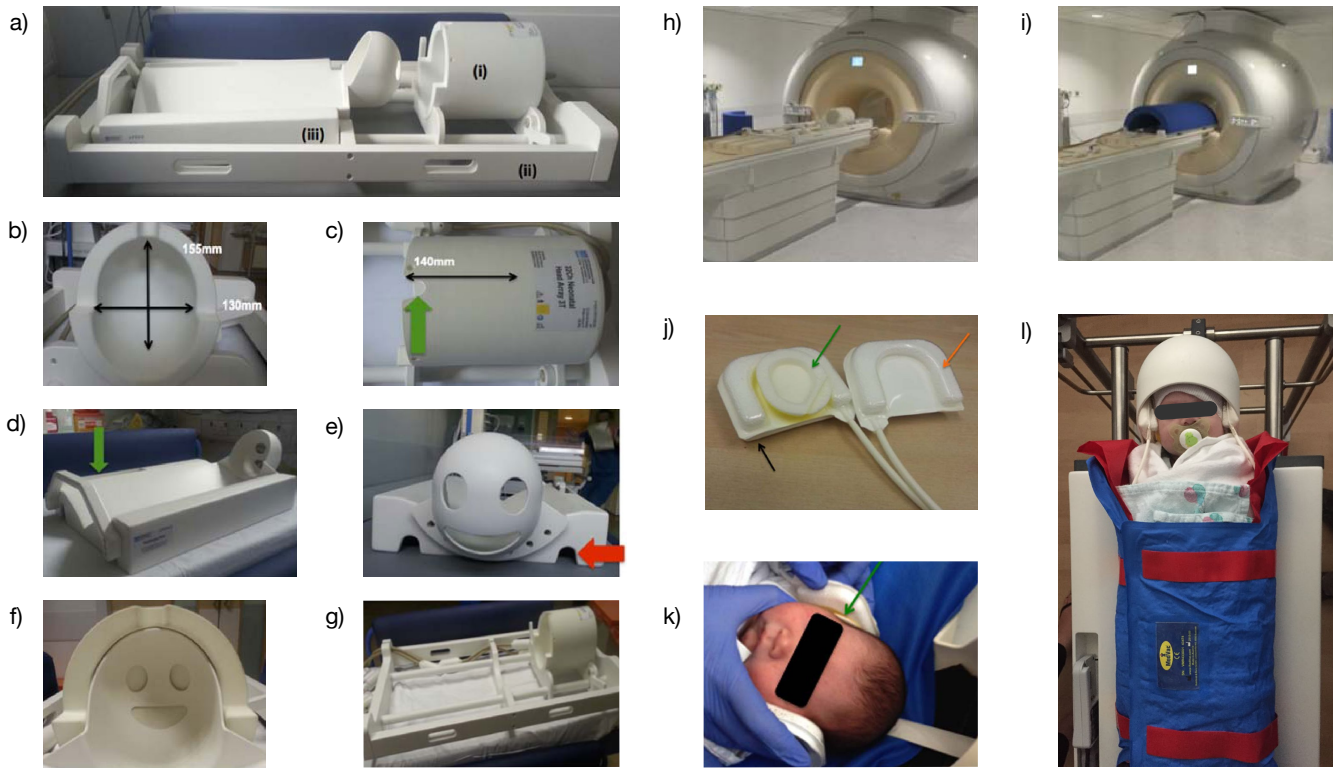

Figure 9 Demonstration of the neonatal brain imaging system (NBIS)

The system consists of three main components: the neonatal head coil (**a**,i), the frame (**a**,ii) and the positioning shell (**a**,iii). The coil is shown from the end view (**b**) and top view (**c**), where the black arrow denotes the inferior-superior length of the coil, and the green arrow indicates a 2 cm gap for respiratory aids. Positioning shell, consisting of a v-shaped base and round headpiece, with pocket for saturation monitor (**d**). The base has a groove to allow it to be placed securely on the rails of the frame (**e**, red arrow). The headpiece has three openings to allow manipulation and visualisation of the infant's position (**e**, **f**). The distance between headpiece and coil is <5 mm to maximise SNR. (**h**) shows a view of the system on the scanner table top, and (**i**) with an acoustic hood in situ, to block out additional scanner noise. Specially-designed positioning and immobilisation devices consist of bead-filled cushions (**j**, orange arrow) backed by an inflatable air cushion (**j**, black arrow), and sit over the top of the ear muffs (**j, k**, green arrow). (**l**) shows a study infant asleep in the shell, and ready for a scan. Adapted from Hughes et al., 2017.

Retrospective motion correction techniques can be employed to acquire optimal images in this population (Cordero-Grande et al., 2018). Traditionally, MR imaging has been exquisitely motion sensitive, often requiring oral sedation to achieve acceptable images in neonatal subjects. In our potentially-unstable population, parents and clinicians are understandably keen to avoid unnecessary use of sedation. Motion correction techniques now enable us to tolerate a baby's natural head movement within the scanner, obtaining structural images (L Cordero-Grande et al., 2016) and diffusion-weighted images (Christiaens et al., 2018) with significantly reduced motion artefact.

2.4 ANALYSIS OF MRI DATA

Analysis of MRI data in this thesis was performed using a variety of image analysis techniques that I will introduce in the following section. Detailed methods for each study are provided in each experimental chapter.

2.4.1 Image registration

Group imaging studies rely on our ability to quantify differences between subjects, ideally using objective methods that provide robust, precise and reproducible measurements.

Image registration is a fundamental part of a great variety of biomedical imaging applications (Toga and Thompson, 2001), and provides the ability to geometrically align one dataset with another. Registration is a prerequisite technique for any imaging study that aims to compare datasets across subjects, imaging modality, or across time. It also allows the creation of a group atlas, which acts as a reference system in which a group of brain images can be compared for statistical analysis.

In general, the process of image registration can be split into three components:

a) **Transformation** – estimating the mapping between the source (the image that will be transformed, or the 'moving' image) and a reference image (the 'target' image). This can be a linear or non-linear process, depending on the application and algorithm used.
b) **Similarity measurement** – assessing the similarity between the transformed source image and the target image. Similarity can be defined in terms of geometric or intensity-based correspondence (Hajnal et al., 2001), and

typically works by identifying reliable anatomically-consistent landmarks (Bookstein, 1989) or by using anatomical surfaces such as ventricular borders or cortical surfaces (Thompson and Toga, 1996). Similarity metrics include cross correlation (CC), which is best for intra-modal registration (Hill et al., 2001) and mutual information (MI), which is suitable for performing registrations between different image modalities (Pluim et al., 2003).

c) **Optimisation** – identifying the global minimum or maximum of the similarity function, implying that the registration has achieved the best fit possible – for example, maximising MI. A common approach is to perform the registration in a multi-resolution fashion, starting with images that have been downsampled to a lower resolution and increasing gradually to higher resolution to fine-tune (Jenkinson and Smith, 2001; Rueckert et al., 1999; Woods et al., 1993). The advantage with this approach is that the registration can be initialised quickly at coarse resolution and improved through several resolution levels to finish with the finer anatomical detail.

Image registration algorithms aim to maximise the similarity between the source and target image by optimising the parameters of the transformation algorithm in between. There are a number of algorithms now available, but they broadly fit into two categories: linear ('rigid' and 'affine') and non-linear.

Linear transformations can account for global differences in size and shape between two images. For example, a rigid-body transformation includes 6 degrees of freedom (3 rotations and 3 translations) and is generally used for within-subject registration. An affine transformation includes 12 degrees of freedom (3 rotations, 3 translations, 3 scalings, 3 skews/shears), and is often used to initialise non-linear registration. Non-linear registration can additionally model local variations in anatomy. The non-linear transformation is usually described by a three-dimensional deformation-field (also called a "displacement-field") that contains information on how each voxel in the subject volume should be warped to reach the target space. Non-linear deformations can be controlled by varying parameters including the number of degrees of freedom (fewer results in a smoother warp), warp resolution (lower results in a smoother warp) and a regularisation term (higher regularisation results in a smoother warp).

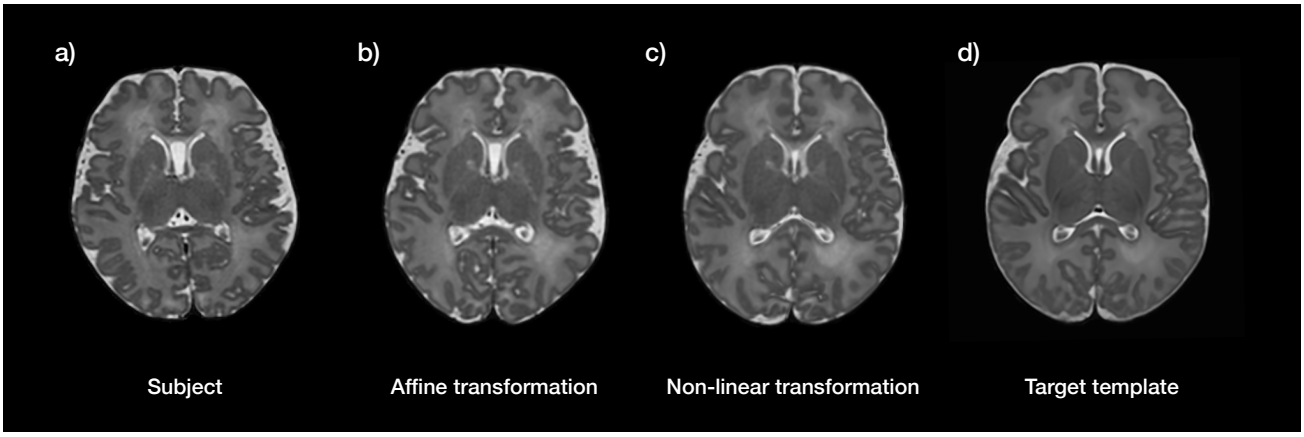

Figure 10 Image registration between a subject source and target template image.
A source image from a single subject (**a**) is aligned to a target template (**d**) through the combination of an affine transformation (**b**) and non-linear transformation (**c**). The subject (**a**) is an infant with coarctation of the aorta, born at 37+3 weeks and scanned at 38+3 weeks. The target (**d**) is a population-average atlas created from a group of 10 infants with and 10 infants without CHD, generated using ANTs (B. B. Avants et al., 2008), and discussed in further detail in Chapter 4.

An example of a subject being registered to template can be viewed in Figure 10, whereby the subject first undergoes an affine transformation to rotate, scale and translate the image into template space (Figure 10b). A non-linear transformation then warps local tissue differences to provide accurate correspondence between subject and template (Figure 10c).

For the studies in this thesis, non-linear image registration between MR images is performed using Advanced Normalisation Tools (ANTs) (B. B. Avants et al., 2008). The symmetric image normalisation (SyN) algorithm that is implemented as part of ANTs was originally developed for the analysis of neurodegenerative brain disorders like dementia and Alzheimer's disease. It is naturally suited to our neonatal population, who are experiencing similarly dramatic changes in brain morphology, albeit in reverse, and it has been shown to perform consistently in brain registration evaluations with high accuracy across subjects (Klein et al., 2009).

2.4.2 Structural MRI analysis

Morphometric analysis of brain MR images is widely used in research studies to quantify alterations in shape and volume of tissue. In this thesis, quantitative analysis of structural MRI data was performed using both tissue segmentation and geometric surface-based methods.

2.4.2.1 Segmentation

Segmentation in brain MRI describes the process of partitioning an image into different regions of interest, according to intensity or anatomical characteristics. Segmentation is complicated by the fact that different brain structures often share similar intensity characteristics. Therefore, *a priori* information is generally required to guide the segmentation algorithm as to the expected location of the structures of interest. The most common way to supply this information to the algorithm is through the use of predefined rules or encoded in the form of atlases.

Segmentation of neonatal brain MR images is widely considered to be a more challenging task than adult brain segmentation. This is due to the greater effect of partial volume between cerebral spinal fluid (CSF) and white matter, a lower contrast-to-noise ratio compared to the adult brain, reduced contrast between grey and white matter, and the large changes in appearance that occur from preterm to term age.

For all experiments in this thesis, we used a segmentation pipeline that has been created and optimised for our acquisitions (Makropoulos et al., 2018, 2016, 2014), which is based on the Expectation–Maximisation (EM) algorithm (Van Leemput et al., 1999). Full technical details of the pipeline are available elsewhere (Makropoulos et al., 2018), and a schematic version is displayed in Figure 11.

To summarise the process, the segmentation pipeline begins with motion-corrected T2-weighted images being skull-stripped using the FSL Brain Extraction Tool (BET) (Smith, 2002), and corrected for intensity inhomogeneity using the N4 algorithm (Tustison et al., 2010). A spatiotemporal neonatal atlas is then registered to the subject's image, and tissue probabilities are propagated to the subject space. Atlas priors are combined with subject-specific tissue priors (obtained using *k*-means) to allow a robust initialisation of the expectation maximisation (EM) algorithm (Van Leemput et al., 1999). An updated form of the original EM algorithm is utilised, with modifications including: a) the spatial proximity of brain structures modelled using a Markov Random Field (MRF) regularisation term; b) a prior relaxation scheme used to account for the large potential anatomical variability in neonatal subjects; c) mislabelled white matter voxels at the CSF-cortical grey matter interface corrected with connected component labelling and knowledge-based rules, d) another partial volume correction implemented for CSF-white matter boundary.

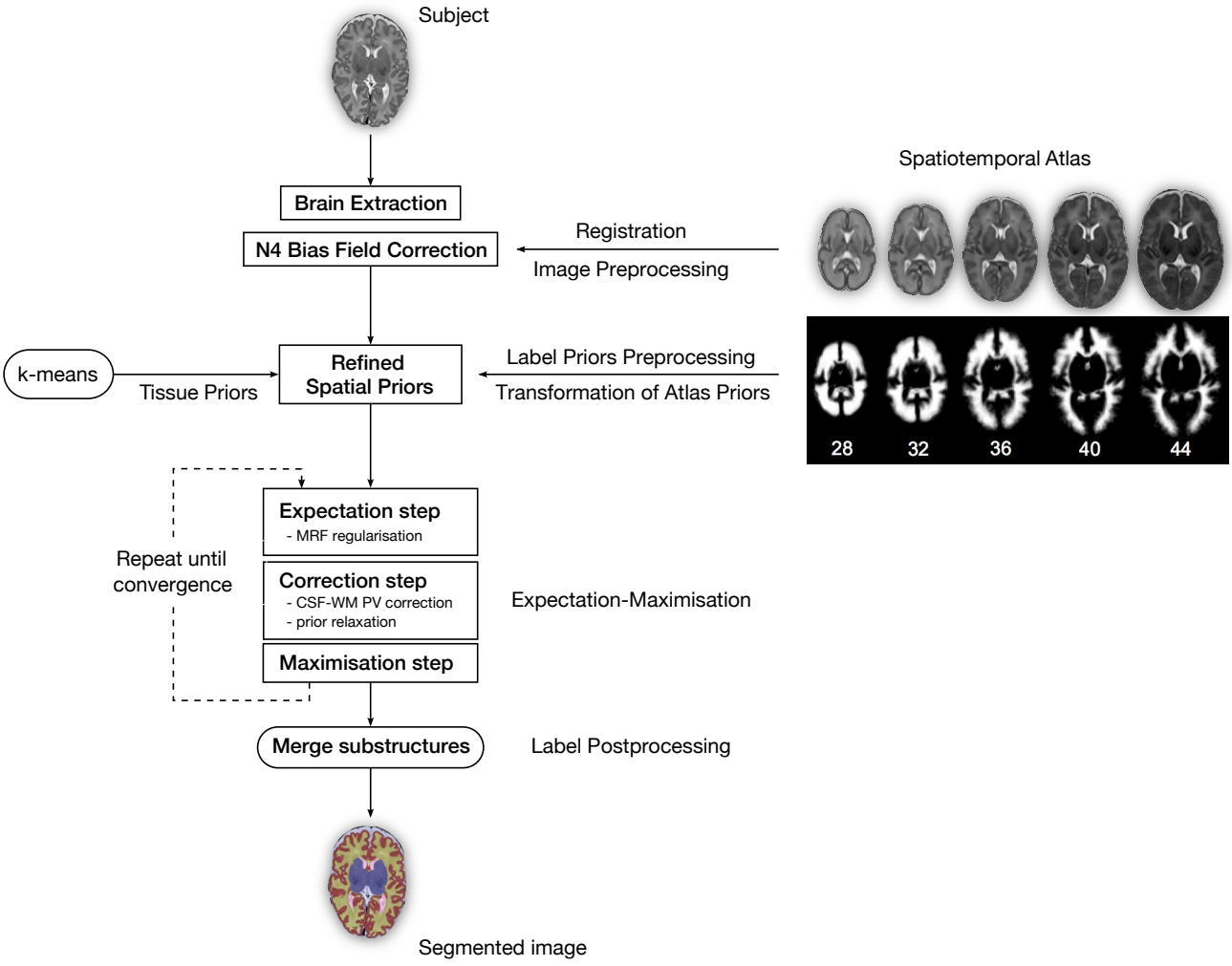

Figure 11 Outline of the tissue segmentation pipeline

The subject's T2-weighted image is brain-extracted and N4 bias field corrected. Atlas priors are propagated and combined with the subject-specific tissue priors. The EM algorithm is initialised with the combined tissue priors and results in the final labelling step. Adapted from Makropoulos et al., 2014. © 2014 IEEE.

2.4.2.2 Geometric surface-based analysis

The geometric shape of brain tissue can be of particular interest in certain patient groups. Gyrification index describes the complexity of cortical folding, and has been used to describe human brain development in a two-dimensional manner since the 1980s (Armstrong et al., 1995; Zilles et al., 1988). To perform this analysis in three-dimensions using a structural MR image, it is first necessary to extract the cortical surface from the scalar MRI volume as a geometric mesh.

Differences in image properties obtained from adult and neonatal brains considerably limits the translation of adult image processing methods to neonatal subjects. In particular, the popular surface analysis framework FreeSurfer (Fischl, 2012) fails when

used on neonatal data, as it relies solely on fitting surfaces to intensity-based tissue segmentation masks (Dale et al., 1999). Adult MRI data have significantly different image intensity distributions to neonatal data, which also vary significantly with gestation. For this reason, it was necessary to develop a custom neonatal surface analysis pipeline (Makropoulos et al., 2018).

The workflow of the surface reconstruction processing pipeline is summarised in Figure 13. The subject's motion-corrected T2-weighted MR image is first bias corrected (Tustison et al., 2010) and the brain is extracted (Smith, 2002). The brain is then segmented into different tissue types using the segmentation framework discussed earlier (Figure 11).

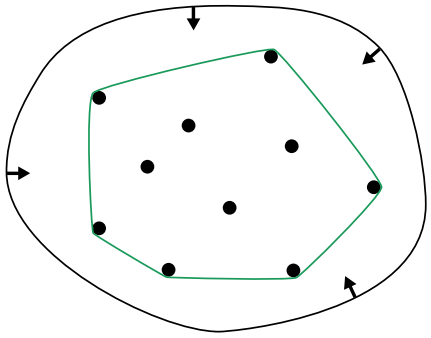

Figure 12 A convex hull – the elastic band analogy
The convex hull is the smallest convex set X of points in a Euclidean plane or space that contains X. For a two-dimensional plane, it is like stretching an elastic band so that it surrounds the entire set X and then releasing it, allowing it to contract around the points. When taut, it encloses the convex hull of X.

Once segmentation is completed, the white matter surface mesh is created first by fitting a closed, genus-0 (no holes), triangulated surface mesh (convex hull, Figure 12) onto the inferred white-matter segmentation boundary. Tissue intensity information from the structural image is used to refine the shape of the mesh to regularise for the effects of partial volume and help avoid incorrect assignment of CSF voxels to either the grey or white matter. The pial surface is then created by deforming the white matter surface mesh towards the grey matter-CSF boundary, by searching for the closest cortical grey matter-CSF image edge outside of the white matter mesh. Full details of the surface reconstruction process have been published previously (Schuh et al., 2017).

The pial surface is required for the calculation of the gyrification index (GI), which is used in Chapter 5 as a measure of cortical folding complexity. The GI is defined as the ratio of the surface area of the pial surface to the surface area of the superficial enclosing surface, where the superficial surface is reconstructed using marching cubes from the morphological closed combined cortical grey matter/white matter mask. Further details of this process are discussed in Chapter 5.

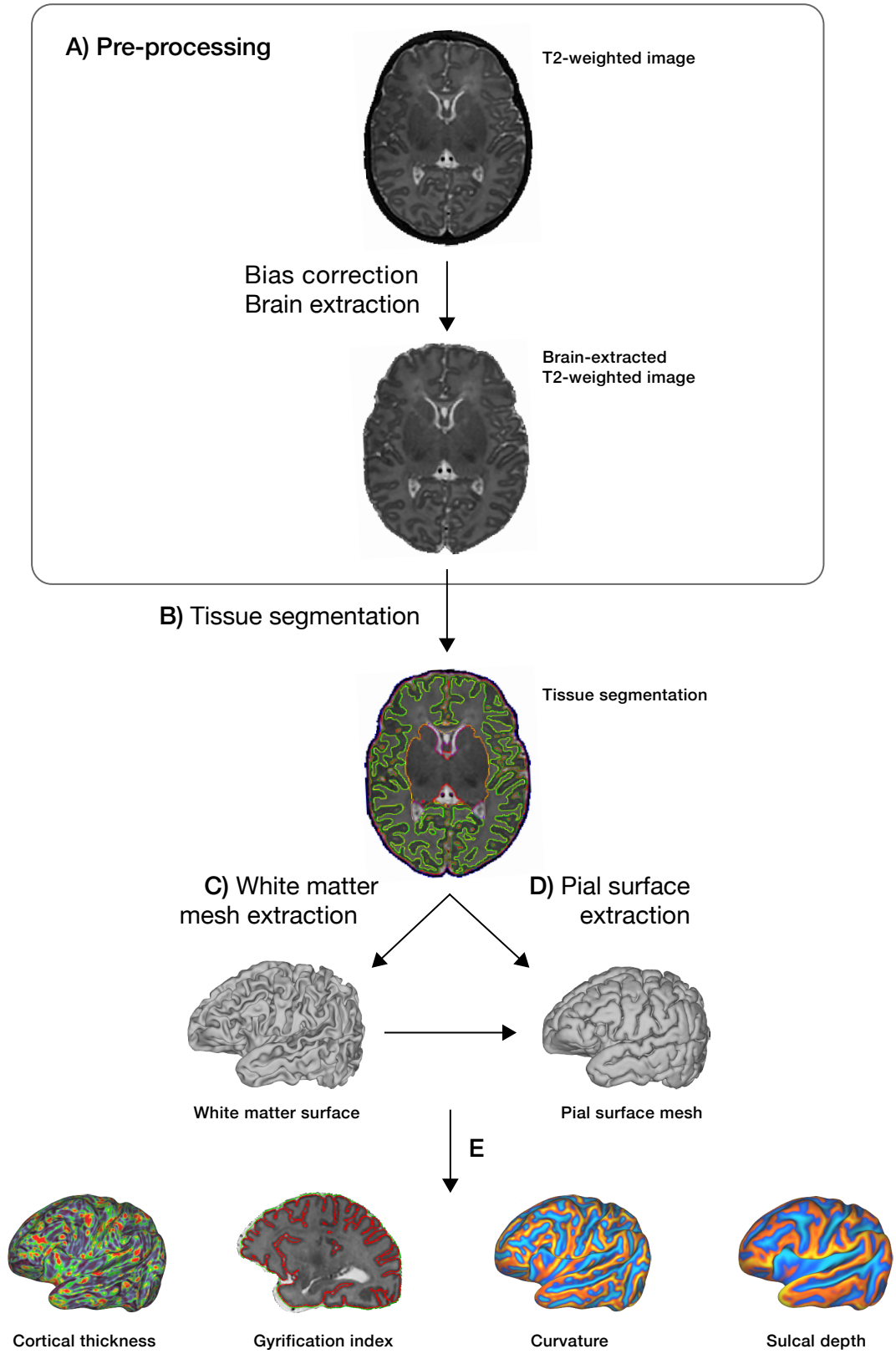

Figure 13 Outline of the surface reconstruction pipeline

Steps include: **A**) pre-processing, including brain extraction and N4 correction; **B**) tissue segmentation (output displayed here as a contour map); **C**) white matter mesh extraction; **D**) expansion of white matter surface to fit the pial surface; **E**) generation of quantitative measures including cortical thickness, curvature, sulcal depth and gyrification index.

2.4.3 Diffusion MRI analysis

Once data has been pre-processed and scalar maps generated using diffusion tensor fitting or another biophysical modelling technique such as NODDI, there are a number of approaches available to perform group-wise comparison studies. In this section, I will consider three common methods: region of interest (ROI), histogram, and voxel-based analysis.

2.4.3.1 Region of interest analysis

This is a simple and intuitive method that involves delineation of a specific region of the brain across different subjects and extracting a summary measure of interest (i.e. mean) from the voxels within it (Mukherjee et al., 2002). An ROI can typically be either outlined and positioned manually on a subject's image or positioned automatically using a segmentation algorithm.

There are many pitfalls associated with an ROI-based approach. Manual placement requires expert knowledge to place the ROI accurately and is highly operator dependent, and so requires inter-/intra-operator reproducibility to be demonstrated as part of any study using this method. Equally, if ROIs are defined manually and directly on the parameter map of interest (e.g. FA), the intensity of the map may wrongly influence the choice of drawn boundary. For example, if a subject's FA map demonstrates higher anisotropy in a particular region, a human rater may be biased to wrongly exclude voxels that should have been within the ROI, with the result of reducing true group differences. To avoid this problem, it is recommended to define ROIs on structural images, or use a b0 map with the same susceptibility-induced distortions as the diffusion-weighted images, but with contrast that is independent of diffusion (Jones and Cercignani, 2010).

2.4.3.2 Histogram analysis

Histogram analysis is another popular method for analysing quantitative MR images between groups. The histogram displays a graph of frequency distribution, showing the proportion of voxels within a certain range of values for a particular parametric map (e.g. FA). The shape of the histogram can be summarised using numerical features, and statistical comparison can be performed between a case and control group of subjects. This is commonly performed across the whole brain, and therefore determines global effects. It can also be performed for regions of interest.

Histogram analysis is also prone to various biases. CSF contamination is a key bias that is common in diffusion-weighted images as the resolution is often low resulting in potentially large partial volume effects. Registration to structural space can be difficult due to geometric distortions. Partial volume effects with CSF may be more substantial if one group of subjects has more atrophic brains than the other (e.g. preterm at term vs term, or CHD vs healthy). This could result in brain volume/morphometry having an undefined and erroneous contribution to differences in diffusion parametric maps.

2.4.3.3 Voxel-based analysis

Voxel-based analysis is becoming increasingly popular for comparing diffusion MR images between two or more groups of subjects to assess the association of diffusion parameters and clinical variables. Voxel-based methods are popular as they are generally highly automated and require minimal intervention from the user, reducing the effect of inter-/intra-observer variability. These methods rely on accurate co-alignment of subject data in order to achieve reliable correspondence from voxel coordinates to the same anatomical structure of each subject within the study. Voxel-based analyses are performed across the brain, removing the need for an *a priori* hypothesis and region of interest selection.

There are various potential sources of bias in voxel-based analyses. Registration is more challenging with diffusion-weighted images, and there is choice about which image should be used to drive the registration. Using the b0 image is one option, although limited contrast may result in poor alignment. This is a concern as local misalignment could easily be interpreted as a signal change (Jones and Cercignani, 2010). For white matter analysis, this source of error can be minimised by using an FA map to drive registration, or by using directionality information encoded within the diffusion tensor to more accurately align white matter tracts (Guimond et al., 2002; Zhang et al., 2006).

Pipelines to achieve voxel-based analysis have many sequential steps, and choices made at each stage of the processing pipeline can have a significant influence on the statistical outcome. Such choices include degree of non-linear warping and amount of regularisation, choice of smoothing kernel and width, choice of statistical analysis method, and how to correct for multiple comparisons. Putting these multiple choices together in a compounding chain means that it is perhaps unsurprising that one study

found that when the same dataset was sent out to nine different research labs, they found nine different plausible results with minimal overlap (Jones et al., 2007).

2.4.3.4 Tract-based spatial statistics

Tract-based spatial statistics (TBSS) is a tool introduced as part of the FSL suite to aim to make voxel-based analyses more consistent and reliable (Smith et al., 2006). TBSS is not dependent on precise spatial alignment. It achieves this by introducing a novel step into the analysis pipeline that projects subject data onto an alignment-invariant tract representation called the 'skeleton'. For white matter, the projection is achieved by searching perpendicular to the skeleton for the maximum value in the FA image, which is assumed to represent the centre of the subject's white matter tract in that region. The selected voxel is then projected back to the corresponding point on the skeleton (Figure 14). This method of projection removes the need for smoothing and increases the statistical power of the method by reducing the number of voxels that require correction for multiple comparisons.

As with all other voxel-based methods of analysis, TBSS relies on robust registration of subject images to a common space. This can be challenging when anatomy is distorted due to pathologies or differing gestational age at scan. In this thesis, the initial steps of the traditional TBSS pipeline have been replaced with a registration method using Advanced Normalization Tools (ANTs) (B. B. Avants et al., 2008) to align each subject's structural T2-weighted images that have been co-registered to the diffusion-weighted maps, for more accurate spatial alignment of the cortex. In

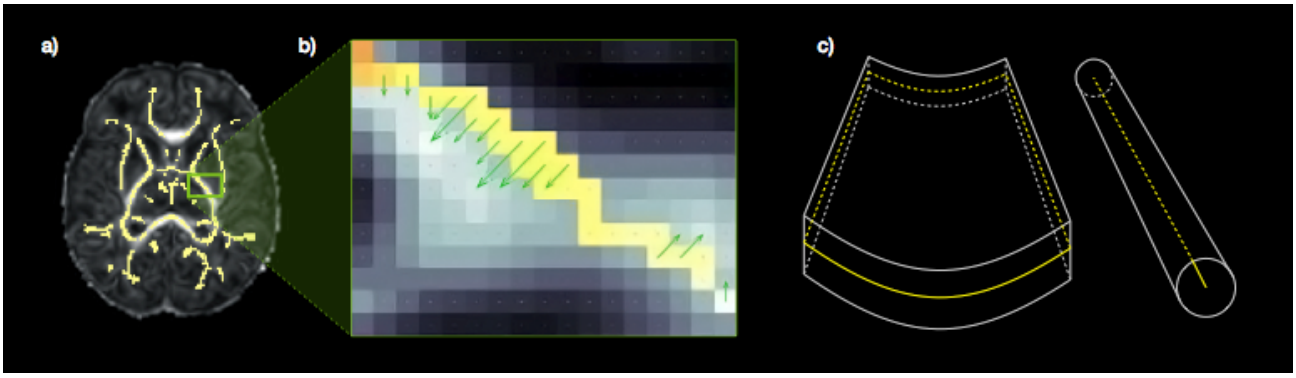

Figure 14 The use of a mean skeleton for tract-based spatial statistics (TBSS) in the white matter and projection of subject data into a common space.

A skeleton (shown in yellow) is generated from either an FA skeleton for white matter analysis (**a**) or a cortical map for grey matter analysis. The skeleton consists of either a "thick sheet" with a thin surface as its skeleton (**c**, left) or a "tube" with a line as its skeleton (**c**, right). Before analysis, individual subject's data is projected (**b**, green arrows) onto an alignment-invariant tract representation (the "mean skeleton" shown in yellow) in a way that is not dependent on perfect non-linear registration (**b**).

addition, the white matter methodology has been adapted for grey matter analysis, by using a cortical mask generated from automated cortical grey matter segmentations to create a cortical grey matter skeleton (Ball et al., 2013). This grey matter-based spatial statistics (GBSS) method ensures that only diffusion measures from voxels that are most likely to be in the grey matter are projected to the skeleton for analysis.

2.5 NEAR-INFRARED SPECTROSCOPY

Near-infrared spectroscopy (NIRS) was introduced in 1977 as a technique that offers non-invasive, real-time, in vivo monitoring of tissue oxygenation (Jöbsis, 1977).

The method relies upon the fact that biological tissue is relatively transparent to light in the near-infrared spectrum (700 – 1000 nm wavelength), and the differential absorption of near-infrared light by chromophores including haemoglobin, myoglobin, and cytochrome aa3. NIRS devices generally use wavelengths in the range of 700 – 750 nm, where the absorption spectra of oxyhaemoglobin and deoxyhaemoglobin are maximally separated with limited overlap with water.

The first application of NIRS in neonatal subjects was in 1985 to monitor cerebral oxygenation in preterm infants (Brazy et al., 1985), and was subsequently used to assess cerebral blood flow in 1988 (Edwards et al., 1988). It has since been used in a variety of neonatal applications including cerebral monitoring during congenital heart disease surgery (Andropoulos et al., 2004; Hirsch et al., 2009), guiding oxygen delivery during transition after birth (Pichler et al., 2014), monitoring cerebral oxygenation in preterm neonates (Hyttel-Sorensen et al., 2015; Pellicer et al., 2013), understanding brain perfusion changes in infants with hypoxic-ischaemic encephalopathy (Wintermark et al., 2014), guiding management of hypotension in preterm neonates (Bonestroo et al., 2011), and evaluating splanchnic perfusion in an attempt to detect early signs of necrotising enterocolitis (Sood et al., 2014).

Despite a wide range of studies in a large number of conditions, the adoption of NIRS in the neonatal setting has been limited. This is likely to be due to the heterogeneity of reference values obtained from different patient populations and manufacturers, the lack of a clear threshold at which a reading is considered abnormal, and the multitude of different models on the market, all yielding different results.

NIRS monitors are available from a number of different manufacturers, each with their own benefits and limitations. The INVOS oximeter was the first to be approved by the

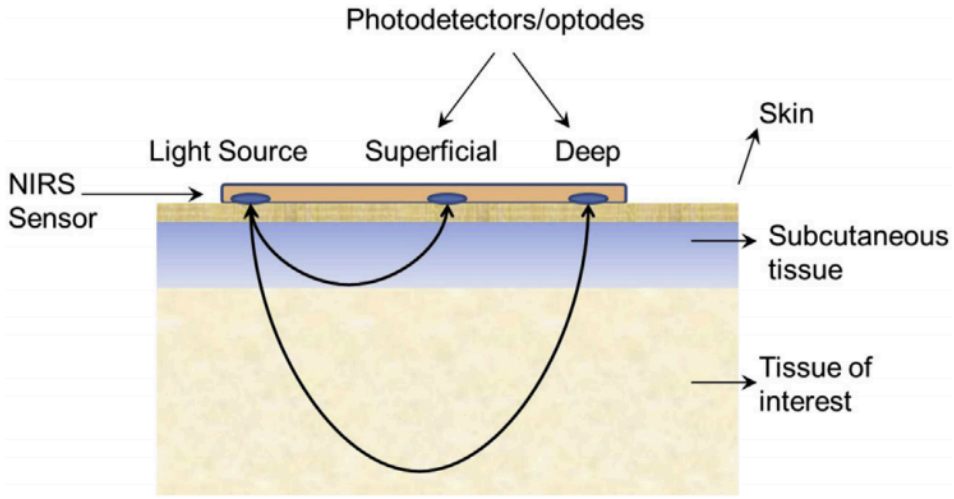

Figure 15 Summary of the original IN Vivo Optical Spectroscopy (INVOS) system
The INVOS monitor uses two photodiode detectors and 'subtracts' the short distance signal from the longer distance in order to diminish the contribution of the skin and scalp.

US FDA in the 1990s. The INVOS 5100C uses two LED sources at 730 nm and 810 nm and two photodetectors (Figure 15). The use of multiple emitter-detector distances, known as spatially-resolved spectroscopy (SRS), introduced the first cost-effective NIRS implementation that attempted to provide an absolute measure of regional tissue oxygen saturation ($rStO_2$).

A newer generation of NIRS technology attempts to improve accuracy and reduce extracranial contamination of the measurement. For example, the Casmed Foresight Elite uses five LED wavelengths (680, 730, 770, 805 and 870 nm) to improve the accuracy of its tissue oxygenation measurements. A study comparing three models (Invos 5100, Foresight 1st generation, and NONIN Equanox) concluded that the Foresight model had the best repeatability and lowest within-subject standard deviation (Hyttel-Sorensen et al., 2014).

For the experiments in this thesis, I opted to use the Casmed Foresight Elite (2nd edition) with neonatal sensors. This was due to the fact that this system had the highest repeatability performance (Hyttel-Sorensen et al., 2014), which was the most important parameter for the spot measurements that I planned to take at the time of MRI scan in order to assess differences in cerebral tissue oxygenation caused by each infant's congenital cardiac condition.

Whether we are dealing with correction of congenital cardiac defects or developing rockets to the moon, we must not let the brilliant glare of technologic success obscure our long-term objective to promote the quality of life.

Joseph K Perloff

"Pediatric Congenital Cardiac becomes a Postoperative Adult", Circulation, 1973

Chapter 3

Background to neurodevelopment in congenital heart disease

3.1 INTRODUCTION

Children born with congenital heart disease (CHD) are at increased risk of developing neurodevelopmental problems across a range of different domains (Gaynor et al., 2015; Marino et al., 2012). These include motor, cognitive, speech and language, behavioural, and executive functioning (Calderon and Bellinger, 2015; Klouda et al., 2016), as well as impaired social communication and repetitive behaviours (Bellinger, 2008; Brandlistuen et al., 2010; Nattel et al., 2017).

Such neurodevelopmental problems are a relatively recent phenomenon, as historically the majority of infants with complex CHD did not survive into childhood. As recently as the 1950s, for all practical purposes, only patent ductus arteriosus, vascular rings and a very occasional case of coarctation of the aorta (CoA) or tetralogy of Fallot (TOF) could be treated surgically with an acceptable success rate in the neonate (Talner and Nadas, 1969). Before 1979, hypoplastic left heart syndrome (HLHS) could only be managed medically and was uniformly fatal, with mean survival time less than one month (Lang P and Norwood WI., 1983; Norwood et al., 1983). These factors led to very high mortality rates: one of the earliest epidemiology studies of CHD mortality in the 1940s from Birmingham, UK, estimated that of ten infants born alive with all forms of CHD, two would have died by the end of the first week, three to four by the end of the first month, and six by the end of the first year (Macmahon et al., 1953). Only three would survive to their tenth birthday. Another study from the 1940s described mortality from CHD per diagnosis in Gothenburg until the age of 7 years old (Carlgren, 1959), which graphically highlights the particularly bleak prognosis for infants born with CoA and transposition of the great arteries (TGA) before routine surgical correction was established (Figure 16).

The last 40 years has seen remarkable surgical and medical advances in CHD (Khairy et al., 2008; Perloff, 1991; Perloff and Warnes, 2001; Wernovsky, 2008), with infant and childhood mortality decreasing by 31% from 1987 to 2005 alone (Khairy et al.,

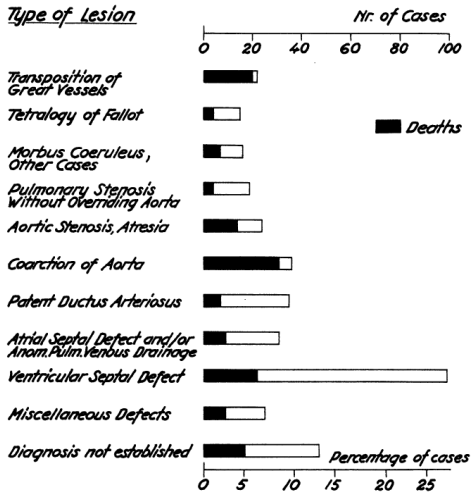

Figure 16 Incidence and mortality rate until 7 years of age in individual types of congenital heart disease from 1941-1950.

Mortality rates in CHD in the early days of surgical repair. Note mortality rate in TGA and CoA. Reproduced from Carlgren 1959, with permission of BMJ Publishing Group Ltd.

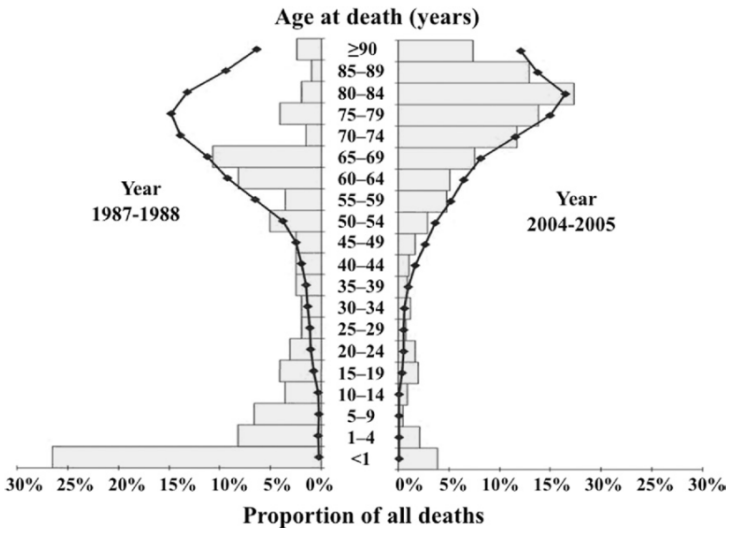

Figure 17 Distribution of Age at Death in Patients With Congenital Heart Disease in 1987 to 1988 and 2004 to 2005

Histogram bars depict the proportion of all deaths (x-axis) according to age at death (y-axis) in the Quebec cohort of patients with congenital heart disease 1987 to 1988 (left) and 2004 to 2005 (right). Black curves represent the corresponding age at death distribution in the general population. Reproduced from Khairy 2010, with permission of Elsevier.

2010), and achieving survival rates of 80-90% even for the most severe forms of CHD (Wernovsky, 2008). As a result, the number of surviving adults now exceeds the number of children with severe defects (Gilboa et al., 2016; Marelli et al., 2007). This contrasts disappointingly with the comparably modest improvements in neurodevelopmental outcomes in recent years (Gaynor et al., 2015).

In this chapter, I introduce evidence from clinical studies of the burden of neurodevelopmental challenges in CHD, the timeline of their manifestation during childhood, and their relation to CHD diagnosis. I describe alterations in brain development and maturation in CHD, from fetal life through to childhood. I finish by considering current hypotheses of how CHD affects the normal development of the brain.

3.2 THE BURDEN OF NEURODEVELOPMENTAL IMPAIRMENT IN CHD

There are a large number of clinical studies that provide an insight into the specific neurodevelopmental deficits experienced by children with CHD. Research has predominantly focused on the more complex CHD patient groups, including single ventricle CHD (such as HLHS) requiring Fontan palliation, or in patients with major bi-ventricular pathology (such as TGA and TOF), who require early surgery in infancy.

The majority of studies have used the Bayley Scales of Infant and Toddler Development (BDIS II) or Bayley III at an age of 6 – 48 months, and frequently report average scores that sit within the normal range for healthy term infants (mean 100, standard deviation ±15). However, almost all studies report poorer neurodevelopmental outcomes in infants with CHD compared to healthy controls or normative data (Mebius et al., 2017).

For the BSID II, the psychomotor development index (PDI) is usually more affected than mental developmental index (MDI). Mean composite scores for PDI have ranged from 69 – 103, and for MDI from 85 to 104 in infants with CHD (Hahn et al., 2016; Latal et al., 2015; Robertson et al., 2004; Williams et al., 2013; Zeng et al., 2015). For the Bayley III, mean cognitive scores have been reported between 91 – 105, mean language scores from 88 – 97, and mean motor scores from 86 – 97 (Andropoulos et al., 2014, 2012; Beca et al., 2013; Gunn et al., 2012b, 2012a; Masoller et al., 2016).

Specific evidence for the different developmental domains are outlined in the following section and summarised in Figure 18.

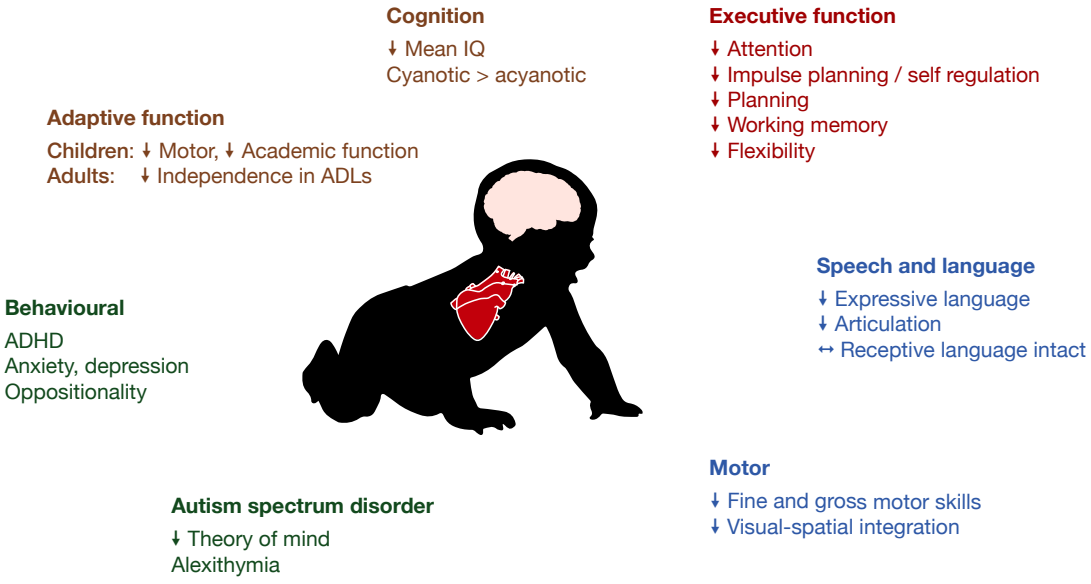

Figure 18 Summary of neurodevelopmental deficits observed in children who underwent corrective surgery for congenital heart disease

Different domains of development can be divided up into four groups – 1. Executive function (red) encompassing cognitive skills required for behaviour regulation and goal-directed activity; 2. Speech / language and motor (blue) which both involve motor ability, coordination and planning; 3. Cognition and adaptive (brown) where adaptive refers to the ability to use cognition to learn and apply skills necessary for everyday life; and 4. Neuropsychiatric (green), including deficits related to autism spectrum disorder, behavioural and psychiatric conditions. ADHD = attention-deficit hyperactivity disorder; ADLs = activities of daily living. Adapted from Nattel et al., 2017, with permission from Elsevier.

3.2.1 Cognitive domains

Children with CHD are at increased risk of cognitive difficulties compared to the healthy population, with consistent evidence that average intellectual quotient (IQ) in children with CHD is reduced by around 5 – 10 points (Bellinger et al., 2015a; Forbess et al., 2002; Goldberg et al., 2000; Krueger et al., 2015; Majnemer et al., 2008; Miatton et al., 2006; Schaefer et al., 2013). IQ scores for children with CHD overlap significantly with their healthy counterparts, with the entire distribution of scores shifted to the left in CHD, and those with a genetic abnormality shifted to an even greater degree (Latal, 2016). This implies that children with CHD may well perform at normal or even high-normal levels, although there will be a greater proportion of those with scores that are below clinically-relevant cut-off values in diagnoses of CHD (Figure 19).

Majnemer et al. found that children who had undergone surgical repair in infancy had IQs within the low average range (90-94) at 5 years (Majnemer et al., 2008). Those with single ventricle repair may demonstrate IQs that are more markedly reduced, with a difference of up 10 points compared to matched controls (Forbess et al., 2002; Goldberg et al., 2000). This is reflected in MDI scores in one study at 14 months of

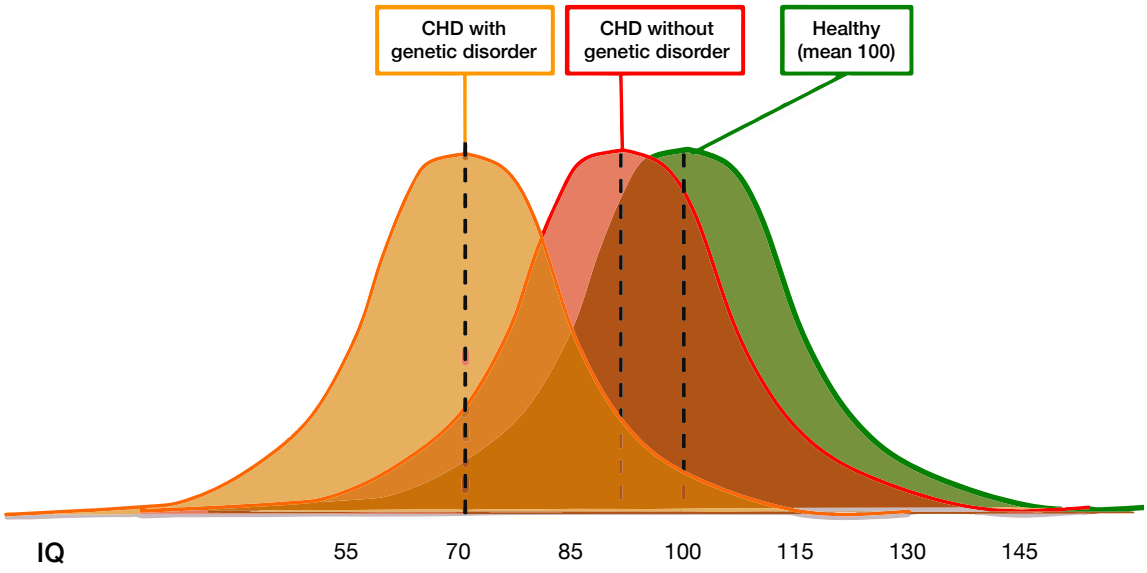

Figure 19 Schematic demonstration of how the IQ of children with CHD with and without genetic abnormalities compare to those of healthy children.

The distributions of IQs of children born with CHD are shifted to the left (poorer IQ), with considerable overlap between groups. This implies that children with CHD may well perform at the normal level or even high-normal level, but that there will be a greater number of infants below the clinically-relevant cut-off values (i.e. <70 represents 2 standard deviations from the mean) in children with CHD. Adapted from (Latal, 2016), with permission from Elsevier Inc.

age in HLHS, with 16% of subjects scoring <70 (equal to >2 SD below normal mean) and 36% of subjects scoring <85 (equal to >1 SD below normal mean) (Newburger et al., 2012). Adolescents with TOF have IQs on average 6-10 points lower than controls, with TOF associated with genetic syndromes (e.g. 22q11) having significantly worse outcomes compared to non-syndromic TOF (Bellinger et al., 2015a).

In adulthood, 'executive function' and other so-called 'higher order' cognitive skills are most impaired compared to the healthy population. Executive function refers to a family of mental processes that are needed to perform complex reasoning, problem solving and planning, with a general agreement that there are three core executive functions: 1) inhibition (self-control, selective attention, cognitive inhibition), 2) working memory, and 3) cognitive flexibility (Diamond, 2013). Executive function is of particular interest for ensuring long-term wellbeing in survivors of CHD, as specific deficits in these domains may cause difficulties in their future lives when performing prerequisite activities of daily living, such as managing finances, and general problem solving.

In adulthood, one recent study that assessed survivors of all subtypes of CHD at a mean age of 33 found that average Wechsler IQ was within the normal range (Tyagi et al., 2017). The authors concluded that this result perhaps emphasises the limitation of generalised measures of cognitive function such as IQ. They did however find significant specific deficits in executive function, divided attention (the ability to respond to multiple tasks simultaneously), and motor function (using the Grooved Pegboard test). Interestingly, total composite scores were worst in TGA, followed by single ventricle physiology, then TOF. Evidence of impaired executive function has also been observed as early as 5-7 years of age, with significant delays in inhibition, cognitive flexibility, despite normal working memory (Calderon et al., 2014)

On average, academic achievements of children with CHD lag behind their healthy peers. A large population-based cohort study of children aged 8 – 9 years old in the US found that children with CHD had 1.24x the odds of not meeting assessment standards in either reading or mathematics (95% CI 1.12 – 1.37), with 44.6% of children with CHD not meeting standards in at least one of these subject areas compared to 37.5% of those without CHD (Oster et al., 2017). Children with complex CHD (including HLHS, TGA, CoA, TOF, pulmonary atresia, tricuspid atresia, truncus arteriosus) required special educational support more frequently than those with simple CHD (adjusted odds ratio 1.46, 95% CI 1.15 – 1.86).

3.2.2 Motor domains

In early childhood, motor development appears to be the most affected developmental domain in CHD. Most studies that assess this domain have found a degree of gross or fine motor impairment, although severe disability is uncommon.

Early in childhood, one study described functional motor impairment at 12 and 18 months following open heart surgery (Limperopoulos et al., 2001). Another study identified motor scores that were 11% below average at 6 – 37 months of age in a mixed cohort of CHD (Mussatto et al., 2015). There is a high prevalence of motor problems in HLHS, with 44 – 48% of children at 12-14 months of age showing significantly abnormal motor performance with scores greater than 2 standard deviations below the mean (Newburger et al., 2012; Tabbutt et al., 2008).

Early motor abnormalities appear to persist into late childhood. Following a cohort of infants who underwent open surgery with cardiopulmonary bypass and assessed at a mean age of 19 months, 42% demonstrated delays in gross or fine motor skills (Limperopoulos et al., 2002). At 5 years of age, these delays persisted with 49% showing gross motor delays, and 39% fine motor delays (Majnemer et al., 2006). In this study, poorer gross motor scores were found if palliative (vs corrective) surgery had been performed, or in the presence of microcephaly at initial surgery (defined as (head circumference <2nd percentile for age and gender). Poorer fine motor scores were associated with longer deep hypothermic circulatory arrest time, palliative surgery, microcephaly and number of hospitalisations (Majnemer et al., 2006). Another study assessing children at 7 – 12 years of age who had undergone cardiac surgery in the first year of life, found that 43% had motor problems, compared to 7% in the healthy matched control group (Holm et al., 2007). Similar findings were reported in a study of 194 children with mixed CHD, assessed at 10 years of age, which found moderate motor abnormalities in 27% and severe disturbances in 32%, significantly worse than their healthy control group (Bjarnason-Wehrens et al., 2007).

3.2.3 Speech and language domains

Expressive language delays in CHD are common in CHD (Bellinger et al., 1999, 1997; Brosig et al., 2007; Hövels-Gürich et al., 2008). This has been specifically shown in HLHS at 3.5 – 6 years of age (Brosig et al., 2007), and in TGA at 2.5 years of age (Bellinger et al., 1997).

Receptive language appears to be less affected. At school age, receptive language was found to be intact at 5 years of age in one study that followed children who had undergone open heart surgery (Majnemer et al., 2008).

Reading ability has been shown to be delayed in adolescents with TOF aged 13-16 years old (Bellinger et al., 2015a), and in adolescents with corrected TGA at 16 years of age (Bellinger et al., 2011).

3.2.4 Adaptive functioning

Adaptive functioning is an age-based construct that describes the ability to learn and use the skills necessary for everyday life (Marino et al., 2012). Children with CHD have lower adaptive functioning scores that persist into adulthood (Warnes et al., 2008). Infants with HLHS are known to be particularly affected (Goldberg et al., 2000; Kern et al., 1998), with one study demonstrating poorer performance in all adaptive behaviour subsets, including worse spatial integration (Goldberg et al., 2000).

3.2.5 Behavioural problems

Children with CHD appear to exhibit a high prevalence of 'internalising' problems (which includes anxiety, depression, and withdrawal) and 'externalising' problems (which includes attention problems and aggression). Parents of children with CHD report these features at similar rates across different studies, ranging from 15 – 25% (Bellinger et al., 2011, 2009; Hövels-Gürich and Konrad, 2002; Hövels-Gürich et al., 2007; Majnemer et al., 2008).

Interestingly the children themselves do not self-report their behavioural or emotional problems, in contrast to their parents. In one study, parents reported increased perceived behavioural or emotional problems in their children aged 7 – 17 with diagnoses including TGA, VSD and pulmonary stenosis, while the children themselves self-reported no impairment (Spijkerboer et al., 2008). A similar finding was made in 328 Fontan survivors, with parents rating their children significantly lower than their children's self-reported measures of physical functioning, emotional and behavioural problems, general behaviour, self-esteem, and general health perceptions (Lambert et al., 2009).

Inattention, impulsivity and hyperactivity have all been reported in children with CHD, with an increased risk of attention dysfunction being particularly reported in TGA and

TOF (Hövels-Gürich and Konrad, 2002; Hövels-Gürich et al., 2007; Shillingford et al., 2008; Shillingford and Wernovsky, 2004).

There have also been a number of studies suggesting that infants with CHD are more likely to exhibit features consistent with autism spectrum disorder (ASD) (Hultman et al., 2002; Wier et al., 2006). ASD describes a group of developmental disabilities that includes impaired socialisation, communication, and repetitive and unusual behaviours (American Psychiatric Association, 2000). Children with CHD have been reported to have communication impairment (Miatton et al., 2007), and reduced social competence (Bellinger, 2008), with higher risk observed in those with 22q11 deletion (Antshel et al., 2007). One study of 195 children at 4 years of age found higher rates of 'possible' autism spectrum disorders than national rates (3.2% vs 1.47%), with risk factors including delayed sternal closure, prematurity, positive genetic findings and various socioeconomic and cultural variables (Bean Jaworski et al., 2017).

Another more specific interpretation is that infants with CHD have problems with 'theory of mind' (their ability to appraise and interpret another's mental state), and alexithymia (difficulty understanding and describing their own emotions), both of which are particularly recognised in CHD (Bellinger, 2008).

3.2.6 Timeline of manifestations of neurodevelopmental impairment

The approximate order in which different neurodevelopmental domains become apparent as a child is summarised in Figure 20. Motor delays are generally the first domain to be affected, with hypotonia, motor asymmetries and feeding difficulties most prevalent (Limperopoulos et al., 2000). At one year of age, the risk of motor delay is greater than the risk of cognitive disability (Snookes et al., 2010). Cognitive impairments start to become more apparent at school age (Miatton et al., 2006), with expressive language, memory impairments, and lower IQ (Bellinger et al., 2015a; Forbess et al., 2002; Goldberg et al., 2000; Krueger et al., 2015; Majnemer et al., 2008; Miatton et al., 2006). Behavioural problems become increasingly apparent with progressing maturity, as discussed previously (Shillingford et al., 2008). Cognitive and motor impairments persist into adolescence, and do not appear to be outgrown as a result of maturational processes (Schaefer et al., 2013). Different combinations of neurodevelopmental challenges for each child with CHD lead to a requirement for

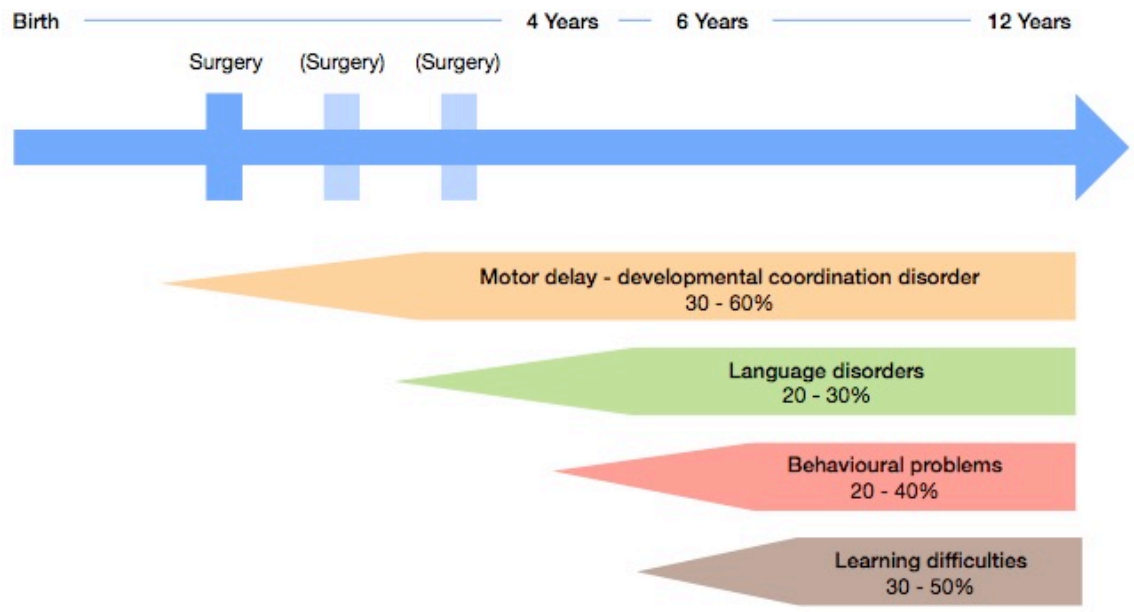

Figure 20 Schematic overview of developmental domains affected in CHD, with their temporal occurrence and estimated prevalence
Adapted from (Latal, 2016) with permission from Elsevier Inc.

some form of special education support in approximately half of those who have undergone neonatal cardiac surgery aged 5 – 10 years old (Shillingford et al., 2008).

3.2.7 Clinical factors that adversely affect neurodevelopmental outcome

A number of outcome studies have attempted to identify perioperative clinical factors that correlate with poorer neurodevelopmental outcome. Lower socioeconomic status is a commonly associated factor (Forbess et al., 2002; Goldberg et al., 2000; Mussatto et al., 2015; Newburger et al., 2012), along with maternal education level (Gaynor et al., 2015). Longer post-repair ICU stay is consistently reported (Forbess et al., 2002; Limperopoulos et al., 2002; Mussatto et al., 2015; Newburger et al., 2012, 2003), which is intuitive as increased ICU stay is generally required to stabilise haemodynamics following more complex surgery, and may additionally involve lengthy exposure to sedatives. Other factors that relate to severity of case and complications and have been associated with impaired neurodevelopmental outcomes include longer length of hypothermic circulatory arrest (Forbess et al., 2002; Goldberg et al., 2000; Majnemer et al., 2008), bypass time (Hövels-Gürich et al., 2007), perioperative seizures (Goldberg et al., 2000), postoperative low cardiac output (Galli et al., 2004; Garcia Guerra et al., 2013; Miller et al., 2007), reduced systemic venous oxygen saturation (Hoffman et al., 2005), need for atrial septostomy (McQuillen et al.,

2006), more cardiac surgeries and tube feeding at discharge (Mussatto et al., 2015). Poorer outcomes have also been associated with constitutional factors such as birthweight less than 2.5 kg (Newburger et al., 2012), microcephaly (Majnemer et al., 2008), and 22q11 (Forbess et al., 2002). In contrast, one study found no association with any perioperative factors in 88 children with HLHS (Tabbutt et al., 2008).

Overall, these studies suggest a cumulative impact of pre-operative, perioperative and post-operative factors that are responsible for increasing the risk of brain injury and subsequent neurodevelopmental impairment in later life.

3.2.8 Advances in surgical and perioperative factors associated with neurodevelopmental impairment

Trials performed over the past 40 years have greatly improved our understanding of how cardiac surgery techniques and associated medical management can impact upon brain injury in the neonatal period. As a result, new strategies have been implemented that have improved outcomes for children with CHD.

The Boston Circulatory Arrest study was a very influential study that compared the incidence of perioperative brain injury in infants with TGA who were randomised to one of: a) deep hypothermic circulatory arrest (DHCA) or b) low-flow cardiopulmonary bypass (Newburger, 1993). In the postoperative period, they found that DHCA was associated with greater 'central nervous system perturbation', including seizures, abnormal EEG monitoring, higher creatine kinase, and longer recovery time to first reappearance of EEG activity following surgery (Newburger, 1993). In infancy and early childhood, follow-up found that children who underwent DHCA were at a higher risk of neurodevelopmental abnormalities at 1 and 4 years of age (Bellinger et al., 1999, 1995). At 8 years of age, DHCA was associated with worse neurodevelopmental outcomes with longer durations of circulatory arrest (>41 minutes), although there was little effect on shorter durations (Wypij et al., 2003). More recently at 16 years of age, few significant variables were found between treatment groups, with occurrence of postoperative seizures being most related to poorer neurodevelopmental outcomes. Despite the eventual similarity between groups at 16 years of age, the scores of both treatment groups were lower than normative populations (Bellinger et al., 2011). Long-term studies like this are extremely valuable in understanding the true extent of modifications to our clinical practices, and this study in particular demonstrates how

early changes in neurodevelopmental outcomes do not necessary reflect longer-term findings.

The effect of regional cerebral perfusion compared to DHCA was compared in infants who underwent the Norwood procedure, which was found to make no difference to neurodevelopmental outcome at 1 year of age (Goldberg et al., 2007). Similarly, in aortic arch repair, comparison between antegrade cerebral perfusion and DHCA showed no difference at 2 years of age, although central infarctions occurred only in the antegrade cerebral perfusion group (Algra et al., 2014).

Various blood parameters have been studied in the perioperative period. One trial studied the effect of two acid-base management strategies during hypothermic cardiopulmonary bypass in a mixed cohort of CHD using an alkalotic alpha-stat strategy and a hypercarbic pH-stat strategy (du Plessis et al., 1997). The pH-state strategy was found to be associated with lower postoperative mortality, shorter recovery time, and shorter length of intubation and intensive care stay.

Another group of trials considered haematocrit levels during cardiopulmonary bypass, finding that haematocrit levels of less than 24% during surgery were associated with worse neurodevelopment psychomotor development index scores at 1 year of age (Jonas et al., 2003; Newburger et al., 2008; Wypij et al., 2008).

Assessment of perioperative glycaemic control has shown that tight glycaemic control does not affect neurodevelopmental outcomes at 1 year of age, length of hospital stay, mortality, or infection rates (Agus et al., 2014, 2012; Sadhwani et al., 2016).

The optimisation of anaesthesia is another area that has been gaining interest in recent years. Cardiac surgery generally necessitates an anaesthetic agent, but the choice of agent and duration of exposure are variables that are potentially modifiable. Preclinical data suggest that general anaesthetics can affect brain development (Jevtovic-Todorovic et al., 2013), although a short duration of anaesthetic (less than 1 hour of sevoflurane) is not thought to affect neurodevelopmental outcome at 2 years of age (Davidson et al., 2016). However, CHD surgery often takes a number of hours, and ongoing anaesthesia may also be required during the post-operative period on intensive care.

A recent study of infants with HLHS found that cumulative volatile anaesthetic agent exposure was associated with worse full-scale IQ and verbal IQ scores at 4-5 years of

age, after correcting for relevant covariates (Diaz et al., 2016). Another study of a mixed cohort of infants undergoing complex cardiac surgery found that volatile anaesthetic agent exposure was associated with lower cognitive scores at 12 months of age (Andropoulos et al., 2014). Evidence remains limited at present, but the limited number of studies to date do raise concern that exposure of neonates to volatile anaesthetic agents may affect their longer term neurodevelopmental outcome. A prospective randomised trial is now required to understand the true effect of these agents.

There are a vast number of modifiable factors in the management of infants with CHD. Studies highlighted above are responsible for improving our knowledge of a number of modifiable perioperative factors that may affect neurodevelopmental outcomes in children undergoing surgery for CHD. Future studies exploring other components of the treatment pathway will allow us to make further improvements for children in the future.

3.2.9 Effect of CHD on quality of life and family impact

Adverse neurodevelopmental outcomes can have a damaging effect on future quality of life (QOL). QOL reflects a measure of the standard of health, comfort, and happiness experienced by an individual. It captures three domains that include physical health and physical functioning, psychological status, and social functioning (Drotar, 2004). QOL can be collected from children as young as 7 years of age, and a number of studies have studied the effect of CHD on QOL scores (Marino et al., 2016). The greatest negative impact of CHD on QOL has been reported in the areas of social and education functioning (Mussatto and Tweddell, 2005). Severity of heart disease has been related to perceived worse physical and psychosocial QOL by parents (Uzark et al., 2008), and although most children reported good overall QOL scores, 20% of children with CHD reported significantly impaired psychosocial scores, which also included those with mild and moderate CHD.

The diagnosis of CHD can have a profound impact upon a family. One study performed a Parental Function Status-II of 100 parents with CHD and showed that 18% scored below one standard deviation, with concerns associated with financial stress, severity of the child's CHD, and lower child functioning (Garcia et al., 2016). In addition, issues including anxiety, depression, and post-traumatic stress disorder

have been reported in the child and family in the years following a diagnosis of CHD (Marino et al., 2016).

3.2.10 Recent improvements in neurodevelopmental outcomes

Despite the highlighted advances in surgical, perioperative care and medical management, the largest aggregated cohort of neurodevelopmental outcomes that has been reported to date in CHD was unable to identify significant improvements in outcomes from 1996 – 2009, even when restricting analyses to homogenous diagnostic subgroups including TGA, TOF and HLHS (Gaynor et al., 2015). After adjustment for patient and preoperative medical factors, both MDI and PDI improved significantly although by only a modest degree (approximately 5-6 points over 14 years) (Figure 21). The analysis suggested that more patients at greater risk for neurodevelopmental impairment are undergoing CHD surgery, and that high-risk patients are surviving more often, creating a growing population that will require significant societal resources. Gaynor and colleagues also (somewhat gloomily) concluded that innate factors (such as genetic syndromes, prematurity, socioeconomic status) may outweigh the impact of modifiable management factors in determining neurodevelopmental outcomes in this population.

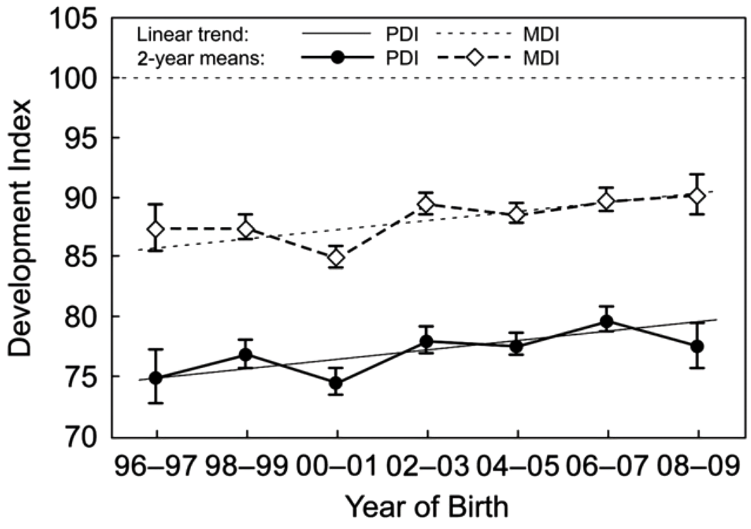

Figure 21 Standardised PDI and MDI by year of birth from 1996 – 2009

Standardised Psychomotor Development Index (PDI) and Mental Development Index (MDI) means by year of birth. The standardised means plot the predicted PDIs and MDIs and standard error bars based on a model with year of birth category adjusting for centre, cardiac class, and other statistically significant predictors at the mean value of the covariates. Overlaid are standardised means plots based on continuous year of birth. The horizontal dotted line represents the normative mean of 100 for both PDI and MDI. Reproduced from Gaynor et al., 2015, with permission of American Academy of Pediatrics.

3.3 EVIDENCE OF ALTERED EARLY BRAIN DEVELOPMENT IN CHD

By now, it is clear that children with CHD are at greater risk of long-term neurodevelopmental deficits. In contrast, the underlying cause for such deficits remains less clear. A growing number of histology and neuroimaging studies have shown evidence of altered early brain development in the fetal and neonatal period. This section describes changes in brain development that have been reported in fetal life, and how neonatal MR imaging has contributed to our understanding of this field.

3.3.1 Post-mortem findings

Post-mortem examinations in the late 80s and early 90s provided an insight into early brain development and the progression of cortical folding during fetal life, both in normal brain development (Armstrong et al., 1995; Zilles et al., 1988) and in those with CHD (Glauser et al., 1990a, 1990b). Findings from a cohort of autopsies of infants with HLHS found an 'immature cortical mantle' in 21% of cases, microcephaly in 27% (defined as below 2nd centile for gestational age), and 'specific recognisable patterns of malformation' in 17% (Glauser et al., 1990b). Acquired lesions were also found in 45% of those with HLHS, of whom half had undergone some form of cardiac procedure, with a combination of hypoxic-ischaemic lesions, periventricular leukomalacia, brainstem necrosis, and intracranial haemorrhage (Glauser et al., 1990a).

Similar findings have been reported in 38 infants dying after cardiac surgery between 1988 – 1992, with white matter damage in virtually all infants and grey matter damage in 68% (Kinney et al., 2005). White matter damage predominantly comprised periventricular leukomalacia (PVL; defined as focal or coalescing foci of necrosis in the white matter associated with diffuse astrogliosis in the surrounding white matter) in 61%, or diffuse white matter gliosis (defined as reactive astrocytes without associated focal necrosis) in 79%. Interestingly, although the clinical profile was virtually identical between both types of white matter lesion, a history of resuscitation at birth was significantly more common in infants with diffuse gliosis (70%) vs. PVL (36%). Grey matter injury tended to be diffuse, implying generalised hypoxic-ischaemic injury. There were few focal infarcts as a result of embolic-related ischaemic events, and no ischaemic events in vascular border zones due to hypotension. The major lesion in the cortex tended to be acute neuronal necrosis, suggesting a timing in the agonal stages

of dying after surgery, while gliosis (indicative of older injury, including before surgery) tended to be present in the thalamus and brainstem.

Overall, these findings suggested that brain development in CHD does not follow a normal trajectory in utero and is associated with increased vulnerability to hypoxic-ischaemic injury during the pre-, intra-, and post-operative periods.

3.3.2 Head circumference

It is well-established that newborn infants with CHD are at greater risk of impaired growth. The rate of microcephaly in different cohorts varies from 12 – 55% (Glauser et al., 1990b; Hinton et al., 2008; Licht et al., 2004; Limperopoulos et al., 1999; Shillingford et al., 2007). The definition of microcephaly varies slightly by publication, with some using less and or equal to the third centile (Hinton et al., 2008; Limperopoulos et al., 1999; Shillingford et al., 2007), less than or equal to the second centile (Glauser et al., 1990b), or more than two standard deviations below the mean (Licht et al., 2004). Small for gestational age birth weight is noted in approximately one fifth of infants (Hinton et al., 2008; Shillingford et al., 2007).

Head circumference represents a simple and widely-available proxy of prenatal brain growth. The American Heart Association acknowledged microcephaly as one of the few recognised risk factors for impaired neurodevelopment in children with CHD (Marino et al., 2012), and has been associated with poorer longer-term outcomes through infancy and school age (Gaynor et al., 2007; Limperopoulos et al., 1999; Matos et al., 2014). Low birth weight was also found to eclipse perioperative measures as the strongest predictor of a worse neurodevelopmental outcome (Gaynor et al., 2007).

A large nationwide cohort study of Danish singleton infants reported smaller head circumference in many types of CHD including HLHS, truncus arteriosus, major ventricular septal defect (VSD), TGA, TOF and anomalous pulmonary venous return (Matthiesen et al., 2016). Only TGA was associated with a smaller head circumference relative to birthweight, which had been noted earlier in a smaller group (Rosenthal, 1996), suggesting that impaired fetal cerebral growth may only be an isolated cerebral phenomenon in infants with TGA.

3.3.3 Fetal and neonatal imaging

Cranial ultrasound is a widely-available bedside tool that can be used to assess cerebral abnormalities in the term CHD population (Latal et al., 2015; Rios et al., 2013; Te Pas et al., 2005; van Houten et al., 1996). Ultrasound has been shown to have both a high sensitivity for cerebral lesions such as periventricular leukomalacia and intraventricular haemorrhage, and has predictive validity to predict major neurodevelopmental impairments in preterm infants (De Vries et al., 2004). The same does not appear to be true for the CHD population, with ultrasound demonstrating very poor sensitivity and specificity for lesions compared to paired MRI in one large study (Rios et al., 2013). Preoperative brain lesions were present in 26% of infants with CHD using MRI, while only 3% showed evidence of lesions in cranial ultrasound, and 80% of these ultrasound-detected lesions were false-positive results. The pattern of brain injury was predominantly white matter injury, with stroke and haemorrhage being much less common (Rios et al., 2013) – a very different pattern to that observed in the preterm population where ultrasound is more effective. Abnormalities detected using ultrasound tend to be mild, consisting of diffuse brain oedema, periventricular white matter injury, and ventricular dilatation, and no significant relationship appears to exist between these and early neurodevelopmental outcome at 1 year of age (Latal et al., 2015).

Advances in MRI have provided new insights into the effect of CHD on brain development. Magnetic resonance spectroscopy is a useful tool to assess metabolic integrity of neurones in particular brain regions. Developmental abnormalities have been noted in CHD fetuses using MR spectroscopy in the form of a lower N-acetylaspartic acid (NAA):Choline ratio during the third trimester, when key neuronal connections are forming (Limperopoulos et al., 2010). The same finding has been noted postnatally, with a 10% reduction in the NAA:Choline ratio in a cohort of newborn infants prior to surgery with TGA and SV physiology (Miller et al., 2007). An abnormally low NAA:Choline ratio in preterm infants has been shown to be predictive of worse motor outcomes (Kendall et al., 2014), but the same has not been reported in CHD.

A derailed trajectory of brain growth in CHD has been elegantly illustrated by studies using fetal ultrasound (Zeng et al., 2015) and fetal MRI (Clouchoux et al., 2013; Limperopoulos et al., 2010), with examples shown in Figure 22. Limperopoulos et al.'s

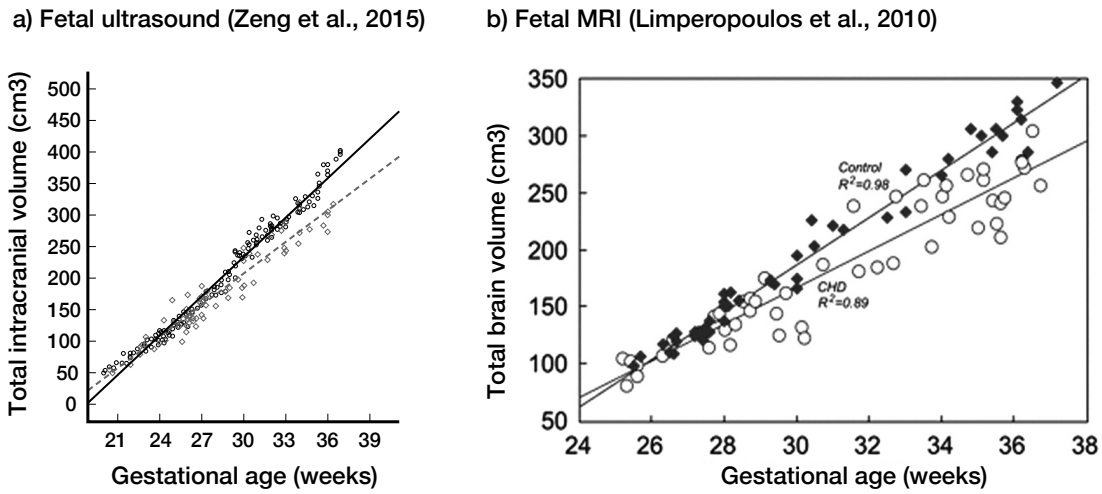

Figure 22 Evidence of altered brain growth trajectories using both ultrasound and fetal MRI
(**a**) Scatterplot of total intracranial volume measured using 3D fetal ultrasound. After the 28th week, the global and regional brain volumes became progressively smaller in CHD fetuses (open circles) relative to controls (closed circles) (Zeng et al., 2015). Reproduced with permission of John Wiley and Sons. (**b**) Relationship between total brain volume and gestational age between infants with CHD (closed diamonds) vs healthy controls (open diamonds) (Limperopoulos et al., 2010). Reproduced with permission of Wolters Kluwer Health, Inc.

pivotal fetal MRI study demonstrated how the brain volumes of a cohort of fetuses with HLHS began to deviate away from normal growth rates in the third trimester (Limperopoulos et al., 2010) (Figure 22b). Similar findings have also been shown using three-dimensional fetal ultrasound, with an impaired trajectory of intracranial volume growth appearing at around 28 weeks in a mixed cohort of CHD (Zeng et al., 2015) (Figure 22a). Limperopoulos's group built upon their initial results to describe significant reductions in cortical volume, cortical gyrification, surface area and white matter volume in the third trimester (Clouchoux et al., 2013). Reduced total brain volume, grey matter volume, and white matter volume have also been shown in a cohort of 24 fetuses with TOF using fetal MRI (Schellen et al., 2015). Fetal studies such as these have convincingly shown that the origins of abnormal brain development in CHD begin in utero.

Smaller brain volumes continue to persist after birth (Hinton et al., 2008; Ibuki et al., 2012; Miller et al., 2007; Shillingford et al., 2007; von Rhein et al., 2015), with MR imaging measures corroborating the smaller head circumferences that have been noted for many years. Interestingly, one study found that while infants with both TGA and single ventricle physiology had significantly reduced brain volumes at 1 year of age, by 3 years of age infants with repaired TGA demonstrated normal brain volumes

while infants with palliated single ventricle physiology remained reduced (Ibuki et al., 2012). This may be evidence for the value of early corrective surgery. In addition to volumes, brain 'maturity' and cortical folding complexity can be assessed using both semi-quantitative radiological scoring methods (Childs et al., 2001) and fully-quantitative objective methods such as gyrification index (Armstrong et al., 1995). Recent studies have demonstrated reduced cortical folding complexity using both methods in newborn infants prior to surgery (Andropoulos et al., 2010; Claessens et al., 2016; Licht et al., 2009; Ortinau et al., 2013), and have suggested that white matter injury is the predominant injury type from qualitative radiological assessment (Mebius et al., 2017). Of note, cortical folding 'immaturity' has been shown to correlate with both pre- and post-operative brain injury (Andropoulos et al., 2010) and eventual outcome (Beca et al., 2009).

The use of more advanced techniques such as neonatal diffusion MRI has enabled new insights into the development of neuronal tissue in this population. Fractional anisotropy (FA) is a measure of the directionality of water diffusion that increases in value as the maturing white matter becomes more organised during normal development. This makes it a valuable marker for white matter maturation. Newborn infants with CHD have been shown to have lower white matter FA compared to healthy controls (Dimitropoulos et al., 2013; Miller et al., 2007; Mulkey et al., 2014; Sethi et al., 2013) with changes that persist into adolescence (Rivkin et al., 2013).

Network analysis of functional MRI data has suggested reduced regional functional connectivity involving critical brain regions in newborns with CHD prior to surgery, albeit in the presence of an intact overall global network topology (De Asis-Cruz et al., 2017). Further studies will be required to ascertain the prognostic ability and diagnostic value of such analyses.

3.4 THE EFFECT OF HAEMODYNAMIC ABNORMALITIES ON BRAIN DEVELOPMENT IN CHD

Circulatory abnormalities as a result of structural defects in CHD can result in altered cerebral blood flow haemodynamics. The earliest quantitative measurements of the distribution of the fetal circulation was performed by Dawes, who used intravascular flow probes in exteriorised fetal lambs to obtain blood saturation measurements from various chambers and vessels, estimated cardiac output, and blood volumes ejected by both left and right ventricles (Dawes et al., 1954). Subsequent work by Rudolph

and Heymann used radionuclide-labelled microspheres to measure organ blood flows, cardiac output, the distribution of blood ejected by the left and right ventricles, also in fetal lambs but under more physiological conditions (Rudolph and Heymann, 1967). This led to some pioneering work to describe alterations in the fetal blood circulation in CHD (Heymann and Rudolph, 1972), and these animal experiments remain the basis for our current understanding of fetal circulation in CHD today.

Recent work using fetal MRI has begun to confirm and build upon this animal work, with phase contrast angiography in 40 late-gestation human fetuses found to confirm flow estimates made by Rudolph using fetal lamb experiments (Prsa et al., 2014). T2 mapping techniques have also been shown to correlate well with conventional blood gas measurements (Nield et al., 2005), which uses the same principle as BOLD MRI (Ogawa et al., 1990) where magnetic properties of blood vary with changes in the oxygen saturation of haemoglobin. The recent combination of phase contrast angiography and T2 mapping has allowed reproducible measurements to be performed on the larger fetal vessels of human fetuses in a non-invasive manner *in vivo*, and so gain a unique insight into the effect of CHD on cerebral haemodynamics (Sun et al., 2015). However, a limitation of work to date is the relatively heterogenous nature of CHD groups studied, making it difficult to draw conclusions about different diagnostic groups.

This section first describes the wide spectrum of CHD diagnoses in the context of three main physiological categories and explains how each may affect cerebral blood flow and oxygen delivery. The evidence for cerebral autoregulation in CHD is discussed, concluding with the effect of both cyanosis and impaired CDO_2 on brain development and neurodevelopmental outcomes.

3.4.1 Disturbed preferential streaming of the normal fetal circulation

In a normal fetus (Figure 23a), there is preferential streaming of oxygenated venous return from the placenta to the fetal circulation via the ductus venosus and foramen ovale, resulting in the most highly oxygenated blood being diverted to the brain. Disturbed preferential streaming occurs in lesions such as TGA and double outlet right ventricle (DORV). In TGA, preferential shunting of oxygenated blood into the left atrium and left ventricle is retained and given the lack of obstruction to either vessel, TGA results in normal flow. However, with the aorta arising from the right ventricle, the

a) Blood flow pattern in a fetus with a normal heart

b) Blood flow pattern in a fetus with transposition of the great arteries

c) Combined ventricular output (%) in pulmonary atresia

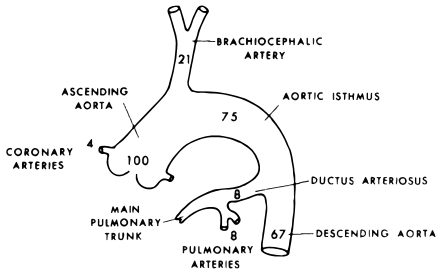

d) Combined ventricular output (%) in aortic atresia

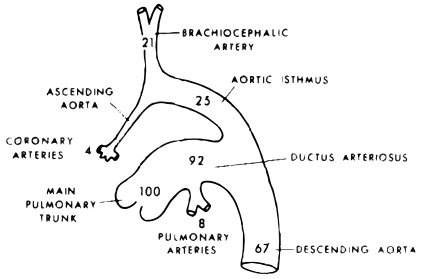

Note: numbers in circles represent percent oxygen saturation; other numbers are pressures in mmHg; m = mean pressure.

Figure 23 Alterations in fetal blood flow patterns in different forms of CHD.

Blood flow patterns in (**a**) a healthy fetus and (**b**) an infant with transposition of the great arteries (TGA). In a fetus with TGA, the pO2 of the blood perfusing the heart, brain and upper body would be lower than normal. (**c**) In pulmonary atresia, blood flow is compromised from the right ventricle to pulmonary trunk, resulting in compensatory increased flow in the aortic isthmus. (**d**) In lesions such as hypoplastic left heart syndrome or aortic atresia, little or no blood is ejected by the left ventricle into the ascending aorta. Therefore, in these cases, coronary, cerebral and upper body blood flow must be provided in a retrograde manner from the main pulmonary trunk through the ductus arteriosus. Figures adapted from Heymann and Rudolph, 1972 with permission from Elsevier Inc.

benefits for selective cerebral blood flow are not realised, resulting in lower oxygenation of blood perfusing the heart, brain and upper body (Figure 23b).

3.4.2 Right ventricular outflow tract obstruction

Right ventricular outflow tract obstruction includes lesions such as TOF, tricuspid atresia, pulmonary atresia with intact ventricular septum, and critical pulmonary valve stenosis (Figure 23c). To maintain descending aortic flow, blood normally carried by the main pulmonary trunk and ductus arteriosus is now handled by the left ventricle, ascending aorta and aortic isthmus, in addition to the flow that is normally carried by them. The aortic arch would therefore be expected to have a wider diameter than in the normal fetal circulation. In TOF, oxygenated blood streams across the foramen ovale into the aorta as usual, but this can be diluted by deoxygenated blood shunting from right to left across the ventricular septal defect.

3.4.3 Obstruction to the left heart

Obstruction to the left heart includes lesions such as HLHS, critical aortic stenosis, aortic atresia, and coarctation of the aorta (Figure 23d). In some fetuses with

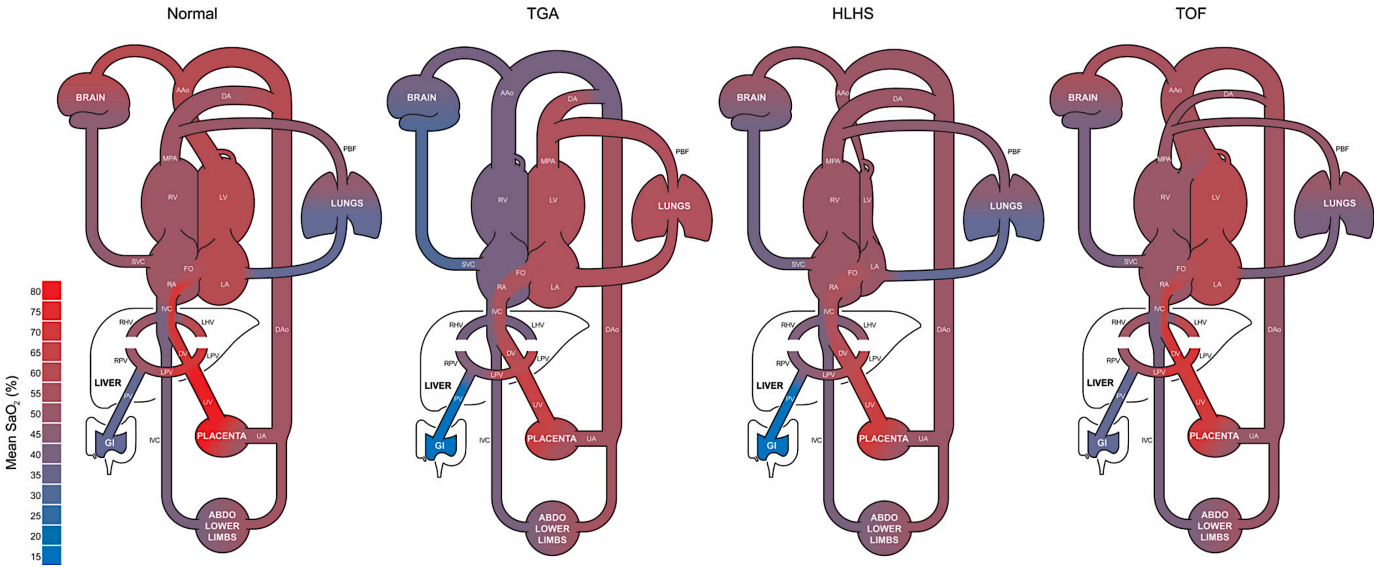

Figure 24 Fetal blood oxygenation in representative examples of transposition of the great arteries (TGA), hypoplastic left heart syndrome (HLHS), and tetralogy of Fallot (TOF).
Reproduced from Sun et al., 2015 with permission of Wolters Kluwer Health, Inc.

coarctation of the aorta, coronary, cerebral and upper body flow must be provided in a retrograde manner from the main pulmonary trunk through the ductus arteriosus, with retrograde flow in the aortic arch. The presence of retrograde flow in the aortic arch can be seen on fetal echocardiography and measured using fetal cardiac MRI. In all cases, the aortic isthmus is relatively small, with varying degrees of hypoplasia. In combination with an overall reduction in combined ventricular output, the whole fetal circulation is supplied by blood of the same oxygen content, resulting in reduced cerebral blood flow and oxygen delivery.

3.4.4 Reduced fetal cerebral oxygen delivery in CHD

Oxygen delivery to the brain in utero relies on both the oxygen content of the blood in the ascending aorta and the cerebral blood flow. There are at least three mechanisms responsible for reduced fetal cerebral oxygen delivery (CDO_2) in CHD. Firstly, structural circulatory defects can cause alterations in normal blood flow that have material effects on the saturation of the blood supplying the brain (Figure 24). As already discussed, structural abnormalities can result in the inability of the fetus to effectively stream oxygenated blood across the foramen ovale towards the cerebral circulation. In TGA, this results in well-oxygenated blood being redirected to the pulmonary circulation rather than the brain, while blood supplying the brain is largely deoxygenated blood returning from the body via the caval veins. In TOF, streaming occurs as normal, but the well-oxygenated blood is diluted by deoxygenated blood

shunting across the ventricular septal defect. In HLHS, there is only one functional ventricle, and so the whole body (including the brain) receives blood of the same oxygen content.

Secondly, suboptimal cardiac output has the potential to cause a reduced total CDO_2. For example, in HLHS, the lack of two functional ventricles results in a reduced combined ventricular output. This has two potential effects: a) the heart is unable to compensate for reduced cerebral oxygenation by increasing cardiac output sufficiently (Donofrio et al., 2003), and b) placental blood flow is likely to be reduced, as the principle driver of placental blood flow is fetal blood pressure (which is dependent on fetal cardiac output), leading to reduced total fetal oxygen delivery in cases with single ventricle hearts (Sun et al., 2015).

Thirdly, umbilical vein oxygen saturations have been shown to be reduced in fetuses with CHD *in vivo* using fetal MRI (Sun et al., 2015), resulting in an overall reduction in oxygen content of the blood delivered to the fetus. This may suggest a degree of abnormal placental function in CHD, and a higher prevalence of a range of placental abnormalities has indeed been reported in infants with CHD (Goff et al., 2011). A histological study of 18 placentas from fetuses with HLHS and 18 gestational age-matched controls found that placentas from pregnancies complicated by fetal HLHS were smaller (447 g vs 538 g, $p=0.02$), and exhibited abnormal parenchymal morphology, with both structural and vascular changes in the villous tree, consistent with placental immaturity (Jones et al., 2015). In addition, this study found an increase in intraparenchymal fibrin deposition, indicating abnormal trophoblast secretion, which could lead to a reduction in available surface area for nutrient and oxygen exchange.

In contrast, an MR imaging study of placental volume between 18 and 39 weeks gestation, in a group of 41 fetuses with mixed CHD vs. 94 healthy controls, found little evidence that placental volume differed between CHD and healthy fetuses during gestation (Andescavage et al., 2015). There were no significant differences in placental volume based on lesion type, cyanotic or acyanotic heart disease, single vs. two-ventricle disease, or reversed/bidirectional flow at the aortic isthmus or ductus. However, with only 8 infants with HLHS, it was arguably underpowered to confirm findings from Jones et al. 2015. The full extent of the effect of CHD on the placenta and its importance therefore remains largely unknown.

3.4.5 Autoregulatory response to reduced cerebral oxygenation

In response to reduced CDO_2, it has been suggested that autoregulatory mechanisms in the fetal brain can vary cerebrovascular resistance to ensure delivery of an appropriate supply of oxygen and other metabolic substrates. Sheep models have shown that arterial oxygen content is an important factor influencing cerebral blood flow (Jones et al., 1981), while fetal hypoxia has been shown to cause a decrease in cerebrovascular resistance in both animal models (Cohn et al., 1974; Kjellmer et al., 1974) and human fetuses (Vyas et al., 1990), resulting in preservation of CDO_2 in the setting of acute hypoxia (Hudak et al., 1986).

In human fetuses subjected to placental insufficiency, studies have shown the presence of an adaptive response known as the 'brain-sparing effect', which involves both an elevated umbilical artery resistance and a lower resistance of the cerebral vasculature in order to maintain adequate cerebral blood flow (Scherjon et al., 1993; Wladimiroff et al., 1987).

Evidence for brain sparing using the cerebral-to-placental resistance ratio (CPR) in CHD has been mixed. Donofrio et al. found that brain sparing occurs in CHD fetuses, with single ventricle conditions most affected (Donofrio et al., 2003). The incidence of CPR <1 was greatest in hypoplastic left ventricle and hypoplastic right ventricle. In contrast, Kaltman et al. found that CPR was similar to normal in CHD (Kaltman et al., 2005), but questioned if this ratio was even appropriate to be used in CHD. The brain sparing effect was originally described in fetuses with placental insufficiency, in fetuses that had structurally normal hearts, and with downstream resistance that was not influenced by fetal haemodynamic effects of obstructive cardiac lesions. Kaltman et al. therefore suggested that caution should be exercised in this population.

Cerebrovascular resistance is measured using the pulsatility index (PI) of the middle cerebral artery (MCA), which is a measure of vascular resistance in the circulatory bed downstream from the point of Doppler sampling. Cerebral vasodilation is detected as a reduction in the pulsatility of blood flow in the MCA. MCA-PI has been shown to be reduced in fetal CHD using Doppler ultrasound (Donofrio et al., 2003; Kaltman et al., 2005). Kaltman et al. showed that fetuses with HLHS had decreased MCA-PI compared to normal fetuses, while fetuses with right-sided obstructive lesions had increased MCA-PI, compared to fetuses with HLHS (Kaltman et al., 2005). They suggested that decreased cerebrovascular resistance in HLHS is a mechanism to

increase cerebral blood flow to compensate for otherwise decreased CDO_2. They also theorised that the increased cerebrovascular resistance in right-sided obstructive lesions is an autoregulatory mechanism to reduce excessive cerebral blood flow resulting from the larger percentage of combined ventricular output that passes through the aorta (since venous return is directed away from the right side). While aortic oxygen saturation in a fetus with a right-sided lesion may be reduced due to intra-cardiac mixing, they suggested that the increased aortic blood flow may actually over-compensate for the decreased arterial oxygen content, requiring autoregulatory mechanisms to increase resistance to compensate.

A retrospective multi-centre study of infants with HLHS found that a lower MCA-PI predicted a better neurodevelopmental outcome at 14 months of age using the BSID II (Williams et al., 2013). This suggests that an autoregulatory response to reduce impedance in the cerebral vasculature and allow increased blood flow in the setting of HLHS may indeed help to compensate for a state of chronic hypoxia.

Quantitative MRI studies of cerebral blood flow (CBF) have had mixed findings. Using arterial spin labelling (ASL), CBF was initially found to be reduced in a cohort of mixed CHD (Licht et al., 2004). However, using phase contrast imaging in fetal subjects, CBF has more recently been shown to be normal in mixed CHD compared to healthy controls (Sun et al., 2015), which is supported by a postnatal study of newborns with mixed CHD that also demonstrated no difference (Lim et al., 2016). The discrepancy may be due to differences in study population case mixes, differing physiology between anaesthetised and sedated subjects, or intrinsic limitations of the two different MR methodologies. A more recent ASL study agreed that global CBF is unchanged in single ventricle neonates compared to controls (Nagaraj et al., 2015), although there were reductions in regional perfusion in the basal ganglia.

Overall, there appears to be consistent evidence that MCA-PI is reduced in CHD in utero, which supports the presence of autoregulatory mechanisms attempting to maintain adequate supply of oxygen and other substrate to the brain. Quantitative cerebral flow studies appear to slightly contradict these findings, with a consensus that fetuses and infants with CHD do not have a significantly different CBF compared to controls, and that reductions in oxygen content of blood supplied to the cerebral circulation are responsible for reduced CDO_2. At present, heterogeneous study groups

and small sample sizes, particularly at the subgroup level, make it hard to draw firm conclusions about cerebral blood flow haemodynamics in CHD.

3.4.6 The impact of reduced cerebral oxygen delivery on brain development

Reduced CDO_2 in utero has been shown to correlate with reduced fetal brain size in third trimester fetuses with CHD (Sun et al., 2015). These findings build upon a previously described study of fetal brain volumes that showed a slowing trajectory of brain growth during the third trimester, which the authors suggested may be a result of acute or chronic oxygen deprivation during this crucial period of development (Limperopoulos et al., 2010).

During the third trimester, there is both a dramatic increase in synapse formation and activity, and an acceleration of cerebral myelination, with increasing demand for metabolic substrate required to support this process (Brody et al., 1987; Hüppi et al., 1998), and blood flow to the brain estimated to represent one quarter of total ventricular output by this stage (Rudolph, 2009). In particular, the cerebral cortex displays accelerated growth and organisation during the third trimester, with dendritic outgrowth, synapse formation and developing cortical connectivity (Kostović and Jovanov-Milosević, 2006), along with a marked three-fold increase in cerebral oxygen consumption and blood flow over the third trimester of gestation in fetal sheep (Gleason et al., 1989). These processes result in an escalating demand on the cardiovascular system to provide adequate resources for normal cerebral development, and an inability to do so will likely slow growth and impair cortical myelination and organisation.

Following birth, CDO_2 continues to be significantly lower than healthy controls (both in absolute value and indexed to brain volume), with the most significant reductions in single ventricle conditions and TGA (Lim et al., 2016). This is perhaps to be expected, as both conditions are known to result in significant cyanosis prior to surgical repair or palliation.

The causative mechanism as to how oxygen might impair brain development in CHD remains unclear, although a number of recent studies have provided new insights into the underlying biology. Important work in the neonatal mouse brain has shown that oxygen tension is an essential regulator of postnatal myelination, mediated via oligodendrocyte precursor cells (OPCs) (Yuen et al., 2014). Oligodendrocytes (OLs)

are the myelinating cells of the central nervous system, and play a finely balanced role in producing normal myelination and angiogenesis. OPC-encoded hypoxia-inducible factor (HIF) function, is an essential regulator of postnatal myelination. Constitutive HIF1/2α stabilisation results in OPC maturation arrest through autocrine activation of canonical Wnt7a/7b. OPCs also show paracrine activity that induces excessive postnatal white matter angiogenesis and directly stimulates endothelial cell proliferation (Yuen et al., 2014). Poor myelination constrains axon outgrowth and synaptogenesis (Fünfschilling et al., 2012), and the integrity of developing axons will be subsequently affected. In addition, mature oligodendrocytes provide metabolic support for axons by supplying ATP, glycolytic substrates, and nutrients (Fünfschilling et al., 2012).

Failure of OPCs to function normally results in cell death, axon damage, and cystic white matter injury, along with severe loss of axons in the corpus callosum (Yuen et al., 2014). Reduced cerebral oxygenation thus results in microstructural abnormalities leading to reduced white matter volume with an overall reduction in size of the brain, associated abnormalities in cortical and deep grey matter, as well as disordered angiogenesis and vascular function. Furthermore, inadequate vascular investment and possible lack of trophic factors for axons in a baby with CHD may result in an immature brain that is more vulnerable to injury during cardiac surgery than a brain that has developed in an environment with normal CDO_2.

The effect of hypoxia on the developing cortex has also been recently investigated using a piglet model with promising results (Morton et al., 2017). The subventricular zone (SVZ) represents the largest source of neural stem/progenitor cells (NSPCs) (Sanai et al., 2005). Morton and colleagues demonstrated that hypoxia reduces proliferation and neurogenesis in the SVZ, which was accompanied by reduced cortical growth. Brains from piglets exposed to perinatal chronic hypoxia had a smaller total brain volume, with a significant reduction in cortical grey matter volume. Animals exposed to hypoxia also had a reduced gyrification index compared to controls, which the authors state were almost identical to those noted in human fetuses with CHD by Clouchoux et al. 2013.

Early progress has been made towards understanding the link between consistent observations of impaired brain development across many decades using numerous different methods and more recent findings of reduced CDO_2 in CHD. Continuing this

work and identifying potential therapeutic targets will be crucial to improving the future neurodevelopmental outcomes in this population.

3.4.7 The impact of cyanosis on neurodevelopmental outcome

While it has only been possible to measure CDO_2 *in vivo* relatively recently, the impact of cyanosis on neurodevelopmental outcomes has been debated for many years. Helen Taussig, in her magnum opus, 'Congenital Malformations of the Heart' (which is generally considered to represent the genesis of paediatric cardiology as an independent field), states that 'extreme anoxaemia does not cause mental retardation' (Taussig, 1947). Campbell and Reynolds reported early data from Guy's Hospital in London about the physical and mental development of children with CHD, finding that degree of cyanosis had a dose-dependent impairment on weight, height, age at walking and age at talking (Campbell and Reynolds, 1949): "in general, the greater the degree of cyanosis, the greater the effect on the patient". However, in terms of intellectual development, they state that "congenital heart disease does not produce any mental deficit or permanent backwardness".

Linde et al. observed that cyanotic children with CHD showed a greater disturbance in growth in weight and height (Linde et al., 1967a). The study also reported "central nervous system disturbance" in cyanotic CHD due to the finding that puberty in these children began as much as 3-4 years after the expected age, and in "very deeply cyanotic" children that puberty had not begun by 18 years of age. A comparison with delayed onset of puberty in children in the Peruvian Highlands led the authors to hypothesise that decreased arterial oxygen saturation may be to blame.

Linde et al. continued to study mental development in CHD, noting that "cyanotic patients scored lower at all ages, particularly in the earlier years, with tests involving gross motor abilities" (Linde et al., 1967b). Overall, cyanotic children performed worse in IQ tests than acyanotic children, who in turn performed worse compared to healthy children and healthy siblings of children with CHD. Linde was keen to mention that while mean IQ scores were reduced, some cyanotic children attained a 'very superior level of intelligence'. The study reports a positive correlation between arterial blood saturation and IQ for children with cyanotic CHD and concludes that lowered arterial oxygen saturation may be a 'primary factor in delay in early mental development'.

A more recent prospective study considered the difference in cognitive function between cyanotic and acyanotic children aged 3.5 – 17 years old before and after surgery (Wray, 2001). They found that children with cyanotic lesions had lower overall IQ scores than acyanotic children, with lower ability levels for mathematics, reading and spelling. The fact that differences between acyanotic and cyanotic children appeared to worsen with age led the authors to suggest that there might be a critical age for correction of cyanotic lesions, after which 'cyanosis and its consequences have deleterious effects on development and cognition' (Wray, 2001).

Confusingly acyanosis has also been found to be a worse predictor of developmental and functional limitations in a prospective study of infants undergoing surgical repair, followed up at 5 years of age (Majnemer et al., 2008). In this study, children with acyanotic lesions had a lower IQ than those with cyanotic lesions. This was attributed to the possibility that acyanotic lesions may be associated with poor cerebral blood flow, beginning in the fetal period and extending until surgical correction. In a separate study, no difference was found in the behaviour and quality of life in 20 children with cyanotic CHD (tetralogy of Fallot) compared to 20 children with acyanotic CHD (VSD), of whom all were operated in infancy, assessed at 7.4 years of age (Hövels-Gürich et al., 2007). Similarly, no difference in neurodevelopmental outcome was noted between acyanotic and cyanotic children in a study assessing 59 children at a median age of almost 14 years of age (Schaefer et al., 2013).

While individual studies through childhood offer conflicting results, a greater consensus is reached in adulthood, although the evidence base is smaller. A recent systematic review identified only five studies of adult survivors of CHD (Tyagi et al., 2014). A consistent finding in four of these studies was that cyanosis and more complex disease were associated with a lower IQ (Daliento, 2005; Utens et al., 1998, 1994; Wernovsky et al., 2000), while the fifth study is less specific and reports only that the CHD group in general had significantly lower IQ scores than healthy controls (Eide et al., 2006). In one of these studies that considered TOF, a history of cyanosis in infancy was associated with greater deficits in executive functioning and complex processing speed (Daliento, 2005). In a more recent mixed cohort of CHD assessed at 18-49 years of age, only those with severe cyanosis performed worse in a range of cognitive tests, while the others were no different on any cognitive measure compared to normative data (Klouda et al., 2016).

3.5 CONCLUSION

Children with CHD are at greater risk of developing neurodevelopmental problems across a range of specific domains. As mortality rates have fallen, and the cohort of CHD survivors grows, such problems have become of increasing importance. Deficits cover domains including motor, cognitive, adaptive functioning, speech and language, and behavioural, with particular prominence in adulthood given to executive function. Despite substantial improvements in surgical and medical care of infants and children with CHD, improvements in neurodevelopmental outcome have been more muted.

Evidence of abnormal early brain development in CHD has progressed from early autopsy findings and head circumference measurements through to sophisticated ultrasound and fetal MRI measures of brain structure, function, and metabolism. Evidence from multiple sources shows a faltering trajectory of brain growth and development in the third trimester at a time when the brain experiences a dramatic increase in metabolic demands. Current explanatory hypotheses converge upon reduced CDO_2 in utero. Early work using fetal MRI has suggested that ascending aorta saturations are reduced in CHD in the third trimester, while animal studies have shown that chronic hypoxia result in reduced myelination, reduced angiogenesis, and reduced proliferation and neurogenesis in the SVZ. Cyanosis has been frequently linked to poorer cognitive and executive function outcomes, and the recent ability to measure CDO_2 *in vivo* offers exciting new opportunities to test these hypotheses.

Chapter 4

Brain injury in congenital heart disease

4.1 ABSTRACT

Objectives Neurodevelopmental impairment has become the most important comorbidity in infants with congenital heart disease (CHD). We aimed to: a) investigate the burden of brain lesions in infants with CHD prior to surgery, and b) explore clinical factors associated with injury.

Study design Prospective observational study.

Setting Single centre UK tertiary neonatal intensive care unit.

Patients 70 newborn infants with major CHD underwent brain MRI prior to surgery.

Main outcome measures Prevalence of cerebral injury including arterial strokes, punctate white matter lesions and haemorrhage; clinical variables associated with injury.

Results Brain lesions were observed in 39% of subjects. Punctate white matter lesions were identified in 33%, subdural haemorrhage without mass effect in 33%, cerebellar haemorrhage in 9%, and arterial infarction in 4%. Punctate lesions were distributed widely throughout the brain, particularly involving the frontal white matter, optic radiations and corona radiata. Punctate lesions exhibited restricted diffusion in 48% of cases and were associated with lower arterial cord pH (7.22 vs 7.30; p=0.03) and days of mechanical ventilation (0-3 vs 0-7 days; p=0.004). Arterial infarction was associated with balloon atrial septostomy (77% vs 23%), lower 1-minute (median 6 vs 9) and 5-minute Apgar scores (8 vs 9), and days of mechanical ventilation (IQR 0-0 vs 2-7 days).

Conclusions Cerebral injury in newborns with CHD prior to surgery is common. Collaborative work between institutions to investigate variation in injury rates may reveal modifiable factors to improve neurodevelopmental outcomes in this population.

This chapter is based upon:, Kelly CJ, Arulkumaran S, Tristão Pereira C, Cordero-Grande L, Hughes EJ, Teixeira RPAG, Steinweg JK, Victor S, Pushparajah K, Hajnal JV, Simpson J, Edwards AD, Rutherford MA, Counsell SJ. Prevalence of brain lesions in newborns with congenital heart disease prior to surgery: an observational study. Submitted.

4.2 INTRODUCTION

Congenital heart disease (CHD) is the most common congenital defect, (Hoffman and Kaplan, 2002) affecting approximately 1% of newborns (EUROCAT, 2015). Historically, few infants born with major CHD survived to adulthood (Mitchell et al., 1971), but advances in diagnostic, interventional and surgical techniques over recent decades have led to dramatic increases in survival (Wren, 2001). Neurodevelopmental impairment has become the most important co-morbidity in this population, with up to half of children with complex CHD experiencing a distinct pattern of neurodevelopmental and behavioural impairment, characterised by mild cognitive impairment, impaired social and communication skills, inattention, and later, deficits in executive function (Marino et al., 2012).

The aetiology of neurodevelopmental impairment in CHD remains poorly understood. It has become clear that neurological insult in CHD begins before surgery, with altered neurological state in the newborn period (Limperopoulos et al., 1999), population studies demonstrating reduced birth weight and head circumference (Matthiesen et al., 2016), and in-utero imaging studies showing a derailed trajectory of brain growth in the third trimester (Clouchoux et al., 2013; Limperopoulos et al., 2010).

Studies of brain injury in pre-surgical newborns have reported lesions including punctate white matter lesions (PWMLs), periventricular leukomalacia, and stroke with a prevalence that varies considerably from 19-52% of cases (Mebius et al., 2017). The cause for such variation between cohorts remains unclear. This study aimed to: 1) characterise brain lesions using MR imaging in a contemporary UK cohort of newborns with major CHD prior to surgery, and 2) assess which clinical factors are associated with brain injury.

4.3 METHODS

4.3.1 Study design and participants

We recruited a prospective cohort of 70 infants with CHD expected to require surgery within one year, born September 2014 – November 2017, from the Neonatal Intensive Care Unit at St Thomas' Hospital, London. Neonates were excluded if there was suspected or confirmed congenital infection or genetic malformation syndrome. The study was approved by the National Research Ethics Service West London committee (07/H0707/105). Informed written parental consent was obtained.

Sequence	TR (ms)	TE (ms)	Flip angle	Acquired voxel size (mm)	Reconstructed voxel size (mm)	Other parameters
Sept 2014 – Nov 2015 (n=18, 26%), Adult 32-channel head coil						
T1-weighted (magnetisation prepared rapid acquisition gradient echo)	17	4.6	13°	0.82 x 0.97 x 1	0.82 x 0.82 x 0.5	TI: 1465 ms
T2-weighted (fast-spin echo)	14,473	160	90°	1.15 x 1.18 x 2	0.86 x 0.86 x 2	-
Diffusion weighted imaging	7,536	49	90°	2 x 2 x 2	1.75 x 1.75 x 2	32 directions, b=0, 750 s/mm^2
Susceptibility-weighted imaging (spoiled gradient-recalled echo)	32	25	12°	0.45 x 0.45 x 1.8	0.4 x 0.4 x 1.8	-
Venogram	18	6.7	10°	0.9 x 0.9 x 2	0.44 x 0.44 x 1	Phase contrast velocity 15 cm/2
Nov 2015 – Nov 2017 (n=52, 74%), Neonatal 32-channel head coil and positioning device (Hughes et al., 2017b)						
T1-weighted (magnetisation prepared rapid acquisition gradient echo)	11	4.6	9°	0.81 x 0.8 x 0.8	0.76 x 0.76 x 0.8	TI: 714 ms
T2-weighted multi-slice turbo spin echo, sagittal and axial, combined in reconstruction	12	156	90°	0.81 x 0.82 x 1.6	0.8 x 0.8 x 0.8	-
Diffusion-weighted imaging (Hutter et al., 2015)	3800	90	90°	1.5 x 1.5 x 3, slice gap -1.5 mm	1.17 x 1.17 x 3, slice gap -1.5 mm	300 directions, b=0, 400, 1000, 2600
Susceptibility-weighted imaging (spoiled gradient-recalled echo)	32	25	12°	0.45 x 0.45 x 1.8	0.4 x 0.4 x 1.8	-
Venogram	18	6.7	10°	0.9 x 0.9 x 2	0.44 x 0.44 x 1	Phase contrast velocity 15 cm/2

Table 1 MRI sequence parameters

4.3.2 MR imaging

MR imaging was performed on a 3-Tesla system (Philips Achieva, Best, Netherlands), situated on the Neonatal Intensive Care Unit at St Thomas' Hospital, as soon as the infant could be safely transferred to the scanner. All examinations were supervised by an experienced paediatrician, and scanned in natural sleep without sedation, as described previously (Hughes et al., 2017b). MRI sequences are described in Table 1, and included a 5 second initial slow ramp-up in acoustic noise to avoid eliciting a startle response. T1-weighted and T2-weighted images were motion-corrected post hoc using a dedicated motion-corrected reconstruction (Cordero-Grande et al., 2018; Lucilio Cordero-Grande et al., 2016; Kuklisova-Murgasova et al., 2012).

4.3.3 Image Review

Images were reported by two neonatal neuroradiologists. All images were subsequently re-reviewed to ensure consistency, and lesions classified (arterial infarction, cerebellar haemorrhage, intraventricular haemorrhage, PWMLs). The location and properties of lesions on T1- and T2-weighted imaging, susceptibility-weighted imaging (SWI) and apparent diffusion coefficient (ADC) map were recorded. Arterial infarcts were defined as occurring within the territory of a major cerebral artery, with restricted diffusion demonstrated as low signal on the ADC map (Rutherford, 2001).

4.3.4 Generation of PWML maps

PWMLs were segmented by a single reader (CTP) from T1-weighted images using ITK-SNAP (Yushkevich et al., 2006), and confirmed by consensus of three authors (SC, CK, CTP). PWMLs were defined as discrete areas of high signal intensity on T1-weighted imaging, usually accompanied by low signal intensity on T2-weighted imaging (Kersbergen et al., 2014; Miller et al., 2003; Wagenaar et al., 2017). T2- and T1-weighted images for each subject were co-registered using a rigid body registration (FLIRT) (Jenkinson and Smith, 2001). A group template was then created from both modalities using symmetric diffeomorphic normalisation for multivariate neuroanatomy and a cross-correlation similarity metric using ANTs (B. Avants et al., 2008). T1-weighted images were non-linearly registered to the template using symmetric diffeomorphic normalisation. These registrations were then used to transform individual lesion maps into template space. Finally, a probabilistic map was calculated from the mean of all lesion maps in template space, visualised using MRtrix3 (Tournier et al., 2012). Descriptive statistics were generated using MATLAB (2015b, MathWorks, US). Total brain volume was calculated using a previously-validated neonatal-specific segmentation pipeline (Makropoulos et al., 2018).

4.3.5 Statistical analysis

Categorical clinical variables were compared using Fisher's exact tests. Continuous variables were tested for normality using the Shapiro-Wilk test. For normally distributed continuous variables, we determined means and standard deviations, and compared groups with the Student's t-test. For non-normal continuous and ordinal

variables, we determined medians and interquartile ranges, and compared groups using the Mann-Whitney U test (P values were not reported for sample sizes less than 5). All analyses were performed using SPSS, V24 (IBM, New York).

4.4 RESULTS

4.4.1 Subject data

We enrolled 70 infants, all of whom were scanned prior to surgery. T1- and T2-weighted images were acquired in 100% of subjects, ADC map in 99% (1 motion corrupted), SWI in 93% (2 motion corrupted, infant awoke in 3), and MRV in 80% (13 awoke before protocol end, 1 poor quality). The median gestational age (GA) at birth was 38.3 weeks (IQR 37.4 – 38.7), and at scan was 39.0 weeks (IQR 38.4 – 39.7). The average age at scan was 5 days (IQR 2-7). Clinical variables are presented in Table 2. No patients experienced birth asphyxia. Antenatal diagnosis of CHD was made in 97% (n=68), of whom all were born at our institution. Both postnatally-diagnosed cases were outborn.

4.4.2 Preoperative brain injury in CHD

Cerebral lesions were identified in 39% (n=27) of cases, including PWMLs in 33% (n=23, Figure 25a), cerebellar haemorrhage in 9% (n=6, Figure 25d), and arterial infarction in 4% (n=3, Figure 25c). Two infants with PWMLs (TGA, pulmonary atresia) had a larger discrete lesion in the deep white matter (Figure 25b). Forty-three infants (61%) had no evidence of lesions, while seven (10%) had more than one lesion type. All cases of arterial infarction were clinically silent, and were located in the left middle cerebral artery territory. There were no cases of sinus venous thrombosis. Asymmetrical transverse sinus flow was noted in 31% of infants (n=22), with reduced left-sided flow in 91% of these (n=20), a common normal anatomical variant (Ayanzen et al., 2000). There were no cases of intraventricular haemorrhage. Other intracranial findings included subdural haemorrhage without mass effect in 33% (n=23, Figure 25e), subependymal cysts in 11% (n=8), cerebellar vermis rotation in 7% (n=5), and extradural haematoma in 1% (n=1, Figure 25f).

Variable	Total (n=70)	No lesion (n=43)	Any lesion (n=27)	P value
Sex				1.0
Female	33 (47%)	20 (61%)	13 (39%)	
Male	37 (53%)	23 (62%)	14 (38%)	
Delivery method				
Normal vaginal delivery	27 (39%)	15 (56%)	12 (44%)	0.46
Forceps vaginal delivery	6 (9%)	4 (67%)	2 (33%)	1.0
Ventouse vaginal delivery	6 (9%)	3 (50%)	3 (50%)	
Emergency caesarean	19 (27%)	14 (74%)	5 (26%)	0.27
Elective caesarean	12 (17%)	7 (58%)	5 (42%)	1.0
Induction of labour	41 (59%)	25 (61%)	16 (39%)	0.67
Prenatal diagnosis	68 (97%)	42 (62%)	26 (38%)	1.0
Outborn	2 (3%)	1 (50%)	1 (50%)	1.0
Gestational age at birth (weeks)	38.3 (37.4-38.7)	38.3 (37.4-38.7)	38.4 (37.6-38.9)	0.45
Gestational age at preoperative MRI (weeks)	39.0 (38.4-39.7)	39.0 (38.3-39.6)	39.3 (38.4-39.9)	0.35
Age at scan (days)	5 (2-7)	5 (2-7)	6 (3-9)	0.15
Birth weight (kg) (mean, SD)*	2.94 (0.57)	2.95 (0.61)	2.94 (0.52)	0.96
Head circumference (cm)	33.5 (32.2-34.5)	33.0 (32.3-34.5)	33.5 (32.0-34.5)	0.91
Apgar score				
1 min	9 (7-9)	9 (8-9)	9 (7-9)	0.33
5 min	9 (9-10)	9 (9-10)	9 (9-10)	0.42
Cord Arterial pH (mean, SD)*	7.29 (0.082)	7.30 (0.065)	7.22 (0.11)	**0.030**
Prostaglandin E2	31 (44%)	16 (52%)	15 (48%)	0.15
Cardiac arrest	0 (0%)	0 (0%)	0 (0%)	n/a
Days mechanical ventilation	0 (0-1)	0 (0-0)	0 (0-2)	**0.029**
Balloon atrial septostomy	13 (19%)	6 (46%)	7 (54%)	0.23
Umbilical	6 (46%)	3 (50%)	3 (50%)	0.67
Femoral	7 (54%)	3 (43%)	4 (57%)	0.42
Heart lesion				
Transposition of the great arteries (TGA)	28 (40%)	18 (64%)	10 (36%)	0.80
Tetralogy of Fallot (TOF)	13 (19%)	10 (77%)	3 (23%)	0.34
Coarctation of aorta (CoA)	11 (16%)	4 (36%)	7 (64%)	0.092
Pulmonary atresia	5 (7%)	2 (40%)	3 (60%)	0.37
Hypoplastic left heart syndrome (HLHS)	4 (6%)	3 (75%)	1 (25%)	1.0
Pulmonary stenosis	3 (4%)	1 (33%)	2 (67%)	0.56
Truncus arteriosus	3 (4%)	2 (67%)	1 (33%)	1.0
Tricuspid atresia	2 (3%)	2 (100%)	0 (0%)	0.52
Large VSD	1 (1%)	1 (100%)	0 (0%)	1.0

Table 2 Clinical characteristics of the CHD cohort.

Data are n (%) or median (IQR), unless otherwise specified. Percentages are column-wise for totals and row-wise for subgroups. “Any lesion” includes arterial infarcts, punctate lesions and cerebellar haemorrhage (there were no cases of intraventricular haemorrhage, and subdural haemorrhage was not included). *denotes normally-distributed variables, summarised by mean and standard deviation (SD).

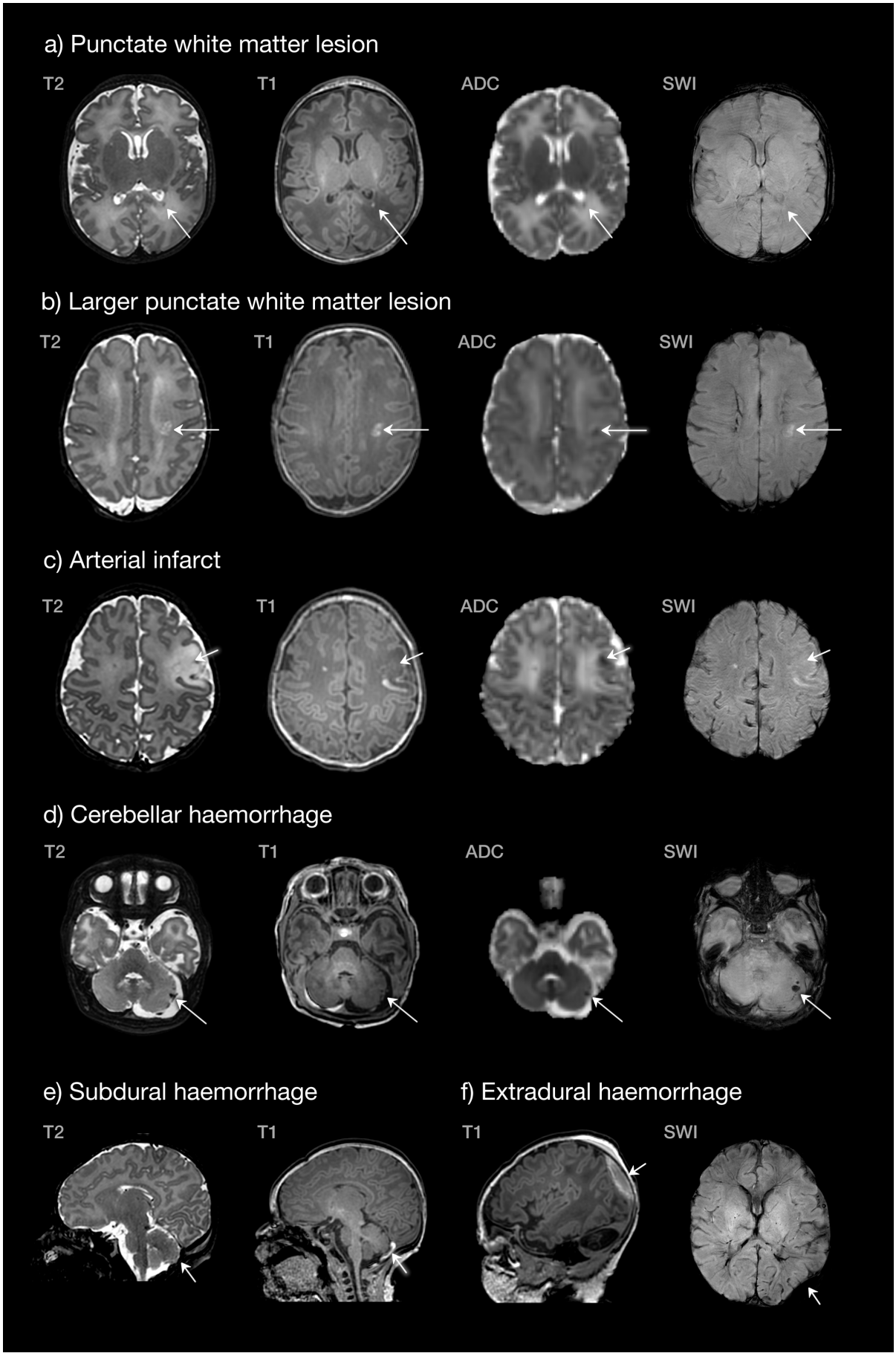

Figure 25 Examples of lesions identified in the congenital heart disease cohort

a) Single punctate white matter lesion in the posterior periventricular white matter (TGA, scanned at 39+6); b) larger punctate white matter lesion in the centrum semiovale (pulmonary atresia, scanned at 37+2); c) left middle cerebral artery infarct (TGA, scanned at 39+5); d) cerebellar haemorrhage (CoA, scanned at 39+3); e) subdural haemorrhage (TGA, scanned at 39+2), f) extradural haemorrhage (CoA, scanned 39+3).

4.4.3 Risk factors for preoperative brain injury

There were no differences in GA at birth between infants with and without any cerebral lesion (p=0.45), PWMLs (p=0.32), or arterial infarcts (p=0.51). There were no differences in the proportion of cases with or without any cerebral injury in infants with abnormal mixing (e.g. TGA; n=34), left-sided lesions (e.g. HLHS, CoA; n=14) and right-sided lesions (e.g. TOF, pulmonary atresia; n=22). However, the only arterial infarcts were in infants with TGA, all of which followed balloon atrial septostomy, but the increase in infarct risk with septostomy was not statistically significant (p=0.09). Arterial infarction occurred in 33% (n=2/6) of infants with septostomy performed via the umbilical vein, compared to 14% (n=1/7) via the femoral vein (Supplemental Table 2). Infants with arterial infarction experienced more days of mechanical ventilation (IQR 2-7 vs 0-0), lower Apgar scores at 1 minute (IQR 6-6 vs 8-9) and 5 minutes (IQR 6-8 vs 9-10). Subdural haemorrhage occurred more frequently with induction of labour (49% vs 10%; p<0.001), normal vaginal delivery (52% vs 21%; p=0.01), ventouse delivery (83% vs 28%; p=0.013), and later GA at birth (p=0.005). Emergency caesarean was associated with reduced risk of subdural (5% vs 43%; p=0.003), with a similar trend observed in elective caesarean (8% vs 38%; p=0.09). PWMLs were associated with increased days of mechanical ventilation (IQR 0-2 vs 0-0; p=0.004) and lower arterial cord pH (7.22 vs 7.30; p=0.03). We did not identify any clinical variables associated with cerebellar haemorrhage.

Genetic testing was performed as part of routine clinical care in 83% of infants (n=58). Microarray was normal in 88% (51/58), with benign copy variant in 7% (4/58) and 22q11 deletion in 5% (3/58). Of those with 22q11, cerebellar haemorrhage was noted in 2/3, cerebellar vermis rotation in 1/3, and PWMLs in 1/3.

4.4.4 Quantitative punctate lesion maps

Quantitative punctate maps were generated from 22 cases (1 infant excluded due to slight motion). PWMLs were distributed widely throughout the brain, involving the frontal white matter, optic radiations, centrum semiovale, and corona radiata (Figure 26). PWMLs exhibited both restricted (48%) and normal (52%) signal on ADC maps, with no significant difference in days of age at scan between groups (p=0.35). There were no cases of haemorrhagic PWMLs identified using SWI. Punctate lesion volume

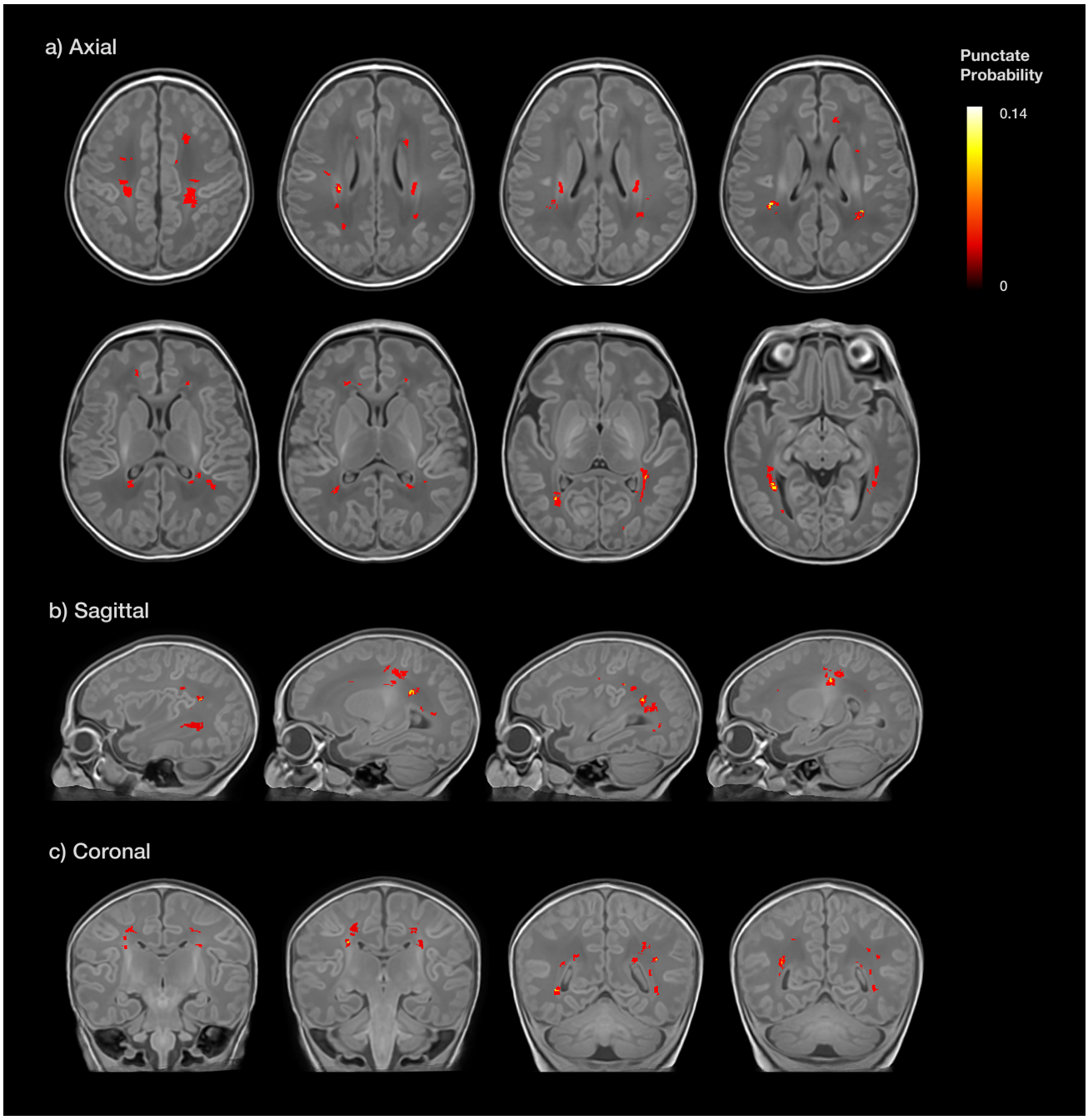

Figure 26 Location of punctate lesions (n=22 included), superimposed onto a T1-weighted group template.
Lesions are demonstrated throughout the white matter including the frontal white matter, optic radiations, centrum semiovale, and corona radiata. A three-dimensional representation of this figure is available at http://goo.gl/uRFaMR

was not statistically associated with any clinical variable, which persisted after removing two outliers with large punctate burdens (CoA n=1, TGA n=1).

4.5 DISCUSSION

To our knowledge, this is the first prospective observational neuroimaging study in the UK of infants with CHD prior to surgery. We found cerebral lesions in 39% of cases. Punctate white matter injury was the predominant lesion type, with few arterial

Study	Date, Location	TGA n	BAS %	Any injury	Punctate WMI %	Arterial infarct %	Subdural %	GA at birth	Out-born %	Antenatal diagnosis %
This study	Sept 14 – Nov 17 ECH, UK	28	46% (13/28)	36% (10/28)	32% (9/28)	11% (3/28)	39% (11/28)	38.5 (IQR 38.1-38.7)	4% (1/28)	96% (27/28)
McQuillen 2006 (McQuillen et al., 2006)	Sept 01 – 05 UBC	29	66% (19/29)	41% (12/29)	7% (2/29)	17% (5/29)	10% (3/29)	-	-	-
Beca 2009 (Beca et al., 2009)	2005 – 2008 SCH Auckland & RCH Melbourne	44	75% (33/44)	30% (13/44)	27% (12/44)	5% (2/44)	-	39 (SD 1.4)	-	14/44 = 32%
Block 2010 (Block et al., 2010)	Sept 01 – Mar 08 UCSF & UBC	62	73% (45/62)	45% (28/62)	21 (13/62)	29% (18/62)	14% (13/92), incl HLHS	39 (IQR 38-40), incl HLHS	-	-
Dimitropoulos 2013 (Dimitropoulos et al., 2013)	Sept 01 – Dec 09 UCSF & UBC	71	76% (54/71)	45% (32/71)	21% (15/71)	24% (17/71)	-	39.3 (weighted median)	68% (81/120) incl other CHD	33% (40/120), incl other CHD
Mulkey 2013 (Mulkey et al., 2013)	Jun 09 – Jun 11 Arkansas CH	14	-	47% (34/73)	-	-	-	-	-	-
Bertholdt 2014 (Bertholdt et al., 2014)	Nov 09 – Jan 12, UCHZ Zurich	22	82% (18/22)	54% (12/22)	27% (6/22)	14% (3/22)	27% (6/22)	40.3 (range 37-.9-42.7)	100%	17% (5/30)
Desai 2015 (Desai et al., 2015)	Aug 09 – Apr 13, Emory, Atlanta	6	-	-	17% (1/6)	-	-	-	-	-
Peyvandi 2016 (Peyvandi et al., 2016)	Sept 01 – 13 UCSF & UBC	96	-	39% (37/96)	21% (20/96)	25% (24/96)	-	Mean 38.9, incl other CHD	52% (80/153)	44% (67/153)
Brossard-Racine 2016 (Brossard-Racine et al., 2016)	Feb 07 – Dec 10 BCH Boston; Jun 11 – Oct 14 CNMC Washington DC	31	48% (15/31)	29% (9/31)	15% (15/103), incl all CHD	3% (3/103), incl all CHD	-	38.5 (SD 1.3), incl all CHD	-	100%
Peyvandi 2017 (Peyvandi et al., 2017)	Sept 01 – 2014 UCSF	49	61% (30/49)	35% (17/49)	14% (7/49)	25% (12/49)	-	39.2 (38.8-39.6)	-	-

Table 3 Comparison of TGA injury rates and characteristics across cohorts

A summary of the TGA components of recent MRI studies to compare injury prevalence across cohorts.

infarcts. PWMLs occurred at a rate over three times higher than in healthy term infants scanned at our institution (Hughes et al., 2017a), with a widespread distribution including frontal white matter, optic radiations, and corona radiata. Brain injury occurred at similar rates in each diagnostic subgroup, and injury was associated with risk factors likely to reflect haemodynamic stability at birth, including arterial cord pH, days of mechanical ventilation, and lower 1 and 5-minute Apgar scores.

Comparisons between cohorts are complicated by the heterogeneity of CHD studies but can be simplified by considering only infants with TGA, who are both well-represented in pre-operative imaging studies and associated with fewest

comorbidities (Table 3). The rate of PWMLs in infants with TGA in this study is consistent with other cohorts, which range from 14%-32% (Beca et al., 2009; Bertholdt et al., 2014; Desai et al., 2015; Peyvandi et al., 2017). The incidence of arterial infarcts has been reported between 5%-29% (Beca et al., 2009; Bertholdt et al., 2014; Block et al., 2010; Dimitropoulos et al., 2013; Peyvandi et al., 2017), with our cohort at the lower end of this range.

We found no cases of venous sinus thrombosis. The placement of central venous catheters in the internal jugular vein has been associated with increased risk of venous sinus thrombosis (Claessens et al., 2017). In contrast to that study (Claessens et al., 2017), our neonatal unit does not place subclavian or internal jugular vein catheters preoperatively, preferring instead umbilical venous catheters or peripherally-inserted long lines. The absence of venous sinus thromboses in our cohort supports the view that internal jugular vein lines should be avoided in this population. We hypothesise that similar differences in clinical practice may reveal other important potential modifiable factors.

The higher burden of PWMLs in our study may be explained, at least in part, by a scan resolution that is higher than many comparable studies, potentially allowing smaller lesions to be discerned. However, this would not explain our low incidence of arterial stroke. Different local definitions of stroke, focal stroke, white matter injury, periventricular leukomalacia, and punctate white matter injury may be responsible, and accurate comparisons are difficult without a consistent approach across institutions.

We evaluated clinical parameters associated with cerebral lesions. We found that PWMLs were associated with lower arterial cord pH, and that arterial infarction was associated with lower 1 and 5-minute Apgar scores, days of mechanical ventilation until time of scan, and balloon atrial septostomy. Comparison of clinical variables with published cohorts is limited by detail available from previous studies. In our cohort, almost all infants were inborn at a tertiary cardiac centre and prenatally diagnosed. Infants with prenatal diagnoses of complex CHD are known to have significantly less preoperative brain injury, thought to be due to improved cardiovascular stability following delivery (Peyvandi et al., 2016).

Subdural haemorrhage is common during term delivery, with an overall incidence of 8 – 15% (Hughes et al., 2017a; Whitby et al., 2004), and up to 28% in complicated

instrumental deliveries (Whitby et al., 2004). In our cohort, subdural haemorrhage occurred five times more frequently than reported in healthy normal vaginal delivery, and ten times more frequently in ventouse delivery (Whitby et al., 2004). At our institution, mothers who do not live locally are induced at around 38 weeks' gestation, while spontaneous labour is preferred for those living nearby. Induction was associated with a rate of subdural haemorrhage almost five times higher than in spontaneous onset of labour, which may partly be related to instrumental delivery being used over three times more frequently in this group. This association between induction and instrumental delivery contrasts with studies of healthy infants (Caughey et al., 2009), and may be explained by a lower threshold for instrumental intervention in labours complicated by CHD, or potentially the use of induction at earlier GAs.

The timing of pre-operative injury in CHD remains uncertain. Fetal MRI studies have not yet reported arterial strokes in utero, and few studies have identified white matter abnormalities prenatally (Brossard-Racine et al., 2016; Limperopoulos et al., 2010). However, perinatal and postnatal injury is likely preceded by a period of abnormal brain development in utero, with reduced cerebral substrate (Rudolph, 2016) and oxygen delivery (Lauridsen et al., 2017; Sun et al., 2015), altered metabolism (Limperopoulos et al., 2010), and a derailed trajectory of fetal brain development in the third trimester (Clouchoux et al., 2013; Limperopoulos et al., 2010). Following birth, there are continued metabolic disturbances (Miller et al., 2007, 2004) and alterations in cerebral oxygen delivery (Kelly et al., 2017; Lim et al., 2016). This chronic impairment may increase susceptibility to ischaemic injury around the time of delivery, a timeline that is supported by the finding that half of our cases exhibited PWMLs with restricted diffusion. If ischaemic, this would suggest an acute insult, although other aetiologies are possible for restricted diffusion, including clusters of activated microglia resulting in increased cellularity (Niwa et al., 2011; Rutherford et al., 2010).

PWMLs were distributed throughout the white matter, in contrast to preterm infants where PWMLs are predominantly observed in the centrum semiovale and corticospinal tracts (Nanba et al., 2007; Tusor et al., 2017). While inflammatory and hypoxic-ischaemic injury to susceptible premyelinating oligodendrocytes (Segovia et al., 2008) may be responsible in both groups, it is possible that spatial differences in lesion distribution reflect developmental differences in the regional vulnerability of premyelinating oligodendrocytes between preterm infants and term infants with CHD. This vulnerability may be compounded by ischaemic vulnerability due to

periventricular vascular anatomy, or by vascular congestion in the path of the medullary veins, leading to small venous infarcts, which may be responsible for the imaging appearances in the two infants with larger PWMLs.

Interestingly, all arterial infarcts in our study occurred following balloon atrial septostomy. There was no statistically increased risk of infarction in this group, although samples sizes were too small to form strong conclusions. Septostomy has been associated with an increased risk of cerebral infarction in some published studies (Dimitropoulos et al., 2013; McQuillen et al., 2006), but not in others (Beca et al., 2009; Bertholdt et al., 2014; Petit et al., 2009). All three arterial infarcts in our group were in the left middle cerebral artery territory, consistent with previous findings (Beca et al., 2009; Block et al., 2010). Prediction of hypoxemia by prenatal echocardiography has proved difficult (Vigneswaran et al., 2017), and need for septostomy is generally assessed postnatally by the clinical team. It is therefore plausible that infants requiring septostomy will have experienced the greatest burden of hypoxia and cardiovascular instability after birth, and are most at risk of cerebral injury. The use of the umbilical vein has been implicated in displacement of pre-existing thrombus from the ductus venosus or hepatic vein during septostomy, increasing the risk of arterial embolic infarction (Chandar and Wolfe, 1994). In this study, the umbilical route was associated with a greater proportion of arterial stroke compared to femoral, although sample sizes were small. Previous studies showed no clear difference between the use of the femoral or umbilical vein (Dimitropoulos et al., 2013; McQuillen et al., 2006).

There were limitations to our study. The heterogeneous nature of the cohort and relatively small subgroup sample sizes hampered our ability to compare risk factors across groups. All infants were from a single centre, and almost all infants had been diagnosed antenatally and were inborn. Comparisons of our results to other centres were made difficult by the variable detail of clinical parameters in previous studies, and variability in radiological definitions across sites.

4.5.1 Conclusions

Cerebral lesions in newborns with CHD prior to surgery are common and are likely to reflect acute injury to a vulnerable brain around the time of delivery. Injury rates show considerable variability between different centres, and large multicentre collaborations

to compare practices may reveal important modifiable factors to improve neurodevelopmental outcomes in this at-risk population.

Chapter 5

Impaired development of the cerebral cortex in infants with congenital heart disease is correlated to reduced cerebral oxygen delivery

5.1 ABSTRACT

Neurodevelopmental impairment is the most common comorbidity associated with complex congenital heart disease (CHD), while the underlying biological mechanism remains unclear. We hypothesised that impaired cerebral oxygen delivery (CDO_2) in infants with CHD is a cause of impaired cortical development, and predicted that cardiac lesions most associated with reduced CDO_2 would demonstrate the greatest impairment of cortical development. We compared 30 newborns with complex CHD prior to surgery and 30 age-matched healthy controls using brain MRI. The cortex was assessed using high resolution, motion-corrected T2-weighted images in natural sleep, analysed using an automated pipeline. CDO_2 was calculated using phase contrast angiography and pre-ductal pulse oximetry, while regional cerebral oxygen saturation was estimated using near-infrared spectroscopy. We found that impaired cortical grey matter volume and gyrification index in newborns with complex CHD was linearly related to reduced CDO_2, and that cardiac lesions associated with the lowest CDO_2 were associated with the greatest impairment of cortical development. These findings suggest that strategies to improve CDO_2 may help reduce brain dysmaturation in newborns with CHD, and may be most relevant for children with CHD whose cardiac defects remain unrepaired for prolonged periods after birth.

This chapter is based upon:

C. J. Kelly, A. Makropoulos, L. Cordero-Grande, J. Hutter, A. Price, E. Hughes, M. Murgasova, R. P. A. G. Teixeira, J. K. Steinweg, S. Kulkarni, L. Rahman, H. Zhang, D. C. Alexander, K. Pushparajah, D. Rueckert, J. V. Hajnal, J. Simpson, A. D. Edwards, M. A. Rutherford, S. J. Counsell, Impaired development of the cerebral cortex in infants with congenital heart disease is correlated to reduced cerebral oxygen delivery., *Sci. Rep.* **7**, 15088 (2017).

5.2 INTRODUCTION

Congenital heart disease (CHD) is the most common congenital disorder in newborns, affecting approximately 1% of births (van der Bom et al., 2011). Of these, approximately half will have severe or moderately severe forms of CHD that require expert cardiology care at birth (Hoffman and Kaplan, 2002). Survival rates through adolescence have improved dramatically (Wernovsky, 2008), and neurodevelopmental impairment has now become the most important comorbidity in this growing population of survivors. Up to half of children with complex CHD experience a distinct pattern of neurodevelopmental and behavioural impairment, characterised by mild cognitive impairment, impaired social and communication skills, inattention, impulsive behaviour and later, impaired executive function (Marino et al., 2012).

Understanding of the biological mechanisms underlying neurodevelopmental delay in this population remains limited. Early animal catheterisation studies suggested that fetal cerebral oxygen delivery (CDO_2) is reduced in CHD, particularly in transposition of the great arteries (TGA) and left-sided lesions (Heymann and Rudolph, 1972). Advances in fetal MRI have since demonstrated a 10% reduction in ascending aortic saturations in a mixed group of CHD (Sun et al., 2015), which may impair normal oligodendrocyte maturation in the developing brain (Yuen et al., 2014).

Brain “immaturity” has been described in CHD before surgery (Licht et al., 2009) using a radiologist-graded scoring system (Childs et al., 2001), and has been associated with impaired neurodevelopment at 2 years of age in children with CHD (Beca et al., 2013). An objective marker of the developing brain’s cortical folding is the gyrification index, first described in the context of autopsy specimens (Elias and Schwartz, 1969; Zilles et al., 1988), and has been shown to increase markedly over the third trimester and during early infancy (Armstrong et al., 1995). Gyrification index may be an important metric when studying neurodevelopment in this population: reduced gyrification index of newborns with CHD has been demonstrated in autopsy specimens (Glauser et al., 1990b), fetal MR imaging studies (Clouchoux et al., 2013), and neonatal MR imaging studies (Claessens et al., 2016; Ortinau et al., 2013), although all studies to date have required varying degrees of manual input, and neonatal studies to date have not attempted to quantify regional differences or to correlate cortical development with cerebral oxygenation delivery.

We hypothesised that impaired CDO_2 in infants with CHD is a cause of impaired cortical development, and predicted that cardiac lesions most associated with most reduced CDO_2 would demonstrate the greatest impairment of cortical development. We aimed to compare the cortex of newborns with CHD prior to surgery versus healthy control infants, assessing cortical folding, cortical grey matter volumes and cerebral blood flow calculated from high resolution magnetic resonance imaging (MRI).

5.3 METHODS

The project was approved by the National Research Ethics Service West London committee (CHD: 07/H0707/105, Controls: 14/LO/1169) and informed written parental consent was obtained prior to imaging. All methods and experiments were performed in accordance with relevant guidelines and regulations.

5.3.1 Participants

A prospective cohort of 33 infants born with complex CHD requiring surgery within one year was recruited from the Neonatal Intensive Care Unit at St Thomas' Hospital, London. Two infants were found to have neonatal arterial ischaemic stroke on MRI (left parietal stroke (n=1) and left frontal stroke (n=1); both TGA post-septostomy) and were excluded from this analysis. A further infant (TGA) was excluded due to unknown date of last menstrual period and lack of ultrasound dating scan.

We therefore studied 30 infants with CHD, born at a median (range) gestational age (GA) of 38^{+3} (34^{+6}-40^{+4}) weeks. A group of healthy controls was matched by GA at birth and at scan, contemporaneously recruited from the postnatal ward at St Thomas' Hospital through the Developing Human Connectome Project (Hughes et al., 2017b), born at a median (range) GA of 38^{+6} (35^{+2}-40^{+6}) weeks. The median GA at imaging was 39^{+2} (37^{+3} - 41^{+4}) weeks for the CHD group and 39^{+1} (36^{+1} - 41^{+6}) weeks for the control group.

5.3.2 MR imaging

T2-weighted, T1-weighted and phase contrast angiography MR imaging was performed on a Philips Achieva 3 Tesla system (Best, The Netherlands) with a 32-channel neonatal head coil and neonatal positioning device (Hughes et al., 2017b),

Variable	Control Newborns n = 30	Newborns with Congenital Heart Disease, n = 30	p value
Gestational age at birth (weeks)	38.9 (38.1 – 39.3)	38.4 (37.9 – 38.9)	0.07
Post-menstrual age at scan (weeks)	39.1 (38.7 – 39.7)	39.3 (38.7 – 39.6)	0.81
Male	16	8	0.06
Birth weight (g)	3220 (2920 – 3550)	3125 (2800 – 3500)	0.37
Birth weight z-score	-0.02 (-0.39 – 0.5)	-0.17 (-0.77 – 0.49)	0.69
Birth head circumference (cm)	34.5 (33 – 35.5)	34 (33 – 35)	0.24
Birth head circumference z-score	0.72 (-0.06 – 1.20)	0.05 (-0.49 – 0.76)	0.11
Heart lesion – no. (%)			
- Transposition of the great arteries (TGA)	-	14 (47)	
- TGA requiring septostomy (% TGA)		5 (36)	
- Coarctation of the aorta	-	4 (13)	
- Hypoplastic left heart syndrome	-	3 (10)	
- Tetralogy of Fallot	-	3 (10)	
- Pulmonary atresia	-	3 (10)	
- Pulmonary stenosis	-	2 (7)	
- Truncus arteriosus	-	1 (3)	

Table 4 Cohort characteristics for macrostructural analysis

GA at birth and PMA at scan are presented as median (interquartile range). Apgar scores reflect condition at birth, ranging from 0 to 10, with lower scores indicating a worse clinical condition. p values calculated using Mann-Whitney U test for continuous data, and Fisher's exact test for categorical variables. z-scores for head circumference and birth weight calculated using UK-WHO 2006 reference data.

situated on the neonatal intensive care unit at St Thomas' Hospital, London. All examinations were supervised by a paediatrician experienced in MR imaging procedures. All infants were scanned in natural sleep without sedation. Pulse oximetry, respiratory rate, temperature and electrocardiography were monitored throughout. Ear protection comprised earplugs moulded from a silicone-based putty (President Putty, Coltene Whaledent, Mahwah, NJ, USA) placed in the external auditory meatus, neonatal earmuffs (MiniMuffs, Natus Medical Inc, San Carlos, CA, USA) and an acoustic hood positioned over the shell. All sequences included a 5 second initial slow ramp-up in acoustic noise to avoid eliciting a startle response.

T2-weighted images were acquired using a multi-slice turbo spin echo (TSE) sequence, acquired in two stacks of 2D slices (in sagittal and axial planes), using parameters: TR: 12 s; TE: 156 ms, flip angle: 90°, slice thickness: 1.6 mm acquired with an overlap of 0.8 mm; in-plane resolution: 0.8x0.8 mm, scan time: 3:12 min per stack. The T1-weighted volumetric magnetisation prepared rapid acquisition gradient echo (MPRAGE) acquisition parameters were as follows: TR: 11 ms, TE: 4.6 ms, TI:

713 ms, flip angle:9°, acquired voxel size:0.8×0.8×0.8mm, FOV:145×145×108mm, SENSE factor:1.2, scan time:4:35min. Quantitative flow imaging was performed using velocity sensitised phase contrast imaging, with a single-slice T1-weighted fast field echo sequence. Scan parameters were: field of view (FOV): 100x100 mm^2, acquisition resolution: 0.6x0.6x4.0mm^2, TR: 6.4 ms, TE: 4.3 ms, flip angle: 10°, 20 repetitions, maximal encoding velocity (vENC): 140cm/s, scan time: 71s.

5.3.3 Structural image reconstruction

T2-weighted images were reconstructed following the scan using a dedicated motion correction algorithm. Retrospective motion-corrected reconstruction (Cordero-Grande et al., 2018; Cordero-Grande et al., 2016) and integration of the information from both acquired orientations (Kuklisova-Murgasova et al., 2012) were used to obtain 0.8 mm isotropic T2-weighted volumes with significantly reduced motion artefacts.

5.3.4 Brain region and tissue segmentation

Motion-corrected T2-weighted images were segmented into tissue type and 87 brain regions using an automated, validated, neonatal-specific pipeline (Makropoulos et al., 2016, 2014) based on the Expectation–Maximisation (EM) technique (Van Leemput et al., 1999), which was optimised for our acquisition parameters. For more details on the individual parts of the segmentation pipeline, we refer the reader to (Makropoulos et al., 2018, 2016, 2014). Each tissue segmentation was manually inspected for accuracy using ITK-SNAP (Yushkevich et al., 2006), and minor corrections performed if necessary.

5.3.5 Gyrification index calculation

Gyrification index was defined as the ratio of the cortical pial surface area and the surface area of the superficial surface enclosing the pial surface (Armstrong et al., 1995; Luders et al., 2006; Zilles et al., 1988). This ratio was calculated for each subject using pial surfaces constructed from the combined grey/white matter mask derived from the segmentations, using a previously-published method (Schuh et al., 2017), as demonstrated in Figure 27. Final cortical surfaces were cleaned using median filtering

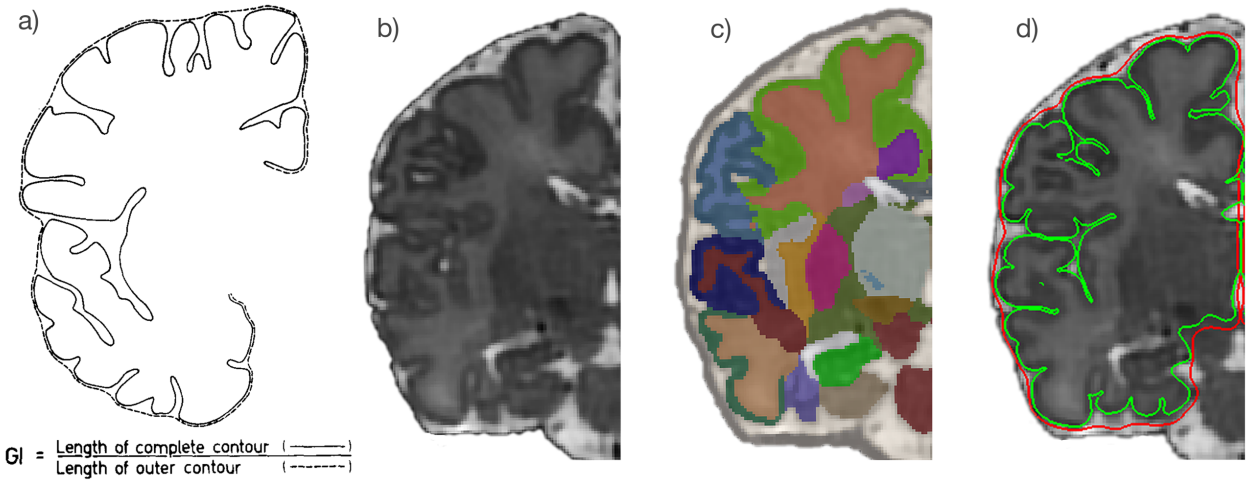

Figure 27 Demonstration of the calculation of gyrification index.

a) Original description of gyrification index in histology setting (Zilles et al., 1988), **b**) Neonatal brain-extracted T2 volume, **c**) Automatic segmentation, **d**) Pial surface mesh (green) and superficial surface (red) created from the segmentation, used to calculate the gyrification index. Figure 3a reproduced from The human pattern of gyrification in the cerebral cortex, Zilles, K., Armstrong, E., Schleicher, A. & Kretschmann, H. J. Anat. Embryol. (Berl). 179, 173–179 (1988). Copyright Springer-Verlag 1988. With permission of Springer.

and Laplacian smoothing. The superficial surface was reconstructed using marching cubes from the morphologically closed combined grey/white matter mask. Morphological closing (performed by 3 dilations followed by 2 erosions) removed small sulci and generated a mask that enclosed the original cGM/WM mask. The gyrification index was calculated initially for the whole brain, and then separately for each major brain region (frontal, parietal, temporal, occipital), using appropriate combinations of the 87 segmented brain regions (Makropoulos et al., 2018).

5.3.6 Cerebral blood flow and cerebral oxygen delivery

To calculate cerebral blood flow, we used a previously-published scanning protocol, acquired in a plane perpendicular to both internal carotid and basilar arteries, at the level of the sphenoid bone (Varela et al., 2012), as demonstrated in Figure 28.

Regions of interest were drawn manually around the three vessels, using Segment v2.0 R4800 (Heiberg et al., 2010), and flow curves generated (Figure 28). An estimate of total cerebral blood flow (CBF) was calculated from the sum of these vessels. This disregards blood flow to some areas of the cerebellum, which is provided by branches of the vertebral arteries and constitutes less than 3% of the total flow to the brain in healthy adults (Nagasawa et al., 2000).

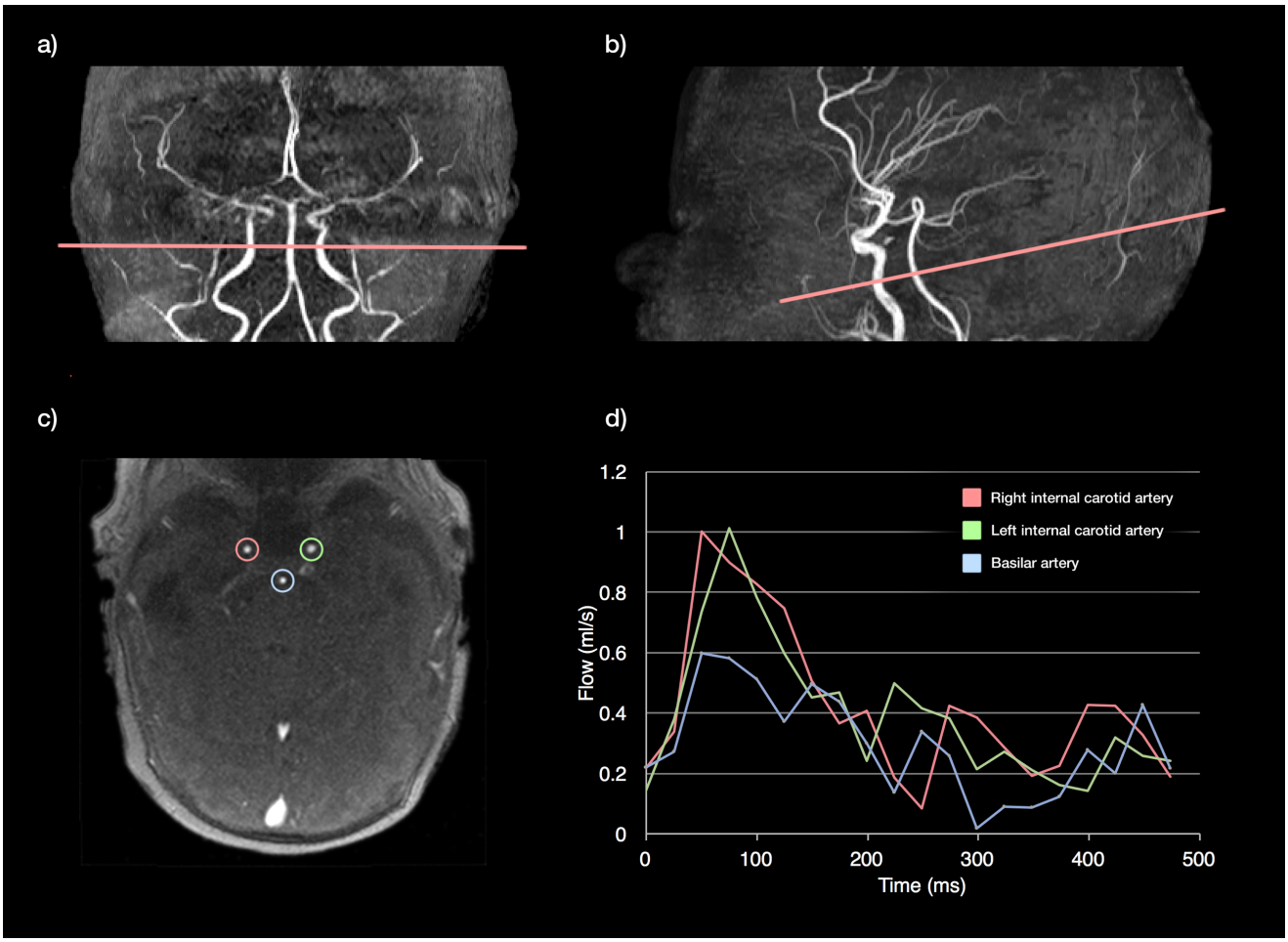

Figure 28 Phase contrast measurements of the cerebral vessels in the neonatal brain.
The plane is planned from a 3D non-contrast angiogram in both coronal (**a**) and sagittal planes (**b**, aiming for the C4 segment of the internal cerebral arteries (ICA) where all three vessels are running approximately parallel). Following the scan, regions of interest are drawn around the three major cerebral vessels: left (green) and right (red) ICAs, and basilar artery (blue), and these regions are propagated through the cardiac cycle (**c**). Flow curves can then be derived across the cardiac cycle (**d**).

Haemoglobin (Hb) levels were measured as part of routine clinical care in all patients at a median of 4 days (range 0 – 10 days) prior to the scan. All newborns with more infrequent Hb monitoring were clinically stable, and we believe all Hb measurements used were representative of levels at time of scan. Arterial oxygen saturation (SaO_2) was measured at the time of scan using a Masimo Radical-7 monitor (Masimo Corp, Irvine, CA) applied to the right hand.

Cerebral oxygen delivery (CDO_2) was calculated using the following formulae (McLellan and Walsh, 2004):

$$CDO_2 \text{ (ml O2/min)} = SaO_2 \text{ x [Hb] (g/dL) x 1.36 x [CBF] (ml/min)}$$

where 1.36 is the amount of oxygen bound per gram of haemoglobin at 1 atmosphere (Hüfner's constant) (Lim et al., 2016).

5.3.7 Regional cerebral oxygen saturation ($rScO_2$)

All newborns had near-infrared spectroscopy $rScO_2$ estimations performed immediately after the scan using a FORE-SIGHT Elite cerebral oxygenation monitor (Casmed, Branford, CT, USA) with neonatal sensor, which was placed over the left frontal region. Measurements were taken for at least three minutes with a sampling frequency of 2 seconds. The output was analysed to obtain mean and standard deviation using a script written in Python (Python Software Foundation, https://www.python.org/). To assess repeatability, the measurement was repeated in a subset of subjects, by disconnecting and removing the sensor from the baby, and reapplying it in a similar location.

5.3.8 Statistical analysis

We automatically matched healthy newborns with babies born with congenital heart disease using an automated method that minimises overall group Euclidean distances between GA and PMA, written in Matlab (R2016, The MathWorks, Inc., Natick, MA, US). We compared group characteristics in newborns with CHD to the healthy control group with the Mann–Whitney U test for continuous data, and Fisher's exact test for categorical variables. Analysis of Covariance (ANCOVA) tests were performed to assess volumetric measurements and gyrification index differences between groups; PMA at scan was included as a covariate. For subsequent regional analyses, outside of the primary hypothesis test, multiple comparisons correction was not performed. Agreement between consecutive readings of rScO2 was analysed using Pearson correlation. Regression analysis was used to compare CDO_2 to brain parameters. Z-scores for birth weight and head circumference were calculated using the SITAR R package (Cole, 2017), using UK-WHO 2006 population reference data (Cole et al., 1998; World Health Organisation, 2006). Statistical analysis was performed with SPSS Statistics v24 (IBM) and graphs were prepared using R Studio (v1.0.136, RStudio Inc, Boston MA). Three-dimensional visualisations were performed in ParaView (Ahrens et al., 2005).

5.4 RESULTS

5.4.1 Demographics

There were no significant differences in GA at birth or at scan between newborns with CHD and healthy controls. There were no significant differences in birthweight, birthweight z-score, head circumference at birth, head circumference z-score, and sex between groups. There were no sex-based differences in total grey matter volume, gyrification index, CDO_2 or regional cerebral oxygen saturations. A summary of CHD diagnoses can be seen in Table 4.

5.4.2 Cerebral oxygen delivery (CDO_2) is positively associated with brain volume and gyrification

Phase contrast measurements, preductal arterial saturations and haemoglobin levels were successfully obtained in 24 of 30 babies with CHD (mean 161, SD 21 g/L). Calculated CDO_2 (median 1638 ml O_2/min, range 1011 – 3023 ml O_2/min) showed a positive association with total brain volume (R^2=0.42, p<0.001), grey matter volume (R^2=0.48, p<0.001, Figure 29a), and whole brain gyrification index (R^2=0.279, p=0.008, Figure 29b). A secondary analysis included days of mechanical ventilation and requirement for prostaglandin E2 in the regression model with no significant effect on the results for brain volume, grey matter volume or gyrification. Indexing CDO_2 per unit of brain volume retained the same trends as without indexing, but weakened both the association with grey matter volume (R^2 = 0.199, p = 0.029, Figure 29c) and with gyrification index (R^2 = 0.127, p = 0.087, Figure 29d).

To understand the relative contribution of CBF and oxygen saturations to CDO_2, we compared correlations between both factors and CDO_2 (Supplementary Figure S1). CBF was more strongly correlated with CDO_2 (R^2=0.643, p < 0.001) than arterial saturations (R^2 = 0.107, p = 0.119), suggesting that blood flow contributed more to the values seen for CDO_2. Subgroup analysis of cerebral haemodynamics by lesion physiology was hampered by small sample sizes, although there was a trend towards higher cerebral blood flows and oxygen delivery in right sided lesions and lower in CHD with abnormal mixing.

Regional cerebral oxygen saturation ($rScO_2$) was measured in all 30 babies with CHD. Consecutive repeat measurements were obtained in 24 of the 30 babies,

demonstrating good repeatability (linear R^2=0.86, p<0.001). $rScO_2$ showed a modest correlation with both whole brain gyrification index (R^2=0.17, p=0.023, Figure 29e), and grey matter volume (R^2=0.21, p=0.011).

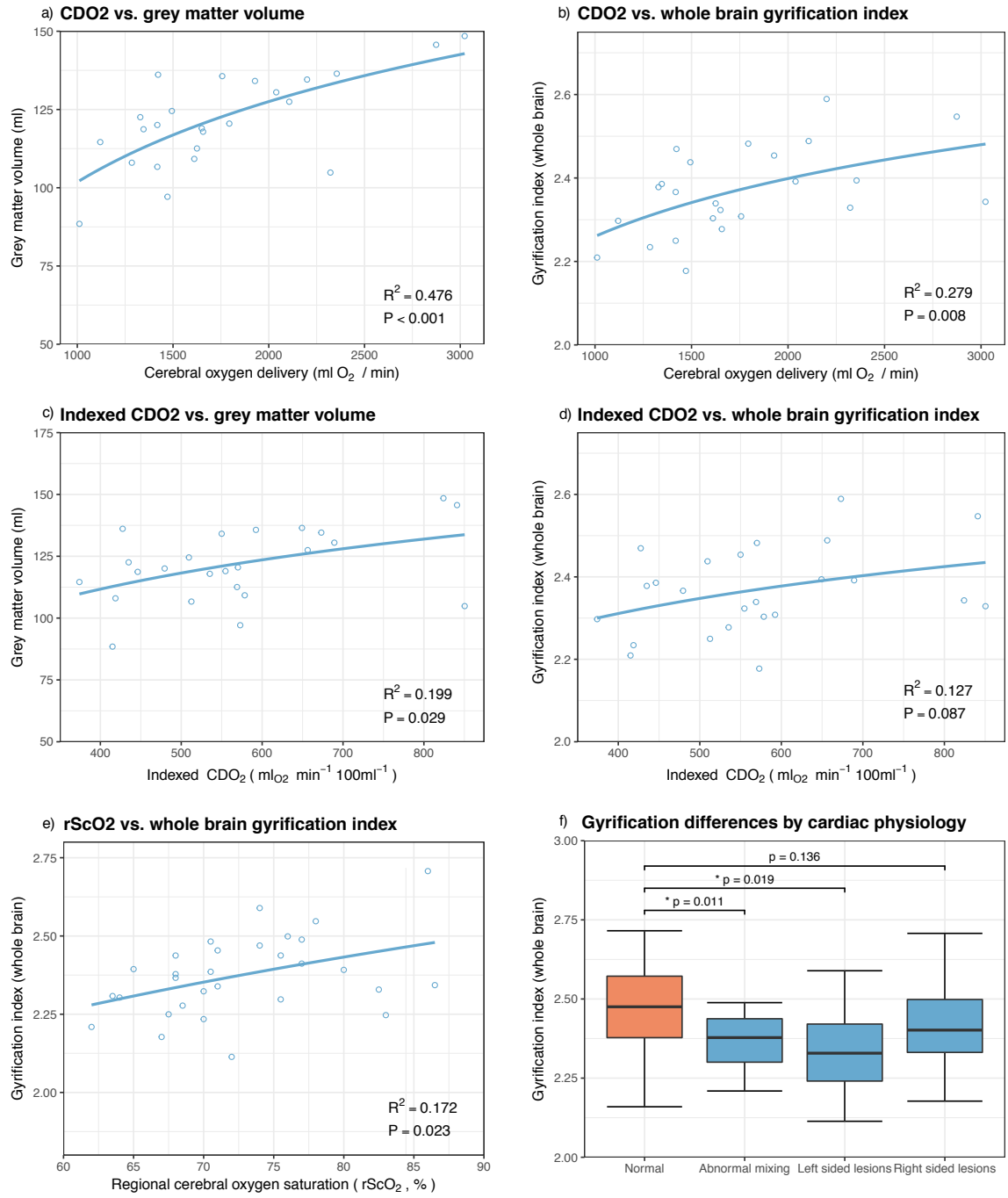

Figure 29 Plots of cerebral oxygen delivery (CDO_2) against measures of cortical development

Cerebral oxygen delivery (CDO_2) demonstrates a positive association with grey matter volume (a) and whole brain gyrification (b). These trends persist after indexing CDO_2 per 100ml brain volume (c and d). Regional cerebral oxygen saturation has a limited positive relationship with gyrification index (e). Abnormal mixing lesions and left sided lesions demonstrate a significantly lower gyrification index, while right-sided lesions are less affected (f).

5.4.3 Cortical volumes are reduced in newborns with CHD

Infants born with CHD had smaller total brain volumes ($p<0.01$) and smaller cortical grey matter volumes ($p<0.01$). Other brain volumes were also smaller, including deep grey matter ($p<0.001$), white matter ($p=0.01$), and cerebellar volume ($p<0.001$). Ventricular volume was not significantly different between groups ($p=0.09$). Extra-cerebral CSF space was increased in the CHD group ($p=0.011$). Volumetric results are summarised in Table 5.

5.4.4 Gyrification index is globally reduced in newborns with CHD

Brain gyrification was reduced in infants with CHD ($p<0.01$, Figure 30a). Regional analysis showed significantly reduced gyrification index in the temporal ($p=0.002$), parietal ($p=0.005$) and occipital ($p=0.018$), and a trend towards reduction in the frontal lobes ($p=0.052$). Regional gyrification differences between groups are described in Table 6, with plots displayed in Figure 30(b-e) and a visualisation on a representative cortical surface in Figure 30(f).

Region	**Volume (ml), mean (SD)**		**ANCOVA**	
	CHD, n=30	Control, n=30	p value	
Whole brain	308 (29.3)	335 (33.9)	< 0.001	*
Cortical grey matter	122 (14.4)	132 (17.4)	0.003	*
Frontal grey matter	41 (5.0)	44 (5.6)	0.011	*
Parietal grey matter	28 (3.2)	31 (4.5)	0.002	*
Temporal grey matter	25 (3.3)	28 (3.9)	< 0.001	*
Occipital grey matter	19 (2.7)	21 (2.8)	0.014	*
Cerebellum	20 (2.3)	22 (2.5)	0.073	Ns
Extra-axial CSF space	78 (20.8)	68 (10.8)	0.011	*

Table 5 Volume differences between newborns with congenital heart disease and healthy controls. Comparison of groups performed with multivariate general linear models, with PMA included as a covariate. Exploratory regional analyses displayed with * = significance and Ns = not significant. Significance did not change with the addition of weight at scan as a covariate.

Region	GI mean (SD)		ANCOVA	
	CHD, n=30	Control, n=30	p value	
Whole brain	2.373 (0.127)	2.464 (0.144)	0.003	*
Frontal lobes	2.112 (0.114)	2.164 (0.124)	0.052	Ns
Parietal lobes	2.820 (0.155)	2.930 (0.194)	0.005	*
Temporal lobes	2.233 (0.145)	2.338 (0.151)	0.002	*
Occipital lobes	2.355 (0.167)	2.454 (0.179)	0.018	Ns

Table 6 Differences in gyrification index between newborns with congenital heart disease and healthy controls

Comparison of groups performed with multivariate general linear models, with PMA included as a covariate. For regional comparisons, p=0.0125 used as a Bonferroni correction threshold, with * representing significance and Ns = not significant.

5.4.5 Gyrification varies between different CHD types

To explore differences further, newborns with CHD were divided into three main physiological groups: 1) Abnormal mixing (i.e. transposition of the great arteries, double-outlet right ventricle), 2) Left sided lesions (i.e. hypoplastic left heart syndrome, coarctation of the aorta), and 3) Right sided lesions (i.e. pulmonary atresia or stenosis), and each group compared to its matched controls. Compared to healthy newborns, gyrification was reduced in mixing (p=0.011) and left sided lesions (p=0.019), but not in right sided lesions (p=0.136) (Figure 29f).

5.4.6 Requirement for septostomy is not associated with cortical volume and gyrification differences

Infants with TGA required septostomy in 5 of 14 cases (36%). We repeated analyses with this as a co-variate in the statistical analysis and found results were unchanged. Within the TGA group, we compared infants with and without a requirement for septostomy, and found no difference in terms of brain volume (p = 0.825) or gyrification (p = 0.19).

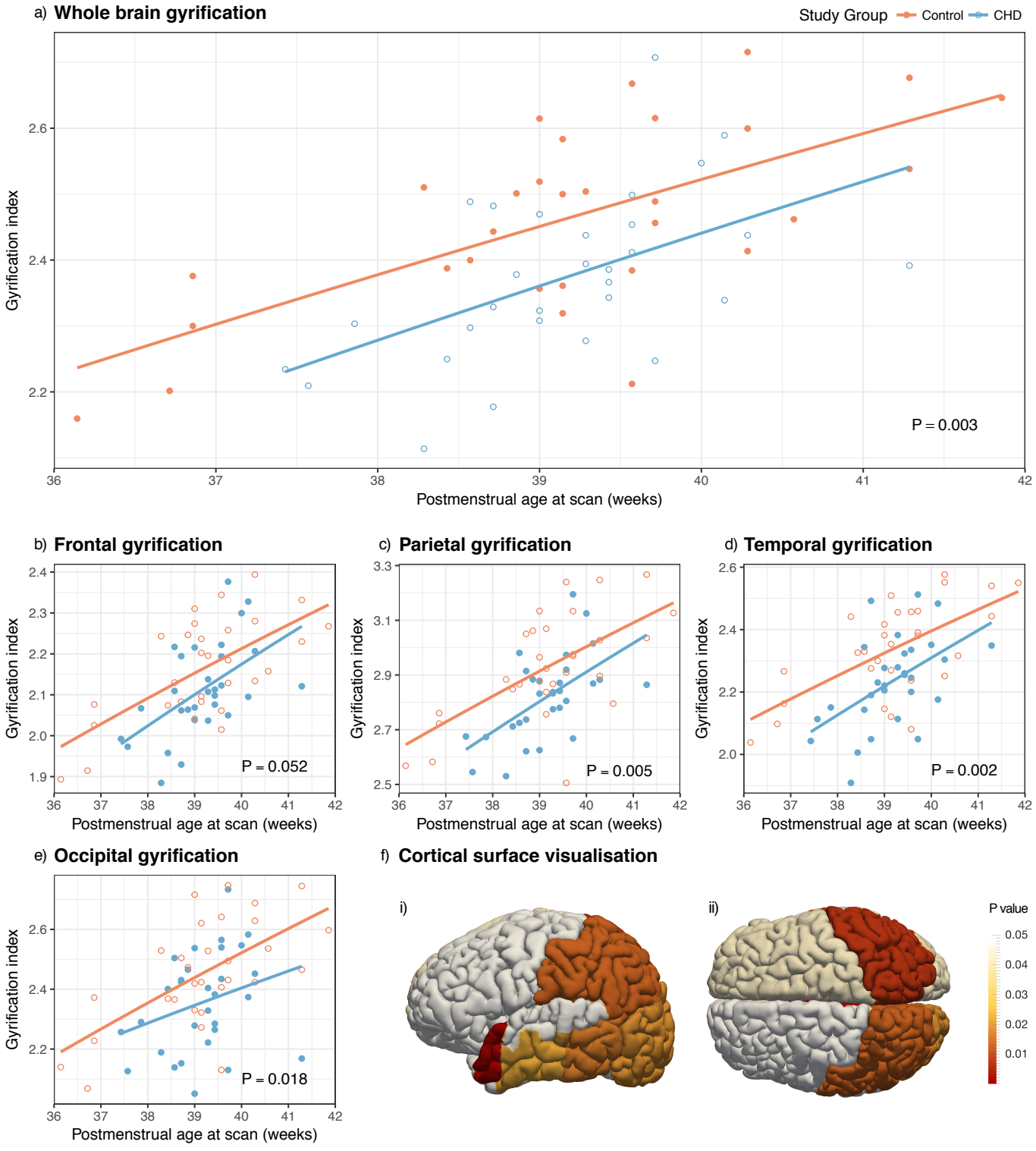

Figure 30 Gyrification index differences between newborns with complex congenital heart disease

Plots showing differences between infants with congenital heart disease (blue) and healthy controls (orange), in the whole brain (a) and exploratory regional analysis (b-e). The cortical surface visualisation (f) demonstrates regions where gyrification is reduced in newborns with congenital heart disease compared to healthy term controls, from the left lateral side (i) and from above (ii); colours represent p values from multivariate general linear models, using postmenstrual age as a covariate; no multiple comparisons correction has been performed in this visualisation.

5.5 DISCUSSION

Reduced CDO_2 in newborns with CHD before surgery is associated with impaired cortical development. Cortical grey matter volumes and gyrification index were lower in newborns with complex CHD when compared to healthy matched controls. The degree of cortical impairment was most significant in mixing and left-sided lesions, which may relate to the fetal cerebral circulatory impairment that has been demonstrated in these groups (Heymann and Rudolph, 1972; Sun et al., 2015).

A recent study of a similar number of infants showed reduced CDO_2 in newborns with mixed complex CHD compared to controls, with the lowest CDO_2 measured in infants with transposition (Lim et al., 2016). Lim and colleagues found that arterial saturations had the greatest influence on CDO_2, and that there were no significant CBF differences between CHD and control infants (Lim et al., 2016). We were unable to replicate these findings due to lack of flow measurements in our control group, but our results suggest that CBF had a greater contribution to the variation of CDO_2 within our CHD cohort. Ascending aorta oxygen saturations were found to be 10% lower in fetuses with CHD when compared to healthy controls using fetal MRI (Sun et al., 2015). Animal studies have shown that a lower oxygen tension environment affects mechanisms that coordinate myelination and angiogenesis during the early phase of brain development (Yuen et al., 2014), and causes diminished proliferation and neurogenesis in the subventricular zone, accompanied by reduced cortical growth (Morton et al., 2017). Taken together with our results, these findings suggest that the developing brain may be adversely affected by the lower oxygen tension environment that is observed in CHD in both fetal and postnatal life.

A limited number of studies have reported altered cortical folding in fetuses and newborns with CHD. An “immature cortical mantle” was first described in an early post-mortem study from a cohort of 41 infants with hypoplastic left heart syndrome (Glauser et al., 1990b). Delayed cortical folding has been described using a radiologist scoring system (Childs et al., 2001) in pre-surgical newborns with CHD, starting at around 30 weeks of gestation (Licht et al., 2009). The same finding in post-surgical infants has been shown to be a strong predictor of later neurodevelopmental outcome (Beca et al., 2013). Specific analysis of the gyrification of the opercula was performed in a cohort of newborns with HLHS and TGA prior to surgery, and demonstrated that opercula in CHD was more “open” and exhibited reduced folding complexity (Awate

et al., 2009). Gyrification index in fetuses with HLHS was found to be reduced compared to controls using a semi-automated analysis technique, and these group differences increased progressively with advancing gestational age (Clouchoux et al., 2013). Our study adds weight to these findings in a more diverse group of CHD.

Cortical development follows a predictable timeline (Armstrong et al., 1995). Most gyri become well defined between 26-28 weeks, becoming more prominent and deeply infolded during the third trimester, with subsequent development of secondary and tertiary gyri (Chi et al., 1977). The frontal third of the brain commences its gyrification slightly before the intermediate and caudal thirds, but also takes longer to reach its adult degree of cortical folding by 48 weeks (compared to 44 and 43 weeks respectively) (Armstrong et al., 1995). We found that gyrification index in our CHD group was most reduced in parietal and temporal regions, and least in the frontal region. This may be due to later completion of gyrification in the frontal region, but also that the pace of gyrification is greatest in parietal, temporal and occipital regions during the time window of our study (Armstrong et al., 1995). Impaired gyrification in infants with CHD may therefore be most apparent in these regions.

To understand gyrification differences further, we examined three subgroups using a cardiac physiology-based categorisation: abnormal mixing, left sided lesions. and right sided lesions. We found significant gyrification differences in the abnormal mixing group, but were unable to form strong conclusions from our left- and right-sided lesion groups due to small subgroup numbers. We were unable to study infants with hypoplastic left heart syndrome separately, a condition known to impair fetal brain development (Clouchoux et al., 2013). There are limited previous studies for comparison, with no pre-surgical neonatal studies for reference. In a previous study of post-surgical infants with transposition, gyrification was reported to be similar to controls (Claessens et al., 2016), which may be explained by smaller group sizes and less closely matched postmenstrual ages at scan. There was unfortunately no control group for their pre-surgery infants for direct comparison.

Our finding of reduced brain volumes in newborns with transposition fits with a recent large population study of 924,422 Dutch liveborn singletons, which found that in contrast to other forms of CHD where both head circumference and birth weight of infants were reduced, only infants with transposition had smaller head circumference relative to birth weight (Matthiesen et al., 2016). Reduced head circumference at birth,

the most widely available proxy of impaired fetal brain growth (Cooke et al., 1977), has often been reported in CHD, most consistently in HLHS and TGA (Donofrio et al., 2003; Limperopoulos et al., 1999; Rosenthal, 1996; Shillingford et al., 2007), but also in tetralogy of Fallot, ventricular septal defects, common arterial trunk, and anomalous pulmonary venous return (Matthiesen et al., 2016). In contrast to other studies, we found that there was no difference in the z-scores of head circumferences between CHD and healthy groups in our cohort. However, brain volumes were significantly reduced in CHD. The discrepancy between head circumference and brain volume is explained by a larger extra-cerebral CSF volume in the CHD group, in the presence of comparable ventricular volumes.

Brain growth trajectories in CHD have been shown to diverge from healthy fetuses in the third trimester, during a period where there is usually an acceleration of energy-demanding brain growth (Limperopoulos et al., 2010), using both fetal ultrasound (Zeng et al., 2015) and fetal MRI (Clouchoux et al., 2013; Limperopoulos et al., 2010; Sun et al., 2015). A limited number of cohorts have also suggested an increased prevalence of ventriculomegaly in fetuses with CHD, as assessed by radiologist assessment (McConnell et al., 1990) and two-dimensional measurements (Brossard-Racine et al., 2014). Increased CSF spaces in CHD has only previously been described in a limited number of studies (Brossard-Racine et al., 2014; Limperopoulos et al., 2010), and may be a marker of cerebral parenchymal growth disturbance.

Our study has a number of limitations. We did not have phase contrast measurements for our control group, limiting analysis of CDO_2 against cortical metrics to those infants with CHD. In addition, our CDO_2 measurements were performed shortly following birth, while the majority of brain development until that point occurs in utero with a fetal circulation. Delayed brain growth and maturation is more like to reflect CDO_2 in utero, which was not measured in this study. There are many influences on early brain growth, and although currently poorly understood, genetic abnormalities are highly prevalent in the CHD population (Blue et al., 2017). It is logical that smaller brains as a direct result of genetic factors with lower metabolic demands will require less blood flow and oxygen delivery, which may explain part of the association demonstrated in this study. We addressed this by calculating the indexed oxygen delivery per unit of brain tissue, and our results support the contention that CDO_2 is reduced even when taking into account differences in brain volume. However, it is not possible to fully determine if lower CDO_2 as a result of CHD has resulted in the development of a

smaller brain, or if extrinsic factors to this analysis (i.e. genetic) have resulted in smaller brains with smaller metabolic demands that require less CDO_2.

5.6 CONCLUSIONS

Cortical folding and cortical grey matter volume is reduced in newborns with congenital heart disease when compared to healthy matched controls. Lower CDO_2 measured in newborns with CHD prior to surgery is associated with reduced cortical grey matter volume and gyrification. This supports the possibility that strategies to improve CDO_2 in infants with CHD could modify the derailing trajectory of brain development. Our finding of reduced CDO_2 may be of greatest importance for children with CHD whose heart defects remain unrepaired for long periods of time after birth, exacerbating deficits in oxygen and other metabolic substrate supply that may have occurred during the prenatal period, and leading to further decrements in brain growth and development after birth.

Chapter 6

Abnormal microstructural development of the cortex in congenital heart disease is related to impaired cerebral oxygen delivery

6.1 ABSTRACT

Neurodevelopmental impairment has become a major remaining challenge in the management of congenital heart disease (CHD). Macroscopic developmental abnormalities of the cerebral cortex in CHD have been reported previously, although the biological basis for this remains unclear. We use high angular resolution diffusion magnetic resonance imaging, phase contrast angiography, and high resolution structural imaging to investigate the link between cerebral oxygen delivery and cortical microstructure development in vivo, in a prospective cohort of infants with CHD prior to surgery. We present evidence that cortical microstructural development is abnormal in infants with CHD, with higher fractional anisotropy (FA) and lower orientation dispersion index (ODI) compared to healthy age-matched controls, correcting for gestational age at birth and scan. There were no differences in mean diffusivity or neurite density index. Secondly, we demonstrate that reduced cortical ODI in CHD is related to impaired cerebral oxygen delivery, supporting the hypothesis that chronic suboptimal cerebral oxygenation is associated with atypical cortical maturation. Thirdly, we show that macrostructural gyrification of the cortex occurs in tandem with microstructural properties including increasing ODI and reducing FA. These results support the interpretation that the primary component of cortical dysmaturation in infants with CHD is impaired development of dendritic arborisation, associated with reduced cerebral oxygen delivery, which is responsible, at least in part, for macrostructural findings in this population. Cortical ODI may prove to be a valuable early indicator of the success of future fetal intervention studies that aim to restore the faltering trajectory of cortical development in CHD.

This chapter is based upon:, Kelly CJ, Christiaens D, Batalle D, Makropoulos A, Cordero-Grande L, Steinweg JK, O'Muircheartaigh J, Khan H, Lee G, Victor S, Alexander DC, Zhang H, Simpson J, Hajnal JV, Edwards AD, Rutherford MA, Counsell SJ. Abnormal microstructural development of the cortex in congenital heart disease is related to impaired cerebral oxygen delivery. Submitted.

6.2 INTRODUCTION

Congenital heart disease (CHD) is the most common congenital abnormality, affecting almost 1% of newborns (van der Bom et al., 2011). Despite improvements in antenatal diagnosis, cardiac surgery and perioperative care, infants with CHD often experience neurological impairment across a range of developmental domains, both in early childhood and later in adult life (Bellinger et al., 2011; Marino et al., 2012), making improvement of neurodevelopmental outcomes a major remaining challenge in the management of CHD. While early research focused on suspected surgical and perioperative factors, it now appears that a more complex set of biological factors may be responsible.

The detrimental effect of CHD on early brain development can be observed via a faltering trajectory of brain growth in the third trimester of pregnancy (Clouchoux et al., 2013; Limperopoulos et al., 2010; Sun et al., 2015; Zeng et al., 2015), and a higher incidence of acquired brain lesions in newborn infants prior to cardiac surgery (Mebius et al., 2017). The developmental morphology of the cortex has become of increasing interest in CHD, with an 'immature cortical mantle' first observed in autopsies of infants with hypoplastic left heart syndrome (HLHS) (Glauser et al., 1990a). Findings of reduced cortical folding have since been quantified *in vivo* using magnetic resonance imaging (MRI) in both fetal (Clouchoux et al., 2013) and pre-surgical neonatal populations (Claessens et al., 2016; Kelly et al., 2017; Ortinau et al., 2013). Factors including reduced fetal cerebral oxygen delivery (Sun et al., 2015) and cerebral metabolic substrate (Rudolph, 2016) are hypothesised to be responsible, at least in part, although precise cellular mechanisms remain unclear.

Linking physiological changes in CHD to brain development is assisted by four recent findings. Firstly, oxygen tension has been shown to regulate development of human cortical radial glial cells, with hypoxia exerting negative effects on gliogenesis by reducing the number of pre-oligodendrocytes while increasing the number of reactive astrocytes (Ortega et al., 2017). Secondly, hypoxia has been shown to reduce proliferation and neurogenesis in the subventricular zone of the piglet brain, accompanied by reduced cortical growth, with preliminary similarities found in the subventricular zone cytoarchitecture in human fetal autopsy specimens (Morton et al., 2017). Thirdly, ascending aorta oxygen saturations have been found to be 10% lower in human fetuses with mixed CHD compared to healthy controls, with saturation

measurements that correlated with fetal brain size (Sun et al., 2015). Finally, microstructural maturation of the cortex, measured using both histology and diffusion anisotropy, has been demonstrated to occur in parallel with macrostructural development (Wang et al., 2017). Taken together, these studies raise the hypothesis that macrostructural changes observed in CHD are the result of altered cortical microstructural development, which is in turn hindered by suboptimal oxygen tension during fetal life in CHD. Diffusion MRI, with newer multi-compartment models such as neurite orientation dispersion and density imaging (NODDI), provides measures that enable this hypothesis to be tested.

Diffusion tensor imaging (DTI) metrics such as fractional anisotropy (FA) are non-specific and reflect many underlying parameters of brain tissue including neuronal density, fibre orientation dispersion, degree of myelination, free-water content, and axonal diameter (Winston et al., 2014). The NODDI model aims to disentangle these different factors by separating the influence of neurite density and orientation dispersion from each other, and from partial volume with CSF, to provide distinct indices: orientation dispersion index (ODI), which captures the degree of dispersion of axonal fibre orientations (e.g. through fanning, bending, crossing) or dendrite orientations, and neurite density index (NDI), represented by the intracellular volume fraction (ICVF) (Zhang et al., 2012). Such techniques have already been used in the preterm population to quantify cortical development, with findings of reducing FA and mean diffusivity (MD) (Ball et al., 2013; McKinstry et al., 2002), and increasing ODI (Eaton-Rosen et al., 2015), with increasing brain maturation until term age, and have identified that impaired postnatal weight, length, and head growth are associated with delayed microstructural development of cortical grey matter (Vinall et al., 2013). Additionally, a diminished decline in cortical FA with maturation in a sheep model of preterm brain injury has been associated with histological findings of reduced dendritic arborisation and dendritic spine density (Dean et al., 2013).

In this study, we aimed to use high angular resolution diffusion imaging (HARDI) and NODDI to test the hypothesis that reduced cerebral oxygen delivery in CHD is associated with impaired cortical microstructural development. We predicted that infants with complex CHD would exhibit higher cortical FA and lower ODI when compared to a group of healthy matched controls, and that infants with the lowest cerebral oxygen delivery would exhibit the most severe impairment of cortical microstructural development.

6.3 MATERIALS AND METHODS

The project was approved by the National Research Ethics Service West London committee (CHD: 07/H0707/105, Controls: 14/LO/1169) and informed written parental consent was obtained prior to imaging. All methods and experiments were performed in accordance with relevant guidelines and regulations.

6.3.1 Participants

A prospective cohort of 54 infants with complex CHD expected to require surgery within one year was recruited from the Neonatal Intensive Care Unit at St Thomas' Hospital, London. Six infants were excluded from the analysis: two infants with suspected coarctation were later assessed to have a normal circulation following postnatal ductus arteriosus closure; two infants were found to have focal arterial ischaemic stroke on MRI involving the cortex (both left middle cerebral artery stroke); one infant had uncertain gestation due to unknown date of last menstrual period and lack of ultrasound dating scan; one infant had incomplete diffusion data due to waking during the scan.

We therefore studied 48 infants with CHD, born at a median GA of 38.8 weeks (IQR 38.0 – 39.1). A control group of 48 healthy infants was matched by GA at birth and scan, recruited contemporaneously from the postnatal ward at St Thomas' Hospital as part of the Developing Human Connectome Project (Hughes et al., 2017b), and born at a median GA of 38.5 weeks (38.1 – 38.9). The median GA at scan was 39.1 weeks (IQR 38.6 – 39.7) for both the CHD group and control group.

6.3.2 MR imaging

T2w, T1w, DWI and PCA MR imaging was performed on a Philips Achieva 3 Tesla system (Best, The Netherlands) with a 32-channel neonatal head coil and neonatal positioning device (Hughes et al., 2017b), situated on the neonatal intensive care unit at St Thomas' Hospital, London. All examinations were supervised by a paediatrician experienced in MR imaging procedures. All infants were scanned in natural sleep without sedation. Pulse oximetry, respiratory rate, temperature and electrocardiography were monitored throughout. Ear protection comprised earplugs moulded from a silicone-based putty (President Putty, Coltene Whaledent, Mahwah, NJ, USA) placed in the external auditory meatus, neonatal earmuffs (MiniMuffs, Natus

Medical Inc, San Carlos, CA, USA) and an acoustic hood positioned over the infant. All sequences included a 5 second initial slow ramp-up in acoustic noise to avoid eliciting a startle response.

T2w images were acquired using a multi-slice turbo spin echo sequence, acquired in two stacks of 2D slices (in sagittal and axial planes), using parameters: repetition time (TR): 12 s; echo time (TE): 156 ms, flip angle: 90°, slice thickness: 1.6 mm acquired with an overlap of 0.8 mm; in-plane resolution: 0.8x0.8 mm, scan time: 3:12 min per stack. The T1w volumetric magnetisation prepared rapid acquisition gradient echo acquisition parameters were as follows: TR: 11 ms, TE: 4.6 ms, TI: 714 ms, flip angle:9°, acquired voxel size:0.8×0.8×0.8mm, field of view (FOV):145×145×108mm, SENSE factor:1.2, scan time:4:35min. DWI with 300 directions was acquired using parameters: TR: 3.8 s, TE: 90 ms, multiband: 4; SENSE: 1.2; resolution: 1.5x1.5x3mm with 1.5mm slice overlap, diffusion gradient encoding: b=0 s/mm (n=20), b=400 s/mm (n=64), b=1000 s/mm (n=88), b=2600 s/mm (n=128) with interleaved phase encoding (Hutter et al., 2018). Quantitative flow imaging was performed using velocity-sensitised phase contrast imaging, with a single-slice T1-weighted fast field echo sequence. Scan parameters were: FOV: 100x100 mm, acquisition resolution: 0.6x0.6x4.0mm, TR: 6.4 ms, TE: 4.3 ms, flip angle: 10°, 20 repetitions, maximal encoding velocity (vENC): 140 cm/s, scan time: 71 s (Varela et al., 2012).

6.3.3 Structural and diffusion-weighted image reconstruction

T2w images were reconstructed using a dedicated neonatal motion correction algorithm. Retrospective motion-corrected reconstruction (Cordero-Grande et al., 2018; Cordero-Grande et al., 2016) and integration of the information from both acquired orientations (Kuklisova-Murgasova et al., 2012) were used to obtain 0.8 mm isotropic T2w volumes with significantly reduced motion artefacts. Diffusion images were reconstructed following the scan using a dedicated multiband reconstruction method described previously (Hutter et al., 2018).

6.3.4 Structural image processing

Motion-corrected T2w images were segmented into tissue type using an automated, neonatal-specific pipeline (Makropoulos et al., 2018, 2016, 2014), which was optimised for our acquisition parameters. Each tissue segmentation was manually

inspected for accuracy using ITK-SNAP (Yushkevich et al., 2006), and minor corrections performed if necessary. Gyrification index was calculated as described previously (Kelly et al., 2017).

6.3.5 Diffusion-weighted image processing

High angular resolution diffusion-weighted imaging (HARDI) data was reconstructed using a slice-to-volume motion correction technique that uses a bespoke spherical harmonics and radial decomposition (SHARD) of multi-shell diffusion data, together with outlier rejection, distortion and slice profile correction (Christiaens et al., 2018). Data was first processed with image denoising (Veraart et al., 2016) and Gibbs ringing suppression (Kellner et al., 2016). A field map was estimated from b=0 images using FSL Topup (Andersson et al., 2003). Reconstruction was run for 10 iterations with Laplacian regularisation, using a SHARD decomposition of rank = 89 (allowing for spherical harmonics order ℓ_{max} = 0, 4, 6, 8 for respective shells), with registration operating at a reduced rank = 15.

Non-brain tissue was removed using FSL BET (Smith, 2002). DTI metrics FA and MD were calculated from b=0 and b=1000 DWI data using MRtrix3 (Tournier et al., 2012). Neurite orientation dispersion and density imaging (NODDI) parameter maps were estimated using NODDI toolbox version 0.9 (Zhang et al., 2012). We used 2.0 x 10^{-3} mm^2 s^{-1} as the intrinsic diffusivity for the intracellular compartment in the NODDI model, as this diffusivity gave the best quality of fit in our data, according to the Bayesian Information Criterion (BIC) (Figure 31). This is consistent with previous NODDI studies in neonates (Eaton-Rosen et al., 2015; Jelescu et al., 2015; Kunz et al., 2014), with the higher value compared to adults (usually 1.7 x 10^{-3} mm^2 s^{-1}) likely reflecting the higher water content of the neonatal brain.

6.3.6 Group template generation and image registration

A multivariate group template was generated from both T1w and T2w images, using symmetric diffeomorphic normalisation for multivariate neuroanatomy and a cross-correlation similarity metric (B. Avants et al., 2008). Each subject's diffusion data were rigidly registered to each subject's T2w image using the MD map (Jenkinson and Smith, 2001). DTI and NODDI maps were then transformed into template space in a single step using concatenated linear and diffeomorphic transformations. Tissue

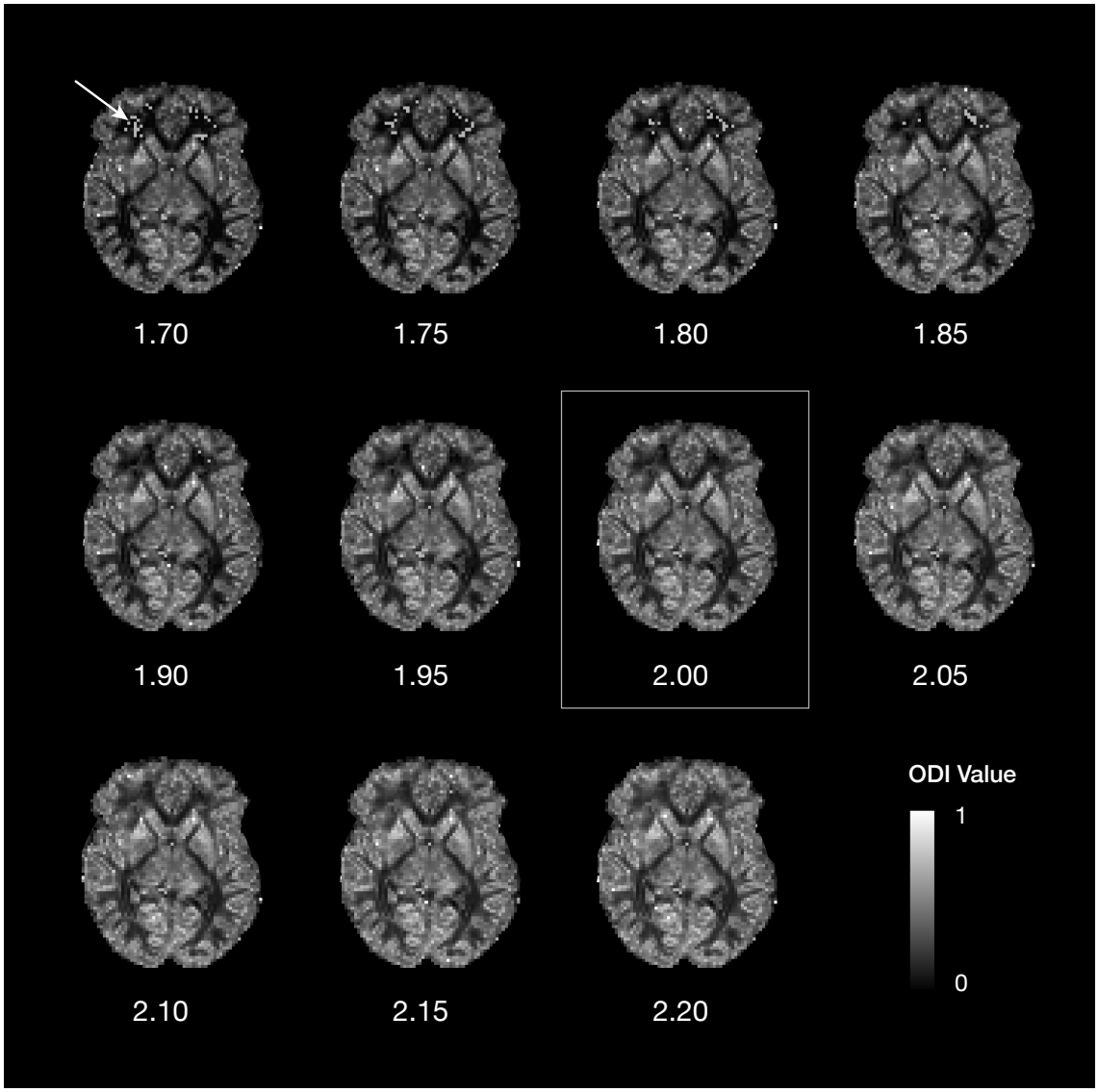

Figure 31 Orientation dispersion index maps for different model values of intrinsic diffusivity
Optimising NODDI model parameters for neonatal data. Figure shows ODI maps for varying intrinsic diffusivity values, of which 2.0 x 10^{-3} mm^2 s^{-1} was found to provide the best fit across the brain. Arrow indicates an example of a cluster of voxels (represented in grey) that failed to fit to the model.

segmentations from T2w images were also transformed into template space using nearest neighbour interpolation.

6.3.7 Cortical analysis of microstructure

We used an approach for aligning cortical data from multiple subjects into a common space to provide voxel-wise spatial characterisation of FA, MD, NDI and ODI, as previously described (Ball et al., 2013; Smith et al., 2006). A mean cortical map was produced by merging cortical grey matter segmentations that had been previously

transformed into template space. This was then skeletonised to retain only a core of highly-probable cortical voxels, represented as a thin curved surface at the centre of the cortex. FA, MD, NDI and ODI measurements from each individual were projected onto the cortical skeleton by searching in a direction perpendicular to the cortical skeleton to identify voxels with the highest probability of being cortical.

6.3.8 Calculation of cerebral oxygen delivery (CDO2)

For infants with CHD, we calculated their cerebral blood flow using a previously-described method (Kelly et al., 2017). Phase contrast angiography was acquired in a plane perpendicular to both internal carotids and basilar arteries at the level of the sphenoid bone (Varela et al., 2012). Haemoglobin measurements were performed as part of routine clinical care, at a median of 3 days (IQR 0 – 5) prior to the scan. Arterial oxygen saturation (SaO_2) was measured at the time of scan using a Masimo Radical-7 monitor (Masimo Corp, Irvine, CA) applied to the right hand.

Cerebral oxygen delivery (CDO_2) was calculated using the following formulae (McLellan and Walsh, 2004):

CDO_2 (ml O2/min) = SaO_2 x [Hb] (g/dL) x 1.36 x [CBF] (ml/min)

where 1.36 is the amount of oxygen bound per gram of haemoglobin at 1 atmosphere (Hüfner's constant) (Lim et al., 2016).

6.3.9 Statistical analysis

Healthy infants were matched to the CHD group by both GA at birth and scan using an R implementation (Leisch, 2017) of the daisy algorithm (Kaufman and Rousseeuw, 1990). In order to investigate the relationship between DWI metrics in the cortical grey matter and clinical factors, cross-subject voxel-wise statistical analysis was performed using FSL Randomise v2.9 (Smith et al., 2006). A general linear model (GLM) was used to assess group differences between diffusion measures of infants with CHD and healthy controls, including both GA at birth and scan as covariates in each model. The effect of CDO_2 on cortical diffusion metrics was performed using a GLM that selected only infants with CHD who had a successful CDO2 measurement (n=39). All images were subject to family-wise error (FWE) correction for multiple comparisons following threshold-free cluster enhancement (TFCE) (Smith and Nichols, 2009) and are shown at $P < 0.05$. Linear regression was used to investigate the association between GI and

Variable	Control Newborns n = 48	Newborns with CHD n = 48	P-value
Gestational age at birth (weeks)	38.8 (38.0 – 39.1)	38.5 (38.1 – 38.9)	0.543
Post-menstrual age at scan (weeks)	39.1 (38.6 – 39.7)	39.1 (38.6 – 39.7)	0.595
Male sex – no. (%)	26 (54%)	27 (56%)	1.0
Birth weight (kg)	3.17 (2.83 – 3.41)	3.10 (2.81 – 3.47)	0.809
Birth head circumference (cm)	34.0 (33.0 – 35.0)	34.0 (33.0 – 35.0)	0.5
Heart lesion – no. (%)			
- Transposition of the great arteries (TGA)	-	21 (44%)	
- TGA requiring septostomy (% TGA)	-	9 (43%)	
- Coarctation of the aorta	-	9 (19%)	
- Tetralogy of Fallot	-	7 (15%)	
- Pulmonary stenosis	-	3 (6%)	
- Hypoplastic left heart syndrome	-	3 (6%)	
- Pulmonary atresia	-	3 (6%)	
- Truncus arteriosus	-	1 (2%)	
- Tricuspid atresia		1 (2%)	

Table 7 Clinical characteristics of the cortical diffusion cohort

GA at birth and PMA at scan are presented as median (interquartile range). P-values calculated using Mann–Whitney U test for continuous data, and Fisher's exact test for categorical variables. Septostomy in TGA was performed prior to imaging in all cases.

diffusion metrics. To assess the relationship of GI and ODI independently of advancing brain maturity, GA at scan was included as a variable in the multiple linear regression model.

Categorical clinical variables were compared using Fisher's exact tests. For continuous clinical variables, we determined medians and interquartile ranges, and compared groups using the Mann-Whitney U test. All analyses of clinical variables were performed using SPSS V24 (IBM, New York).

6.4 RESULTS

The analysis included 96 newborn infants: 48 infants with confirmed complex CHD scanned prior to surgery without evidence of arterial ischaemic stroke, and 48 age-matched healthy infants. Clinical characteristics of both groups are shown in Table 7. There were no significant differences in gestational age (GA) at birth, GA at scan and

sex between groups. T1-weighted (T1w), T2-weighted (T2w), and diffusion-weighted images (DWI) were acquired in all infants. Phase contrast angiography (PCA) was acquired with acceptable quality in 81% of infants with CHD (n=39).

6.4.1 Cortical orientation dispersion index (ODI) is reduced in infants with complex CHD

Infants with CHD demonstrated widespread changes in cortical ODI, with the most significant reductions observed posteriorly in the posterior parietal cortex, insula cortex, cingulate cortex, primary motor cortex, supplementary motor area, and occipital regions (Figure 32a, corrected for GA at birth and scan). There were no regions where ODI was higher in infants with CHD. There were no differences in NDI between groups. GA at scan was positively associated with cortical ODI.

6.4.2 Cortical fractional anisotropy (FA) is higher in infants with CHD

Cortical FA was higher in infants with CHD with effects seen in predominantly midline cortical structures (Figure 32b, corrected for GA at birth and scan). There were no regions where FA was lower in infants with CHD. There were no differences in mean diffusivity between groups. Cortical FA was negatively associated with GA at scan.

6.4.3 Reduced cerebral oxygen delivery is associated with impaired ODI

Cerebral oxygen delivery (CDO_2) at time of scan was positively associated with cortical ODI across many regions of the cortex (FWE-corrected for multiple comparisons, $p < 0.05$), with the most significant associations found in the bilateral temporal lobes, occipital lobes, cingulate cortex, and right insula cortex (Figure 33). To demonstrate this linear relationship, mean ODI data were extracted for each subject from significant voxels in the grey matter skeleton and plotted against CDO_2 at time of scan ($R^2 = 0.637$, Figure 34). There were no voxels with a negative association between the two variables. To assess the relative contribution of each component of CDO_2, we repeated the analysis substituting CDO_2 for either cerebral blood flow (CBF) or pre-ductal arterial saturation at time of scan. Considered alone, neither component demonstrated voxels that reached significance for either a positive or negative relationship with ODI. There were no significant associations between CDO_2 and FA, MD or NDI.

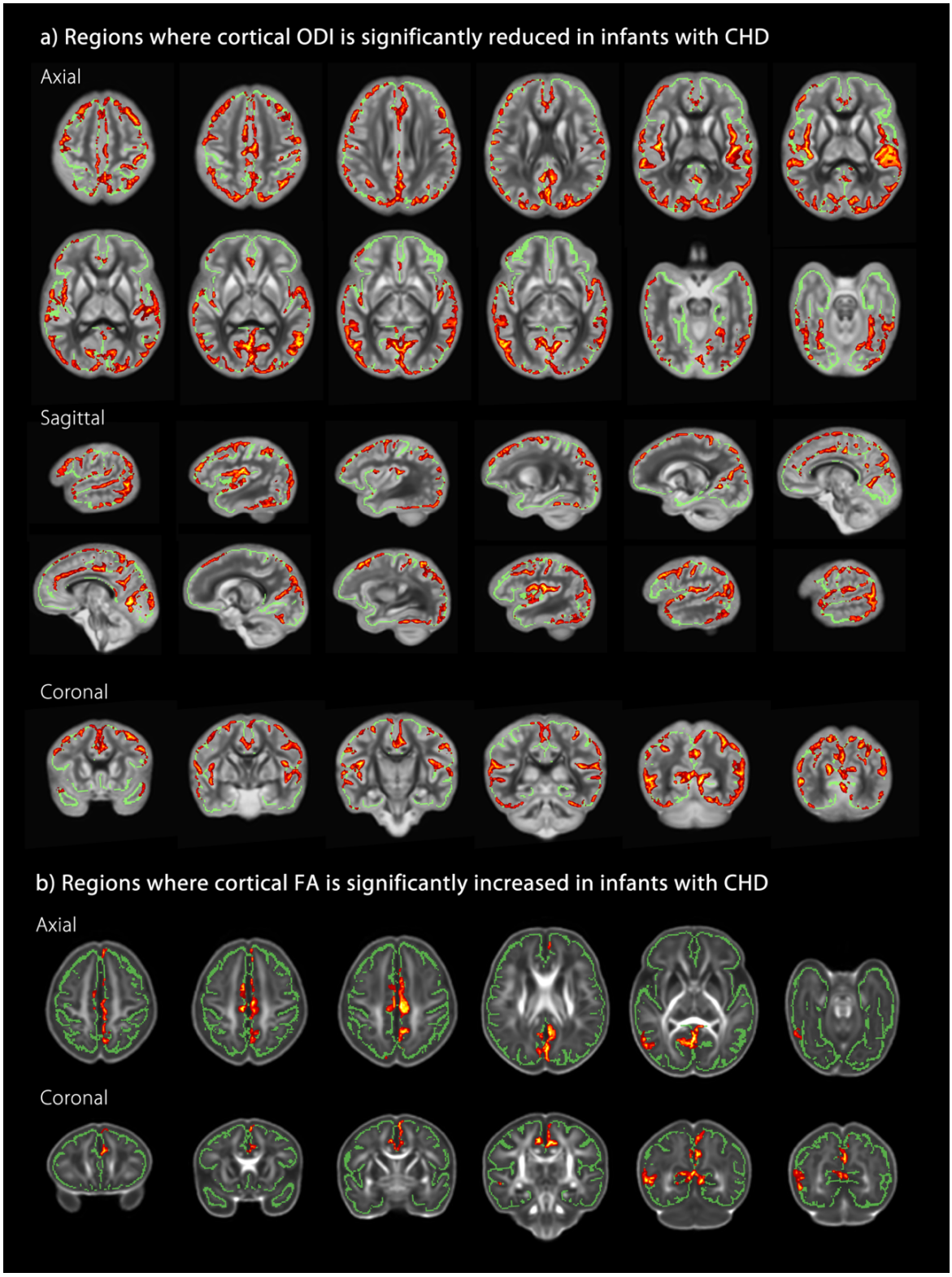

Figure 32 Infants with CHD (n=48) exhibit impaired microstructural development compared to healthy age-matched controls (n=48).

(A) Regions where ODI is significantly reduced in infants with CHD, overlaid on the mean ODI template. (B) Regions where cortical FA is significantly increased in infants with CHD, overlaid on the mean FA template. Red-Yellow indicates $p<0.05$ after FWE correction for multiple comparisons following TFCE. Results are shown overlaid on the mean cortical skeleton (green). Both analyses included GA at birth and at scan in the general linear model as covariates. Number of permutations was 10,000. Left–right orientation is according to radiological convention.

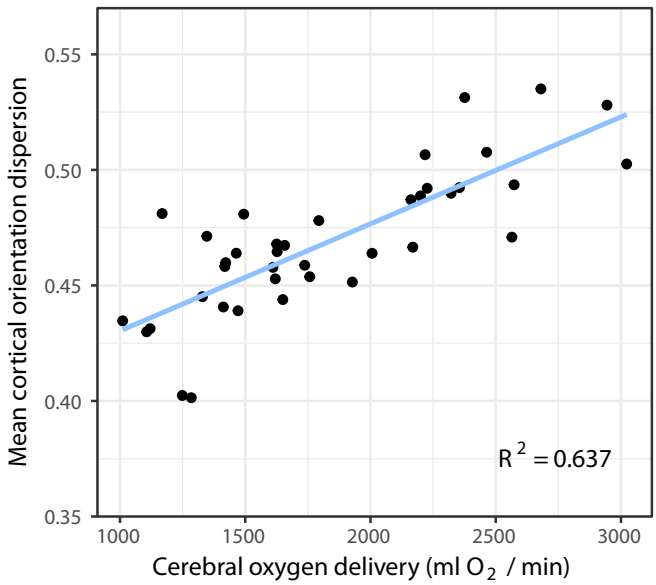

Figure 34 Visualisation of the linear relationship between CDO2 and cortical ODI within significant voxels from analysis displayed in Figure 33.

Mean ODI data were extracted for each subject from significant voxels in the statistic image after FWE-correction for multiple comparisons at P < 0.05.

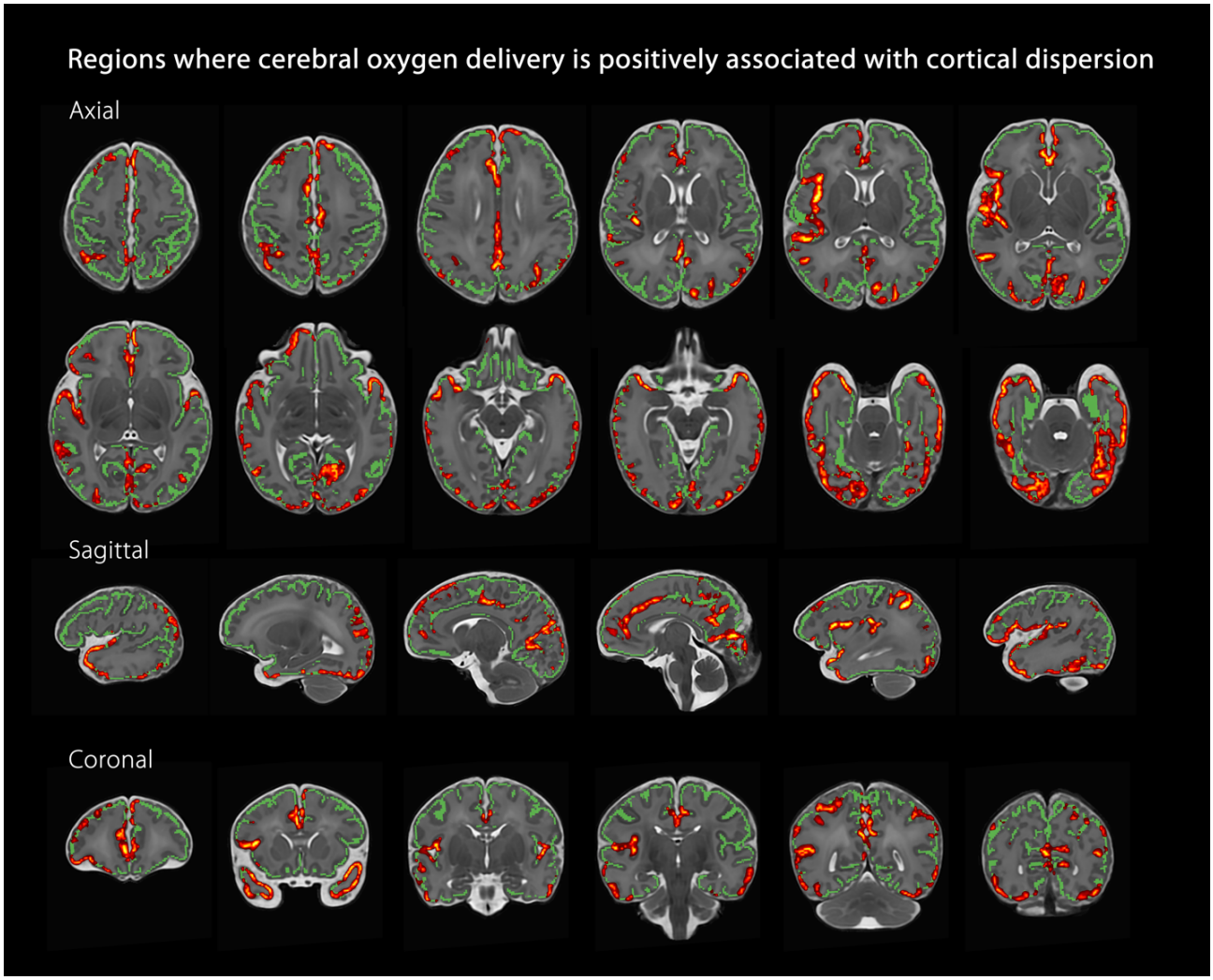

Figure 33 Regions where cerebral oxygen delivery is positively associated with cortical orientation dispersion in infants with CHD (n=40)

Red-Yellow indicates p<0.05 after FWE correction for multiple comparisons following TFCE. Results are shown overlaid on the group T2-weighted template and the mean cortical skeleton (green). Number of permutations was 10,000. Left–right orientation is according to radiological convention.

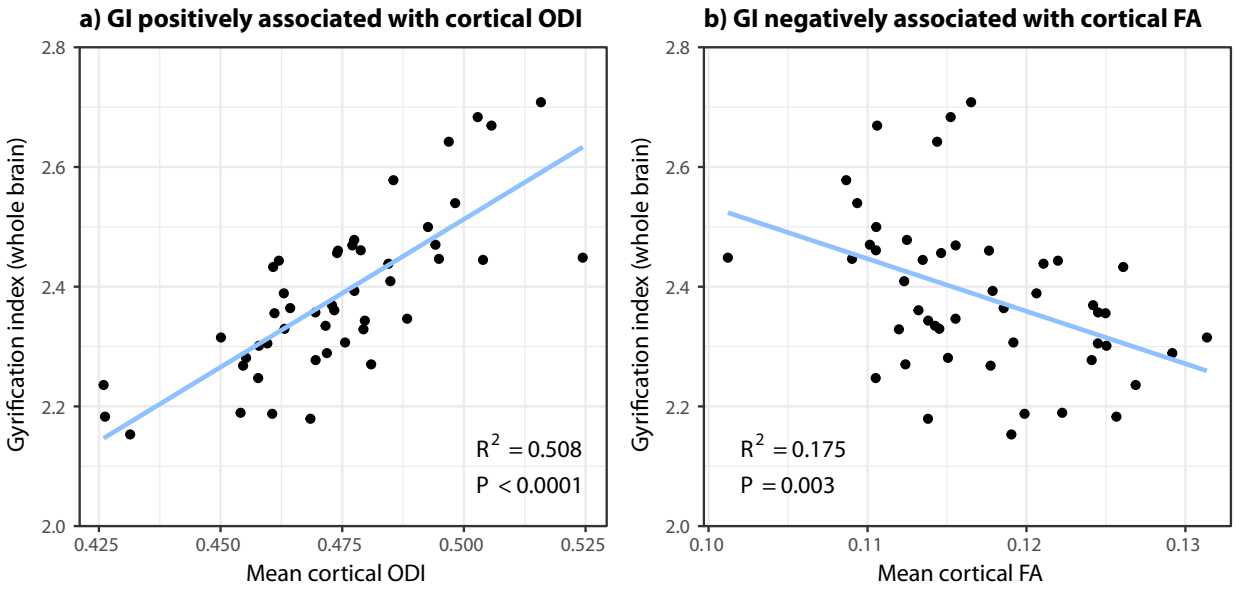

Figure 35 The linear relationship between gyrification index (GI) and cortical diffusion measures ODI and FA in newborn infants with CHD (n = 48).

GI is (a) positively associated with cortical ODI and (b) negatively associated with cortical FA.

6.4.4 Relationship between cortical microstructure and macrostructure in CHD

We have previously reported reduced gyrification index (GI) in our cohort of infants with CHD in Chapter 5. However, the relationship between cortical microstructure and macrostructure has not been assessed in this group. We found that GI was significantly positively associated with mean cortical ODI (R^2 = 0.589, P < 0.0001) and negatively with FA (R^2 = 0.175, P = 0.003) (Figure 35). The linear relationship between GI and cortical ODI persisted following inclusion of GA at scan in the linear regression model (β = 0.642, P < 0.0001), but not for cortical FA (β = -0.304, P = 0.09). Cortical grey matter volume was significantly positively correlated with cortical ODI (R^2 = 0.170, P = 0.004), but not with cortical FA. There was no relationship between total brain volume and microstructural measures (FA: R^2 = 0.011, P = 0.49; ODI: R^2 = 0.034, P = 0.207).

6.5 DISCUSSION

Long-term neurodevelopmental impairment is a major remaining challenge for infants with congenital heart disease, yet our understanding of the underlying biological substrate remains limited. Our study establishes that the microstructural development of the cerebral cortex in infants with CHD is atypical in the newborn period compared to healthy controls, and importantly that the degree of impairment is related to reduced cerebral oxygen delivery. We speculate that hindered microstructural

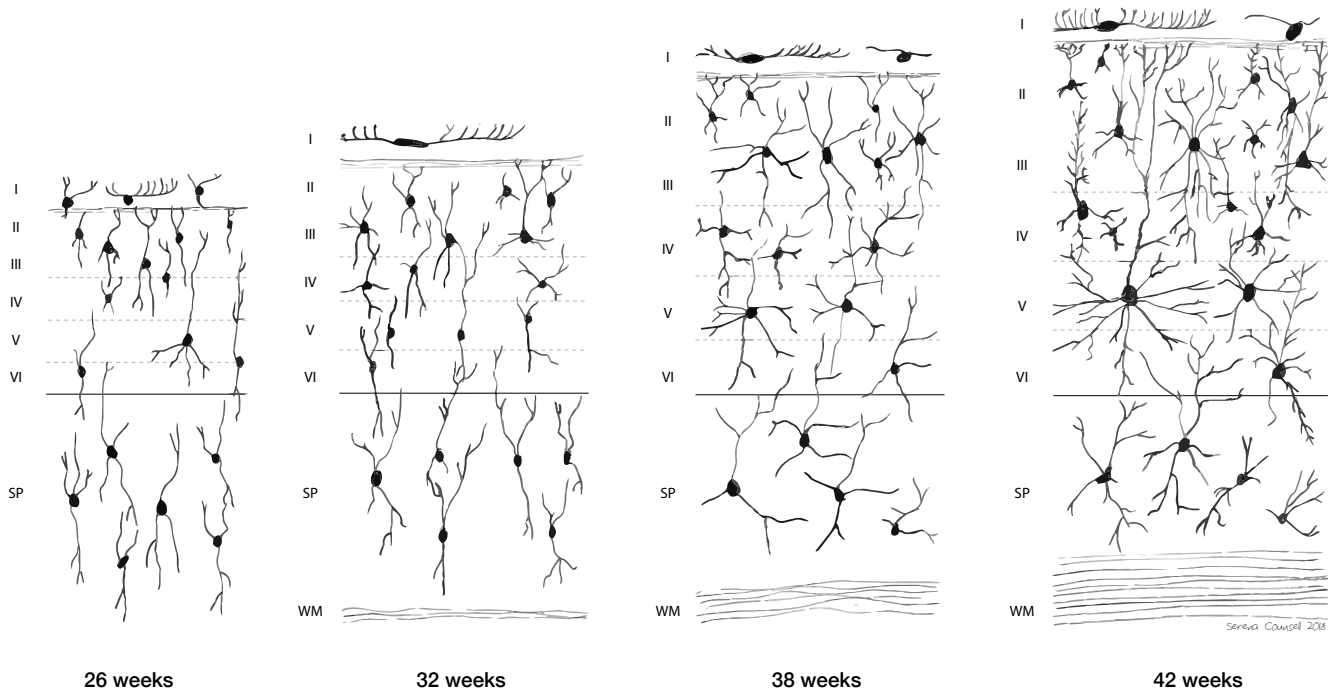

Figure 36 Schematic diagram depicting the development of cortical layers with increasing maturation
Demonstration of cortical and subplate neurons, with increasing elaboration of their dendritic spines. Adapted from Mrzljak et al., 1988 with permission of John Wiley and Sons.

development underlies the abnormal macrostructural changes in brain development that have been observed through reduced birth head circumference (Matthiesen et al., 2016), smaller brain volumes (Limperopoulos et al., 2010) and immature cortical folding (Claessens et al., 2016; Clouchoux et al., 2013; Glauser et al., 1990b; Kelly et al., 2017; Ortinau et al., 2013), and that strategies to optimise cerebral oxygenation in utero may offer the potential to ameliorate brain development in this population.

We found that cortical ODI was widely reduced in the CHD group, with associated but more sparsely distributed areas of higher FA. These findings suggest a hindered trajectory of normal brain development, with increased sensitivity to tissue changes using the more advanced NODDI model. As the brain matures in utero, cortical neurons migrate outwards towards the pial surface, populating the cortex (Bystron et al., 2008) and resulting in a highly directional, parallel, columnar microstructure. This can be observed with diffusion tensor imaging (DTI) as tensors with high FA, oriented radially to the cortical surface (McKinstry et al., 2002). As the cortex matures (Figure 36), an increasingly dense and complex cytoarchitecture forms, with dendritic arborisation, glial proliferation, differentiation of radial glia and synapse formation (Bystron et al., 2008; Mrzljak et al., 1988; Rakic, 2003), associated with an observed increase in cortical ODI (Eaton-Rosen et al., 2015). Increasing cytoarchitecture complexity also restricts water diffusion more evenly in all directions, with a

consequent reduction in FA (Ball et al., 2013; McKinstry et al., 2002). The link between diffusion imaging studies and underlying tissue biology is supported by prior evidence that NODDI-derived dispersion measures match their histological counterparts in adult postmortem specimens (Grussu et al., 2017), and by correlations found between maturation of dendritic arbors at the cellular level and loss of diffusion anisotropy with cortical development in the rhesus macaque (Wang et al., 2017) and fetal sheep (Dean et al., 2013).

While reduced cortical folding complexity in newborns with CHD has previously been reported in our cohort (Kelly et al., 2017), and others (Claessens et al., 2016; Licht et al., 2009; Ortinau et al., 2012), the link between cortical macrostructural and microstructural development in these infants has not been investigated previously. We found that gyrification index (GI) was positively associated with mean cortical ODI, independent of their association with increasing maturity. GI was also negatively but more weakly associated with mean cortical FA. Of interest, total brain volume was not associated with either FA or ODI. Taken together, these results suggest that macrostructural abnormalities observed in infants with CHD may be related to underlying impairments in dendritic arborisation.

Changes in cortical orientation dispersion were more pronounced posteriorly than frontally, which is consistent with previously described sequence of cortical development maturing earlier in the occipital cortex, and completing later in frontal regions (Armstrong et al., 1995; Delpolyi et al., 2005; van der Knaap et al., 1996). Differences were also seen prominently in the region of the operculum, a region that has been repeatedly highlighted in infants with CHD. Findings of an ‘open operculum’ with exposed insular cortex have been reported in CHD (Awate et al., 2010; Glauser et al., 1990b; Licht et al., 2004; Mahle et al., 2002; Tatum et al., 1989), and has been associated with a poor outcome (Chen et al., 1996).

Having established group differences between infants with CHD and healthy controls, we investigated the effect of CDO_2 on development of cortical ODI. There was a widespread positive relationship between ODI and CDO_2, supporting the hypothesis that impaired oxygen delivery to the developing brain may be associated with delayed cortical microstructural development. There was no relationship between cerebral blood flow alone and ODI, suggesting that impaired CDO_2 rather than alternative proposed metabolic substrates (Rudolph, 2016) may be most influential. These results

support recent laboratory studies, with oxygen tension shown to regulate the development of human cortical radial glia cells. Moderate and severe levels of hypoxia exert negative effects on gliogenesis, mediated via reduced numbers of pre-oligodendrocytes and increased numbers of reactive astrocytes derived from cortical radial glia cells (Ortega et al., 2017). Equally, diminished subventricular zone neurogenesis as a result of chronic hypoxia may represent a cellular mechanism that underlies immature cortical development in the CHD population (Morton et al., 2017). Taken together, these studies support the view that oxygenation of the developing brain is a crucial factor to optimise in order to restore the derailing trajectory of cortical development in this population. Future serial imaging to assess cortical development in CHD through infancy and early childhood would allow us to understand if microstructural differences observed in the newborn period are simply delayed with potential for catch-up in later childhood, or if such abnormalities are permanent and persist into childhood. Such work may offer insights into whether early surgical repair may help prevent further divergence, resulting in better long-term neurodevelopmental outcomes.

There were limitations to our study. Firstly, quantitative estimates obtained from microstructural studies are invariably model-dependent, exhibiting biases and limitations that are related to model assumptions. Despite this, NODDI indices have been shown to correlate with histological changes in neurite geometrical configuration (Grussu et al., 2017), and offers a valuable proxy to underlying biological changes in microstructure. Secondly, CDO_2 was also measured in the postnatal period, while the most influential period on brain growth would have been in utero, and particularly during the third trimester. Despite this, we feel that postnatal CDO_2 remains a useful surrogate for severity of cardiac circulatory compromise to date, taking into account both measures of cerebral blood flow and degree of hypoxia as a result of structural changes in congenital heart disease. Thirdly, the underlying genetic basis of CHD is becoming increasingly better-understood (Zaidi and Brueckner, 2017), and may represent a key contributor not only to structural heart disease and associated impaired CDO_2, but also to intrinsic abnormalities in microstructural development of the brain.

There are currently no validated neuroprotective therapies available for infants with CHD. Our demonstration that reduced CDO_2 is associated with impaired cortical maturation in this population supports the development of strategies to optimise fetal

CDO_2. Strategies including the provision of supplemental oxygen to mothers during pregnancy may enable restoration of fetal cerebral oxygen tension to levels required to prevent or reverse abnormal corticogenesis. In addition, the use of newer microstructural measures such as ODI may provide a crucial leading indicator in the postnatal period to assess the impact of novel interventions on cortical development before child neurodevelopmental outcomes can be assessed at a later age.

Chapter 7

Summary

7.1 CONCLUSIONS

With the increasing survival of infants with complex CHD, greater attention is turning to long-term outcomes and quality of life in this important population (Marino et al., 2012). Neurodevelopmental outcomes have not improved at the same pace as surgical and medical advances in recent decades (Gaynor et al., 2015), emphasising the need to better-understand the neural substrate that underlies poorer neurodevelopmental outcomes in children with CHD. Through this understanding, we hope to make progress towards identifying interventions with the potential to restore early brain development to a normal healthy trajectory, while establishing more sensitive imaging tools to quantify abnormalities in brain macro- and microstructural development. There is also considerable potential to discover valuable improvements in clinical practice through large-scale collaborations to compare existing variable practices across different institutions.

The primary hypothesis of this thesis was that infants with CHD have impaired early brain development and are more susceptible to injury. This was tested using two methodological approaches. Firstly, qualitative radiological analysis of a prospective cohort of 70 infants with complex CHD was performed in Chapter 4, which found evidence of brain lesions in 39% of subjects. The prevalence of punctate white matter lesions was consistent with previously reported cohorts, distributed widely throughout the brain, including frontal white matter, optic radiations and corona radiata. However, a low rate of ischaemic stroke was found compared to previously studied cohorts. Relevant clinical variables were considered, suggesting that clinical variables related to haemodynamic stability at birth may be most related to arterial infarction. There were no cases of venous sinus thrombosis in our group, which is interesting in the context of a recent previous study that reported thrombosis in 8% (Claessens et al., 2017). Differences may be due to local variation in clinical practice, where our institution uses entirely different vascular access routes for central lines while preparing our infants for surgery. This difference alone provides insight into the

potential benefits of a wider collaborative project and offers encouragement for the future.

As a second approach to address the primary hypothesis, quantitative analysis was performed using analysis of both structural and diffusion data. In Chapter 5, both total brain volume and cortical grey matter volume were found to be reduced in infants with CHD compared to healthy age-matched controls. Cortical surface analysis showed that cortical folding, quantified using gyrification index, was reduced in CHD, primarily affecting parietal, temporal and occipital regions. In Chapter 6, diffusion analysis of the cortex demonstrated that infants with CHD have regions of increased FA and reduced ODI compared to healthy age-matched controls. The effect was most pronounced posteriorly and affected frontal regions least. The link between macrostructural abnormalities found in this thesis and by other groups (Claessens et al., 2016; Clouchoux et al., 2013; Limperopoulos et al., 2010; Miller et al., 2007; Ortinau et al., 2013) and microstructural findings was established through the demonstration of a strong positive relationship between gyrification index and ODI. Overall, these findings support the interpretation that impaired microstructural development of the cortex in CHD is predominantly due to abnormal dendritic arborisation, which is in turn related to impaired development of cortical gyrification. Such results corroborate animal studies in the fetal macaque showing that microstructural development of the cortex is coupled to the formation of gyri and sulci (Wang et al., 2017), and make progress towards understanding the macrostructural abnormalities that have been well-reported in the newborn population with CHD.

The second hypothesis of this thesis was that reduced cerebral oxygen delivery (CDO_2) in CHD is associated with impaired development of the cerebral cortex. In Chapter 5, the macrostructure of the cortex was investigated, with both cortical grey matter volume and gyrification index found to be positively associated with CDO_2. In Chapter 6, cortical microstructure was investigated, with widespread regions of the brain showing a linear association between CDO_2 and ODI. Interestingly, there was no association between cerebral blood flow alone and ODI, suggesting that the role of alternative metabolic substrates (e.g. Rudolph, 2016) may be less influential. Taken together, these *in vivo* studies suggest that CDO_2 plays an important role in the normal development of cortical microstructure, which in turn is associated with development of cortical macrostructure.

The findings in this thesis are potentially valuable for the development of future therapies for CHD. Animal studies have suggested that oxygen plays a key role in brain development (Morton et al., 2017; Yuen et al., 2014), but there have been limited studies investigating this *in vivo* (Sun et al., 2015). The associations shown in this thesis between CDO_2 and markers of brain development offer support to potential therapies to improve cerebral oxygenation during the crucial third trimester of pregnancy, such as maternal oxygen supplementation. In addition, macrostructural and microstructural measures described in this thesis could potentially act as markers of brain dysmaturation for interventional trials, providing a leading indicator in the newborn period while waiting for long-term neurodevelopmental follow-up. Earlier indicators enable faster feedback and iteration, while better sensitivity through tools including diffusion MRI reduce the chance of an avoidable type II error.

7.2 FUTURE PERSPECTIVES

Below are some possible directions for future study, to extend upon the work presented in this thesis:

7.2.1 Follow up of our prospective cohort

The infants presented in this thesis undertook a comprehensive range of novel structural and diffusion imaging examinations, developed for the Developing Human Connectome Project, that have not been performed in a cohort with CHD before. Follow-up of this cohort is ongoing at around the children's second birthday. Once this phase is complete, we will begin to understand the predictive value and clinical utility of these newer imaging techniques.

7.2.2 Further uses of acquired neonatal diffusion data

There are a number of different biophysical models that attempt to model tissue microstructure from diffusion-weighted imaging. While this thesis considered only diffusion tensor and NODDI methods, it may be interesting to compare additional models using this dataset. In particular, Spherical Mean Technique (Kaden et al., 2016) provides a new way to estimate tissue microstructure that is not confounded by the effects of fibre crossings and orientation dispersion, which are ubiquitous in the brain. It also avoids some of the limitations of NODDI such as the use of a fixed intrinsic diffusivity.

Structural network analysis using diffusion-weighted imaging has demonstrated global differences in white matter network topology in adolescents with CHD (Panigrahy et al., 2015). Functional MRI has already been used in neonates to show that the density of rich club nodes in CHD was diminished, with reduced connectivity among some critical brain hubs (De Asis-Cruz et al., 2017).

While this thesis did not acquire functional MRI data, there is an exciting opportunity to interrogate the network structure of the white matter using diffusion tractography, and relate these to subsequent outcomes.

7.2.3 Genetic influences in CHD

CHD has been known to be associated with a number of genetic conditions for many years. More recently, it has been suggested that up to 30% of children with CHD have manifestations of a multi-systemic syndrome (Marino et al., 2012). Common associations include Trisomy 21 and 22q11.2 deletion (DiGeorge syndrome), which are both independently associated with poorer neurodevelopmental outcome (Atallah et al., 2007; Visootsak et al., 2011). Others include CHARGE syndrome, Noonan's syndrome, Williams syndrome, VACTERL, and many others (Pierpont et al., 2007).

Through more advanced genetic sequencing, we may begin to understand the genetic underpinnings of CHD in those who do not appear to have an overt genetic syndrome. For example, recent studies have shown that previously unknown copy number variants (CNVs) may be present and potentially causative in up to 20% of non-syndromic children (Soemedi et al., 2012; Thienpont et al., 2007). Another example is how the apolipoprotein E (APOE) ε2 allele, which encodes the APOE E2 protein, is associated with poor neurological outcome in children with CHD following cardiopulmonary bypass. Infants with this allele have been shown to have significantly worse BSID scores, independent of cardiac defect, ethnicity of socioeconomic status (Gaynor et al., 2003, 2014). Whole-exome sequencing will bring even greater insights. One study of 1200 CHD patients found that patients with both CHD and neurodevelopmental disorders had a much higher burden of damaging *de novo* mutations, particularly in genes with likely roles in both heart and brain development (Homsy et al., 2015). This suggests that clinical phenotyping may help to identify those at greatest risk of neurodevelopmental impairment, enabling earlier intervention.

However, studies performed to date have highlighted that CHD is extremely heterogeneous, which is further complicated by the relative lack of observed genotype-phenotype correlations (Zaidi and Brueckner, 2017).

Genetic material has been collected from most infants recruited as part of this thesis, although our sample size is not yet of a size typically required for genetic group studies. Aggregation of genetic testing and analysis with other centres, using the latest sequencing techniques and linked to MR imaging, could help to further identify the genetic underpinning of a greater proportion of CHD and its effect on neurodevelopmental outcomes, and help translate these findings into precision medicine for the care of children born with CHD.

7.2.4 Future management of children with CHD at St Thomas'

Work presented in this thesis highlights that children with CHD are at greater risk of brain injury and dysmaturation. Through incidental findings in asymptomatic infants, the research presented in this thesis has enabled early referral for specialist neurological follow up in a number of cases. There is a strong argument that all infants with CHD should undergo neurodevelopmental follow-up, including early brain imaging (ideally fetal and neonatal), as part of their routine clinical care. This would offer benefits not only for the individual but would also enable larger studies to be performed using the high-quality imaging possible at our institution. Routine neurodevelopmental follow-up in infants with complex CHD is recommended by American guidelines (Marino et al., 2012), but implementation of such practices in the UK has been limited to date.

7.2.5 Variation in clinical practice

There is considerable variation in clinical practice between different centres globally. A number of research cohorts of infants with CHD exist across the world, which are each relatively small individually, but when combined would provide a rich source of information about the most influential factors in early brain injury and dysmaturation, and subsequent outcome. The aggregation of data through multi-centre collaborations would be of great value for the future.

7.2.6 The effect of fetal CDO_2 on measures of macro- and microstructure

One key limitation of this thesis is that all imaging was performed in the neonatal period. Further work could build upon the results presented in this thesis by obtaining measures of CDO_2 in utero (e.g. Sun et al, 2015), and correlating these with subsequent neonatal structural and diffusion measures of brain development. This direct link between fetal environment and subsequent outcome would be very valuable.

7.2.7 Relating fetal haemodynamics to imaging findings and outcome

As part of the normal fetal clinical service at the Evelina Children's Hospital, a number of measures of fetal haemodynamic status are measured (RI, PI, CPR etc), which were not recorded as part of this thesis. By retrospectively collecting this data, there is the opportunity to better-understand how autoregulatory mechanisms may impact upon, or highlight, ongoing abnormalities in fetal brain development, and correlate this with future neurodevelopmental outcome.

7.2.8 Timing of injury

Although the weight of evidence suggests that pre-surgical brain injury occurs around the time of delivery, there have been few serial imaging studies in CHD to ascertain precise timing of injury. In addition, T1-weighted imaging in fetal MRI has historically been limited compared to neonatal imaging, due to technical constraints, meaning that punctate white matter injury may not have been detected with equally high sensitivity.

New fetal imaging sequences that offer motion-corrected T1-weighted imaging may allow a greater insight into timing of injury in the late third trimester, and image registration techniques to co-register each individual's fetal and neonatal imaging may reveal subtle changes in fetal imaging that had not been detected previously.

7.2.9 Identification of candidate therapies to intervene in abnormal brain development and injury

Few studies have found promising neuroprotective effects in CHD. A recent study tested the neuroprotective effect of erythropoietin in cardiac surgery (Andropoulos et al., 2013). However, although it was found to be safe, there was no difference in

neurodevelopmental outcome at 1 year of age. The study was underpowered to definitively detect changes in neurodevelopmental outcome, and so the authors recommend a larger study.

Other studies are currently looking at the effect of maternal progesterone therapy during pregnancy (https://clinicaltrials.gov/ct2/show/NCT02133573), and the effect of anaesthetic agent dexmedetomidine during surgery (https://clinicaltrials.gov/ct2/show/NCT01915277).

There are a number of exciting potential future therapies. Maternal supplemental oxygen during pregnancy is an attractive intervention given the results from this thesis and others (particularly Sun et al. 2015). Following a recent maternal hyperoxygenation study (Porayette et al., 2016), trials are planned to start in Toronto shortly. The possibility of SVZ-stabilising therapeutics has been suggested by Morton et al. 2017 that are designed to protect or restore the neurogenic potential of NSPCs. HIF-stabilisers have been suggested in the context of animal work showing this potential (Yuen et al., 2014). There are a large number of neuroprotective agents that have shown promise in the preterm/HIE population (e.g. allopurinol, phentolamine, dextromethorphan, sodium nitroprusside, ketamine etc), which could be applied to the CHD population in future intervention studies.

7.2.10 Summary

Ultimately, the challenge of improving neurodevelopmental outcomes in CHD will rely on a collaborative and an integrated approach to future research. Through a combination of cell biology, molecular biology, genetics, and sophisticated models of brain development, we will be able to understand the underlying causes of brain dysmaturation in this population, and identify the optimum window and most promising therapeutics for treatment to improve long-term neurodevelopmental outcomes in CHD.

Bibliography

Agus, M.S.D., Asaro, L.A., Steil, G.M., Alexander, J.L., Silverman, M., Wypij, D., Gaies, M.G., 2014. Tight Glycemic Control After Pediatric Cardiac Surgery in High-Risk Patient Populations: A Secondary Analysis of the Safe Pediatric Euglycemia After Cardiac Surgery Trial. Circulation 129, 2297–2304. doi:10.1161/CIRCULATIONAHA.113.008124

Agus, M.S.D., Steil, G.M., Wypij, D., Costello, J.M., Laussen, P.C., Langer, M., Alexander, J.L., Scoppettuolo, L.A., Pigula, F.A., Charpie, J.R., Ohye, R.G., Gaies, M.G., 2012. Tight Glycemic Control versus Standard Care after Pediatric Cardiac Surgery. N. Engl. J. Med. 367, 1208–1219. doi:10.1056/NEJMoa1206044

Ahrens, J., Geveci, B., Law, C., 2005. ParaView: An End-User Tool for Large Data Visualization. Elsevier.

Algra, S.O., Jansen, N.J.G., van der Tweel, I., Schouten, A.N.J., Groenendaal, F., Toet, M., van Oeveren, W., van Haastert, I.C., Schoof, P.H., de Vries, L.S., Haas, F., 2014. Neurological injury after neonatal cardiac surgery: a randomized, controlled trial of 2 perfusion techniques., Circulation. doi:10.1161/CIRCULATIONAHA.113.003312

Allen, J.S., Damasio, H., Grabowski, T.J., 2002. Normal Neuroanatomical Variation in the Human Brain : An MRI-Volumetric Study 358, 341–358. doi:10.1002/ajpa.10092

American Psychiatric Association, 2000. Diagnostic and Statistical Manual of Mental Disorders, Fourth Edition: DSM-IV-TR®, Diagnostic and Statistical Manual of Mental Disorders. American Psychiatric Association.

Andersson, J.L.R., Skare, S., Ashburner, J., 2003. How to correct susceptibility distortions in spin-echo echo-planar images: Application to diffusion tensor imaging. Neuroimage 20, 870–888. doi:10.1016/S1053-8119(03)00336-7

Andescavage, N., Yarish, A., Donofrio, M., Bulas, D., Evangelou, I., Vezina, G., McCarter, R., Duplessis, A., Limperopoulos, C., 2015. 3-D volumetric MRI evaluation of the placenta in fetuses with complex congenital heart disease.

Placenta 36, 1024–1030. doi:10.1016/j.placenta.2015.06.013

Andropoulos, D.B., Ahmad, H.B., Haq, T., Brady, K., Stayer, S. a, Meador, M.R., Hunter, J. V, Rivera, C., Voigt, R.G., Turcich, M., He, C.Q., Shekerdemian, L.S., Dickerson, H. a, Fraser, C.D., Dean McKenzie, E., Heinle, J.S., Blaine Easley, R., 2014. The association between brain injury, perioperative anesthetic exposure, and 12-month neurodevelopmental outcomes after neonatal cardiac surgery: a retrospective cohort study. Paediatr. Anaesth. 24, 266–74. doi:10.1111/pan.12350

Andropoulos, D.B., Brady, K., Easley, R.B., Dickerson, H.A., Voigt, R.G., Shekerdemian, L.S., Meador, M.R., Eisenman, C.A., Hunter, J. V., Turcich, M., Rivera, C., McKenzie, E.D., Heinle, J.S., Fraser, C.D., 2013. Erythropoietin neuroprotection in neonatal cardiac surgery: A phase I/II safety and efficacy trial. J. Thorac. Cardiovasc. Surg. 146, 124–131. doi:10.1016/j.jtcvs.2012.09.046

Andropoulos, D.B., Easley, R.B., Brady, K., McKenzie, E.D., Heinle, J.S., Dickerson, H.A., Shekerdemian, L., Meador, M., Eisenman, C., Hunter, J. V., Turcich, M., Voigt, R.G., Fraser, C.D., 2012. Changing expectations for neurological outcomes after the neonatal arterial switch operation. Ann. Thorac. Surg. 94, 1250–1256. doi:10.1016/j.athoracsur.2012.04.050

Andropoulos, D.B., Hunter, J. V., Nelson, D.P., Stayer, S.A., Stark, A.R., McKenzie, E.D., Heinle, J.S., Graves, D.E., Fraser, C.D., 2010. Brain immaturity is associated with brain injury before and after neonatal cardiac surgery with high-flow bypass and cerebral oxygenation monitoring. J. Thorac. Cardiovasc. Surg. 139, 543–556. doi:10.1016/j.jtcvs.2009.08.022

Andropoulos, D.B., Stayer, S.A., Diaz, L.K., Ramamoorthy, C., 2004. Neurological monitoring for congenital heart surgery. Anesth. Analg. 99, 1365–1375. doi:10.1213/01.ANE.0000134808.52676.4D

Antshel, K.M., Aneja, A., Strunge, L., Peebles, J., Fremont, W.P., Stallone, K., AbdulSabur, N., Higgins, A.M., Shprintzen, R.J., Kates, W.R., 2007. Autistic spectrum disorders in velo-cardio facial syndrome (22q11.2 deletion). J. Autism Dev. Disord. 37, 1776–1786. doi:10.1007/s10803-006-0308-6

Armstrong, E., Schleicher, A., Omran, H., Curtis, M., Zilles, K., 1995. The ontogeny of

human gyrification. Cereb. Cortex 5, 56–63. doi:10.1093/cercor/5.1.56

Assaf, Y., Basser, P.J., 2005. Composite hindered and restricted model of diffusion (CHARMED) MR imaging of the human brain. Neuroimage 27, 48–58. doi:10.1016/j.neuroimage.2005.03.042

Assaf, Y., Blumenfeld-Katzir, T., Yovel, Y., Basser, P.J., 2008. AxCaliber: A method for measuring axon diameter distribution from diffusion MRI. Magn. Reson. Med. 59, 1347–1354. doi:10.1002/mrm.21577

Atallah, J., Joffe, A.R., Robertson, C.M.T., Leonard, N., Blakley, P.M., Nettel-Aguirre, A., Sauve, R.S., Ross, D.B., Rebeyka, I.M., 2007. Two-year general and neurodevelopmental outcome after neonatal complex cardiac surgery in patients with deletion 22q11.2: A comparative study. J. Thorac. Cardiovasc. Surg. 134, 772–779. doi:10.1016/j.jtcvs.2007.03.007

Avants, B., Duda, J.T., Kim, J., Zhang, H., Pluta, J., Gee, J.C., Whyte, J., 2008. Multivariate Analysis of Structural and Diffusion Imaging in Traumatic Brain Injury. Acad. Radiol. 15, 1360–1375. doi:10.1016/j.acra.2008.07.007

Avants, B.B., Epstein, C.L., Grossman, M., Gee, J.C., 2008. Symmetric diffeomorphic image registration with cross-correlation: Evaluating automated labeling of elderly and neurodegenerative brain. Med. Image Anal. 12, 26–41. doi:10.1016/j.media.2007.06.004

Awate, S.P., Yushkevich, P., Song, Z., Licht, D., Gee, J.C., 2009. Multivariate high-dimensional cortical folding analysis, combining complexity and shape, in neonates with congenital heart disease. Lect. Notes Comput. Sci. (including Subser. Lect. Notes Artif. Intell. Lect. Notes Bioinformatics) 5636 LNCS, 552–563. doi:10.1007/978-3-642-02498-6_46

Awate, S.P., Yushkevich, P.A., Song, Z., Licht, D.J., Gee, J.C., 2010. Cerebral cortical folding analysis with multivariate modeling and testing: Studies on gender differences and neonatal development. Neuroimage 53, 450–459. doi:10.1016/j.neuroimage.2010.06.072

Ayanzen, R.H., Bird, C.R., Keller, P.J., McCully, F.J., Theobald, M.R., Heiserman, J.E., 2000. Cerebral MR venography: Normal anatomy and potential diagnostic pitfalls. Am. J. Neuroradiol. 21, 74–78.

Bakker, C.J.G., Hoogeveen, R.M., Viergever, M.A., Mali, W.P.T.M., 1999. Construction of a protocol for measuring blood flow by 2D phase contrast {MR} angiography 9, 119–127.

Bakker, C.J.G., Kouwenhoven, M., Hartkamp, M.J., Hoogeveen, R.M., Mali, W.P.T.M., 1995. Accuracy and precision of time-averaged flow as measured by nontriggered 2D phase-contrast MR angiography, a phantom evaluation. Magn. Reson. Imaging 13, 959–965. doi:10.1016/0730-725X(95)02005-E

Ball, G., Srinivasan, L., Aljabar, P., Counsell, S.J., Durighel, G., Hajnal, J. V, Rutherford, M.A., Edwards, A.D., 2013. Development of cortical microstructure in the preterm human brain. Proc. Natl. Acad. Sci. U. S. A. 110, 9541–6. doi:10.1073/pnas.1301652110

Basser, P.J., Mattiello, J., LeBihan, D., 1994. MR diffusion tensor spectroscopy and imaging. Biophys. J. 66, 259–267. doi:10.1016/S0006-3495(94)80775-1

Bean Jaworski, J.L., Flynn, T., Burnham, N., Chittams, J.L., Sammarco, T., Gerdes, M., Bernbaum, J.C., Clancy, R.R., Solot, C.B., Zackai, E.H., McDonald-McGinn, D.M., Gaynor, J.W., 2017. Rates of autism and potential risk factors in children with congenital heart defects. Congenit. Heart Dis. 12, 421–429. doi:10.1111/chd.12461

Beaulieu, C., 2002. The basis of anisotropic water diffusion in the nervous system - A technical review. NMR Biomed. 15, 435–455. doi:10.1002/nbm.782

Beca, J., Gunn, J., Coleman, L., Hope, A., Whelan, L.-C., Gentles, T., Inder, T., Hunt, R., Shekerdemian, L., 2009. Pre-operative brain injury in newborn infants with transposition of the great arteries occurs at rates similar to other complex congenital heart disease and is not related to balloon atrial septostomy. J. Am. Coll. Cardiol. 53, 1807–11. doi:10.1016/j.jacc.2009.01.061

Beca, J., Gunn, J.K., Coleman, L., Hope, A., Reed, P.W., Hunt, R.W., Finucane, K., Brizard, C., Dance, B., Shekerdemian, L.S., 2013. New White matter brain injury after infant heart surgery is associated with diagnostic group and the use of circulatory arrest. Circulation 127, 971–979. doi:10.1161/CIRCULATIONAHA.112.001089

Behrens, T.E.J., Woolrich, M.W., Jenkinson, M., Johansen-Berg, H., Nunes, R.G.,

Clare, S., Matthews, P.M., Brady, J.M., Smith, S.M., 2003. Characterization and Propagation of Uncertainty in Diffusion-Weighted MR Imaging. Magn. Reson. Med. 50, 1077–1088. doi:10.1002/mrm.10609

Bellinger, D.C., 2008. Are children with congenital cardiac malformations at increased risk of deficits in social cognition? Cardiol. Young 18, 3–9. doi:10.1017/S104795110700176X

Bellinger, D.C., Jonas, R.A., Rappaport, L.A., Wypij, D., Wernovsky, G., Kuban, K.C., Barnes, P.D., Holmes, G.L., Hickey, P.R., Strand, R.D., 1995. Developmental and neurologic status of children after heart surgery with hypothermic circulatory arrest or low-flow cardiopulmonary bypass., The New England journal of medicine. doi:10.1097/00008506-199507000-00007

Bellinger, D.C., Newburger, J.W., Wypij, D., Kuban, K.C.K., duPlesssis, A.J., Rappaport, L. a, 2009. Behaviour at eight years in children with surgically corrected transposition: The Boston Circulatory Arrest Trial. Cardiol. Young 19, 86–97. doi:10.1017/S1047951108003454

Bellinger, D.C., Rappaport, L.A., Wypij, D., Wernovsky, G., Newburger, J.W., 1997. Patterns of Developmental Dysfunction after Surgery during Infancy to Correct Transposition of the Great Arteries. J. Dev. Behav. Pediatr. doi:10.1097/00004703-199704000-00001

Bellinger, D.C., Rivkin, M.J., Demaso, D., Robertson, R.L., Stopp, C., Dunbar-Masterson, C., Wypij, D., Newburger, J.W., 2015a. Adolescents with tetralogy of Fallot: Neuropsychological assessment and structural brain imaging. Cardiol. Young 25, 338–347. doi:10.1017/S1047951114000031

Bellinger, D.C., Watson, C.G., Rivkin, M.J., Robertson, R.L., Roberts, A.E., Stopp, C., Dunbar-Masterson, C., Bernson, D., DeMaso, D.R., Wypij, D., Newburger, J.W., 2015b. Neuropsychological status and structural brain imaging in adolescents with single ventricle who underwent the fontan procedure. J. Am. Heart Assoc. 4, 1–17. doi:10.1161/JAHA.115.002302

Bellinger, D.C., Wypij, D., Kuban, K.C., Rappaport, L. a., Hickey, P.R., Wernovsky, G., Jonas, R. a., Newburger, J.W., 1999. Developmental and neurological status of children at 4 years of age after heart surgery with hypothermic circulatory arrest

or low-flow cardiopulmonary bypass., Circulation. doi:10.1161/01.CIR.100.5.526

Bellinger, D.C., Wypij, D., Rivkin, M.J., Demaso, D.R., Robertson, R.L., Dunbar-Masterson, C., Rappaport, L.A., Wernovsky, G., Jonas, R.A., Newburger, J.W., 2011. Adolescents with d-transposition of the great arteries corrected with the arterial switch procedure: Neuropsychological assessment and structural brain imaging. Circulation 124, 1361–1369. doi:10.1161/CIRCULATIONAHA.111.026963

Bernier, P.-L., Stefanescu, A., Samoukovic, G., Tchervenkov, C.I., 2010. The challenge of congenital heart disease worldwide: epidemiologic and demographic facts. Semin. Thorac. Cardiovasc. Surg. Pediatr. Card. Surg. Annu. 13, 26–34. doi:10.1053/j.pcsu.2010.02.005

Bernstein, M., King, K., Zhou, X., 2004. Handbook of MRI Pulse Sequences 1st Edition. Academic Press.

Bertholdt, S., Latal, B., Liamlahi, R., Prêtre, R., Scheer, I., Goetti, R., Dave, H., Bernet, V., Schmitz, A., Von rhein, M., Knirsch, W., Sennhauser, F.H., Plecko, B.R., Kretschmar, O., Batinic, K., Dimitropoulos, A., Kellenberger, C., Makki, M., Hug, M.I., Bürki, C., Weiss, M., Hagmann, C., 2014. Cerebral lesions on magnetic resonance imaging correlate with preoperative neurological status in neonates undergoing cardiopulmonary bypass surgery. Eur. J. Cardio-thoracic Surg. 45, 625–632. doi:10.1093/ejcts/ezt422

Bjarnason-Wehrens, B., Dordel, S., Schickendantz, S., Krumm, C., Bott, D., Sreeram, N., Brockmeier, K., 2007. Motor development in children with congenital cardiac diseases compared to their healthy peers. Cardiol. Young 17, 487–498. doi:10.1017/S1047951107001023

Bloch, F., 1946. Nuclear induction. Phys. Rev. 70, 460–474. doi:10.1103/PhysRev.70.460

Block, A.J., McQuillen, P.S., Chau, V., Glass, H., Poskitt, K.J., Barkovich, A.J., Esch, M., Soulikias, W., Azakie, A., Campbell, A., Miller, S.P., 2010. Clinically silent preoperative brain injuries do not worsen with surgery in neonates with congenital heart disease. J. Thorac. Cardiovasc. Surg. 140, 550–557. doi:10.1016/j.jtcvs.2010.03.035

Blue, G.M., Kirk, E.P., Giannoulatou, E., Sholler, G.F., Dunwoodie, S.L., Harvey, R.P., Winlaw, D.S., 2017. Advances in the Genetics of Congenital Heart Disease. J. Am. Coll. Cardiol. 69, 859–870. doi:10.1016/j.jacc.2016.11.060

Bonestroo, H.J.C., Lemmers, P.M.A., Baerts, W., van Bel, F., 2011. Effect of Antihypotensive Treatment on Cerebral Oxygenation of Preterm Infants Without PDA. Pediatrics 128, e1502–e1510. doi:10.1542/peds.2010-3791

Bookstein, F.L., 1989. Principal Warps: Thin-Plate Splines and the Decomposition of Deformations. IEEE Trans. Pattern Anal. Mach. Intell. doi:10.1109/34.24792

Brandlistuen, R.E., Stene-Larsen, K., Holmstrom, H., Landolt, M.A., Eskedal, L.T., Vollrath, M.E., 2010. Motor and Social Development in 6-Month-Old Children with Congenital Heart Defects. J. Pediatr. 156, 265–269.e1. doi:10.1016/j.jpeds.2009.08.035

Brant Zawadzki, M., Davis, P.L., Crooks, L.E., 1983. NMR demonstration of cerebral abnormalities: Comparison with CT. Am. J. Neuroradiol. 4, 117–124. doi:10.2214/ajr.140.5.847

Brazy, J.E., Lewis, D. V, Mitnick, M.H., Jöbsis vander Vliet, F.F., 1985. Noninvasive monitoring of cerebral oxygenation in preterm infants: preliminary observations. Pediatrics 75, 217–25.

Brody, B.A., Kinney, H.C., Kloman, A.S., Gilles, F.H., 1987. Sequence of central nervous system myelination in human infancy. I. An autopsy study of myelination. J. Neuropathol. Exp. Neurol. 46, 283–301.

Brosig, C.L., Mussatto, K.A., Kuhn, E.M., Tweddell, J.S., 2007. Neurodevelopmental Outcome in Preschool Survivors of Complex Congenital Heart Disease: Implications for Clinical Practice. J. Pediatr. Heal. Care 21, 3–12. doi:10.1016/j.pedhc.2006.03.008

Brossard-Racine, M., du Plessis, a J., Vezina, G., Robertson, R., Bulas, D., Evangelou, I.E., Donofrio, M., Freeman, D., Limperopoulos, C., 2014. Prevalence and spectrum of in utero structural brain abnormalities in fetuses with complex congenital heart disease. AJNR. Am. J. Neuroradiol. 35, 1593–9. doi:10.3174/ajnr.A3903

Brossard-Racine, M., du Plessis, A., Vezina, G., Robertson, R., Donofrio, M.,

Tworetzky, W., Limperopoulos, C., 2016. Brain Injury in Neonates with Complex Congenital Heart Disease: What Is the Predictive Value of MRI in the Fetal Period? Am. J. Neuroradiol. 1–9. doi:10.3174/ajnr.A4716

Brown, R., 1828. XXVII. A brief account of microscopical observations made in the months of June, July and August 1827, on the particles contained in the pollen of plants; and on the general existence of active molecules in organic and inorganic bodies. Philos. Mag. 4, 161–173. doi:10.1080/14786442808674769

Bystron, I., Blakemore, C., Rakic, P., 2008. Development of the human cerebral cortex: Boulder Committee revisited. Nat. Rev. Neurosci. 9, 110–122. doi:10.1038/nrn2252

Calderon, J., Bellinger, D.C., 2015. Executive function deficits in congenital heart disease: why is intervention important? Cardiol. Young 1–9. doi:10.1017/S1047951115001134

Calderon, J., Jambaqué, I., Bonnet, D., Angeard, N., 2014. Executive functions development in 5- to 7-year-old children with transposition of the great arteries: Longitudinal study. Dev. Neuropsychol. 39, 365–384. doi:10.1080/87565641.2014.916709

Campbell, M., Reynolds, G., 1949. The physical and mental development of children with congenital heart disease. Arch. Dis. Child. 24, 294–302.

Carlgren, L., 1959. The incidence of congenital heart disease in children born in Gothenburg 1941–1950. Br. Heart J. 40–50.

Caughey, A.B., Sundaram, V., Kaimal, A.J., Cheng, Y.W., Gienger, A., Little, S.E., Lee, J.F., Wong, L., Shaffer, B.L., Tran, S.H., Padula, A., McDonald, K.M., Long, E.F., Owens, D.K., Bravata, D.M., 2009. Maternal and neonatal outcomes of elective induction of labor. Evid. Rep. Technol. Assess. (Full. Rep). 1–257.

Chandar, J.S., Wolfe, S.B., 1994. Displacement of preexisting thrombus by umbilical vein catheterization. Pediatr. Cardiol. 15, 311–312. doi:10.1007/BF00798126

Chen, C.Y., Zimmerman, R.A., Faro, S., Parrish, B., Wang, Z., Bilaniuk, L.T., Chou, T.Y., 1996. MR of the cerebral operculum: Abnormal opercular formation in infants and children. Am. J. Neuroradiol. 17, 1303–1311.

Chi, J.G., Dooling, E.C., Gilles, F.H., 1977. Gyral development of the human brain. Ann. Neurol. 1, 86–93. doi:10.1002/ana.410010109

Childs, A.M., Ramenghi, L.A., Cornette, L., Tanner, S.F., Arthur, R.J., Martinez, D., Levene, M.I., 2001. Cerebral maturation in premature infants: quantitative assessment using MR imaging. AJNR. Am. J. Neuroradiol. 22, 1577–1582.

Christiaens, D., Cordero-Grande, L., Pietsch, M., Hutter, J., Edwards, A.D., Deprez, M., Hajnal, V., Tournier, J., 2018. Multi-shell SHARD reconstruction from scattered slice diffusion MRI data in the neonatal brain. ISMRM (Paris) Accepted.

Claessens, N.H.P., Algra, S.O., Jansen, N.J.G., Groenendaal, F., de Wit, E., Wilbrink, A.A., Haas, F., Schouten, A.N.J., Nievelstein, R.A.J., Benders, M.J.N.L., de Vries, L.S., 2017. Clinical and neuroimaging characteristics of cerebral sinovenous thrombosis in neonates undergoing cardiac surgery. J. Thorac. Cardiovasc. Surg. 1–10. doi:10.1016/j.jtcvs.2017.10.083

Claessens, N.H.P.P., Moeskops, P., Buchmann, A., Latal, B., Knirsch, W., Scheer, I., Isgum, I., de Vries, L.S., Benders, M.J.N.L.N.L., von Rhein, M., Išgum, I., de Vries, L.S., Benders, M.J.N.L.N.L., von Rhein, M., 2016. Delayed cortical gray matter development in neonates with severe congenital heart disease. Pediatr. Res. 80, 668–674. doi:10.1038/pr.2016.145

Clouchoux, C., du Plessis, A.J., Bouyssi-Kobar, M., Tworetzky, W., McElhinney, D.B., Brown, D.W., Gholipour, A., Kudelski, D., Warfield, S.K., McCarter, R.J., Robertson, R.L., Evans, A.C., Newburger, J.W., Limperopoulos, C., 2013. Delayed Cortical Development in Fetuses with Complex Congenital Heart Disease. Cereb. Cortex 23, 2932–2943. doi:10.1093/cercor/bhs281

Cohn, H.E., Sacks, E.J., Heymann, M.A., Rudolph, A.M., 1974. Cardiovascular responses to hypoxemia and acidemia in fetal lambs. Am. J. Obstet. Gynecol. 120, 817–24.

Cole, T.J., 2017. Super Imposition by Translation and Rotation Growth Curve Analysis (R Package).

Cole, T.J., Freeman, J. V., Preece, M.A., 1998. British 1990 growth reference centiles for weight, height, body mass index and head circumference fitted by maximum penalized likelihood. Stat. Med. 17, 407–429. doi:10.1002/(SICI)1097-

0258(19980228)17:4<407::AID-SIM742>3.0.CO;2-L

Cooke, R.W.I., Lucas, A., Yudkin, P.L.N., Pryse-Davies, J., 1977. Head circumference as an index of brain weight in the fetus and newborn. Early Hum. Dev. 1, 145–149. doi:10.1016/0378-3782(77)90015-9

Cordero-Grande, L., Hughes, E., Price, A., Hutter, J., Edwards, A., Hajnal, J., 2016. 3D motion corrected SENSE reconstruction for multishot multislice MRI, in: Proc International Society for Magnetic Resonance in Medicine.

Cordero-Grande, L., Hughes, E.J., Hutter, J., Price, A.N., Hajnal, J. V., 2018. Three-dimensional motion corrected sensitivity encoding reconstruction for multi-shot multi-slice MRI: Application to neonatal brain imaging. Magn. Reson. Med. 79, 1365–1376. doi:10.1002/mrm.26796

Cordero-Grande, L., Teixeira, R.P.A.G., Hughes, E.J., Hutter, J., Price, A.N., Hajnal, J. V, 2016. Sensitivity Encoding for Aligned Multishot Magnetic Resonance Reconstruction. IEEE Trans. Comput. Imaging 2, 266–280. doi:10.1109/TCI.2016.2557069

Dale, A.M., Fischl, B., Sereno, M.I., 1999. Cortical surface-based analysis. I. Segmentation and surface reconstruction. Neuroimage 9, 179–94. doi:10.1006/nimg.1998.0395

Daliento, L., 2005. Health related quality of life in adults with repaired tetralogy of Fallot: psychosocial and cognitive outcomes. Heart 91, 213–218. doi:10.1136/hrt.2003.029280

Davidson, A.J., Disma, N., De Graaff, J.C., Withington, D.E., Dorris, L., Bell, G., Stargatt, R., Bellinger, D.C., Schuster, T., Arnup, S.J., Hardy, P., Hunt, R.W., Takagi, M.J., Giribaldi, G., Hartmann, P.L., Salvo, I., Morton, N.S., Von Ungern Sternberg, B.S., Locatelli, B.G., Wilton, N., Lynn, A., Thomas, J.J., Polaner, D., Bagshaw, O., Szmuk, P., Absalom, A.R., Frawley, G., Berde, C., Ormond, G.D., Marmor, J., McCann, M.E., 2016. Neurodevelopmental outcome at 2 years of age after general anaesthesia and awake-regional anaesthesia in infancy (GAS): An international multicentre, randomised controlled trial. Lancet 387, 239–250. doi:10.1016/S0140-6736(15)00608-X

Dawes, G.S., Mott, J.C., Widdicombe, J.G., 1954. The foetal circulation in the lamb. J.

Physiol. 126, 563–587. doi:10.1113/jphysiol.1954.sp005227

De Asis-Cruz, J., Donofrio, M.T., Vezina, G., Limperopoulos, C., 2017. Aberrant brain functional connectivity in newborns with congenital heart disease before cardiac surgery. NeuroImage Clin. 17, 31–42. doi:10.1016/j.nicl.2017.09.020

De Vries, L.S., Van Haastert, I.L.C., Rademaker, K.J., Koopman, C., Groenendaal, F., 2004. Ultrasound abnormalities preceding cerebral palsy in high-risk preterm infants. J. Pediatr. 144, 815–820. doi:10.1016/j.jpeds.2004.03.034

Dean, J.M., McClendon, E., Hansen, K., Azimi-Zonooz, A., Chen, K., Riddle, A., Gong, X., Sharifnia, E., Hagen, M., Ahmad, T., Leigland, L.A., Hohimer, A.R., Kroenke, C.D., Back, S.A., 2013. Prenatal cerebral ischemia disrupts MRI-defined cortical microstructure through disturbances in neuronal arborization. Sci. Transl. Med. 5. doi:10.1126/scitranslmed.3004669

Delpolyi, A.R., Mukherjee, P., Gill, K., Henry, R.G., Partridge, S.C., Veeraraghavan, S., Jin, H., Lu, Y., Miller, S.P., Ferriero, D.M., Vigneron, D.B., Barkovich, A.J., 2005. Comparing microstructural and macrostructural development of the cerebral cortex in premature newborns: Diffusion tensor imaging versus cortical gyration. Neuroimage 27, 579–586. doi:10.1016/j.neuroimage.2005.04.027

Desai, N.K., Hamrick, S.E.G., Strickland, M.J., Matthews, E., McMaster, L., Mahle, W.T., 2015. White Matter Injury and the Inflammatory Response Following Neonatal Cardiac Surgery. Pediatr. Cardiol. 36, 942–949. doi:10.1007/s00246-015-1104-x

Diamond, A., 2013. Executive functions. Annu. Rev. sychology 64, 135–68. doi:10.1146/annurev-psych-113011-143750

Diaz, L.K., Gaynor, J.W., Koh, S.J., Ittenbach, R.F., Gerdes, M., Bernbaum, J.C., Zackai, E.H., Clancy, R.R., Rehman, M.A., Pennington, J.W., Burnham, N., Spray, T.L., Nicolson, S.C., 2016. Increasing cumulative exposure to volatile anesthetic agents is associated with poorer neurodevelopmental outcomes in children with hypoplastic left heart syndrome. J. Thorac. Cardiovasc. Surg. 152, 482–489. doi:10.1016/j.jtcvs.2016.03.095

Dimitropoulos, A., McQuillen, P., Sethi, V., 2013. Brain injury and development in newborns with critical congenital heart disease. Neurology 81, 241–8.

doi:10.1212/WNL.0b013e31829bfdcf

Dobbing, J., Sands, J., 1973. Quantitative growth and development of human brain. Arch. Dis. Child. 48, 757–767. doi:10.1136/adc.48.10.757

Donofrio, M.T., Bremer, Y.A., Schieken, R.M., Gennings, C., Morton, L.D., Eidem, B.W., Cetta, F., Falkensammer, C.B., Huhta, J.C., Kleinman, C.S., 2003. Autoregulation of cerebral blood flow in fetuses with congenital heart disease: the brain sparing effect. Pediatr. Cardiol. 24, 436–43. doi:10.1007/s00246-002-0404-0

Drotar, D., 2004. Measuring child health: Scientific questions, challenges and recommendations. Ambul. Pediatr. 4, 353–357. doi:10.1367/1539-4409(2004)4<353:MCHSQC>2.0.CO;2

du Plessis, A.J., Jonas, R.A., Wypij, D., Hickey, P.R., Riviello, J., Wessel, D.L., Roth, S.J., Burrows, F.A., Walter, G., Farrell, D.M., Walsh, A.Z., Plumb, C.A., del Nido, P., Burke, R.P., Castaneda, A.R., Mayer, J.E., Newburger, J.W., 1997. Perioperative effects of alpha-stat versus ph-stat strategies for deep hypothermic cardiopulmonary bypass in infants. J. Thorac. Cardiovasc. Surg. 114, 991–1001. doi:10.1016/S0022-5223(97)70013-8

Eaton-Rosen, Z., Melbourne, A., Orasanu, E., Cardoso, M.J., Modat, M., Bainbridge, A., Kendall, G.S., Robertson, N.J., Marlow, N., Ourselin, S., 2015. Longitudinal measurement of the developing grey matter in preterm subjects using multi-modal MRI. Neuroimage 111, 580–589. doi:10.1016/j.neuroimage.2015.02.010

Edwards, A.D., Wyatt, J.S., Richardson, C., Delpy, D.T., Cope, M., Reynolds, E.O.R., 1988. Cotside Measurement of Cerebral Blood Flow in Ill Newborn Infants By Near Infrared Spectroscopy. Lancet (London, England) 2, 770–1.

Eide, M.G., Skjærven, R., Irgens, L.M., Bjerkedal, T., Øyen, N., 2006. Associations of birth defects with adult intellectual performance, disability and mortality: Population-based cohort study. Pediatr. Res. 59, 848–853. doi:10.1203/01.pdr.0000219172.16638.f9

Einstein, A., 1905. Über die von der molekularkinetischen Theorie der Wärme geforderte Bewegung von in ruhenden Flüssigkeiten suspendierten Teilchen. Ann. Phys. 322, 549–560. doi:10.1002/andp.19053220806

Elias, H., Schwartz, D., 1969. Surface areas of the cerebral cortex of mammals determined by stereological methods. Science 166, 111–113. doi:10.1126/science.166.3901.111

EUROCAT, 2015. Eurocat Prevalence Tables [WWW Document]. URL http://www.eurocat-network.eu/accessprevalencedata/prevalencetables (accessed 11.2.17).

Fischl, B., 2012. NeuroImage FreeSurfer 62, 774–781. doi:10.1016/j.neuroimage.2012.01.021

Forbess, J.M., Visconti, K.J., Hancock-Friesen, C., Howe, R.C., Bellinger, D.C., Jonas, R. a, 2002. Neurodevelopmental outcome after congenital heart surgery: results from an institutional registry. Circulation 106, I95–I102. doi:10.1161/01.cir.0000032915.33237.72

Fünfschilling, U., Supplie, L.M., Mahad, D., Boretius, S., Saab, A.S., Edgar, J., Brinkmann, B.G., Kassmann, C.M., Tzvetanova, I.D., Möbius, W., Diaz, F., Meijer, D., Suter, U., Hamprecht, B., Sereda, M.W., Moraes, C.T., Frahm, J., Goebbels, S., Nave, K.-A., 2012. Glycolytic oligodendrocytes maintain myelin and long-term axonal integrity. Nature 485, 517–21. doi:10.1038/nature11007

Galli, K.K., Zimmerman, R. a, Jarvik, G.P., Wernovsky, G., Kuypers, M.K., Clancy, R.R., Montenegro, L.M., Mahle, W.T., Newman, M.F., Saunders, A.M., Nicolson, S.C., Spray, T.L., Gaynor, J.W., Galli, K.K., 2004. Periventricular leukomalacia is common after neonatal cardiac surgery. J. Thorac. Cardiovasc. Surg. 127, 692–704. doi:10.1016/j.jtcvs.2003.09.053

Garcia Guerra, G., Robertson, C.M.T., Alton, G.Y., Joffe, A.R., Dinu, I.A., Nicholas, D., Ross, D.B., Rebeyka, I.M., 2013. Quality of life 4 years after complex heart surgery in infancy. J. Thorac. Cardiovasc. Surg. 145, 482–488.e2. doi:10.1016/j.jtcvs.2012.03.050

Garcia, R.U., Aggarwal, S., Natarajan, G., 2016. Parental perception of functional status and impact on the family of children with congenital heart surgery. Early Hum. Dev. 96, 45–51. doi:10.1016/j.earlhumdev.2016.03.004

Gaynor, J., Gerdes, M., Zackai, E., 2003. Apolipoprotein E genotype and neurodevelopmental sequelae of infant cardiac surgery. J. Thorac. ….

doi:10.1067/S0022-5223(03)01188-7

Gaynor, J.W., Kim, D.S., Arrington, C.B., Atz, A.M., Bellinger, D.C., Burt, A.A., Ghanayem, N.S., Jacobs, J.P., Lee, T.M., Lewis, A.B., Mahle, W.T., Marino, B.S., Miller, S.G., Newburger, J.W., Pizarro, C., Ravishankar, C., Santani, A.B., Wilder, N.S., Jarvik, G.P., Mital, S., Russell, M.W., 2014. Validation of association of the apolipoprotein e ε2 allele with neurodevelopmental dysfunction after cardiac surgery in neonates and infants. J. Thorac. Cardiovasc. Surg. 148, 2560–2568. doi:10.1016/j.jtcvs.2014.07.052

Gaynor, J.W., Stopp, C., Wypij, D., Andropoulos, D.B., Atallah, J., Atz, A.M., Beca, J., Donofrio, M.T., Duncan, K., Ghanayem, N.S., Goldberg, C.S., Hovels-Gurich, H., Ichida, F., Jacobs, J.P., Justo, R., Latal, B., Li, J.S., Mahle, W.T., McQuillen, P.S., Menon, S.C., Pemberton, V.L., Pike, N.A., Pizarro, C., Shekerdemian, L.S., Synnes, A., Williams, I., Bellinger, D.C., Newburger, J.W., 2015. Neurodevelopmental outcomes after cardiac surgery in infancy. Pediatrics 135, 816–825. doi:10.1542/peds.2014-3825

Gaynor, J.W., Wernovsky, G., Jarvik, G.P., Bernbaum, J., Gerdes, M., Zackai, E., Nord, A.S., Clancy, R.R., Nicolson, S.C., Spray, T.L., 2007. Patient characteristics are important determinants of neurodevelopmental outcome at one year of age after neonatal and infant cardiac surgery. J. Thorac. Cardiovasc. Surg. 133. doi:10.1016/j.jtcvs.2006.10.087

Gilboa, S.M., Devine, O.J., Kucik, J.E., Oster, M.E., Riehle-Colarusso, T., Nembhard, W.N., Xu, P., Correa, A., Jenkins, K., Marelli, A.J., 2016. Congenital Heart Defects in the United States: Estimating the Magnitude of the Affected Population in 2010. Circulation 134, 101–109. doi:10.1161/CIRCULATIONAHA.115.019307

Glauser, T.A., Rorke, L.B., Weinberg, P.M., Clancy, R.R., 1990a. Acquired neuropathologic lesions associated with the hypoplastic left heart syndrome. Pediatrics 85, 991–1000.

Glauser, T.A., Rorke, L.B., Weinberg, P.M., Clancy, R.R., 1990b. Congenital brain anomalies associated with the hypoplastic left heart syndrome. Pediatrics 85, 984–90.

Gleason, C.A., Hamm, C., Jones, M.D., 1989. Cerebral blood flow, oxygenation, and

carbohydrate metabolism in immature fetal sheep in utero. Am J Physiol 256, R1264–R1268.

Goff, D.A., McKay, E.M., Davey, B.T., Thacker, D., Khalek, N., Miesnik, S.R., Moldenhauer, J.S., Huff, D.S., Rychik, J., 2011. Abstract 11260: Placental Abnormalities in Fetal Congenital Heart Disease. Circulation 124, A11260 LP-A11260.

Goldberg, C.S., Bove, E.L., Devaney, E.J., Mollen, E., Schwartz, E., Tindall, S., Nowak, C., Charpie, J., Brown, M.B., Kulik, T.J., Ohye, R.G., 2007. A randomized clinical trial of regional cerebral perfusion versus deep hypothermic circulatory arrest: Outcomes for infants with functional single ventricle. J. Thorac. Cardiovasc. Surg. 133. doi:10.1016/j.jtcvs.2006.11.029

Goldberg, C.S., Schwartz, E.M., Brunberg, J.A., Mosca, R.S., Bove, E.L., Schork, M.A., Stetz, S.P., Cheatham, J.P., Kulik, T.J., Goldberg, C.S., 2000. Neurodevelopmental outcome of patients after the Fontan operation: A comparison between children with hypoplastic left heart syndrome and other functional single ventricle lesions. J. Pediatr. 137, 646–652. doi:10.1067/mpd.2000.108952

Grussu, F., Schneider, T., Tur, C., Yates, R.L., Tachrount, M., Ianuş, A., Yiannakas, M.C., Newcombe, J., Zhang, H., Alexander, D.C., DeLuca, G.C., Gandini Wheeler-Kingshott, C.A.M., 2017. Neurite dispersion: a new marker of multiple sclerosis spinal cord pathology? Ann. Clin. Transl. Neurol. 4, 663–679. doi:10.1002/acn3.445

Guimond, A., Guttmann, C.R.G., Warfield, S.K., Westin, C.-F., 2002. Deformable registration of DT-MRI data based on transformation invariant tensor characteristics, in: Proceedings IEEE International Symposium on Biomedical Imaging. IEEE, pp. 761–764. doi:10.1109/ISBI.2002.1029369

Gunn, J.K., Beca, J., Hunt, R.W., Olischar, M., Shekerdemian, L.S., 2012a. Perioperative amplitude-integrated EEG and neurodevelopment in infants with congenital heart disease. Intensive Care Med. 38, 1539–1547. doi:10.1007/s00134-012-2608-y

Gunn, J.K., Beca, J., Penny, D.J., Horton, S.B., D'Udekem, Y.A., Brizard, C.P.,

Finucane, K., Olischar, M., Hunt, R.W., Shekerdemian, L.S., 2012b. Amplitude-integrated electroencephalography and brain injury in infants undergoing norwood-type operations. Ann. Thorac. Surg. 93, 170–176. doi:10.1016/j.athoracsur.2011.08.014

Hahn, E., Szwast, A., Cnota, J., Levine, J.C., Fifer, C.G., Jaeggi, E., Andrews, H., Williams, I.A., 2016. Association between fetal growth, cerebral blood flow and neurodevelopmental outcome in univentricular fetuses. Ultrasound Obstet. Gynecol. 47, 460–465. doi:10.1002/uog.14881

Hajnal, J. V., Doran, M., Hall, A.S., Collins, A.G., Oatridge, A., Pennock, J.M., Young, I.R., Bydder, G.M., 1991. Mr imaging of anisotropically restricted diffusion of water in the nervous system: Technical, anatomic, and pathologic considerations. J. Comput. Assist. Tomogr. doi:10.1097/00004728-199101000-00001

Hajnal, J. V., Hill, D.L.G., Hawkes, D.J., 2001. Medical Image Registration. CRC Press, p. 392.

Hansen, E., Poole, T. a, Nguyen, V., Lerner, M., Wigal, T., Shannon, K., Wigal, S.B., Batra, A.S., 2012. Prevalence of ADHD symptoms in patients with congenital heart disease. Pediatr. Int. 54, 838–43. doi:10.1111/j.1442-200X.2012.03711.x

Heiberg, E., Sjögren, J., Ugander, M., Carlsson, M., Engblom, H., Arheden, H., 2010. Design and validation of Segment - freely available software for cardiovascular image analysis. BMC Med. Imaging 10, 1. doi:10.1186/1471-2342-10-1

Heymann, M.A., Rudolph, A.M., 1972. Effects of congenital heart disease on fetal and neonatal circulations. Prog. Cardiovasc. Dis. 15, 115–143. doi:10.1016/0033-0620(72)90015-1

Hill, D.L.G., Batchelor, P.G., Holden, M., Hawkes, D.J., 2001. Medical image registration. Phys. Med. Biol. 46, R1–R45. doi:10.1088/0031-9155/46/3/201

Hinton, R.B., Andelfinger, G., Sekar, P., Hinton, A.C., Gendron, R.L., Michelfelder, E.C., Robitaille, Y., Benson, D.W., 2008. Prenatal Head Growth and White Matter Injury in Hypoplastic Left Heart Syndrome. Pediatr Res 64, 364–369. doi:10.1021/ja8019214.Optimization

Hirsch, J.C., Charpie, J.R., Ohye, R.G., Gurney, J.G., 2009. Near-infrared spectroscopy: What we know and what we need to know-A systematic review of

the congenital heart disease literature. J. Thorac. Cardiovasc. Surg. 137, 154–159.e12. doi:10.1016/j.jtcvs.2008.08.005

Hoffman, G.M., Mussatto, K.A., Brosig, C.L., Ghanayem, N.S., Musa, N., Fedderly, R.T., Jaquiss, R.D.B., Tweddell, J.S., 2005. Systemic venous oxygen saturation after the Norwood procedure and childhood neurodevelopmental outcome. J. Thorac. Cardiovasc. Surg. 130, 1094–1100. doi:10.1016/j.jtcvs.2005.06.029

Hoffman, J.I.E., Kaplan, S., 2002. The incidence of congenital heart disease. J. Am. Coll. Cardiol. 39, 1890–1900. doi:10.1016/S0735-1097(02)01886-7

Hofman, M.B.M., Visser, F.C., Van Rossum, A.C., Vink, G.Q.M., Sprenger, M., Westerhof, N., 1995. In vivo validation of magnetic resonance blood volume flow measurements with limited spatial resolution in small vessels. Magn. Reson. Med. 33, 778–784. doi:10.1002/mrm.1910330606

Holm, I., Fredriksen, P.M., Fosdahl, M.A., Olstad, M., Vøllestad, N., 2007. Impaired Motor Competence in School-aged Children With Complex Congenital Heart Disease. Arch. Pediatr. Adolesc. Med. 161, 945. doi:10.1001/archpedi.161.10.945

Homsy, J., Zaidi, S., Shen, Y., Ware, J.S., Samocha, K.E., Karczewski, K.J., DePalma, S.R., McKean, D., Wakimoto, H., Gorham, J., Jin, S.C., Deanfield, J., Giardini, A., Porter, G.A., Kim, R., Bilguvar, K., Lopez-Giraldez, F., Tikhonova, I., Mane, S., Romano-Adesman, A., Qi, H., Vardarajan, B., Ma, L., Daly, M., Roberts, A.E., Russell, M.W., Mital, S., Newburger, J.W., Gaynor, J.W., Breitbart, R.E., Iossifov, I., Ronemus, M., Sanders, S.J., Kaltman, J.R., Seidman, J.G., Brueckner, M., Gelb, B.D., Goldmuntz, E., Lifton, R.P., Seidman, C.E., Chung, W.K., 2015. De novo mutations in congenital heart disease with neurodevelopmental and other congenital anomalies. Science (80-.). 350, 1262–1266. doi:10.1126/science.aac9396

Hövels-Gürich, H., Konrad, K., 2002. Long term behavioural outcome after neonatal arterial switch operation for transposition of the great arteries. Arch. Dis. … 506–510.

Hövels-Gürich, H.H., Bauer, S.B., Schnitker, R., Willmes-von Hinckeldey, K., Messmer, B.J., Seghaye, M.C., Huber, W., 2008. Long-term outcome of speech and language in children after corrective surgery for cyanotic or acyanotic

cardiac defects in infancy. Eur. J. Paediatr. Neurol. 12, 378–386. doi:10.1016/j.ejpn.2007.10.004

Hövels-Gürich, H.H., Konrad, K., Skorzenski, D., Minkenberg, R., Herpertz-Dahlmann, B., Messmer, B.J., Seghaye, M.C., 2007. Long-term behavior and quality of life after corrective cardiac surgery in infancy for tetralogy of fallot or ventricular septal defect. Pediatr. Cardiol. 28, 346–354. doi:10.1007/s00246-006-0123-z

Hudak, M.L., Koehler, R.C., Rosenberg, A.A., Traystman, R.J., Jones, M.D., 1986. Effect of hematocrit on cerebral blood flow. Am. J. Physiol. Circ. Physiol. 251, H63–H70. doi:10.1152/ajpheart.1986.251.1.H63

Hughes, E., Carney, O., Tusor, N., Pegoretti, K., Arulkumaran, S., Cordeo-Grande, L., Kelly, C., Barnett, M., Krishnan, M., Steinweg, J., Allsop, J., Gomes, A.D.S., Wurie, J., Bueno-Conde, J., Fox, M., Strang, A., Sharma, M., Victor, S., Serena, C., Edwards, D., Hajnal, J., Rutherford, M., 2017a. The type and prevalence of incidental findings on magnetic resonance imaging of the low risk term born neonatal brain, in: ISMRM 25th Annual Meeting & Exhibition.

Hughes, E., Winchman, T., Padormo, F., Teixeira, R., Wurie, J., Sharma, M., Fox, M., Hutter, J., Cordero-Grande, L., Price, A.N., Allsop, J., Bueno-Conde, J., Tusor, N., Arichi, T., Edwards, A.D., Rutherford, M.A., Counsell, S.J., Hajnal, J. V, 2017b. A dedicated neonatal brain imaging system. Magn. Reson. Med. 78, 794–804. doi:10.1002/mrm.26462

Hultman, C.M., Sparen, P., Cnattingius, S., 2002. Perinatal risk factors for infantile autism. Epidemiology 13, 417–423. doi:10.1097/01.EDE.0000016968.14007.E6

Hüppi, P.S., Warfield, S., Kikinis, R., Barnes, P.D., Zientara, G.P., Jolesz, F. a, Tsuji, M.K., Volpe, J.J., 1998. Quantitative magnetic resonance imaging of brain development in premature and mature newborns. Ann. Neurol. 43, 224–235. doi:10.1002/ana.410430213

Hutter, J., Price, A.N., Cordero-Grande, L., Hughes, E.J., Tournier, J.-D., Batalle, D., Counsell, S.J., Edwards, A.D., Hajnal, J. V, 2015. Multi-band accelerated multi-shell HARDI neonatal diffusion for the developing Human Connectome Project, in: ISMRM.

Hutter, J., Tournier, J.D., Price, A.N., Cordero-Grande, L., Hughes, E.J., Malik, S.,

Steinweg, J., Bastiani, M., Sotiropoulos, S.N., Jbabdi, S., Andersson, J., Edwards, A.D., Hajnal, J.V., 2018. Time-efficient and flexible design of optimized multishell HARDI diffusion. Magn. Reson. Med. 79, 1276–1292. doi:10.1002/mrm.26765

Hyttel-Sorensen, S., Hessel, T.W., Greisen, G., 2014. Peripheral tissue oximetry: Comparing three commercial near-infrared spectroscopy oximeters on the forearm. J. Clin. Monit. Comput. 28, 149–155. doi:10.1007/s10877-013-9507-9

Hyttel-Sorensen, S., Pellicer, a., Alderliesten, T., Austin, T., van Bel, F., Benders, M., Claris, O., Dempsey, E., Franz, a. R., Fumagalli, M., Gluud, C., Grevstad, B., Hagmann, C., Lemmers, P., van Oeveren, W., Pichler, G., Plomgaard, a. M., Riera, J., Sanchez, L., Winkel, P., Wolf, M., Greisen, G., 2015. Cerebral near infrared spectroscopy oximetry in extremely preterm infants: phase II randomised clinical trial. Bmj 350, g7635–g7635. doi:10.1136/bmj.g7635

Ibuki, K., Watanabe, K., Yoshimura, N., Kakimoto, T., Matsui, M., Yoshida, T., Origasa, H., Ichida, F., 2012. The improvement of hypoxia correlates with neuroanatomic and developmental outcomes: Comparison of midterm outcomes in infants with transposition of the great arteries or single-ventricle physiology. J. Thorac. Cardiovasc. Surg. 143, 1077–1085. doi:10.1016/j.jtcvs.2011.08.042

Jelescu, I.O., Veraart, J., Adisetiyo, V., Milla, S.S., Novikov, D.S., Fieremans, E., 2015. One diffusion acquisition and different white matter models: How does microstructure change in human early development based on WMTI and NODDI? Neuroimage 107, 242–256. doi:10.1016/j.neuroimage.2014.12.009

Jenkinson, M., Smith, S., 2001. A global optimisation method for robust affine registration of brain images. Med. Image Anal. 5, 143–156. doi:10.1016/S1361-8415(01)00036-6

Jespersen, S.N., Kroenke, C.D., Østergaard, L., Ackerman, J.J.H., Yablonskiy, D.A., 2007. Modeling dendrite density from magnetic resonance diffusion measurements. Neuroimage 34, 1473–1486. doi:10.1016/j.neuroimage.2006.10.037

Jevtovic-Todorovic, V., Absalom, A.R., Blomgren, K., Brambrink, A., Crosby, G., Culley, D.J., Fiskum, G., Giffard, R.G., Herold, K.F., Loepke, A.W., Ma, D., Orser,

B.A., Planel, E., Slikker, W., Soriano, S.G., Stratmann, G., Vutskits, L., Xie, Z., Hemmings, H.C., 2013. Anaesthetic neurotoxicity and neuroplasticity: An expert group report and statement based on the BJA Salzburg Seminar. Br. J. Anaesth. 111, 143–151. doi:10.1093/bja/aet177

Jöbsis, F.F., 1977. Noninvasive, infrared monitoring of cerebral and myocardial oxygen sufficiency and circulatory parameters. Science 198, 1264–7.

Johnson, M.A., Pennock, J.M., Bydder, G.M., Steiner, R.E., Thomas, D.J., Hayward, R., Bryant, D.R., Payne, J.A., Levene, M.I., Whitelaw, A., 1983. Clinical NMR imaging of the brain in children: normal and neurologic disease. AJR. Am. J. Roentgenol. 141, 1005–1018. doi:10.2214/ajr.141.5.1005

Jonas, R.A., Wypij, D., Roth, S.J., Bellinger, D.C., Visconti, K.J., Du Plessis, A.J., Goodkin, H., Laussen, P.C., Farrell, D.M., Bartlett, J., McGrath, E., Rappaport, L.J., Bacha, E.A., Forbess, J.M., Del Nido, P.J., Mayer, J.E., Newburger, J.W., Baumgartner, W.A., Starnes, V.A., Fraser, C.D., Park, S.J., 2003. The influence of hemodilution on outcome after hypothermic cardiopulmonary bypass: Results of a randomized trial in infants. J. Thorac. Cardiovasc. Surg. 126, 1765–1774. doi:10.1016/j.jtcvs.2003.04.003

Jones, D.K., 2004. The Effect of Gradient Sampling Schemes on Measures Derived from Diffusion Tensor MRI: A Monte Carlo Study. Magn. Reson. Med. 51, 807–815. doi:10.1002/mrm.20033

Jones, D.K., Cercignani, M., 2010. Twenty-five pitfalls in the analysis of diffusion MRI data. NMR Biomed. 23, 803–820. doi:10.1002/nbm.1543

Jones, D.K., Chitnis, X.A., Job, D., Khong, P.L., Leung, L.T., Marenco, S., Smith, S.M., Symms, M.R., 2007. What Happens When Nine Different Groups Analyze the Same DT-MRI Data Set Using Voxel-Based Methods ? Proc. Int. Soc. Magn. Reson. Med. 15, 2007. doi:citeulike-article-id:9188257

Jones, H.N., Olbrych, S.K., Smith, K.L., Cnota, J.F., Habli, M., Ramos-Gonzales, O., Owens, K.J., Hinton, A.C., Polzin, W.J., Muglia, L.J., Hinton, R.B., 2015. Hypoplastic left heart syndrome is associated with structural and vascular placental abnormalities and leptin dysregulation. Placenta 36, 1078–1086. doi:10.1016/j.placenta.2015.08.003

Jones, M.D., Traystman, R.J., Simmons, M.A., Molteni, R.A., 1981. Effects of changes in arterial O_2 content on cerebral blood flow in the lamb. Am. J. Physiol. 240, H209–H215.

Kaden, E., Kelm, N.D., Carson, R.P., Does, M.D., Alexander, D.C., 2016. Multi-compartment microscopic diffusion imaging. Neuroimage 139, 346–359. doi:10.1016/j.neuroimage.2016.06.002

Kaltman, J.R., Di, H., Tian, Z., Rychik, J., 2005. Impact of congenital heart disease on cerebrovascular blood flow dynamics in the fetus. Ultrasound Obstet. Gynecol. 25, 32–6. doi:10.1002/uog.1785

Kansagra, A.P., Mabray, M.C., Ferriero, D.M., Barkovich, A.J., Xu, D., Hess, C.P., 2016. Microstructural maturation of white matter tracts in encephalopathic neonates. Clin. Imaging 40, 1009–1013. doi:10.1016/j.clinimag.2016.05.009

Kaufman, L., Rousseeuw, P.J., 1990. Finding Groups in Data, Wiley Series in Probability and Statistics. John Wiley & Sons, Inc., Hoboken, NJ, USA. doi:10.1002/9780470316801

Keil, B., Alagappan, V., Mareyam, A., McNab, J.A., Fujimoto, K., Tountcheva, V., Triantafyllou, C., Dilks, D.D., Kanwisher, N., Lin, W., Grant, P.E., Wald, L.L., 2011. Size-optimized 32-channel brain arrays for 3 T pediatric imaging. Magn. Reson. Med. 66, 1777–1787. doi:10.1002/mrm.22961

Kellner, E., Dhital, B., Kiselev, V.G., Reisert, M., 2016. Gibbs-ringing artifact removal based on local subvoxel-shifts. Magn. Reson. Med. 76, 1574–1581. doi:10.1002/mrm.26054

Kelly, C.J., Makropoulos, A., Cordero-Grande, L., Hutter, J., Price, A., Hughes, E., Murgasova, M., Teixeira, R.P.A.G., Steinweg, J.K., Kulkarni, S., Rahman, L., Zhang, H., Alexander, D.C., Pushparajah, K., Rueckert, D., Hajnal, J. V., Simpson, J., Edwards, A.D., Rutherford, M.A., Counsell, S.J., 2017. Impaired development of the cerebral cortex in infants with congenital heart disease is correlated to reduced cerebral oxygen delivery. Sci. Rep. 7, 15088. doi:10.1038/s41598-017-14939-z

Kendall, G.S., Melbourne, A., Johnson, S., Price, D., Bainbridge, A., Gunny, R., Huertas-Ceballos, A., Cady, E.B., Ourselin, S., Marlow, N., Robertson, N.J., 2014.

White matter NAA/Cho and Cho/Cr ratios at MR spectroscopy are predictive of motor outcome in preterm infants. Radiology 271, 230–238. doi:10.1148/radiol.13122679

Kern, J.H., Hinton, V.J., Nereo, N.E., Hayes, C.J., Gersony, W.M., 1998. Early developmental outcome after the Norwood procedure for hypoplastic left heart syndrome. Pediatrics 102, 1148–52. doi:10.1542/peds.102.5.1148

Kersbergen, K.J., Benders, M.J.N.L., Groenendaal, F., Koopman-Esseboom, C., Nievelstein, R.A.J., Van Haastert, I.C., De Vries, L.S., 2014. Different patterns of punctate white matter lesions in serially scanned preterm infants. PLoS One 9. doi:10.1371/journal.pone.0108904

Khairy, P., Fernandes, S.M., Mayer, J.E., Triedman, J.K., Walsh, E.P., Lock, J.E., Landzberg, M.J., 2008. Long-term survival, modes of death, and predictors of mortality in patients with Fontan surgery. Circulation 117, 85–92. doi:10.1161/CIRCULATIONAHA.107.738559

Khairy, P., Ionescu-Ittu, R., MacKie, A.S., Abrahamowicz, M., Pilote, L., Marelli, A.J., 2010. Changing mortality in congenital heart disease. J. Am. Coll. Cardiol. 56, 1149–1157. doi:10.1016/j.jacc.2010.03.085

Kinney, H.C., Panigrahy, A., Newburger, J.W., Jonas, R.A., Sleeper, L.A., 2005. Hypoxic-ischemic brain injury in infants with congenital heart disease dying after cardiac surgery. Acta Neuropathol. 110, 563–578. doi:10.1007/s00401-005-1077-6

Kjellmer, I., Karlsson, K., Olsson, T., Rosén, K.G., 1974. Cerebral Reactions during Intrauterine Asphyxia in the Sheep. I. Circulation and Oxygen Consumption in the Fetal Brain. Pediatr. Res. 8, 50–57. doi:10.1203/00006450-197401000-00009

Klein, A., Andersson, J., Ardekani, B.A., Ashburner, J., Avants, B., Chiang, M.C., Christensen, G.E., Collins, D.L., Gee, J., Hellier, P., Song, J.H., Jenkinson, M., Lepage, C., Rueckert, D., Thompson, P., Vercauteren, T., Woods, R.P., Mann, J.J., Parsey, R. V., 2009. Evaluation of 14 nonlinear deformation algorithms applied to human brain MRI registration. Neuroimage 46, 786–802. doi:10.1016/j.neuroimage.2008.12.037

Klouda, L., Franklin, W.J., Saraf, A., Parekh, D.R., Schwartz, D.D., 2016.

Neurocognitive and executive functioning in adult survivors of congenital heart disease. Congenit. Heart Dis. 1–8. doi:10.1111/chd.12409

Kostović, I., Jovanov-Milosević, N., 2006. The development of cerebral connections during the first 20-45 weeks' gestation. Semin. Fetal Neonatal Med. 11, 415–22. doi:10.1016/j.siny.2006.07.001

Krueger, J.J., Brotschi, B., Balmer, C., Bernet, V., Latal, B., 2015. Postoperative Hyperglycemia and 4-Year Neurodevelopmental Outcome in Children Operated for Congenital Heart Disease. J. Pediatr. 167, 1253–1258.e1. doi:10.1016/j.jpeds.2015.07.007

Kuklisova-Murgasova, M., Quaghebeur, G., Rutherford, M.A., Hajnal, J. V, Schnabel, J.A., 2012. Reconstruction of fetal brain MRI with intensity matching and complete outlier removal. Med. Image Anal. 16, 1550–1564. doi:10.1016/j.media.2012.07.004

Kunz, N., Zhang, H., Vasung, L., O'Brien, K.R., Assaf, Y., Lazeyras, F., Alexander, D.C., Hüppi, P.S., 2014. Assessing white matter microstructure of the newborn with multi-shell diffusion MRI and biophysical compartment models. Neuroimage 96, 288–299. doi:10.1016/j.neuroimage.2014.03.057

Lambert, L.M., Minich, L.L., Newburger, J.W., Lu, M., Pemberton, V.L., McGrath, E.A., Atz, A.M., Xu, M., Radojewski, E., Servedio, D., McCrindle, B.W., 2009. Parent-Versus Child-Reported Functional Health Status After the Fontan Procedure. Pediatrics 124, e942–e949. doi:10.1542/peds.2008-1697

Lang P, Norwood WI., 1983. Hemodynamic assessment after palliative surgery for hypoplastic left heart syndrome. Circulation 68, 104–108.

Latal, B., 2016. Neurodevelopmental Outcomes of the Child with Congenital Heart Disease. Clin. Perinatol. 43, 173–185. doi:10.1016/j.clp.2015.11.012

Latal, B., Kellenberger, C., Dimitropoulos, A., Hagmann, C., Balmer, C., Beck, I., Bernet, V., 2015. Can preoperative cranial ultrasound predict early neurodevelopmental outcome in infants with congenital heart disease? Dev. Med. Child Neurol. 57, 639–644. doi:10.1111/dmcn.12701

Lauridsen, M.H., Uldbjerg, N., Henriksen, T.B., Petersen, O.B., Stausbøl-Grøn, B., Matthiesen, N.B., Peters, D.A., Ringgaard, S., Hjortdal, V.E., 2017. Cerebral

Oxygenation Measurements by Magnetic Resonance Imaging in Fetuses With and Without Heart DefectsCLINICAL PERSPECTIVE. Circ. Cardiovasc. Imaging 10, e006459. doi:10.1161/CIRCIMAGING.117.006459

Lauterbur, P.C., 1973. Image Formation by Induced Local Interactions: Examples Employing Nuclear Magnetic Resonance. Nature 242, 190–191. doi:10.1038/242190a0

Leisch, F., 2017. e1071 Probability Theory R Package.

Licht, D.J., Shera, D.M., Clancy, R.R., Wernovsky, G., Montenegro, L.M., Nicolson, S.C., Zimmerman, R.A., Spray, T.L., Gaynor, J.W., Vossough, A., 2009. Brain maturation is delayed in infants with complex congenital heart defects. J. Thorac. … 137, 529-36; discussion 536–7. doi:10.1016/j.jtcvs.2008.10.025

Licht, D.J., Wang, J., Silvestre, D.W., Nicolson, S.C., Montenegro, L.M., Wernovsky, G., Tabbutt, S., Durning, S.M., Shera, D.M., Gaynor, J.W., Spray, T.L., Clancy, R.R., Zimmerman, R.A., Detre, J.A., 2004. Preoperative cerebral blood flow is diminished in neonates with severe congenital heart defects. J. Thorac. Cardiovasc. Surg. 128, 841–9. doi:10.1016/j.jtcvs.2004.07.022

Lim, J.M., Kingdom, T., Saini, B., Chau, V., Post, M., Blaser, S., Macgowan, C., Miller, S.P., Seed, M., 2016. Cerebral oxygen delivery is reduced in newborns with congenital heart disease. J. Thorac. Cardiovasc. Surg. 152, 1095–103. doi:10.1016/j.jtcvs.2016.05.027

Limperopoulos, C., Majnemer, a., Shevell, M.I., Rosenblatt, B., Rohlicek, C., Tchervenkov, C., 1999. Neurologic Status of Newborns With Congenital Heart Defects Before Open Heart Surgery. Pediatrics 103, 402–408. doi:10.1542/peds.103.2.402

Limperopoulos, C., Majnemer, a, Shevell, M.I., Rosenblatt, B., Rohlicek, C., Tchervenkov, C., 2000. Neurodevelopmental status of newborns and infants with congenital heart defects before and after open heart surgery. J. Pediatr. 137, 638–45. doi:10.1067/mpd.2000.109152

Limperopoulos, C., Majnemer, A., Shevell, M.I., Rohlicek, C., Rosenblatt, B., Tchervenkov, C., Darwish, H.Z., 2002. Predictors of developmental disabilities after open heart surgery in young children with congenital heart defects. J.

Pediatr. 141, 51–8. doi:10.1067/mpd.2002.125227

Limperopoulos, C., Majnemer, A., Shevell, M.I., Rosenblatt, B., Rohlicek, C., Tchervenkov, C., Darwish, H.Z., 2001. Functional limitations in young children with congenital heart defects after cardiac surgery. Pediatrics 108, 1325–1331. doi:10.1542/peds.108.6.1325

Limperopoulos, C., Tworetzky, W., McElhinney, D.B., Newburger, J.W., Brown, D.W., Robertson, R.L., Guizard, N., McGrath, E., Geva, J., Annese, D., Dunbar-Masterson, C., Trainor, B., Laussen, P.C., Du Plessis, A.J., 2010. Brain volume and metabolism in fetuses with congenital heart disease: Evaluation with quantitative magnetic resonance imaging and spectroscopy. Circulation 121, 26–33. doi:10.1161/CIRCULATIONAHA.109.865568

Linde, L., Dunn, O., Schireson, R., Rasof, B., 1967a. Growth in children with congenital heart disease. J. Pediatr. 70, 413–419.

Linde, L., Rasof, B., Dunn, O., 1967b. Mental development in congenital heart disease. J. Pediatr. 71, 198–203.

Luders, E., Thompson, P.M., Narr, K.L., Toga, A.W., Jancke, L., Gaser, C., 2006. A curvature-based approach to estimate local gyrification on the cortical surface. Neuroimage 29, 1224–1230. doi:10.1016/j.neuroimage.2005.08.049

Macmahon, B., McKeown, T., Record, R.G., 1953. The Incidence and Life Expectation of Children With Congenital Heart Disease. Heart 15, 121–129. doi:10.1136/hrt.15.2.121

Mahle, W.T., Tavani, F., Zimmerman, R.A., Nicolson, S.C., Galli, K.K., Gaynor, J.W., Clancy, R.R., Montenegro, L.M., Spray, T.L., Rosetta, M., Wernovsky, G., Kurth, C.D., Chiavacci, R.M., Wernovsky, G., Kurth, C.D., 2002. An MRI study of neurological injury before and after congenital heart surgery. Circulation 106, I109-14. doi:10.1161/01.cir.0000032908.33237.b1

Majnemer, A., Limperopoulos, C., Shevell, M., Rohlicek, C., Rosenblatt, B., Tchervenkov, C., 2008. Developmental and functional outcomes at school entry in children with congenital heart defects. J. Pediatr. 153, 55–60. doi:10.1016/j.jpeds.2007.12.019

Majnemer, A., Limperopoulos, C., Shevell, M., Rosenblatt, B., Rohlicek, C.,

Tchervenkov, C., 2006. Long-term neuromotor outcome at school entry of infants with congenital heart defects requiring open-heart surgery. J. Pediatr. 148, 72–77. doi:10.1016/j.jpeds.2005.08.036

Makropoulos, A., Aljabar, P., Wright, R., Hüning, B., Merchant, N., Arichi, T., Tusor, N., Hajnal, J. V., Edwards, A.D., Counsell, S.J., Rueckert, D., 2016. Regional growth and atlasing of the developing human brain. Neuroimage 125, 456–478. doi:10.1016/j.neuroimage.2015.10.047

Makropoulos, A., Gousias, I., Ledig, C., Aljabar, P., Serag, A., Hajnal, J., Edwards, A.D., Counsell, S., Rueckert, D., 2014. Automatic Whole Brain MRI Segmentation of the Developing Neonatal Brain. IEEE Trans. Med. Imaging 0062, 1–16. doi:10.1109/TMI.2014.2322280

Makropoulos, A., Robinson, E.C., Schuh, A., Wright, R., Fitzgibbon, S., Bozek, J., Counsell, S.J., Steinweg, J., Passerat-Palmbach, J., Lenz, G., Mortari, F., Tenev, T., Duff, E.P., Bastiani, M., Cordero-Grande, L., Hughes, E., Tusor, N., Tournier, J.-D., Hutter, J., Price, A.N., Murgasova, M., Kelly, C., Rutherford, M.A., Smith, S.M., Edwards, D.A., Hajnal, J. V, Jenkinson, M., Rueckert, D., 2018. The Developing Human Connectome Project: a Minimal Processing Pipeline for Neonatal Cortical Surface Reconstruction. Neuroimage In press. doi:https://doi.org/10.1101/125526

Marelli, A.J., Mackie, A.S., Ionescu-Ittu, R., Rahme, E., Pilote, L., 2007. Congenital heart disease in the general population: Changing prevalence and age distribution. Circulation 115, 163–172. doi:10.1161/CIRCULATIONAHA.106.627224

Marino, B.S., Cassedy, A., Drotar, D., Wray, J., 2016. The Impact of Neurodevelopmental and Psychosocial Outcomes on Health-Related Quality of Life in Survivors of Congenital Heart Disease. J. Pediatr. 174, 11–22.e2. doi:10.1016/j.jpeds.2016.03.071

Marino, B.S., Lipkin, P.H., Newburger, J.W., Peacock, G., Gerdes, M., Gaynor, J.W., Mussatto, K.A., Uzark, K., Goldberg, C.S., Johnson, W.H., Li, J., Smith, S.E., Bellinger, D.C., Mahle, W.T., 2012. Neurodevelopmental Outcomes in Children With Congenital Heart Disease: Evaluation and Management: A Scientific Statement From the American Heart Association. Circulation 126, 1143–1172.

doi:10.1161/CIR.0b013e318265ee8a

Masoller, N., Sanz-Cortés, M., Crispi, F., Gómez, O., Bennasar, M., Egaña-Ugrinovic, G., Bargalló, N., Martínez, J.M., Gratacós, E., 2016. Severity of Fetal Brain Abnormalities in Congenital Heart Disease in Relation to the Main Expected Pattern of in utero Brain Blood Supply. Fetal Diagn. Ther. 39, 269–278. doi:10.1159/000439527

Matos, S.M., Sarmento, S., Moreira, S., Pereira, M.M., Quintas, J., Peixoto, B., Areias, J.C., Areias, M.E.G., 2014. Impact of Fetal Development on Neurocognitive Performance of Adolescents with Cyanotic and Acyanotic Congenital Heart Disease. Congenit. Heart Dis. 9, 373–381. doi:10.1111/chd.12152

Matthiesen, N.B., Henriksen, T.B., Gaynor, J.W., Agergaard, P., Bach, C.C., Hjortdal, V.E., Østergaard, J.R., 2016. Congenital Heart Defects and Indices of Fetal Cerebral Growth in a Nationwide Cohort of 924 422 Liveborn Infants. Circulation 133, 566–575. doi:10.1161/CIRCULATIONAHA.115.019089

McConnell, J.R., Fleming, W.H., Chu, W.K., Hahn, F.J., Sarafian, L.B., Hofschire, P.J., Kugler, J.D., 1990. Magnetic resonance imaging of the brain in infants and children before and after cardiac surgery. A prospective study. Am. J. Dis. Child. 144, 374–8.

McKinstry, R.C., Mathur, A., Miller, J.H., Ozcan, A., Snyder, A.Z., Schefft, G.L., Almli, C.R., Shiran, S.I., Conturo, T.E., Neil, J.J., 2002. Radial organization of developing preterm human cerebral cortex revealed by non-invasive water diffusion anisotropy MRI. Cereb. Cortex 12, 1237–1243. doi:10.1093/cercor/12.12.1237

McLellan, S.A., Walsh, T.S., 2004. Oxygen delivery and haemoglobin. Contin. Educ. Anaesthesia, Crit. Care Pain 4, 123–126. doi:10.1093/bjaceaccp/mkh033

McQuillen, P.S., Hamrick, S.E.G., Perez, M.J., Barkovich, A.J., Glidden, D. V., Karl, T.R., Teitel, D., Miller, S.P., 2006. Balloon atrial septostomy is associated with preoperative stroke in neonates with transposition of the great arteries. Circulation 113, 280–285. doi:10.1161/CIRCULATIONAHA.105.566752

Mebius, M.J., Kooi, E.M.W., Bilardo, C.M., Bos, A.F., 2017. Brain Injury and Neurodevelopmental Outcome in Congenital Heart Disease: A Systematic

Review. Pediatrics 140. doi:10.1542/peds.2016-4055

Miatton, M., De Wolf, D., François, K., Thiery, E., Vingerhoets, G., 2007. Neuropsychological Performance in School-Aged Children with Surgically Corrected Congenital Heart Disease. J. Pediatr. 151. doi:10.1016/j.jpeds.2007.02.020

Miatton, M., De Wolf, D., François, K., Thiery, E., Vingerhoets, G., 2006. Neurocognitive consequences of surgically corrected congenital heart defects: A review. Neuropsychol. Rev. 16, 65–85. doi:10.1007/s11065-006-9005-7

Miller, S.P., Cozzio, C.C., Goldstein, R.B., Ferriero, D.M., Partridge, J.C., Vigneron, D.B., Barkovich, A.J., 2003. Comparing the diagnosis of white matter injury in premature newborns with serial MR imaging and transfontanel ultrasonography findings. Am. J. Neuroradiol. 24, 1661–1669.

Miller, S.P., McQuillen, P.S., Hamrick, S., Xu, D., Glidden, D. V, Charlton, N., Karl, T., Azakie, A., Ferriero, D.M., Barkovich, a J., Vigneron, D.B., 2007. Abnormal brain development in newborns with congenital heart disease. N. Engl. J. Med. 357, 1928–38. doi:10.1056/NEJMoa067393

Miller, S.P., McQuillen, P.S., Vigneron, D.B., Glidden, D. V., Barkovich, A.J., Ferriero, D.M., Hamrick, S.E.G., Azakie, A., Karl, T.R., 2004. Preoperative brain injury in newborns with transposition of the great arteries. Ann. Thorac. Surg. 77, 1698–1706. doi:10.1016/j.athoracsur.2003.10.084

Mitchell, S.C., Korones, S.B., Berendes, H.W., 1971. Congenital heart disease in 56,109 births. Incidence and natural history. Circulation 43, 323–32.

Morton, P.D., Korotcova, L., Lewis, B.K., Bhuvanendran, S., Ramachandra, S.D., Zurakowski, D., Zhang, J., Mori, S., Frank, J.A., Jonas, R.A., Gallo, V., Ishibashi, N., 2017. Abnormal neurogenesis and cortical growth in congenital heart disease. Sci. Transl. Med. 9, eaah7029. doi:10.1126/scitranslmed.aah7029

Moseley, M.E., Cohen, Y., Kucharczyk, J., Mintorovitch, J., Asgari, H.S., Wendland, M.F., Tsuruda, J., Norman, D., 1990. Diffusion-weighted MR imaging of anisotropic water diffusion in cat central nervous system. Radiology 176, 439–445. doi:10.1148/radiology.176.2.2367658

Mrzljak, L., Uylings, H.B., Kostovic, I., Van Eden, C.G., 1988. Prenatal Development of

Neurons in the Human Prefrontal Cortex: I. A Qualitative Golgi Study. J. Comp. Neurol. 271, 355–386. doi:10.1002/cne.902710306

Mukherjee, P., Miller, J.H., Shimony, J.S., Philip, J. V, Nehra, D., Snyder, A.Z., Conturo, T.E., Neil, J.J., McKinstry, R.C., 2002. Diffusion-tensor MR imaging of gray and white matter development during normal human brain maturation. AJNR.American J. Neuroradiol. 23, 1445–1456.

Mulkey, S.B., Ou, X., Ramakrishnaiah, R.H., Glasier, C.M., Swearingen, C.J., Melguizo, M.S., Yap, V.L., Schmitz, M.L., Bhutta, A.T., 2014. White matter injury in newborns with congenital heart disease: a diffusion tensor imaging study. Pediatr. Neurol. 51, 377–83. doi:10.1016/j.pediatrneurol.2014.04.008

Mulkey, S.B., Swearingen, C.J., Melguizo, M.S., Schmitz, M.L., Ou, X., Ramakrishnaiah, R.H., Glasier, C.M., Bradley Schaefer, G., Bhutta, A.T., 2013. Multi-tiered analysis of brain injury in neonates with congenital heart disease. Pediatr. Cardiol. 34, 1772–1784. doi:10.1007/s00246-013-0712-6

Mussatto, K., Tweddell, J., 2005. Quality of life following surgery for congenital cardiac malformations in neonates and infants. Cardiol. Young 15 Suppl 1, 174–8.

Mussatto, K.A., Hoffmann, R., Hoffman, G., Tweddell, J.S., Bear, L., Cao, Y., Tanem, J., Brosig, C., 2015. Risk factors for abnormal developmental trajectories in young children with congenital heart disease. Circulation 132, 755–761. doi:10.1161/CIRCULATIONAHA.114.014521

Nagaraj, U.D., Evangelou, I.E., Donofrio, M.T., Vezina, L.G., McCarter, R., du Plessis, A.J., Limperopoulos, C., 2015. Impaired Global and Regional Cerebral Perfusion in Newborns with Complex Congenital Heart Disease. J. Pediatr. 167, 1018–1024. doi:10.1016/j.jpeds.2015.08.004

Nagasawa, S., Kawanishi, M., Tada, Y., Kawabata, S., Ohta, T., 2000. Intra-operative measurement of cortical arterial flow volumes in posterior circulation using Doppler sonography. Neurol. Res. 22, 194–6.

Nanba, Y., Matsui, K., Aida, N., Sato, Y., Toyoshima, K., Kawataki, M., Hoshino, R., Ohyama, M., Itani, Y., Goto, A., Oka, A., 2007. Magnetic Resonance Imaging Regional T1 Abnormalities at Term Accurately Predict Motor Outcome in Preterm Infants. Pediatrics 120, e10–e19. doi:10.1542/peds.2006-1844

Nattel, S.N., Adrianzen, L., Kessler, E.C., Andelfinger, G., Dehaes, M., Côté-Corriveau, G., Trelles, M.P., 2017. Congenital Heart Disease and Neurodevelopment: Clinical Manifestations, Genetics, Mechanisms, and Implications. Can. J. Cardiol. 33, 1543–1555. doi:10.1016/j.cjca.2017.09.020

Newburger, J.W. et al., 1993. A comparison of the perioperative neurologic effects of hypothermic circulatory arrest vs low-flow cardiopulmonary bypass in infant heart surgery. New Engl 329.

Newburger, J.W., Jonas, R. a, Soul, J., Kussman, B.D., Bellinger, D.C., Laussen, P.C., Robertson, R., Mayer, J.E., del Nido, P.J., Bacha, E. a, Forbess, J.M., Pigula, F., Roth, S.J., Visconti, K.J., du Plessis, A.J., Farrell, D.M., McGrath, E., Rappaport, L. a, Wypij, D., 2008. Randomized trial of hematocrit 25% versus 35% during hypothermic cardiopulmonary bypass in infant heart surgery. J. Thorac. Cardiovasc. Surg. 135, 347–54, 354.e1–4. doi:10.1016/j.jtcvs.2007.01.051

Newburger, J.W., Sleeper, L. a., Bellinger, D.C., Goldberg, C.S., Tabbutt, S., Lu, M., Mussatto, K. a., Williams, I. a., Gustafson, K.E., Mital, S., Pike, N., Sood, E., Mahle, W.T., Cooper, D.S., Dunbar-Masterson, C., Krawczeski, C.D., Lewis, A., Menon, S.C., Pemberton, V.L., Ravishankar, C., Atz, T.W., Ohye, R.G., Gaynor, J.W., 2012. Early developmental outcome in children with hypoplastic left heart syndrome and related anomalies: The single ventricle reconstruction trial. Circulation 125, 2081–2091. doi:10.1161/CIRCULATIONAHA.111.064113

Newburger, J.W., Wypij, D., Bellinger, D.C., Du Plessis, A.J., Kuban, K.C.K., Rappaport, L.A., Almirall, D., Wessel, D.L., Jonas, R.A., Wernovsky, G., 2003. Length of stay after infant heart surgery is related to cognitive outcome at age 8 years. J. Pediatr. 143, 67–73. doi:10.1016/S0022-3476(03)00183-5

Nield, L.E., Qi, X.-L.L., Valsangiacomo, E.R., Macgowan, C.K., Wright, G.A., Hornberger, L.K., Yoo, S.-J., 2005. In vivo MRI measurement of blood oxygen saturation in children with congenital heart disease. Pediatr. Radiol. 35, 179–185. doi:10.1007/s00247-004-1305-6

Nieuwenhuys, R., Voogd, J., van Huijzen, C., 2008. The Human Central Nervous System. Springer Berlin Heidelberg, Berlin, Heidelberg. doi:10.1007/978-3-540-34686-9

Niwa, T., De Vries, L.S., Benders, M.J.N.L., Takahara, T., Nikkels, P.G.J., Groenendaal, F., 2011. Punctate white matter lesions in infants: New insights using susceptibility-weighted imaging. Neuroradiology 53, 669–679. doi:10.1007/s00234-011-0872-0

Norwood, W.I., Lang, P., Hansen, D.D., 1983. Physiologic Repair of Aortic Atresia–Hypoplastic Left Heart Syndrome. N. Engl. J. Med. 308, 23–26. doi:10.1056/NEJM198301063080106

Ogawa, S., Lee, T.M., Kay, A.R., Tank, D.W., 1990. Brain magnetic resonance imaging with contrast dependent on blood oxygenation. Proc. Natl. Acad. Sci. U. S. A. 87, 9868–72. doi:10.1073/pnas.87.24.9868

Orasanu, E., Melbourne, A., Cardoso, M.J., Modat, M., Taylor, A.M., Thayyil, S., Ourselin, S., 2014. NeuroImage : Clinical Brain volume estimation from post-mortem newborn and fetal MRI 6, 438–444. doi:10.1016/j.nicl.2014.10.007

Ortega, J.A., Sirois, C.L., Memi, F., Glidden, N., Zecevic, N., 2017. Oxygen Levels Regulate the Development of Human Cortical Radial Glia Cells. Cereb. Cortex 27, 3736–3751. doi:10.1093/cercor/bhw194

Ortinau, C., Alexopoulos, D., Dierker, D., Van Essen, D., Beca, J., Inder, T., 2013. Cortical folding is altered before surgery in infants with congenital heart disease. J. Pediatr. 163, 1507–10. doi:10.1016/j.jpeds.2013.06.045

Ortinau, C., Beca, J., Lambeth, J., Ferdman, B., Alexopoulos, D., Shimony, J.S., Wallendorf, M., Neil, J., Inder, T., 2012. Regional alterations in cerebral growth exist preoperatively in infants with congenital heart disease. J. Thorac. Cardiovasc. Surg. 143, 1264–70. doi:10.1016/j.jtcvs.2011.10.039

Oster, M.E., Watkins, S., Hill, K.D., Knight, J.H., Meyer, R.E., 2017. Academic Outcomes in Children With Congenital Heart Defects. Circ. Cardiovasc. Qual. Outcomes 10, e003074. doi:10.1161/CIRCOUTCOMES.116.003074

Panigrahy, A., Schmithorst, V.J., Wisnowski, J.L., Watson, C.G., Bellinger, D.C., Newburger, J.W., Rivkin, M.J., 2015. Relationship of white matter network topology and cognitive outcome in adolescents with d-transposition of the great arteries. NeuroImage Clin. 7, 438–448. doi:10.1016/j.nicl.2015.01.013

Papadakis, N.G., Murrills, C.D., Hall, L.D., Huang, C.L.H., Adrian Carpenter, T., 2000.

Minimal gradient encoding for robust estimation of diffusion anisotropy. Magn. Reson. Imaging 18, 671–679. doi:10.1016/S0730-725X(00)00151-X

Pellicer, A., Greisen, G., Benders, M., Claris, O., Dempsey, E., Fumagalli, M., Gluud, C., Hagmann, C., Hellström-Westas, L., Hyttel-Sorensen, S., Lemmers, P., Naulaers, G., Pichler, G., Roll, C., Van Bel, F., Van Oeveren, W., Skoog, M., Wolf, M., Austin, T., 2013. The SafeBoosC phase II randomised clinical trial: A treatment guideline for targeted near-infrared-derived cerebral tissue oxygenation versus standard treatment in extremely preterm infants. Neonatology 104, 171–178. doi:10.1159/000351346

Perloff, J.K., 1991. Congenital heart disease after childhood: an expanding patient population. 22nd Bethesda Conference, Maryland, October 18-19, 1990. J. Am. Coll. Cardiol. 18, 311–42.

Perloff, J.K., Warnes, C.A., 2001. Challenges posed by adults with repaired congenital heart disease. Circulation 103, 2637–43.

Petit, C.J., Rome, J.J., Wernovsky, G., Mason, S.E., Shera, D.M., Nicolson, S.C., Montenegro, L.M., Tabbutt, S., Zimmerman, R.A., Licht, D.J., 2009. Preoperative brain injury in transposition of the great arteries is associated with oxygenation and time to surgery, not balloon atrial septostomy. Circulation 119, 709–716. doi:10.1161/CIRCULATIONAHA.107.760819

Peyvandi, S., De Santiago, V., Chakkarapani, E., Chau, V., Campbell, A., Poskitt, K.J., Xu, D., Barkovich, A.J., Miller, S., McQuillen, P., 2016. Association of Prenatal Diagnosis of Critical Congenital Heart Disease With Postnatal Brain Development and the Risk of Brain Injury. JAMA Pediatr. 170, e154450. doi:10.1001/jamapediatrics.2015.4450

Peyvandi, S., Kim, H., Lau, J., Barkovich, A.J., Campbell, A., Miller, S., Xu, D., McQuillen, P., 2017. The association between cardiac physiology, acquired brain injury and postnatal brain growth in critical congenital heart disease. J. Thorac. Cardiovasc. Surg. doi:10.1016/j.jtcvs.2017.08.019

Pichler, G., Cheung, P.Y., Aziz, K., Urlesberger, B., Schmölzer, G.M., 2014. How to monitor the brain during immediate neonatal transition and resuscitation? A systematic qualitative review of the literature. Neonatology 105, 205–210.

doi:10.1159/000357162

Pierpont, M.E., Basson, C.T., Benson, D.W., Gelb, B.D., Giglia, T.M., Goldmuntz, E., McGee, G., Sable, C.A., Srivastava, D., Webb, C.L., 2007. Genetic Basis for Congenital Heart Defects: Current Knowledge: A Scientific Statement From the American Heart Association Congenital Cardiac Defects Committee, Council on Cardiovascular Disease in the Young: Endorsed by the American Academy of Pediatrics. Circulation 115, 3015–3038. doi:10.1161/CIRCULATIONAHA.106.183056

Pluim, J.P.W., Maintz, J.B.A.A., Viergever, M.A., 2003. Mutual-information-based registration of medical images: A survey. IEEE Trans. Med. Imaging 22, 986–1004. doi:10.1109/TMI.2003.815867

Porayette, P., Madathil, S., Sun, L., Jaeggi, E., Grosse-Wortmann, L., Yoo, S.J., Hickey, E., Miller, S.P., Macgowan, C.K., Seed, M., 2016. MRI reveals hemodynamic changes with acute maternal hyperoxygenation in human fetuses with and without congenital heart disease. Prenat. Diagn. 36, 274–281. doi:10.1002/pd.4762

Prastawa, M., Gilmore, J.H., Lin, W., Gerig, G., 2005. Automatic segmentation of MR images of the developing newborn brain q 9, 457–466. doi:10.1016/j.media.2005.05.007

Prsa, M., Sun, L., van Amerom, J., Yoo, S.-J., Grosse-Wortmann, L., Jaeggi, E., Macgowan, C., Seed, M., 2014. Reference ranges of blood flow in the major vessels of the normal human fetal circulation at term by phase-contrast magnetic resonance imaging. Circ. Cardiovasc. Imaging 7, 663–70. doi:10.1161/CIRCIMAGING.113.001859

Purcell, E., Torrey, H., Pound, R., 1946. Resonance Absorption by Nuclear Magnetic Moments in a Solid. Phys. Rev. 69, 37–38. doi:10.1103/PhysRev.69.37

Rakic, P., 2003. Developmental and evolutionary adaptations of cortical radial glia. Cereb. Cortex 13, 541–549. doi:10.1093/cercor/13.6.541

Rios, D.R., Welty, S.E., Gunn, J.K., Beca, J., Minard, C.G., Goldsworthy, M., Coleman, L., Hunter, J. V., Andropoulos, D.B., Shekerdemian, L.S., 2013. Usefulness of Routine Head Ultrasound Scans Before Surgery for Congenital Heart Disease.

Pediatrics 131, 1765–1770. doi:10.1542/peds.2012-3734

Rivkin, M.J., Watson, C.G., Scoppettuolo, L.A., Wypij, D., Vajapeyam, S., Bellinger, D.C., Demaso, D.R., Robertson, R.L., Newburger, J.W., 2013. Adolescents with d-transposition of the great arteries repaired in early infancy demonstrate reduced white matter microstructure associated with clinical risk factors. J. Thorac. Cardiovasc. Surg. 146, 543–549.e1. doi:10.1016/j.jtcvs.2012.12.006

Robertson, D.R., Justo, R.N., Burke, C.J., Pohlner, P.G., Graham, P.L., Colditz, P.B., 2004. Perioperative predictors of developmental outcome following cardiac surgery in infancy. Cardiol. Young 14, 389–395. doi:10.1017/S104795110400407X

Rosenthal, G.L., 1996. Patterns of prenatal growth among infants with cardiovascular malformations: possible fetal hemodynamic effects. Am. J. Epidemiol. 143, 505–513. doi:10.1093/oxfordjournals.aje.a008771

Rudolph, A.M., 2016. Impaired cerebral development in fetuses with congenital cardiovascular malformations: Is it the result of inadequate glucose supply? Pediatr. Res. 80, 172–177. doi:10.1038/pr.2016.65

Rudolph, A.M., 2009. Congenital Diseases of the Heart, Congenital Diseases of the Heart. Wiley-Blackwell, Oxford, UK. doi:10.1002/9781444311822

Rudolph, A.M., Heymann, M.A., 1967. The circulation of the fetus in utero. Methods for studying distribution of blood flow, cardiac output and organ blood flow. Circ. Res. 21, 163–84.

Rueckert et al., D., 1999. Nonrigid registration using free-form deformations: application to breast MR images. IEEE Trans. Med. Imag. 18, 712–21. doi:10.1109/42.796284

Rutherford, M.A., 2001. MRI of the Neonatal Brain. Saunders Ltd, Philadelphia.

Rutherford, M.A., Supramaniam, V., Ederies, A., Chew, A., Bassi, L., Groppo, M., Anjari, M., Counsell, S., Ramenghi, L.A., 2010. Magnetic resonance imaging of white matter diseases of prematurity. Neuroradiology 52, 505–521. doi:10.1007/s00234-010-0700-y

Sadhwani, A., Asaro, L.A., Goldberg, C., Ware, J., Butcher, J., Gaies, M., Smith, C.,

Alexander, J.L., Wypij, D., Agus, M.S.D., 2016. Impact of Tight Glycemic Control on Neurodevelopmental Outcomes at 1 Year of Age for Children with Congenital Heart Disease: A Randomized Controlled Trial. J. Pediatr. 174, 193–198.e2. doi:10.1016/j.jpeds.2016.03.048

Sanai, N., Alvarez-Buylla, A., Berger, M.S., 2005. Neural Stem Cells and the Origin of Gliomas. N. Engl. J. Med. 353, 811–822. doi:10.1056/NEJMra043666

Schaefer, C., von Rhein, M., Knirsch, W., Huber, R., Natalucci, G., Caflisch, J., Landolt, M.A., Latal, B., 2013. Neurodevelopmental outcome, psychological adjustment, and quality of life in adolescents with congenital heart disease. Dev. Med. Child Neurol. 55, 1143–1149. doi:10.1111/dmcn.12242

Schellen, C., Ernst, S., Gruber, G.M., Mlczoch, E., Weber, M., Brugger, P.C., Ulm, B., Langs, G., Salzer-Muhar, U., Prayer, D., Kasprian, G., 2015. Fetal MRI detects early alterations of brain development in Tetralogy of Fallot. Am. J. Obstet. Gynecol. 213, 392e1-392e7. doi:10.1016/j.ajog.2015.05.046

Scherjon, S.A., Smolders-DeHaas, H., Kok, J.H., Zondervan, H.A., 1993. The “brain-sparing” effect: antenatal cerebral Doppler findings in relation to neurologic outcome in very preterm infants. Am. J. Obstet. Gynecol. 169, 169–75.

Schmahmann, J.D., Pandya, D.N., 2006. Fiber Pathways of the Brain. Oxford University Press. doi:10.1093/acprof:oso/9780195104233.003.0014

Schuh, A., Makropoulos, A., Wright, R., Robinson, E., Tusor, N., Steinweg, J., Hughes, E., Cordero Grande, L., Price, A., Hutter, J., Hajnal, J., Rueckert, D., 2017. A deformable model for the reconstruction of the neonatal cortex, in: IEEE 14th International Symposium on Biomedical Imaging (ISBI).

Segovia, K.N., McClure, M., Moravec, M., Ning, L.L., Wan, Y., Gong, X., Riddle, A., Craig, A., Struve, J., Sherman, L.S., Back, S.A., 2008. Arrested oligodendrocyte lineage maturation in chronic perinatal white matter injury. Ann. Neurol. 63, 520–530. doi:10.1002/ana.21359

Sethi, V., Tabbutt, S., Dimitropoulos, A., Harris, K.C., Chau, V., Poskitt, K., Campbell, A., Azakie, A., Xu, D., Barkovich, A.J., Miller, S.P., McQuillen, P.S., 2013. Single-ventricle anatomy predicts delayed microstructural brain development. Pediatr. Res. 73, 661–7. doi:10.1038/pr.2013.29

Shillingford, A.J., Glanzman, M.M., Ittenbach, R.F., Clancy, R.R., Gaynor, J.W., Wernovsky, G., 2008. Inattention, hyperactivity, and school performance in a population of school-age children with complex congenital heart disease. Pediatrics 121, e759-67. doi:10.1542/peds.2007-1066

Shillingford, A.J., Ittenbach, R.F., Marino, B.S., Rychik, J., Clancy, R.R., Spray, T.L., Gaynor, J.W., Wernovsky, G., 2007. Aortic morphometry and microcephaly in hypoplastic left heart syndrome. Cardiol. Young 17, 189–195. doi:10.1017/S1047951107000248

Shillingford, A.J., Wernovsky, G., 2004. Academic performance and behavioral difficulties after neonatal and infant heart surgery. Pediatr. Clin. North Am. 51, 1625–1639. doi:10.1016/j.pcl.2004.07.007

Smith, S.M., 2002. Fast robust automated brain extraction. Hum. Brain Mapp. 17, 143–155. doi:10.1002/hbm.10062

Smith, S.M., Jenkinson, M., Johansen-Berg, H., Rueckert, D., Nichols, T.E., Mackay, C.E., Watkins, K.E., Ciccarelli, O., Cader, M.Z., Matthews, P.M., Behrens, T.E.J., 2006. Tract-based spatial statistics: voxelwise analysis of multi-subject diffusion data. Neuroimage 31, 1487–505. doi:10.1016/j.neuroimage.2006.02.024

Smith, S.M., Nichols, T.E., 2009. Threshold-free cluster enhancement: Addressing problems of smoothing, threshold dependence and localisation in cluster inference. Neuroimage 44, 83–98. doi:10.1016/j.neuroimage.2008.03.061

Snookes, S.H., Gunn, J.K., Eldridge, B.J., Donath, S.M., Hunt, R.W., Galea, M.P., Shekerdemian, L., 2010. A systematic review of motor and cognitive outcomes after early surgery for congenital heart disease. Pediatrics 125, e818-27. doi:10.1542/peds.2009-1959

Soemedi, R., Wilson, I.J., Bentham, J., Darlay, R., Töpf, A., Zelenika, D., Cosgrove, C., Setchfield, K., Thornborough, C., Granados-Riveron, J., Blue, G.M., Breckpot, J., Hellens, S., Zwolinkski, S., Glen, E., Mamasoula, C., Rahman, T.J., Hall, D., Rauch, A., Devriendt, K., Gewillig, M., O'sullivan, J., Winlaw, D.S., Bu'lock, F., Brook, J.D., Bhattacharya, S., Lathrop, M., Santibanez-Koref, M., Cordell, H.J., Goodship, J.A., Keavney, B.D., 2012. Contribution of global rare copy-number variants to the risk of sporadic congenital heart disease. Am. J. Hum. Genet. 91,

489–501. doi:10.1016/j.ajhg.2012.08.003

Sood, B., Cortez, J., McLaughlin, K., Gupta, M., Amaram, A., Kolli, M., Zajac, M., Pizzino, J., Schoettle, B., Chen, X., 2014. Near infrared spectroscopy as a biomarker for necrotising enterocolitis following red blood cell transfusion. J. Near Infrared Spectrosc. 22, 375. doi:10.1255/jnirs.1135

Spijkerboer, A.W., Utens, E.M.W.J., Bogers, A.J.J.C., Verhulst, F.C., Helbing, W.A., 2008. Long-term behavioural and emotional problems in four cardiac diagnostic groups of children and adolescents after invasive treatment for congenital heart disease. Int. J. Cardiol. 125, 66–73. doi:10.1016/j.ijcard.2007.02.025

Stejskal, E.O., Tanner, J.E., 1965. Spin Diffusion Measurements: Spin Echoes in the Presence of a Time-Dependent Field Gradient. J. Chem. Phys. 42, 288–292. doi:10.1063/1.1695690

Sun, L., Macgowan, C.K., Sled, J.G., Yoo, S.-J., Manlhiot, C., Porayette, P., Grosse-Wortmann, L., Jaeggi, E., McCrindle, B.W., Kingdom, J., Hickey, E., Miller, S., Seed, M., 2015. Reduced Fetal Cerebral Oxygen Consumption is Associated With Smaller Brain Size in Fetuses With Congenital Heart Disease. Circulation 131, 114.013051. doi:10.1161/CIRCULATIONAHA.114.013051

Tabbutt, S., Nord, A.S., Jarvik, G.P., Bernbaum, J., Wernovsky, G., Gerdes, M., Zackai, E., Clancy, R.R., Nicolson, S.C., Spray, T.L., Gaynor, J.W., 2008. Neurodevelopmental Outcomes After Staged Palliation for Hypoplastic Left Heart Syndrome. Pediatrics 121, 476–483. doi:10.1542/peds.2007-1282

Talner, N.S., Nadas, A.S., 1969. Regional Plan to Aid Infants with Heart Disease. N. Engl. J. Med. 281, 794–795. doi:10.1056/NEJM196910022811414

Tatum, W.O., Coker, S.B., Ghobrial, M., Abd-Allah, S., 1989. The open opercular sign: diagnosis and significance. Ann. Neurol. 25, 196–9. doi:10.1002/ana.410250216

Taussig, H.B., 1947. Congenital Malformations of the Heart (Second Printing). New York, The Commonwealth Fund.

Te Pas, A.B., van Wezel-Meijler, G., Bökenkamp-Gramann, R., Walther, F.J., 2005. Preoperative cranial ultrasound findings in infants with major congenital heart disease. Acta Paediatr. 94, 1597–603. doi:10.1080/08035250510041150

Thienpont, B., Mertens, L., De Ravel, T., Eyskens, B., Boshoff, D., Maas, N., Fryns, J.P., Gewillig, M., Vermeesch, J.R., Devriendt, K., 2007. Submicroscopic chromosomal imbalances detected by array-CGH are a frequent cause of congenital heart defects in selected patients. Eur. Heart J. 28, 2778–2784. doi:10.1093/eurheartj/ehl560

Thompson, P., Toga, A.W., 1996. A surface-based technique for warping three-dimensional images of the brain. IEEE Trans. Med. Imaging 15, 402–417. doi:10.1109/42.511745

Thomsen, C., Henriksen, O., Ring, P., 1987. In vivo measurement of water self diffusion in the human brain by magnetic resonance imaging. Acta Radiol 28, 353–361. doi:10.3109/02841858709177362

Toga, A.W., Thompson, P.M., 2001. The role of image registration in brain mapping. Image Vis. Comput. 19, 3–24. doi:10.1016/S0262-8856(00)00055-X

Tournier, J.D., Calamante, F., Connelly, A., 2012. MRtrix: Diffusion tractography in crossing fiber regions. Int. J. Imaging Syst. Technol. 22, 53–66. doi:10.1002/ima.22005

Tuch, D.S., Reese, T.G., Wiegell, M.R., Makris, N., Belliveau, J.W., Van Wedeen, J., 2002. High angular resolution diffusion imaging reveals intravoxel white matter fiber heterogeneity. Magn. Reson. Med. 48, 577–582. doi:10.1002/mrm.10268

Tusor, N., Benders, M.J., Counsell, S.J., Nongena, P., Moegamad, A., Falconer, S., Chew, A., Gonzalez-cinca, N., Hajnal, J. V, Chatzi, V., Kersbergen, K.J., Kennea, N., Azzopardi, D. V, Edwards, A.D., 2017. Punctate White Matter Lesions Associated With Altered Brain Development And Adverse Motor Outcome In Preterm Infants. Sci. Rep. 1–9. doi:10.1038/s41598-017-13753-x

Tustison, N.J., Avants, B.B., Cook, P.A., Zheng, Y., Egan, A., Yushkevich, P.A., Gee, J.C., 2010. N4ITK : Improved N3 Bias Correction 29, 1310–1320.

Tyagi, M., Austin, K., Stygall, J., Deanfield, J., Cullen, S., Newman, S.P., 2014. What do we know about cognitive functioning in adult congenital heart disease? Cardiol. Young 24, 13–19. doi:10.1017/S1047951113000747

Tyagi, M., Fteropoulli, T., Hurt, C.S., Hirani, S.P., Rixon, L., Davies, A., Picaut, N., Kennedy, F., Deanfield, J., Cullen, S., Newman, S.P., 2017. Cognitive dysfunction

in adult CHD with different structural complexity. Cardiol. Young 27, 851–859. doi:10.1017/S1047951116001396

Utens, E.M., Bieman, H.J., Verhulst, F.C., Meijboom, F.J., Erdman, R.A., Hess, J., 1998. Psychopathology in young adults with congenital heart disease. Follow-up results. Eur. Heart J. 19, 647–51. doi:10.1053/euhj.1997.0824

Utens, E.M.W.J., Verhulst, F.C., Erdman, R.A.M., Meijboom, F.J., Duivenvoorden, H.J., Bos, E., Roelandt, J.R.T.C., Hess, J., 1994. Psychosocial functioning of young adults after surgical correction for congenital heart disease in childhood: a follow-up study. J. Psychosom. Res. 38, 745–758. doi:10.1016/0022-3999(94)90027-2

Uzark, K., Jones, K., Slusher, J., Limbers, C.A., Burwinkle, T.M., Varni, J.W., 2008. Quality of Life in Children With Heart Disease as Perceived by Children and Parents. Pediatrics 121, e1060–e1067. doi:10.1542/peds.2006-3778

van der Bom, T., Zomer, A.C., Zwinderman, A.H., Meijboom, F.J., Bouma, B.J., Mulder, B.J.M., 2011. The changing epidemiology of congenital heart disease. Nat. Rev. Cardiol. 8, 50–60. doi:10.1038/nrcardio.2010.166

van der Knaap, M.S., van Wezel-Meijler, G., Barth, P.G., Barkhof, F., Adèr, H.J., Valk, J., 1996. Normal gyration and sulcation in preterm and term neonates: appearance on MR images. Radiology 200, 389–96. doi:10.1148/radiology.200.2.8685331

van Houten, J.P., Rothman, A., Bejar, R., 1996. High incidence of cranial ultrasound abnormalities in full-term infants with congenital heart disease. Am. J. Perinatol. 13, 47–53. doi:10.1055/s-2007-994202

Van Leemput, K., Maes, F., Vandermeulen, D., Suetens, P., 1999. Automated model-based bias field correction of MR images of the brain. IEEE Trans. Med. Imaging 18, 885–896. doi:10.1109/42.811268

Varela, M., Groves, A.M., Arichi, T., Hajnal, J. V., 2012. Mean cerebral blood flow measurements using phase contrast MRI in the first year of life. NMR Biomed. 25, 1063–1072. doi:10.1002/nbm.2771

Veraart, J., Novikov, D.S., Christiaens, D., Ades-aron, B., Sijbers, J., Fieremans, E., 2016. Denoising of diffusion MRI using random matrix theory. Neuroimage 142, 394–406. doi:10.1016/j.neuroimage.2016.08.016

Vigneswaran, T. V., Zidere, V., Miller, O.I., Simpson, J.M., Sharland, G.K., 2017. Usefulness of the Prenatal Echocardiogram in Fetuses With Isolated Transposition of the Great Arteries to Predict the Need for Balloon Atrial Septostomy. Am. J. Cardiol. 119, 1463–1467. doi:10.1016/j.amjcard.2017.01.017

Vinall, J., Grunau, R.E., Brant, R., Chau, V., Poskitt, K.J., Synnes, A.R., Miller, S.P., 2013. Slower Postnatal Growth Is Associated with Delayed Cerebral Cortical Maturation in Preterm Newborns. Sci. Transl. Med. 5, 168ra8-168ra8. doi:10.1126/scitranslmed.3004666

Visootsak, J., Mahle, W.T., Kirshbom, P.M., Huddleston, L., Caron-Besch, M., Ransom, A., Sherman, S.L., Caron-, M., Ransom, A., Sherman, S.L., 2011. Neurodevelopmental outcomes in children with Down syndrome and congenital heart defects. Am. J. Med. Genet. Part A 155, 2688–2691. doi:10.1002/ajmg.a.34252

von Rhein, M., Buchmann, A., Hagmann, C., Dave, H., Bernet, V., Scheer, I., Knirsch, W., Latal, B., 2015. Severe Congenital Heart Defects Are Associated with Global Reduction of Neonatal Brain Volumes. J. Pediatr. 1–6. doi:10.1016/j.jpeds.2015.07.006

von Smoluchowski, M., 1906. Zur kinetischen Theorie der Brownschen Molekularbewegung und der Suspensionen. Ann. Phys. 326, 756–780. doi:10.1002/andp.19063261405

Vyas, S., Nicolaides, K.H., Bower, S., Campbell, S., 1990. Middle cerebral artery flow velocity waveforms in fetal hypoxaemia. Br. J. Obstet. Gynaecol. 97, 797–803.

Wagenaar, N., Chau, V., Groenendaal, F., Kersbergen, K.J., Poskitt, K.J., Grunau, R.E., Synnes, A., Duerden, E.G., de Vries, L.S., Miller, S.P., Benders, M.J.N.L., 2017. Clinical Risk Factors for Punctate White Matter Lesions on Early Magnetic Resonance Imaging in Preterm Newborns. J. Pediatr. 182, 34–40.e1. doi:10.1016/j.jpeds.2016.11.073

Wang, X., Studholme, C., Grigsby, P.L., Frias, A.E., Cuzon Carlson, V.C., Kroenke, C.D., 2017. Folding, But Not Surface Area Expansion, Is Associated with Cellular Morphological Maturation in the Fetal Cerebral Cortex. J. Neurosci. 37, 1971–1983. doi:10.1523/JNEUROSCI.3157-16.2017

Warnes, C.A., Williams, R.G., Bashore, T.M., Child, J.S., Connolly, H.M., Dearani, J.A., Del Nido, P., Fasules, J.W., Graham, T.P., Hijazi, Z.M., Hunt, S.A., King, M.E., Landzberg, M.J., Miner, P.D., Radford, M.J., Walsh, E.P., Webb, G.D., Smith, S.C., Jacobs, A.K., Adams, C.D., Anderson, J.L., Antman, E.M., Buller, C.E., Creager, M.A., Ettinger, S.M., Halperin, J.L., Krumholz, H.M., Kushner, F.G., Lytle, B.W., Nishimura, R.A., Page, R.L., Riegel, B., Tarkington, L.G., Yancy, C.W., 2008. ACC/AHA 2008 guidelines for the management of adults with congenital heart disease: Executive summary - A report of the American College of Cardiology/American Heart Association Task Force on practice guidelines (writing committee to develop guidelines fo. Circulation 118, 2395–2451. doi:10.1161/CIRCULATIONAHA.108.190811

Wernovsky, G., 2008. The paradigm shift toward surgical intervention for neonates with hypoplastic left heart syndrome. Arch. Pediatr. Adolesc. Med. 162, 849–854.

Wernovsky, G., Licht, D.J., 2016. Neurodevelopmental Outcomes in Children With Congenital Heart Disease-What Can We Impact? Pediatr. Crit. Care Med. 17, S232-42. doi:10.1097/PCC.0000000000000800

Wernovsky, G., Stiles, K.M., Gauvreau, K., Gentles, T.L., duPlessis, A.J., Bellinger, D.C., Walsh, A.Z., Burnett, J., Jonas, R.A., Mayer, J.E., Newburger, J.W., 2000. Cognitive Development After the Fontan Operation. Circulation 102, 883–889. doi:10.1161/01.CIR.102.8.883

Whitby, E., Griffiths, P., Rutter, S., Smith, M., Sprigg, A., Ohadike, P., Davies, N., Rigby, A., Paley, M., 2004. Frequency and natural history of subdural haemorrhages in babies and relation to obstetric factors. Lancet 363, 846–851. doi:10.1016/S0140-6736(04)15730-9

Wier, M.L., Yoshida, C.K., Odonli, R., Grether, J.K., Croen, L.A., 2006. Congenital anomalies associated with autism spectrum disorders. Dev. Med. Child Neurol. 48, 500–507. doi:10.1017/S001216220600106X

Williams, I.A., Fifer, C., Jaeggi, E., Levine, J.C., Michelfelder, E.C., Szwast, A.L., 2013. The association of fetal cerebrovascular resistance with early neurodevelopment in single ventricle congenital heart disease. Am. Heart J. 165, 544–550.e1. doi:10.1016/j.ahj.2012.11.013

Winston, G.P., Micallef, C., Symms, M.R., Alexander, D.C., Duncan, J.S., Zhang, H., 2014. Advanced diffusion imaging sequences could aid assessing patients with focal cortical dysplasia and epilepsy. Epilepsy Res. 108, 336–339. doi:10.1016/j.eplepsyres.2013.11.004

Wintermark, P., Hansen, a., Warfield, S.K., Dukhovny, D., Soul, J.S., 2014. Near-infrared spectroscopy versus magnetic resonance imaging to study brain perfusion in newborns with hypoxic-ischemic encephalopathy treated with hypothermia. Neuroimage 85, 287–293. doi:10.1016/j.neuroimage.2013.04.072

Wladimiroff, J.W., vd Wijngaard, J.A., Degani, S., Noordam, M.J., van Eyck, J., Tonge, H.M., 1987. Cerebral and umbilical arterial blood flow velocity waveforms in normal and growth-retarded pregnancies. Obstet. Gynecol. 69, 705–9.

Wolf, R.L., Ehman, R.L., Riederer, S.J., Rossman, P.J., 1993. Analysis of systematic and random error in MR volumetric flow measurements. Magn. Reson. Med. 30, 82–91. doi:10.1002/mrm.1910300113

Woods, R.P., Mazziotta, J.C., Cherry, S.R., 1993. MRI-PET registration with automated algorithm. J. Comput. Assist. Tomogr. 17, 536–46.

World Health Organisation, 2006. WHO Child Growth Standards (UK) [WWW Document]. URL http://www.who.int/childgrowth/en/

Wray, J., 2001. Congenital heart disease and cardiac surgery in childhood: effects on cognitive function and academic ability. Heart 85, 687–691. doi:10.1136/heart.85.6.687

Wren, C., 2001. Survival with congenital heart disease and need for follow up in adult life. Heart 85, 438–443. doi:10.1136/heart.85.4.438

Wypij, D., Jonas, R.A., Bellinger, D.C., Del Nido, P.J., Mayer, J.E., Bacha, E.A., Forbess, J.M., Pigula, F., Laussen, P.C., Newburger, J.W., 2008. The effect of hematocrit during hypothermic cardiopulmonary bypass in infant heart surgery: Results from the combined Boston hematocrit trials. J. Thorac. Cardiovasc. Surg. 135, 355–360. doi:10.1016/j.jtcvs.2007.03.067

Wypij, D., Newburger, J.W., Rappaport, L.A., DuPlessis, A.J., Jonas, R.A., Wernovsky, G., Lin, M., Bellinger, D.C., 2003. The effect of duration of deep hypothermic circulatory arrest in infant heart surgery on late neurodevelopment: The Boston

Circulatory Arrest Trial. J. Thorac. Cardiovasc. Surg. 126, 1397–1403. doi:10.1016/S0022-5223(03)00940-1

Yuen, T.J., Silbereis, J.C., Griveau, A., Chang, S.M., Daneman, R., Fancy, S.P.J., Zahed, H., Maltepe, E., Rowitch, D.H., 2014. Oligodendrocyte-encoded HIF function couples postnatal myelination and white matter angiogenesis. Cell 158, 383–96. doi:10.1016/j.cell.2014.04.052

Yushkevich, P.A., Piven, J., Hazlett, H.C., Smith, R.G., Ho, S., Gee, J.C., Gerig, G., 2006. User-guided 3D active contour segmentation of anatomical structures: Significantly improved efficiency and reliability. Neuroimage 31, 1116–1128. doi:10.1016/j.neuroimage.2006.01.015

Zaidi, S., Brueckner, M., 2017. Genetics and Genomics of Congenital Heart Disease. Circ. Res. 120, 923–940. doi:10.1161/CIRCRESAHA.116.309140

Zeng, S., Zhou, Q.C., Zhou, J.W., Li, M., Long, C., Peng, Q.H., 2015. Volume of intracranial structures on three-dimensional ultrasound in fetuses with congenital heart disease. Ultrasound Obstet. Gynecol. 46, 174–181. doi:10.1002/uog.14677

Zhang, H., Hubbard, P.L., Parker, G.J.M., Alexander, D.C., 2011. Axon diameter mapping in the presence of orientation dispersion with diffusion MRI. Neuroimage 56, 1301–1315. doi:10.1016/j.neuroimage.2011.01.084

Zhang, H., Schneider, T., Wheeler-Kingshott, C. a, Alexander, D.C., 2012. NODDI: practical in vivo neurite orientation dispersion and density imaging of the human brain. Neuroimage 61, 1000–16. doi:10.1016/j.neuroimage.2012.03.072

Zhang, H., Yushkevich, P.A., Alexander, D.C., Gee, J.C., 2006. Deformable registration of diffusion tensor MR images with explicit orientation optimization. Med. Image Anal. 10, 764–785. doi:10.1016/j.media.2006.06.004

Zilles, K., Armstrong, E., Schleicher, A., Kretschmann, H.J., 1988. The human pattern of gyrification in the cerebral cortex. Anat. Embryol. (Berl). 179, 173–179. doi:10.1007/BF00304699